The University Of Sheffield.

Novel Gas Diffusion Layers for Proton Exchange Membrane Fuel Cells

Isaac Chukwuemezu Okereke

A Thesis submitted in accordance with the requirements for the degree of Doctor of Philosophy

The University of Sheffield

Faculty of Engineering

Department of Mechanical Engineering

October 2022

The candidate confirms that the work submitted is his own and that appropriate credit has been given where reference has been made to the works of others.

Acknowledgements

My greatest appreciation and gratitude go to God almighty for the grace, favor, health, and mercies He has shown me during this PhD study ,and for always being there for me.

I would like to express my sincere gratitude to my supervisors; Professors Mohamed Pourkashanian, Lin Ma, Derek Ingham, Drs Kevin Hughes, and Mohammed Ismail. Their tremendous support, help, comprehensive guidance, and thorough examinations during weekly meetings provided me with good knowledge on the subject area. Their questions and feedback really challenged me a lot. However, special thanks must go to Professor Derek Ingham and Dr Mohammed Ismail. Professor Derek Ingham was kind and very supportive of having me back in the UK (in Sheffield) after a master's programme in Leeds. Upon my arrival in Sheffield, he has been like a father; showing understanding, cautioned where necessary, and offered helpful and technical advice. Dr Mohammed Ismail, once a senior colleague at Leeds and present Supervisor, has been more than a personal Tutor but a confidant, a mentor and technical advisor. I would always be deeply indebted to them for all they had done for me.

I would also like to thank the Tertiary Education Trust Fund (TETFund) and Akwa Ibom State University, Nigeria for their financial support by funding my PhD study at the University of Sheffield, United Kingdom.

Sincere and earnest thanks go to every member of my extended family, of whom I am forever grateful to Dr. and Mrs. Emmanuel Edoho. On their own (and out of love), with no prompting, facilitated my successful arrival and stay in Sheffield. I am also grateful to Dr & Mrs. Umoren, who happily accepted me in their home and facilitated my meeting with Dr. Kingsley Udofa. Dr. Udofa has helped my family and I in so many ways, I can't mention. I am grateful to friends here in Sheffield and in Nigeria; Utiaruk Asukpa, Ediomo Ukpong, Ms. Adelaide Okra, Dr. Esuene Sampson, Dr. Godfrey Udeh, Dr.Kelachi Omehia, Wayne, Daniel Okuo, Steven Aderinto, and the members of the Fuel cell research group: Florence, Mustafa, Fatma, Jinbei, Fernando, and Alan.

I cannot thank my parents; Professor Chiedu S. Okereke, Mrs. Nse Okereke, and Mrs. Nkoyo Udo Tom for all they have been to me in the course of this work. God will continue to bless and strengthen them for everything (even those of which I cannot completely fulfill my gratitude for). I love you so much. Also, my brother and sister, Chukwunonso & Lindy Okereke together with my nieces; Amayah and Ava.

Finally, after God, I am most thankful and indebted to my wife who has been a pillar of support. My personal confidante, carer, helper, and has never ceased to be there when I needed her. Words cannot express all she has been to me.

But of all, I am most thankful to God for the day he made me hold my daughter Ndidiamaka Alma Okereke in my arms (She's brought so much light, joy, hope, favor, and has colored my life in a lot of ways).

Therefore, this work is dedicated to God almighty and to my daughter, Ndidiamaka Alma Okereke.

Abstract

Polymer electrolyte membrane fuel cells (PEMFCs) have a great potential in becoming a major alternative to fossil fuel combustion technology. One of its major components is the gas diffusion layer (GDL). It is a porous carbon fibre-based material (which is mostly coated with a microporous layer (MPL)) that provides pathways for the transport of reactant gases, excess water, heat, and electrons during PEMFC operation. Hence, there is a need for an effective design of the GDL to optimize the PEMFC performance. One of the efficient and cost-effective tools to optimise fuel cell performance is numerical modelling using for example computational fluid dynamics (CFD) software. However, the anisotropy of the GDL and its anisotropic transport properties are not fully captured in the PEMFC numerical models reported in the literature, leading to unrealistic predictions of the PEMFC performance. In this thesis, a comprehensive 3-D numerical model of a PEMFC, incorporating realistic experimentally measured multidimensional values of the GDL transport properties (gas permeability, diffusivity, thermal conductivity, and electrical conductivity) has been developed to investigate the sensitivity of the fuel cell performance to these anisotropic transport properties. Also, a 2-D model of the transport of reactant species in cathode GDL of the PEMFC was developed. Further, numerical investigations were conducted to study the sensitivity of the PEMFC performance to (i) the interfacial contact resistances between the PEMFC components and (ii) that of a double side MPL-coated GDL. Finally, the impact of a linear porosity gradient distribution in the cathode GDL on the PEMFC global performance and the local distribution of the current density and oxygen concentration in the cathode side of the membrane electrode assembly (MEA) has been investigated. Results from the research show that at low fluid velocities and

gas permeability, the transport of the gas reactant species from the channel to the catalyst reaction sites is dominated and controlled by the diffusion mechanism in the GDL. GDL anisotropy has significant impact on the PEMFC performance, overlooking it results in either significant overestimation (if the in-plane values of the transport properties are only considered) or underestimation (if the through-plane values of the transport properties are only considered) of the modelled fuel cell. Also, when designing the carbon fibre paper GDLs, it is recommended that the carbon fibres are more oriented in the through-plane direction than in the through-plane direction to maximise traverse transport properties, in particular electrical conductivity, thermal conductivity, and gas diffusivity. Furthermore, the fuel cell performance is more sensitive to the porosity of the MPL facing the bipolar plate than the MPL facing the catalyst layer. As the porosity of the MPL facing the bipolar plate is predominantly the limiting factor for the distribution of oxygen concentration within the cathode GDL. Also, the grading of the cathode porous transport medium of the PEMFC shows that at optimum design with increasing gradient, the PEMFC global performance as well as the local distribution of the key parameters is improved.

PUBLICATIONS, CONFERENCES AND WORKSHOPS

Journal Papers

1. I.C. Okereke, M.S. Ismail, D. Ingham, K.J. Hughes, L. Ma, M. Pourkashanian," The effects of GDL anisotropic transport properties on the PEFC performance," International Journal of Numerical Methods for Heat & Fluid Flow, DOI: https://doi.org/10.1108/HFF-05-2022-0284. – **Chapter 4.**

2. I.C. Okereke, M.S. Ismail, D. Ingham, K.J. Hughes, L. Ma, M. Pourkashanian, "Single and double sided MPL coated GDLs: A numerical study," – **Chapter 5.** Manuscript accepted for publication in Energies journal, titled "Single and Double-sided Coated Gas Diffusion Layers used in Polymer Electrolyte Fuel Cells: A Numerical Study". **https://doi.org/10.3390/en16114363**

3. I.C. Okereke, M.S. Ismail, D. Ingham, K.J. Hughes, L. Ma, M. Pourkashanian," Graded GDL and MPL porosities: a numerical study. – **Chapter 6.** The manuscript is in preparation for submission to an international journal.

Poster Presentations

1. A poster on "The effects of GDL anisotropic transport properties on PEFC performance '' (The Department of Mechanical Engineering Conference and Poster Event – 25 June 2020, University of Sheffield). **(Chapters 4).**

Workshops and Presentations

1) Attended and presented at the 5th Sheffield-Kyushu Workshop on Electrochemical Energy Conversion (SKWEEC-5), Sheffield, UK.
2) Attended and presented at the 1st UK-Japan Symposium on Advanced Materials for Hydrogen and Fuel Cells, - 09 December 2021, Sheffield, UK.

NOMENCLATURE

Roman symbols

a	Specific surface area, $\mathrm{m^{-1}}$
A	Cross sectional area, $\mathrm{m^2}$
ac	Water activity
c	Concentration, $\mathrm{mol/m^3}$
$\mathrm{C_p}$	Specific heat capacity
D	Diffusion coefficient, $\mathrm{m^2/s}$
$\mathrm{D_s}$	Capillary diffusion coefficient, $\mathrm{m^2/s}$
E	Cell potential, V
$\mathrm{E_0}$	Reference potential, V
$\mathrm{E_r}$	Equilibrium potential, V
F	Faraday' constant, C/mol
i	Current density, $\mathrm{A/m^2}$
$\mathrm{i_0}$	Exchange current density, $\mathrm{A/m^2}$
$\mathrm{i_{op}}$	Operating current density, $\mathrm{A/m^2}$
j	Volumetric transfer current, $\mathrm{A/m^3}$
K	Permeability, $\mathrm{m^2}$
$\mathrm{K_r}$	Relative permeabliity
M	Molecular weight, kg/mol
P	Pressure, Pa
$\mathrm{P_c}$	Capillary pressure
r	Fibre radius
R	Universal gas constant, J/mol·K
s	water saturation
S	Source term in conservation equations
T	Cell operating temperature, K
$\vec{u}$	Fluid velocity vector, m/s
$\vec{v}$	Molar-averaged velocity vector, m/s

V_{cell}	Operating cell voltage
R_c	Contact resistance, $\Omega \cdot m^2$
X	Mole fraction
Y	Mass fraction

Greek symbols

σ	Electrical or ionic conductivity, S/m; surface tension (N/m)
μ	Dynamic viscosity, Pa·s
η	Over-potential, V
ρ	Density, kg/m^3; electrical resistivity ($\Omega \cdot m$)
ϕ	Electrical or ionic Potential, V
∝	Transfer coefficient; empirical constant
ε	Porosity
Ƙ	Thermal conductivity, W/m·K
ξ	Stoichiometric ratio
ε_p	Percolation threshold
β	Inertial coefficient
Λ	Membrane water content
θ_c	Contact angle

Subscripts

a	Anode
act	Activation; active area
c	Cathode
ch	Channel
e	Energy
eff	Effective
f	Volume fraction
F	Fluid
g	Gases
i, j	Species

mem	Membrane phase
s	Saturated water vapor
sol	Solid phase
v	Water vapor
$_{=}$	In-plane
$_{\perp}$	Through-plane

Superscripts

eff	Effective
ref	Reference
τ	Tortuosity

Abbreviations

AC	Alternating current
AEM	Anion exchange membrane
AFC	Alkaline fuel cell
BoP	Balance of plant
BPP	Bipolar plate
CCS	Carbon coated substrate
CCUS	Carbon capture and storage
CFD	Computational Fluid Dynamics
CHP	Combined heat and power
CL	Catalyst layer
DC	Direct current
DMFC	Direct methanol fuel cell
EIS	Electrochemical impedance spectroscopy
EMT	Effective medium theory
FBG	Fibre Bragg Grating
FCEV	Fuel cell electric vehicle
FDM	Finite difference method
FEM	Finite element method

FVM	Finite volume method
GDE	Gas diffusion electrode
GDL	Gas diffusion layer
GDM	Gas diffusion media
GE	General Electric
GHG	Greenhouse gas
ICE	Internal combustion engine
IEA	International energy agency
HOR	Hydrogen oxidation reaction
LSM	Lanthanum strontium manganite
LB	Lattice Boltzmann
LHV	Lower heating value
MEA	Membrane electrode assembly
MCFC	Molten carbonate fuel cell
MPL	Microporous layer
MPS	Macro porous substrate
ORR	Oxygen reduction reaction
PAFC	Phosphoric acid fuel cell
PAN	Polyacrylonitrile
PEM	Polymer electrolyte membrane
PEMFC	Proton exchange membrane fuel cell
PFSA	Polyflourosulfonic acid
PSD	Pore size distribution
PTC	Parallel thermal conductance
PTFE	Polytetrafluoroethylene
PVA	Polyvinyl alcohol
RH	Relative humidity
SEM	Scanning electron microscope
SOFC	Solid oxide fuel cell
SPE	Solid polymer electrolyte

TEM	Transmission electron microscopy
TFE	Tetraflouroethylene
X-CT	X-ray computed tomography
Redox	Reduction-oxidation
SIMPLE	Semi-implicit methods for pressure linked equations
wt.%	Percentage based on weight

Chemical symbols

CO	Carbon monoxide
CO_2	Carbon dioxide
CH_4	Methane
e^-	Electron
H^+	Proton
H_2	Hydrogen molecule
H_2O	Water molecule
O_2	Oxygen molecule
N_i	Nickel
rGO	Graphene oxide

Contents

LIST OF FIGURES

LIST OF TABLES

1 INTRODUCTION

1.1 Energy – Sources, energy systems, sustainability, and security

Primary energy is energy in its raw form before being processed or converted into other forms of energy such as heat, electricity, or power for transport. Examples are coal, oil, or gas (before being burned) or solar or wind energy. These raw forms of energy are generally referred to as energy sources. The process of conversion of these raw forms of energy into useful energy (to do work) is the energy generation system/technology with the most used system being the combustion of fossil fuels. Increased global population growth and the global socio-economic activities has escalated energy demand [1]. According to the world energy reports [2,3] presently a large percentage (about 70%) of the energy used globally is generated from the combustion of fossils fuels (coal, natural gas, and oil) with only a small percentage generated from other sources such as nuclear, hydro, solar, wind, geothermal, etc. The IEA Global Energy Review on CO_2 emissions for the year 2021 [4] reports that global carbon dioxide emissions from fossil fuel combustions and industrial processes reached their highest ever annual level in 2021, increased 6% from the 2020 record to a total of 36.3 Gt, with a 2.1 Gt increase in emissions from that of 2020, as shown in Figure 1.1.

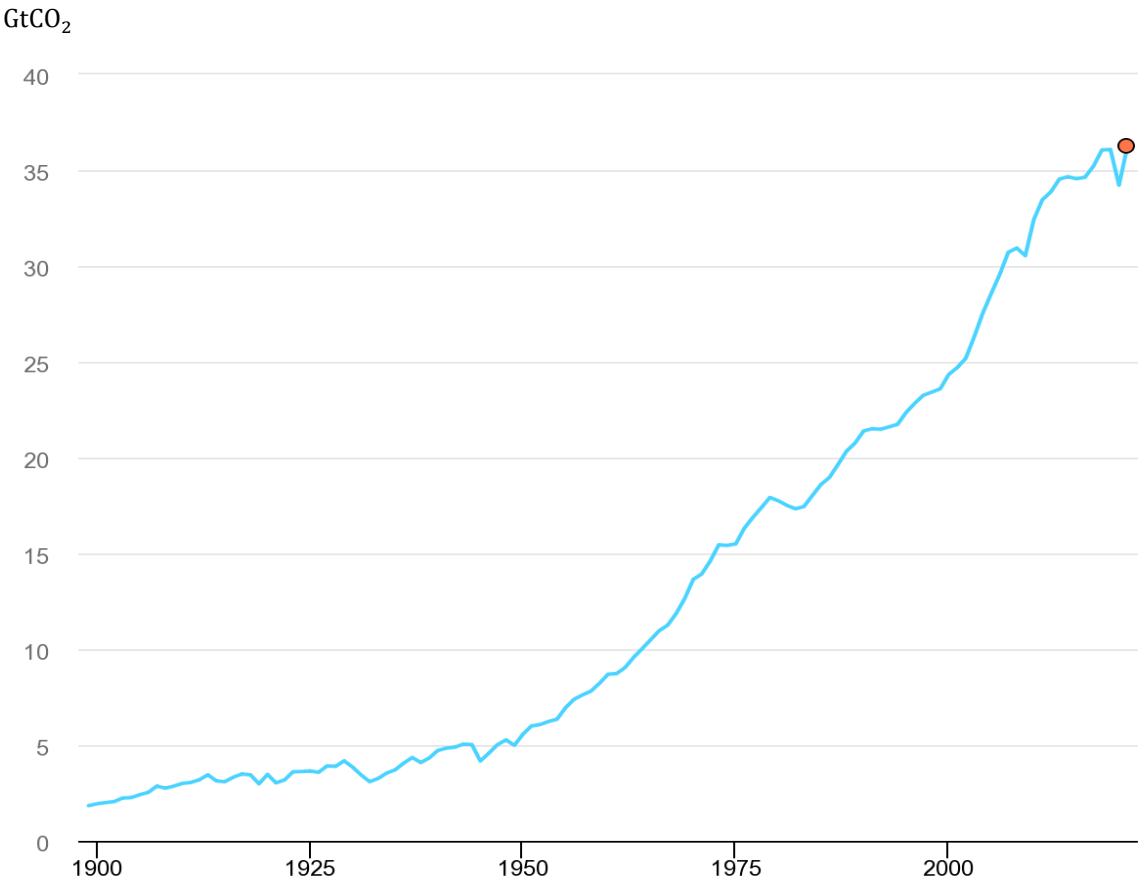

Figure 1.1 CO_2 emissions from energy combustion and industrial processes, 1900 to 2021. All emission estimates are expressed in Gt CO_2 [4].

Though, the report also states that despite the rebound in coal for power generation within the year 2021, renewables had the highest share of global electricity generation when compared to coal with an all-time high exceeding 8000 TWh. This increase in renewables for electricity generation helped reduced the global rise in CO_2 emissions by 220 Mt in the year 2021. According to “our world in data” [5] the energy production is responsible for 87% of global emission of GHGs with rich countries (Europe, USA, China) producing the highest percentage of these emissions. The world still lacks large-scale fossil fuels alternatives that are cheap, safe, and sustainable, with fossil technologies still producing about 65% of the world

energy consumed (as at 2021) and renewables generating an increased global supply of about 30% power (with a steady rise of about 10% in the year 2021). For energy generation systems security and sustainability, there is the need to develop large scale technologies to fast track the transition from fossils to clean energy sources especially for use in the transport and heating sectors [6]. The over-reliance on fossil fuels combustion technology as the major energy generation system is constantly leading to the weakening of fossils combustion energy systems – with global hydrocarbon reserves being depleted at increasing rates, making the need to diversity energy sources and systems very crucial to meet energy demands, ensure energy security and minimize environmental hazards [3], thereby threatening global energy production and distribution security [1, 3]. Though, as at present there is yet to be any reported shortage of fossil fuels globally, there has been documented reports indicating serious local and global environmental fatigue and degradation as well as health hazards (from the combustion of fossil fuels) to human, animal, and plant population globally. It has been reported by [3,7] that about 67% of energy consumed globally is generated from the combustion of fossil fuels with tonnes of carbon dioxide (CO_2) emitted into the atmosphere, thus causing global warming together with local and global environmental degradation. Approximately 17% of CO_2 emissions come from internal combustion engines (ICEs) of cars, trucks and generating sets. According to [6] there has been a rapid increase in fossil fuels and CO_2 emissions from 1950 – following the global industrial revolution as shown in Figure 1.2.

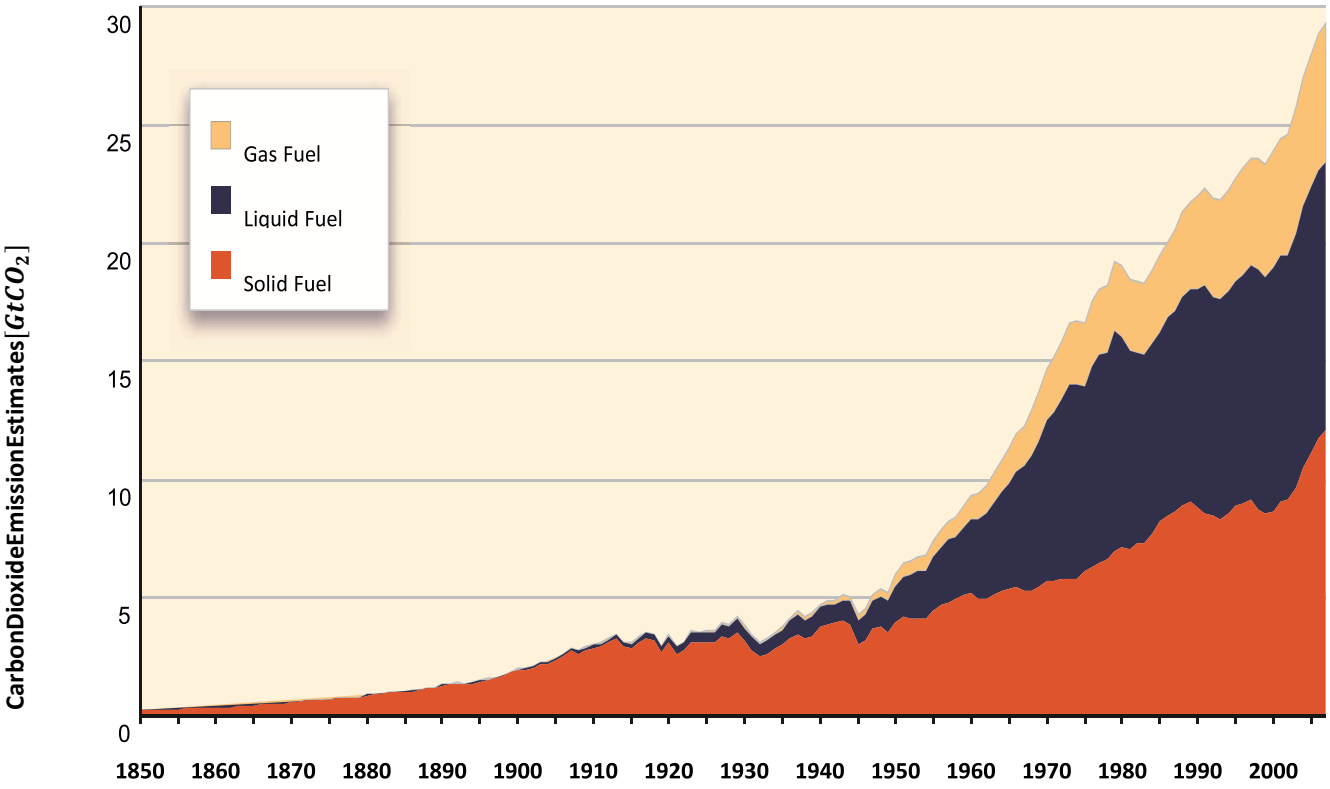

Figure 1.2 Global CO_2 emissions from fossil fuel burning, 1850 to 2007. Gas fuel includes flaring of natural gas. All emission estimates are expressed in Gt CO_2 [6].

It has been reported by [6] that an estimated 113 million US residents, as of 1998, live in regions that do not meet the US National Air Quality Standards. To sustain industrial growth and global development without leading to environmental fatigue and eventual failure, the energy sources and systems must have to be diversified – and even localised (distribution of electricity) and sustainable sources and system must be developed. Localised energy distribution are autonomous energy distribution systems that involve the distribution of power generated locally using several many mini-power plants or microgrids. The system is contrary to the traditional, centralized electricity distribution system which requires/involves a large-scale grid system. Rather, for this system, several mini power plants or microgrids are dispersed over different areas near energy consumers instead of a

few mega ones. This helps to reduce transmission losses and vulnerability of having to transmit energy over wide areas. This will help reduce the effects and damages on the environment as well as the threat to human, animal, and plant populations. A transition to alternative fuels and clean energy generation technology will help sustain energy mobility and global energy security [1,2,3]. This will help provide the necessary security and sustainability in the supply and distribution of power. Reducing over reliance on fossil fuels in transportation and electric energy generation has been on the front burner of discussions amongst industrialized nations, developing and even under-developed countries. This development has led to increased research into renewable energy sources and systems as well as alternative fuel sources such as biomass and hydrogen. With the increasing importance of the transport sector to global economy, and limited application of renewable energy in this sector, hydrogen fuel cells are currently receiving significant global attention as potential alternatives for power generation owing to their clean electrochemical energy conversion process (with no combustion), low-to-zero noise emission (as there is no moving part), high efficiency, high power densities under rapid changes in load, and easy start up and shutdowns.

1.2 Hydrogen as an alternative clean fuel

Though the most abundant element in the universe, hydrogen is not a primary source of energy as it does not naturally occur as a fuel. Hydrogen must be manufactured or extracted from different processes such as the reforming of methane, coal gasification and the electrolysis of water. However, hydrogen is a versatile energy carrier and a clean, important energy storage medium. According

to [8] the utilization of hydrogen in clean forms produced from renewables, such as hydro, solar, nuclear, etc. or fossil fuels with carbon capture and storage (CCUS) will go a long way in reducing harmful emissions/ pollutants to the environment in the transport, chemicals sectors and improve and guarantee energy security. Hydrogen technologies have gained momentum in their demand and utilization lately, especially within the year 2020. According to [4], in 2018 global demand for pure hydrogen was about 74 million tonnes (Mt), of which 38.2 Mt was used in oil refining and 31.5 Mt in ammonia production. There was a further 42 Mt of demand for hydrogen mixed with other gases such as carbon monoxide. Of this, 12 Mt was used in methanol production and 4 Mt in direct-reduced iron (DRI) for steel. There are four main global sources for the commercial production of hydrogen, namely natural gas, oil, coal, and electrolysis. Hydrogen production from natural gas accounts for 48% of commercial hydrogen in the market while oil, coal, and electrolysis of water contributes 30%, 18% and 4% of the world's hydrogen production source respectively. About 10 countries have adopted hydrogen technologies as alternative energy carriers/energy currencies. In 2020, almost 70MW of hydrogen electrolysers were installed around the globe, to generate hydrogen from fossil fuels, thereby expanding hydrogen production capacity by 15%. Its demand, according to [9], in the year 2020, rose to about 90 Mt. 70 Mt was used as pure hydrogen and less than 20 Mt was mixed with carbon-containing gases which is used in the production of methanol and steel.

Hydrogen production

A large scale of the hydrogen used in energy generation is manufactured from the high temperature steam reforming of methane (CH_4) under pressures of 3-25 bars.

The reversible chemical reactions involved in the steaming reforming of methane into hydrogen are as follows:

Steam reforming (SR): $\mathrm{CH_4 + H_2O \leftrightarrows CO + 3H_2}$ $[\Delta \mathrm{H_{SR}} = 206 \mathrm{kJmol^{-1}}]$ **(1.1)**

Water-gas shift reaction: $\mathrm{CO + H_2O \leftrightarrows CO_2 + H_2}$ $[\Delta \mathrm{H_{WGSR}} = -41 \mathrm{kJmol^{-1}}]$ **(1.2)**

Direct steam reforming: $\mathrm{CH_4 + 2H_2O \leftrightarrows CO_2 + 4H_2}$ $[\Delta \mathrm{H_{SR}} = 165 \mathrm{kJmol^{-1}}]$ **(1.3)**

The reforming of methane into hydrogen accounts for about 70 million tonnes of world hydrogen production [9], followed by the gasification of coal or biomass using high temperature steam and oxygen in pressurised reactions to produce carbon monoxide (CO). A small fraction of it is produced from the electrolysis of water using Alkaline, PEM, and solid oxide electrolysers. Also, hydrogen can be produced from renewable sources such as agricultural wastes, sewage, paper, and other biomass materials [9]. Hydrogen can be produced from steam reforming of bio-oils and pyrolysis as well as thermochemical conversion processes. Also, it can be produced by other processes such as photo-fermentation, bio-photolysis of water using green algae and cyanobacteria, dark fermentation, and hybrid reactor systems.

Hydrogen demand and usage

Hydrogen is used in production industry for oil-refining, metal refining, ammonia production, methanol production, steel production, and in food processing. It is blended into natural gas network for heating homes. In power generation, it is one of the leading options for storing renewable energy. It can be used, together with ammonia, in gas turbines to increase power system flexibility. Also, hydrogen-based ammonia can be used in coal- fired power plants to reduce emissions. A representation of hydrogen production, logistics and its end use is shown in Figure 1.3.

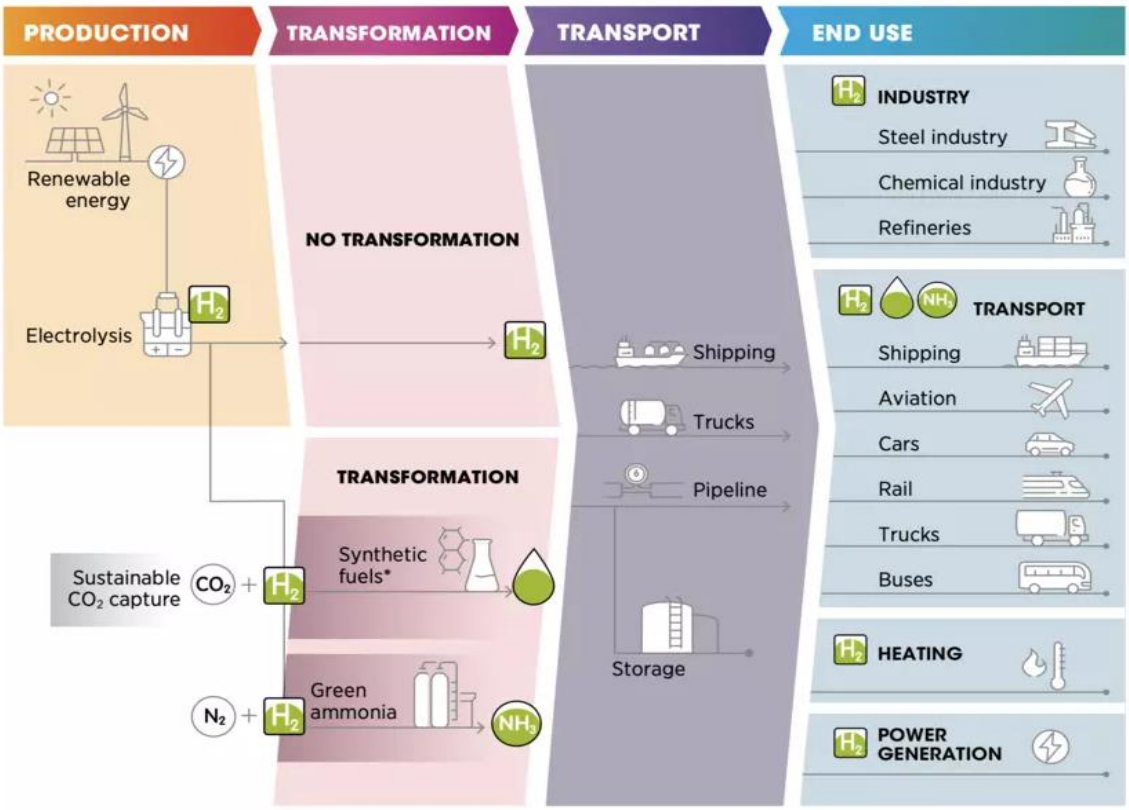

Figure 1.3 Hydrogen production, transformation, and usage [9].

Usage in the transport sector

The huge economic importance of the global transport sector has led to a high demand of other sources of energy, with high efficiencies, to sustain global mobility. According to [1,10], the European Commission has laid down a plan for alternative fuels to replace 20% of conventional fossil fuels in the transport sector, by the year 2030. Hydrogen has been projected to be the long-term replacement to conventional fossil fuels. Its main attraction, as an important alternative to fossils, is its low-to-zero emission of CO_2, with water and heat being the end production from the electrochemical reaction-making it the cleanest chemical fuel. Though, according to the IEA [9], it is still proving difficult to fully integrate hydrogen into the transport fuel

mix. Its use in the transport sector, as of 2020, was barely 0.01% with fuel cell electric vehicle (FCEVs) global stocks being less than 0.01% as compared to electric vehicles which was 0.3%. That notwithstanding, it's global trade and stocks in FCEVs grew by an average of 70% annually within the year 2017-2020. As at the middle of the year 2021,40000 FCEVs were in use globally with the USA and Korea having the largest shares. There has been an increasing rise in stock for FCEVs globally within the period of 2017 -2020, with cars leading and followed by buses [11]. However, the greatest drawback in the full utilisation of hydrogen technologies in the transport sector has been the inadequate deployment of infrastructure. Hydrogen refuelling stations compared to electric vehicles charging points is still very low. Hydrogen-based fuels (ammonia) are also attracting attention for use in large ocean-going vessels, with investors announcing plans to make 100% ammonia- fuelled marine engines available as early as 2023 and to offer ammonia retrofit packages for existing vessels from 2025. Hydrogen is also attracting serious attention in the air industry. Airbus recently set a target year of 2035 to develop novel hydrogen aircraft concepts for commercial flights with passenger capacity of 200 and above and flight range of 3700km. The Commonwealth Scientific and Industrial Research Organization (CSIRO) reports that "hydrogen can significantly reduce aviation emissions in the long-term and that growing hydrogen industry momentum can provide an opportunity for airport applications as early as 2025" [12]. Zero Avia and Universal Hydrogen are also developing hydrogen fuelled small aircrafts for short range flights. In February 2021, KLM tested their first hydrogen -based synthetic kerosene as drop-in fuel, in Netherland [11]. There have lately been great focus in the application of hydrogen to electric generation with Japan targeting 1 GW of hydrogen electricity by 2030. Korea has also set a target of 1.5 GW fuel

cell capacity by 2022 and 15 GW by 2040. Generally, the demand for hydrogen has grown since 1975 with 6% of global natural gas and 2% of global coal going into its production.

1.3 Fuel Cell technology: basic principles

A fuel cell is an electrochemical device, consisting of an electrolyte which is sandwiched between negative (anode) and positive (cathode) electrodes, and converts the chemical energy from hydrogen and other fuels directly into electricity. The building block of a fuel cell consists of an electrolyte in contact with an anode and a cathode on either side. The most common reactants used in fuel cells are hydrogen, which is the reducing agent in the electrochemical reaction, and oxygen which is the oxidizing agent. The electrochemical reactions take place within the electrodes of the cell producing electricity [13] heat, and water as by-products. The electrochemical reaction in the fuel cell is represented as follows:

Anode: $2H_2 \rightarrow 4H^+ + 4e^-$ (oxidation) **(1.4)**

Cathode: $O_2 + 4H^+ + 4e^- \rightarrow 2H_2O$ (reduction) **(1.5)**

Overall reaction: $2H_2 + O_2 \rightarrow 2H_2O$ + heat (**1.6)**

The fuel cells convert the chemical energy stored in fuels (hydrogen, methane, methanol, etc.) directly into electricity. They operate at higher efficiencies, with low environmental impact compared to conventional fossil combustion technologies as they convert chemical energy directly into electricity. Their operation does not require any mechanical moving parts or the undergoing of thermodynamic processes of heat generation, steam production, thermal-to-mechanical energy conversion, and mechanical-electrical energy conversion which makes them less

expensive compared to hydrocarbon combustion technologies. In addition, because combustion is avoided, fuel cells produce power with minimal pollutant emission. Though they are like conventional battery cells in many ways (as they both consist of an anode and cathode in contact with an electrolyte and undergo electrochemical reactions to generate electricity), they differ in several respects. Conventional battery cells are energy storage devices in which all the energy available is stored within the battery itself. Batteries stop producing electricity once the chemical reactants are consumed (i.e., discharged) whereas fuel cells do not run down nor require to be recharged as the chemical reactants are externally supplied and only require to be refilled. In principle, the fuel cell produces power for as long as fuel is supplied. To improve their efficiencies, some fuel cells can be coupled with combined heat and power systems. Individual cells can be combined to form fuel cell stacks and these stacks can also be combined to form larger fuel cell system [14]. A schematic representation of a typical fuel cell is shown in Figure 1.4.

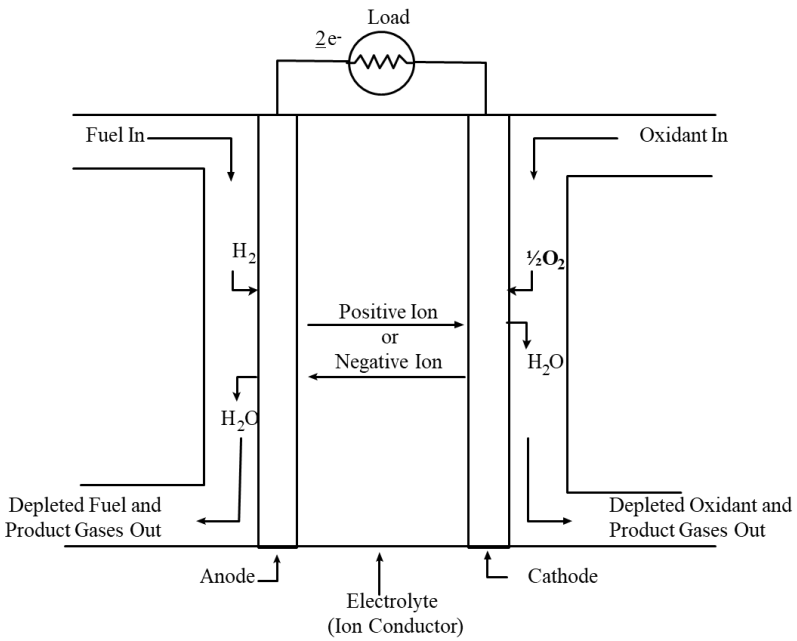

Figure 1.4 Schematic of a typical fuel cell [16].

1.3.1 Fuel cell system

Individual fuel cell units are electrically connected to form fuel cell stacks to achieve the required power output capacity. The fuel stack forms the heart of operation of the fuel cell system. However, the fuel cell system still requires other important supporting components for its functionality and to produce electric power. A fuel cell system's arrangement depends on its type of electrolyte and its application, the type of fuel required for its operation, the operating conditions such as temperature and pressure, as well as the fuel cell stack design characteristics. The balance of plant (BoP) for a typical fuel cell system comprises several components with the following functions: fuel supply/preparation, air/oxidant supply, thermal management, water management, electric power conditioning, and (in the case of polymer electrolyte membrane fuel cells) humidifiers. Figure 1.5 shows a schematic of a typical fuel cell system while its subsystems are explained in detail in the following subsections.

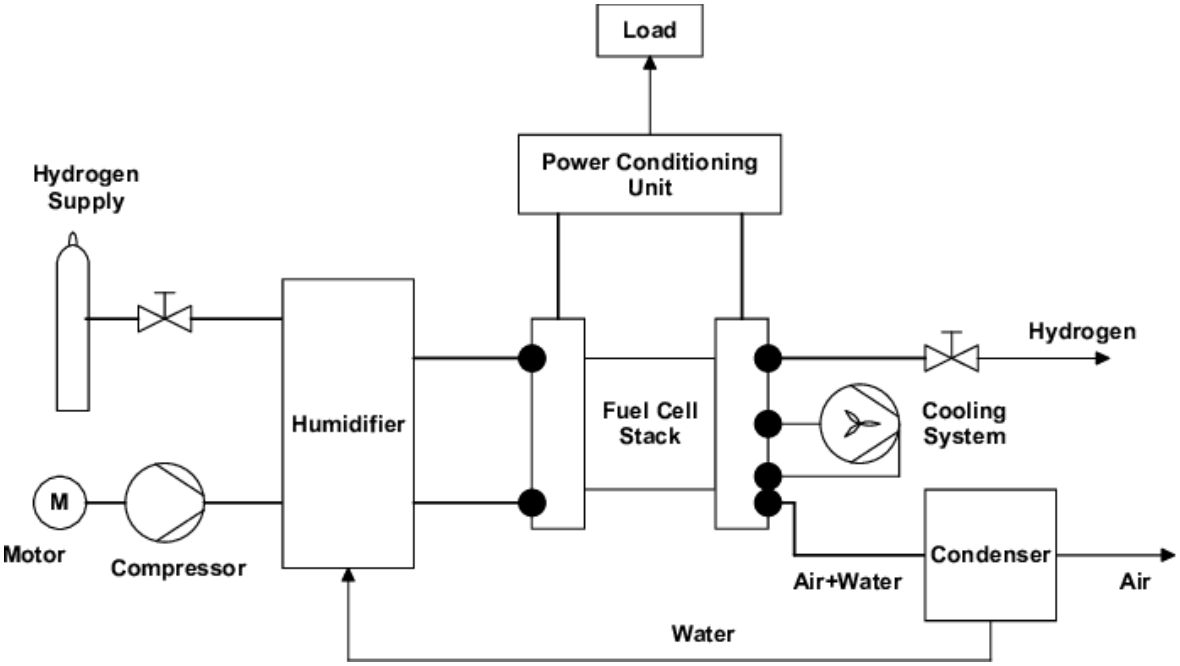

Figure 1.5 Schematic diagram of a typical fuel cell system.

The fuel cell stack

The amount of electricity generated by a single fuel cell depends on its size, the operating temperature of the cell, the operating pressures and the inlet gas pressures, as well as the type of fuel cell. Generally, a stand-alone fuel cell generates less than 1.0 V of electric voltage which is insufficient in most applications requiring higher loads. Hence, units of fuel cells need to be combined or arranged in series to form a fuel cell stack. Typical fuel cell stacks may consist of hundreds of fuel cells. A schematic diagram of the fuel cell stack is shown in Figure 1.6.

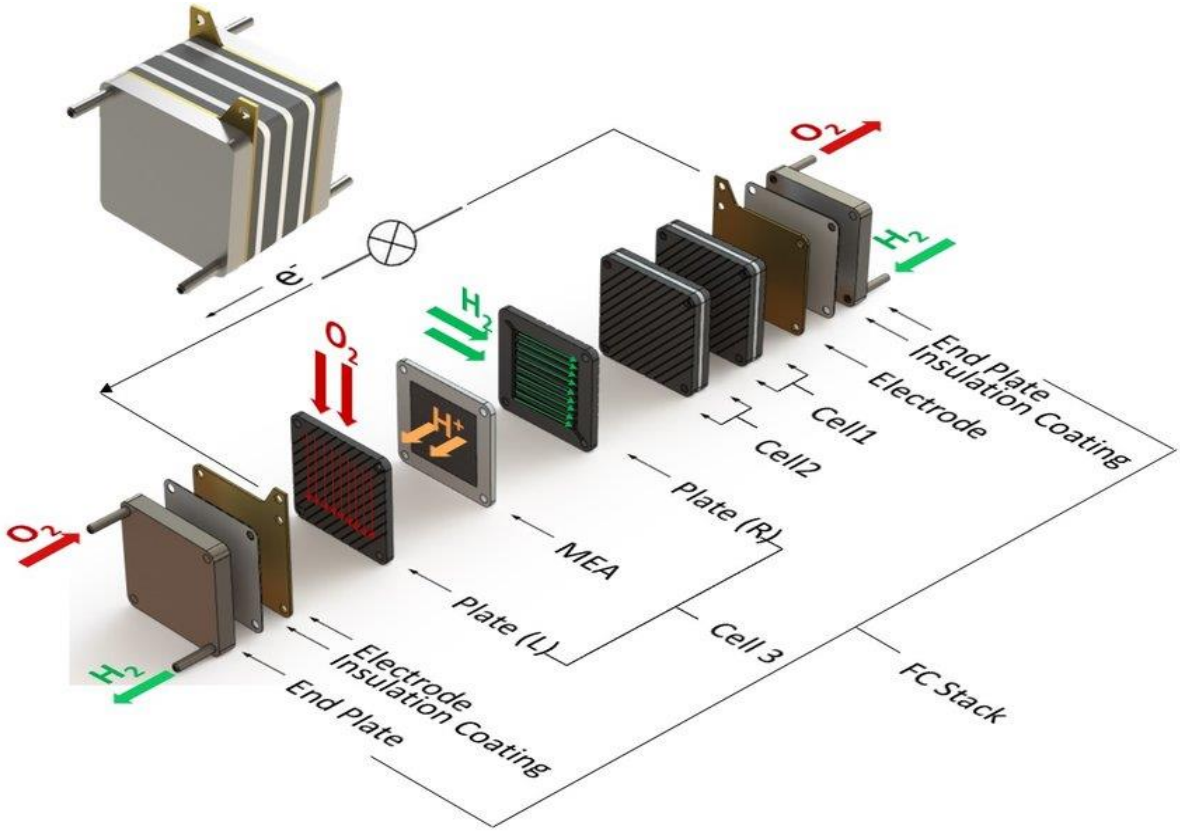

Figure 1.6 Schematic diagram of a fuel cell stack [17].

The fuel processor

Except for cases where hydrogen is used in pure forms or fuel cells that run on /or internally reform their fuels from natural gas, etc., the fuel must be externally prepared then fed into the cell. This process involves the removal of impurities (such as CO_2 and CO) and thermal conditioning. An external reformer is used to convert the hydrocarbon and reformate, where the fuel cell requires a hydrogen-rich feed mixture, methanol, gasoline, or gasified coal. In some fuel cell systems, there are multiple reactions to oxidise the CO, converting it into CO_2. A sorbent bed is then used to remove impurities such as sulphur compound from the fuel before feeding it into the fuel cell. High temperature fuel cells, operating at temperatures above 550℃, such as molten carbonate fuel cells (MCFC) and solid oxide fuel cells (SOFC) can internally reform their fuel before it is feed to the fuel cell stack.

Electric power conditioners

Electric power conditioning/conditioners is required to adapt the direct current (DC) produced by the fuel cell into alternating current (AC) so it can be used for application.

Air Supply Equipment

Comprises air compressors or blowers and air filters. The air compressors help improve the fuel cell performance by increasing the gas pressures at inlet. Some fuel cells systems also have expanders which recover power from the higher-pressure exhaust gases.

Thermal management

All fuel cells require careful management of the heat within the fuel cell stack. Therefore, heat-conducting materials are used in the fuel cell stack to remove excess heat so as to allow for improved efficiency of the fuel cell. Some fuel cell systems are combined with heat and power generation as well as with combined heating systems.

Water management

Proper water management systems are used to ensure the smooth and effective operation of the fuel to avoid flooding and dehydration (which can lead to damages of the electrolyte membrane).

Humidifiers

Many fuel cell systems, especially polymer electrolyte membrane fuel cells use humidifiers to humidify the inlet air to keep the membrane hydrated for continuous and efficient operation. They humidifiers consist of a thin membrane which may be made of the same material as the polymer electrolyte membrane, PEM.

1.4 Advantages and limitations of fuel cells

The advantages of the fuel cells include the following:

- Most fuel cells run on pure hydrogen and therefore they are generally pollution free, with water, and heat as by-products, hence drawing serious attention in terms of research and development.
- High efficiency in the energy conversion process, since there is no combustion or energy loss in mechanical component movement, as can be

seen when compared with other energy generation systems in Figure 1.7.

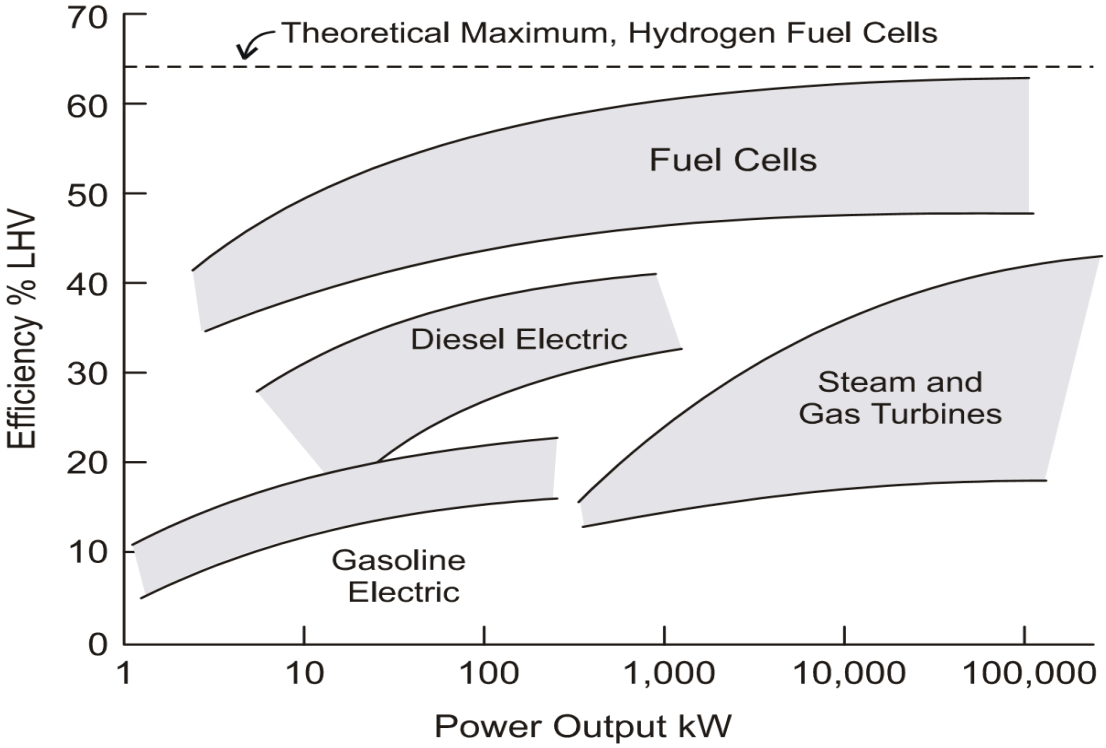

Figure 1.7 Power Generating Systems Efficiency Comparison [15].

- Unlike batteries that must be disposed of once their chemicals are used up, fuel cell reactions do not deplete and can produce electricity for as long as the reactants are supplied.
- They are quiet in operation as they do not have moving parts and have low mass.
- They are simple in operation therefore saving cost of maintenance.
- Low to zero emissions which makes them environmentally friendly.
- The heat by-product from its operation can be used in combined heating and power (CHP).

- They are scalable, unlike battery cells. Individual cells can be combined to form fuel cell stacks and these stacks can also be combined to form larger fuel cell system.

Fuel cells are however limited in use since:

- There is currently no hydrogen infrastructure to supply coast-to-coast delivery of hydrogen fuel.
- The process of producing large quantities of hydrogen (reforming methane) is too expensive.
- Platinum, as a catalyst is used for low-temperature fuel cells but are very rare and expensive. Also, they are easily poisoned and degraded.

1.5 Types of fuel cells and their applications

Fuel cells are generally classified based on the type of electrolyte material used in the fuel cell [14]. Based on their electrolytes, there are five major types of fuel cells that are being researched and developed for electricity generation, namely: alkaline fuel cell (AFC), phosphoric acid fuel cell (PAFC), molten carbonate fuel cell (MCFC), solid oxide fuel cell (SOFC), and polymer electrolyte fuel cells. The polymer electrolyte fuel cells are further differentiated into two types based on the fuel used for its electrochemical reaction. Proton exchange membrane fuel cells (PEMFC) run on hydrogen while the direct methanol fuel cell use methanol as its fuel. Also, fuel cells can be broadly classified into two groups based on the operating temperature which is determined by the electrolyte used for the fuel cell. For the low-medium temperature fuel cells such as AFC, PAFC, PEMFC, and DMFC, the hydrocarbon

fuels are converted into hydrogen my externally attached reformers before being fed into the cells. High temperature fuel cells such as MCFC and SOFC internally convert CO and methane (without the use of reformers) into hydrogen or even oxidise them directly [14]. Table 1.1, which is followed by a brief description of each fuel cell type - except for PEMFC (which is described in detail in Section 1.6), summarises the data for the different types of fuel cells.

Table 1.1 Data for different types of fuel cells [14,16].

	AFC	PEMFC	DMFC	PAFC	MCFC	SOFC
Operating temperature (℃)	60-250	30-80	60-130	150-220	600-700	800-1000
Electrolyte	Mobilized or Immobilized Potassium Hydroxide in asbestos matrix	Hydrated Polymeric Ion Exchange Membranes	Hydrated Polymeric Ion Exchange Membranes	Immobilized Liquid Phosphoric Acid in SiC	Immobilized Liquid Molten Carbonate in LiAlO2	Yttria stabilized Zirconia (YSZ)
Electrodes	Transition metals	Carbon	Carbon	Carbon	Nickel and Nickel Oxide	Perovskite and perovskite / metal cermet
Catalyst	Platinum	Platinum	Platinum-ruthenium (anode) and	Platinum		

			platinum (cathode)		Electrode material	Electrode material
Charge carrier	OH^-	H^+	H^+	H^+	Co_3^{2-}	O^{2-}
Anode reaction	$H_2 + 2OH^- \rightarrow 2H_2O + 2e^-$	$H_2 \rightarrow 2H^+ + 2e^-$	$CH_3OH + H_2O \rightarrow CO_2 + 6H^+ 6e^-$	$H_2 \rightarrow 2H^+ 2e^-$	$H_2 + CO_3^{2-} \rightarrow H_2O + CO_2 + 2e^-$	$H^2 + O^{2-} \rightarrow H_2O + 2e^-$
Cathode reaction	$^1/_2\, O_2 + H_2O + 2e^- \rightarrow 2OH^-$	$^1/_2\, O_2 + 2H^+ + 2e^- \rightarrow H_2O$	$^3/_2\, O_2 + 6H^+ + 6e^- \rightarrow 3H_2O$	$^1/_2\, O_2 + 2H^+ + 2e^- \rightarrow H_2O$	$^1/_2\, O_2 + CO_2 + 2e^- \rightarrow CO_3^{2-}$	$^1/_2\, O_2 + 2e^- \rightarrow O^{2-}$
Catalyst materials	Anode: Ni Cathode: Ag	Anode: Pt Cathode: Pt	Anode: Pt-Ru Cathode: Pt	Anode: Pt-Ru Cathode: Pt	Anode: Ni-5Cr Cathode: NiO(Li)	Anode: Ni-YSZ Cathode: Lanthanum Strontium Manganite (LSM)
Applications	Transportation, space, military, energy storage system			Combined heat and power for decentralized stationary power systems	Combined heat and power for decentralized stationary power systems, and for transportation (trains, boats, etc.)	

Output power	Small plants 5- 150kW Modular	Small plants 5- 250kW Modular	Small plants <5kW	Small-medium sized plants 50kW- 1MW	Small power plants 100kW-2MW	Small power plants 5- 250kW
Main producers	AFC Energy (UK) UTC Power (USA) Acta Power (Italy)	Ballard (Canada) Heliocentris (Germany)	SFC Energy (Germany)	UTC Power (USA) Fuji Electric (Japan)	Fuel cell energy (USA)	Ceramic fuel cells (Australia) SOFC Power (Italy Ceres Power (UK)

Alkaline Fuel Cell (AFC)

AFCs happen to be one of the first fuel cell technologies developed and used for power generation. They were the first fuel cell to be extensively researched and developed for use by NASA in their Gemini Apollo and Space shuttles to produce power and water on-board [18,19]. They operate at a higher efficiency of 60-70%, compared to other fuel cells and combustion technology, due to the rate of their electrochemical reactions and low activation overpotential. This implies that the activation barrier required to be overcome in the electrochemical reactions is low.

A higher ORR kinetics allows for the use of less expensive non- noble metals such as iron, nickel (at the anode) and cheaper catalysts such as silver or iron at the

cathode. AFCs are made of an aqueous solution of potassium hydroxides (KOH) as the electrolyte and a variety of non-noble metals like iron, silver, nickel as their electrocatalysts [19]. The AFCs use 85 wt. % concentration of potassium hydroxide as electrolytes for high temperature operations (between $120 \text{ and } 250℃$) and a less concentration of 35 wt.% of KOH for temperature operations lower than 120℃. Their electrolytes are retained in a matrix (asbestos), and they are CO_2 intolerant with the charge carrier being OH^- ions and a cell output power of 5 kW (in small plants and applications) to 150kW (in modular plants). Figure 1.8 depicts the AFC and its operations. Their greatest drawback and limitation in application is the fact that they are intolerant to and poisoned by CO_2, which reacts with the hydroxides ions in the electrolyte to form potassium carbonates (K_2CO_2). The electrolytes suffer from wettability and increased corrosion.

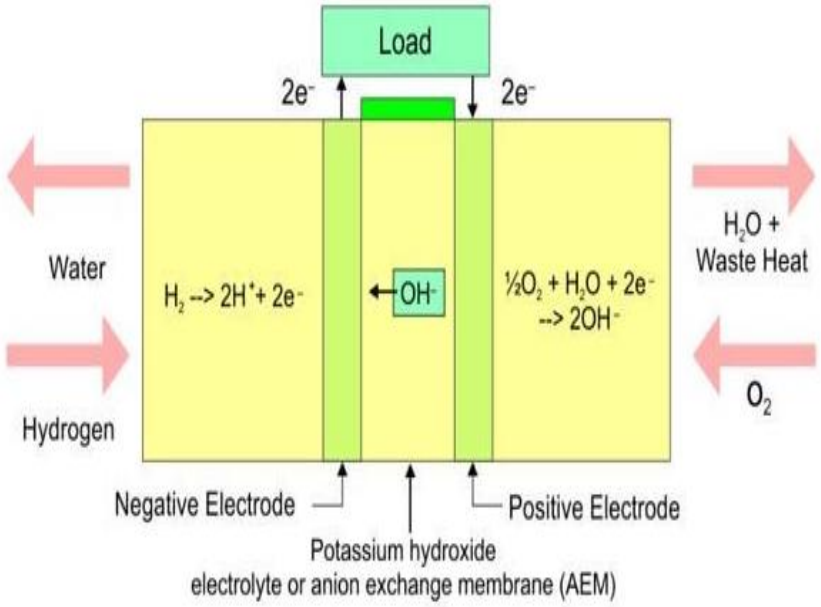

Figure 1.8 The basic structure of the AFC [19].

Phosphoric Acid Fuel Cells (PAFCs)

PAFCs operate at a typical temperature of $150 \text{ and } 220℃$ [14]. They are the first generation of modern fuel cells to be mass produced and commercialised [14,20] and are widely developed/ manufactured and use in stationary power generation in the U.S and Japan [20]. PAFCs are generally made of 100% concentrated liquid phosphoric acid (H_3PO_4) which is held in a Teflon -bonded silicon carbide matrix (S_iC), porous carbon anode cathode electrodes and platinum electrocatalyst o+ anode and cathode. The phosphoric acid electrolyte, unlike the alkaline, are more tolerant to carbon monoxide concentration of about 1.5% (which broadens the choice of fuel for use) in the hydrogen obtained from the reforming of methane. Another advantage of the phosphoric acid electrolyte is that it can be operated above the boiling point of water, a limitation on other acid electrolytes that require water for conductivity. The diagram of a typical PAFC is as shown in the figure below. They have been widely used for stationary application -field tests and demonstrations in the US and Japan, though some have been used to power city buses. According to [20], “PAFCs are more than 85% efficient when used for the co-generation of electricity and heat, but they are less efficient at generating electricity alone (37-42%) slightly more than the efficiency of fossil combustion-based power generation plants (of 33%)”. They are less sensitive to CO (to about 1.5%) compared to AFCs and PEFCs. They can operate at low to medium temperature ($150 - 220℃$), allowing the use of cheaper materials in their manufacture, and flexible design for heat management [14]. Their disadvantages are that the ORR in the cathode side of the cell is slower compared to AFCs therefore requiring the use of expensive platinum electro catalysts. They still do require expensive fuel reforming processes to achieve good performance and the highly corrosive nature of the

concentrated phosphoric acid (H_3PO_4) requires the use of expensive materials as bipolar plates [20]. Figure 1.9 shows the basic structure of the PAFC.

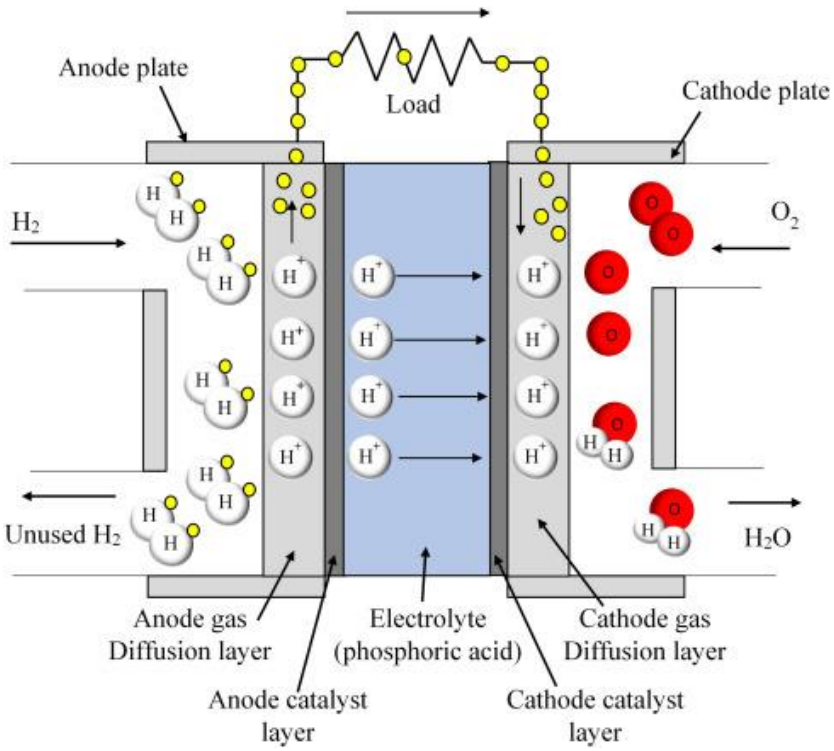

Figure 1.9 The basic structure of the PAFC [21].

Molten Carbonate Fuel Cell (MCFC)

MCFCs are high -temperature fuel cells, operating at temperatures between $600 \text{ and } 700℃$ [14,19,20]. Their electrotypes are a mixture of high temperature molten carbonate salt which is retained in a porous, chemically inert ceramic matrix of lithium aluminate or lithium aluminium oxide (L_iAlO_2). The molten carbonate salts provide ionic conduction. At high operating temperatures, they do not require noble metals as catalysts for their electrochemical reactions and most of the hydrocarbon fuels can be reformed internally reducing cost. When coupled with gas or steam

turbines, they are about 65% efficient considerably higher than the 37-42% efficiencies of PAFC plant. Where their waste heat is reused in CHP, they have an overall efficiency of 85%. However, their high temperature operation combined with the corrosive molten carbonate salts results in component wear and corrosion thereby decreasing their cell life. The basic structure of the MCFC is shown in Figure 1.10.

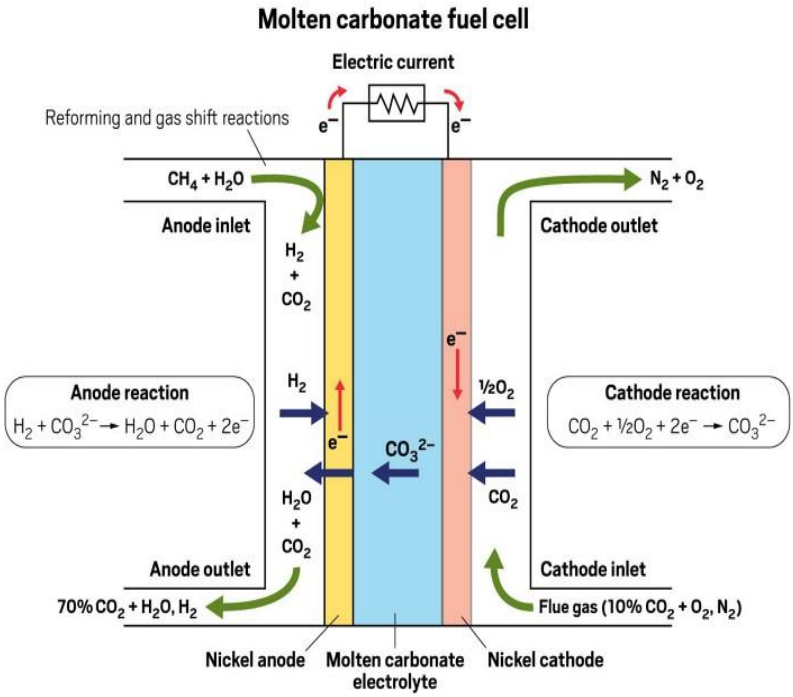

Figure 1.10 The basic structure of the MCFC.

Solid Oxide Fuel Cell (SOFC)

The SOFC was first developed by Baur and Preiss in the year 1937. They used a hard nonporous ceramic compound of metal oxides such as calcium oxide or zirconium oxides [14,19,20] They are highly efficient with about 60% efficiency in the conservation of fuel to electricity and in the use of their waste heat for co-

generation, they have an 85% fuel use efficiency. They are high temperature fuel cells with an operating temperature ranging from $800 - 1000℃$. Therefore, they can achieve high reaction rates without the use of precious metals as electro catalyst and are able to use natural gas directly or internally reform them for their use. This helps reduce manufacturing costs associated with adding a hydrocarbon fuel reformer to the cell system. They also can tolerate several orders of magnitude of sulphur and are also CO tolerant with the CO being used as fuel in the system. However, they have low and difficult start up due to their high thermal operation and very low lifetime. They are also limited in use (especially in the transport sector) because of their high temperatures, excessive large and brittle (ceramic) electrolyte. The basic structure of the SOFC is shown in Figure 1.11.

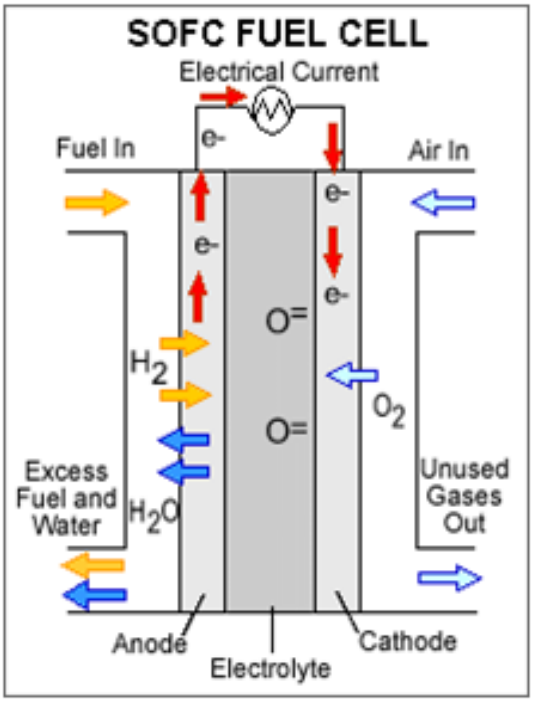

Figure 1.11 The basic structure of the Solid Oxide Fuel Cell (SOFC).

Direct Methanol Fuel Cell (DMFC)

DMFCs are a subcategory of proton exchange fuel cell in which a polymer membrane is used as their electrolytes but methanol, instead of hydrogen, is used as the fuel. They were invented in the 1990s by researchers in NASA and the US jet propulsion laboratory [22]. The anode electro catalyst is made of platinum-ruthenium which oxidises the methanol fuel while platinum catalyst is used in the cathode for the oxygen reduction reaction. The platinum-ruthenium catalyst used in the anode allows the hydrogen to be directly reformed from methanol within the fuel cell, therefore removing the need for an external fuel reformer. The methanol fuel is inexpensive and easy to transport and stored. However, there are still some drawbacks in the use or commercialization of the DMFCs. They have very low efficiency of 30%-40% and are mostly used for mobile electronic devices or chargers and portable power packs. They operate at $60℃$ to $130℃$ range of temperature [23]. Figure 1.12 shows the basic structure of the DMFC.

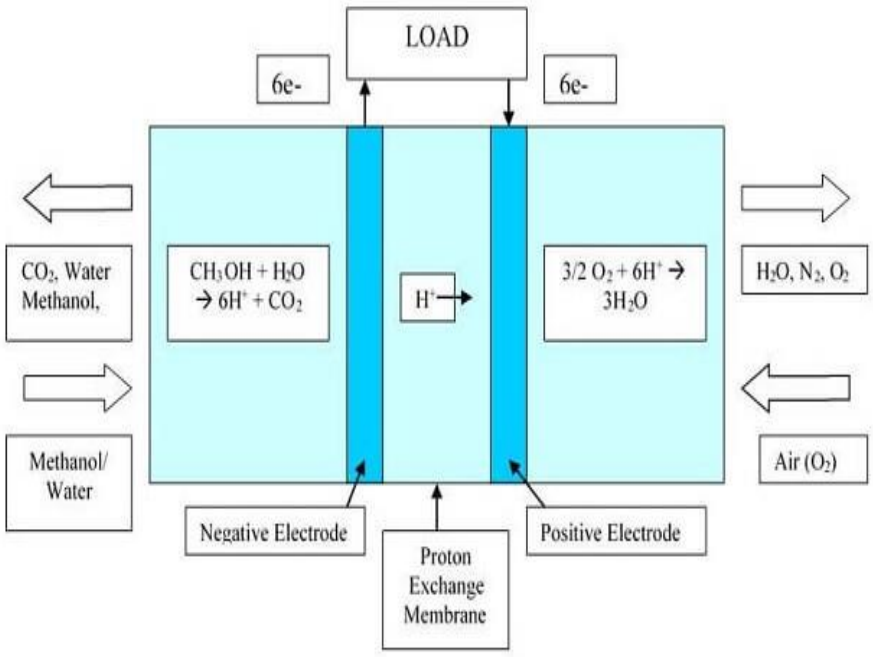

Figure 1.12 The basic structure of the DMFC [23].

1.6 PEM fuel cells

PEM fuel cells were invented and first demonstrated in the year 1960 by Thomas Grubb and Leonard Niedrach (both employees of General Electric) for the United States Navy ships. General Electric went further to develop the first PEM fuel cell that was used in the US space programs in the 1960s as a replacement for alkaline fuel cells used in space shuttles [22]. The hydrogen for the GE first invented PEM fuel cell unit was produced by mixing water and lithium hydride in disposable canisters. The solid polymer used electrolyte was an acid that allowed the use of CO_2 unlike that of alkaline fuel cells. In the late 1980s, they were employed by Perry Technologies and Ballard Power systems for powering submarines and buses, respectively. Energy Partners, 1993, first demonstrated the PEM fuel cell's automotive applicability by using it to power passenger vehicles. In the early days

of its development, the polymer electrolyte membrane or proton exchange membrane (PEM) fuel cell was generally referred to as a solid polymer electrolyte (SPE) fuel cell, due to the solid polymer membrane used as the electrolyte for the cell. They are opposites of PEM electrolysers which decomposes water into oxygen and hydrogen atoms by the passage of electric current. Instead, they produce electricity from the electrochemical reaction (oxidation, and reduction of hydrogen and oxygen respectively). PEMFCs can generate high power density. They have light/low weight and volume compared to other fuel cell types. They have a solid polymer as their electrolyte with porous carbon electrodes containing platinum as the electrocatalyst. They operate on pure hydrogen, reformed from methane [14]. Their light weight and low volume make them potential technology for mobile and portable applications as well as in automobiles [13,14]. They are widely used in transport applications, offering many advantages over fossil fuel combustion engines and other fuel cells due to their excellent dynamic characteristics, light weight, and an operational efficiency of 40%. They are also applied in small-scale stationary power generation (producing power of 5 kW at 30% efficiency) as well as for portable fuel cell applications. Their distinguishing features include the ability to operate at temperatures as low as room temperature to temperatures of 100 °C (though most PEM fuel cells operate at 80 °C), low operational pressures, between 1-5 atm, and with efficiency of about 58%. This allows them the advantage of quick start up (with less time for warm-up), components durability - as the components are not damaged by excess heat and high temperature and therefore less expensive materials are required, except for the precious platinum electrocatalyst required for the hydrogen oxidation reaction. Due to the solid polymer film used as electrolyte in the PEMFC and its low temperature operation, the challenges of sealing and liquid

circulation (commonly associated with AFCs) assembly and handling are less complex compared to the other types of fuel cells [14,15]. The major drawback for PEM fuel cell technology is its expensive platinum electro catalyst which is intolerant to carbon monoxide (CO), therefore requiring external reactor (to reduce carbon monoxide) this adds to the cost in design and operation. As the cell needs to be operated with pure hydrogen.

PEM fuel cells are primarily applied for use in the transport sector such as for cars, buses, and heavy trucks, due to their high-power densities, light weight, quick start-up, and excellent dynamic characteristics. They have been used in buses in Vancouver and Chicago by Ballard systems and have also been experimented in vehicles produced by Daimler Chrysler. They are widely used also for stationary/ distributed power generation, and for portable applications.

1.6.1 The operation of a PEM fuel cell

At the heart of the PEM fuel cell is the membrane electrode assembly (MEA) which consists of a solid proton conducting polymer membrane (electrolyte) sandwiched between negative (anode) and positive (cathode) porous electrically conductive electrodes made from either carbon cloth or carbon fibre paper [22]. Figure 1.13 shows a schematic of the MEA which consists of a platinum catalyst, supported on carbon, integrated between the membrane and the gas diffusion media. The platinum electrocatalyst helps activate and speed up the redox reactions of the fuel cell. The MEA is sandwiched between bipolar plates, also known as the flow-field plates or separator plates and houses the gas flow channels.

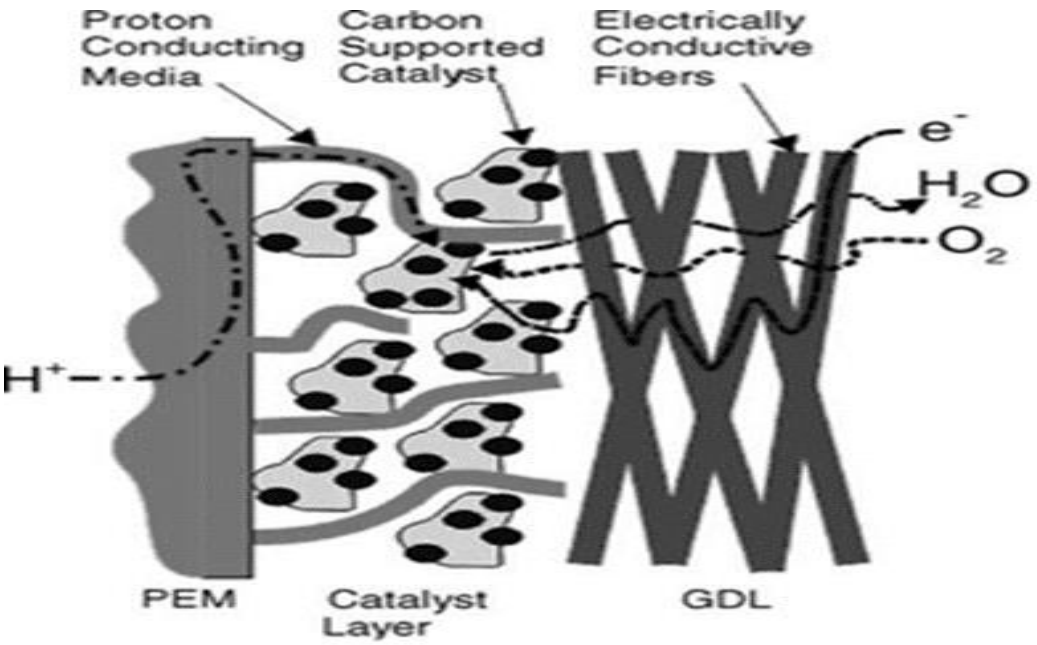

Figure 1.13 A schematic diagram of the MEA. https://commons.wikimedia.org/wiki/File:Transport_of_Gases,_p%2B_and_e-_in_PEMFC.png

PEM fuel cells, like other fuel cells and batteries, are galvanic cells and the redox reactions between the hydrogen fuel and the oxidant (oxygen) forms the basis for the conversion of chemical energy of the fuel directly into DC electricity. Generally, for any chemical reaction to occur the reactants need to be in direct contact, so electrons can be exchanged, and bonds formed. This would require the anode and the cathode of the PEM fuel cell to be in direct contact for the redox reaction between the hydrogen and oxygen to take place. The result of this arrangement is the production of heat without any useful work (power generation) as the electrons would pass directly between the anode and the cathode. Hence, to generate useful electricity (which is the main purpose of the PEM fuel cell), the anode and cathode must be separated by placing an electrolyte between them. This electrolyte is electrically non-conductive, impermeable to gases but are ionically conductive-allowing the transport of protons to the cathode catalyst site. The electrons then

must travel from the anode through the anode current collector to an external circuit – thereby producing electric current- before travelling to the cathode catalyst sites to complete the reaction. The electrochemical reactions in the anode and cathode are two halves of a spontaneous redox reaction that occur simultaneously at the surface of the platinum catalyst of each electrode. In the anode catalyst sites, hydrogen which is fed into the cell from the flow inlets through the gas flow field channels etched on the bipolar plates travels by convection to the porous gas diffusion layer and is diffused into the catalyst sites. At the catalyst sites, hydrogen is catalytically spilt into protons and electrons. The HOR is represented as:

$$H_2 \rightarrow 2H^+ + 2e^- \quad \textbf{(1.7)}$$

The protons travel through the membrane while the electrons travel from the external circuit to the cathode catalyst sites where oxygen has been delivered through the same process of convection and diffusion. The oxygen molecules combine with the protons and electrons (gaining electrons-reduction) to form water molecules. This oxygen reduction reaction (ORR) in the cathode is represented as:

$$½O_2 + 2H^+ + 2e^- \rightarrow H_2O \quad \textbf{(1.8)}$$

The overall redox reaction is represented as follows:

$$½O_2 + H_2 \rightarrow H_2O \quad \textbf{(1.9)}$$

A schematic of the PEM fuel cell with its operation principle is as shown in Figure 1.14.

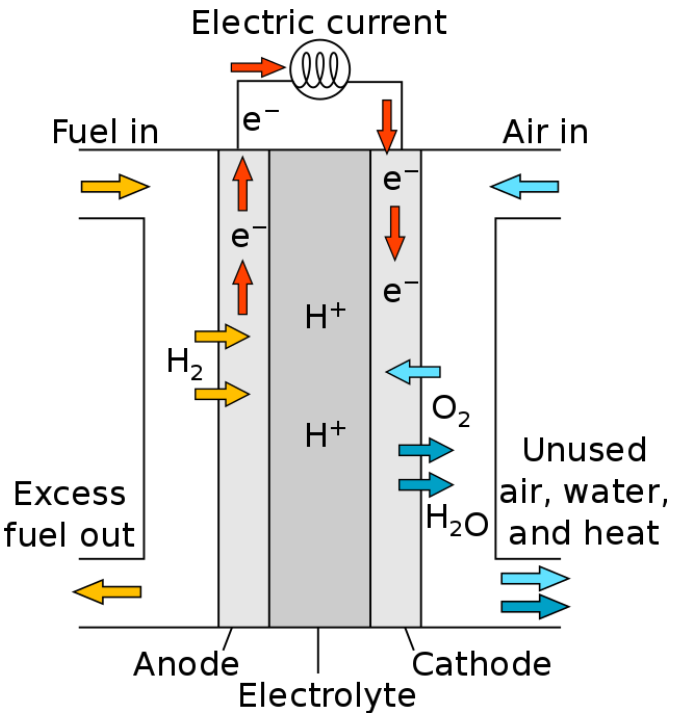

Figure 1.14 The basic principle of operation of a PEM fuel cell.

1.6.2 Polymer electrolytes

The solid polymer electrolyte is what distinguishes the PEM fuel cell from other fuel cells. It is a thin membrane of plastic-like film that is typically made of perfluorocarbon-sulfonic acid ionomer (PFSA) which is a copolymer of tetrafluoroethylene (TFE) and various perflourosulfonate monomers. They conduct the hydrogen proton from the anode catalyst layer to the cathode catalyst layer (while repelling the electrons) and as well separates the reactant gases in the PEM fuel cell. They are produced generally using sulphonated fluoro-polymers-fluoroethylenes (Nafion by Dupont) [22]. The fluoroethylene polymer is basically made from the modification or polymerisation of polyethylene, of which the molecular structure is based in ethylene. This process, known as perflourination, involves the substitution of the hydrogen molecules with fluorine which results in the

formation of a modified/polymerised material called PTFE and sold as Teflon [14,22]. Proton transport in the PEM fuel cell takes place within the membrane via ionic groups of the polymer structure and depends largely on the organic bonds of the groups (the polymer structure and hydrogen) as well as the vapour water molecules in the membrane. Polymer electrolyte membranes, because of their acidic nature, require the presence of water molecules to transport the hydrogen ions to the cathode reaction site, as the hydrogen ions must be coupled with these water molecules during the ion exchange transport. The hydrogen proton moves through the hydrogen bonding (H-bonding) networks which exists between the hydronium ion and water, in which proton transfer and sequential molecular rotation occur simultaneously. The protons get attached to and move from one water molecule to the next via the hydrogen-bonds. This mechanism (Grothuss mechanism) facilitate the mobility of the hydrogen proton within the electrolyte of the fuel cell. Hence the reactant gases need to be humidified for optimum membrane ionic conductivity. The membranes are designed so that the polymer tubes are partly hydrophilic and hydrophobic as the same time. The sulfonic acids groups on the inner part of the of the tubes make the inner part of the tubes hydrophilic hence allowing for effective ionic conductivity while the outer parts are hydrophobic due to the fluorinated materials there. Membranes are ionically conductive and are electrically non-conductive as well as impermeable to gases, and with low equivalent weight (weight of polymer relative to the number of available acid sites). They are durable and resistant to chemical attack and do not react to the reactant gases. The PTFE polymer membrane is thermally and chemically stable owing to its PTFE backbone. Typical polymer electrolyte membranes are characterised by their equivalent weight which is inversely proportional to the ion exchange capacity.

Typical values are between 800 to 1150 milliequivalents per dry gram of polymer [22]. Several types of membranes are commercially manufactured and marketed by various dealers. Nafion, the most used polymer electrolyte membrane, is manufactured by Dupont and others by Dow chemical company. GORE-SELECT® Membranes are manufactured by GORE technologies, and Celtec® membranes are developed by BASF. Ballard Power Systems, a PEM fuel cell manufacturing company, have been developing their own proprietary polymer membranes as well.

1.6.3 Catalyst layers

The anode and cathode catalyst layers form the heart of the Membrane electrode assembly, MEA [20]. They are the functional and critical components of the MEA, producing high intrinsic activities for the PEM fuel cell. Basically, they provide surface area for the reactions to take place. The catalyst layers facilitate the HOR in the anode as well as the ORR in the cathode. They provide the sites for the redox reaction to occur simultaneous without being consumed in the process. They are typically made of platinum due to its high electro-catalyst activity, stability, and electrical conductivity. They lie in contact (on both sides) with the electrolyte membrane and the gas diffusion media. The catalyst layer is also referred to as the triple phase boundary as it comprises the ionomer (the electrolyte), the solid phase- carbon particles that conducts the electrons to and from the catalyst sites and provides supports to the electro catalysts, the liquid or dissolved water phase- which helps conduct the hydrogen protons within the electrolytes membrane and keeps the membrane hydrated, and then the void region or pores for reactant and liquid water transport. Figure 1.15 shows the structure of a typical catalyst layer. The catalyst is applied in two ways, either on the electrolyte membrane (catalyst coated

membrane) or in the carbon gas diffusion medium or porous transport layer and then bounded to the membrane to form the MEA. The platinum used as electro catalyst for the PEM fuel cell is very rare and expensive, therefore contributing to the drawbacks in PEM fuel cells being commercially viable. However, catalyst developers have developed other ways of solving this challenge by using platinum nanoparticles (with reduced loadings of 0.2-0.4 mg/cm^2) supported on carbon powders such as VULCAN XC72R, providing more surface area for reactions. Also, the catalyst is designed to be rough and porous to allow for maximum surface areas of the platinum loading to be in contact with the reactant gases.

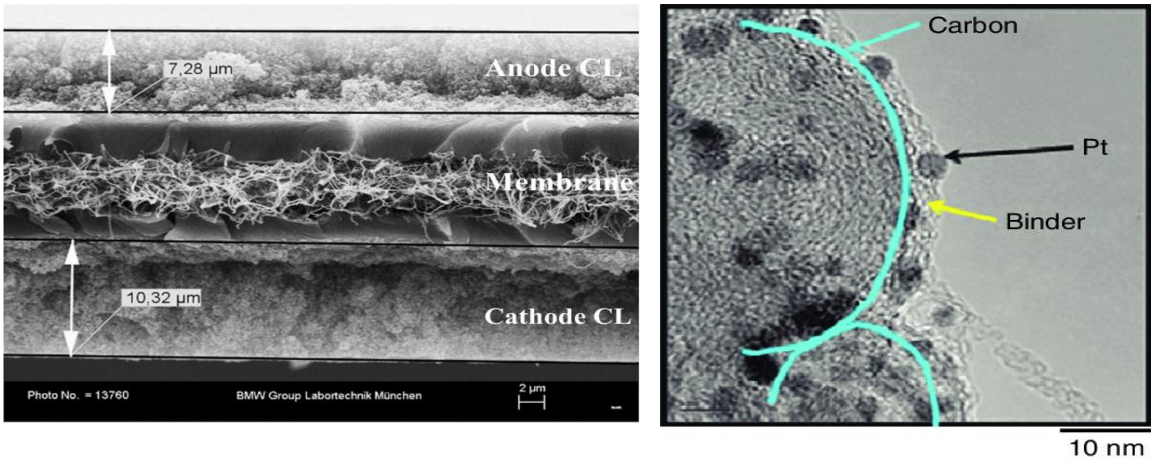

(a) **(b)**

Figure 1.15 Structure of the catalyst layer (a) SEM-micrograph of the catalyst coated membrane; (b) TEM-micrograph of the carbon support with dispersed catalyst agglomerates and binder [22].

1.6.4 Bipolar plates and channel configuration

The bipolar plates (BPP) are made from graphite, and they house the gas channels which transport the reactant gases from the inlet manifolds of the PEM fuel cell to the MEA [22]. They are good conductors of electrons and heat and are chemically

stable and are not easily poisoned. They provide mechanical strength to the PEM fuel cell and allow for the gas flow channels to be engraved. According to [16] the gas flow fields can be machined on either side of the plates forming anode and cathode plates in either side hence the term bipolar plate. In the fuel cell stack, they connect series of PEM fuel cell stacks together, as shown in figure 1.6. The bipolar plates electrically connect the anode of one cell to the cathode of the adjacent cell. They are also known as separator plates. They function to:

- Electrically connect each fuel cell in series in the fuel cell stack.
- Separate the gases in adjacent cell components (i.e., anode of once cell and cathode of the adjacent cell in the fuel cell stack) from mixing. Hence, the bipolar plates must be impermeable to the reactant gases.
- They provide mechanical support and strength hence, they must lightweight.
- They help conduct heat away from the MEA and PEM fuel cells.

The flow field or configuration of the channels within the bipolar plates provide uniform and adequate supply of the gas reactants to the membrane electrode assembly/ gas diffusion layers while minimizing pressure drop. There are basically three types of channel configurations in the design of the bipolar plates of PEM fuel cells namely, the parallel, serpentine, and interdigitated flow field designs/channel configurations. The parallel flow field design of the gas channel allows for uniform distribution of the gas reactants and requires less mass flow per channel with less pressure drop. However, the drawback in this design is that for continuous operations, liquid water accumulates the channels and leads to blockage so that the velocity of flow is insufficient to push the water out. Also, the amount of water in each channels varies leading to uneven distribution of the gas reactants. Owing to

its short channel designs, the pressure drop in the stack becomes higher. The single-pass serpentine channel configuration is the most used channel configuration. Patented and mostly used by Ballard system. It has continuous gas flow path from the beginning of the inlet manifold to the outlet manifold and ensures gas distribution across the entire active surface of the fuel cell. Though pressure drops, due to wall friction and lengthy channel turns, the velocity of flow is sufficient to push out liquid water in the channel therefore freeing the other channels from obstruction. The only disadvantage of this design is that the gas reactants are depleted along the channels, hence an adequate or high amount of the gas needs to be supplied. The multi-pass or parallel serpentine flow field is a compromise between the parallel flow field and the serpentine flow field which is patented by General Motors [16]. This design consists of a multitude of parallel channels meandering through the entire bipolar plate in the form of a serpentine configuration. It lowers pressure drop which could have resulted in large energy losses. However, there is a possibility of one of the channels being blocked thereby hindering the flow of gas reactants. It integrates a cooling mechanism within the bipolar plates. Interdigitated flow fields have discontinued channels, unlike the serpentine flow field designs, they do not connect the inlets to the outlet manifolds. The gas reactants travel in a direction parallel to the active surface for the interdigitated flow field configuration. The channels are dead ended forcing flow of gases, under pressure, through the porous gas diffusion layer to the flow channels connected to the stack manifolds. It prevents flooding and enhances PEM fuel cell performance, promotes forced correction which helps avoid/minimize gas diffusion limitations. However, they also result to high pressure drops between the inlet and the outlets, compared

to other flow field patterns. The different gas channel configurations described above are shown in Figure 1.16.

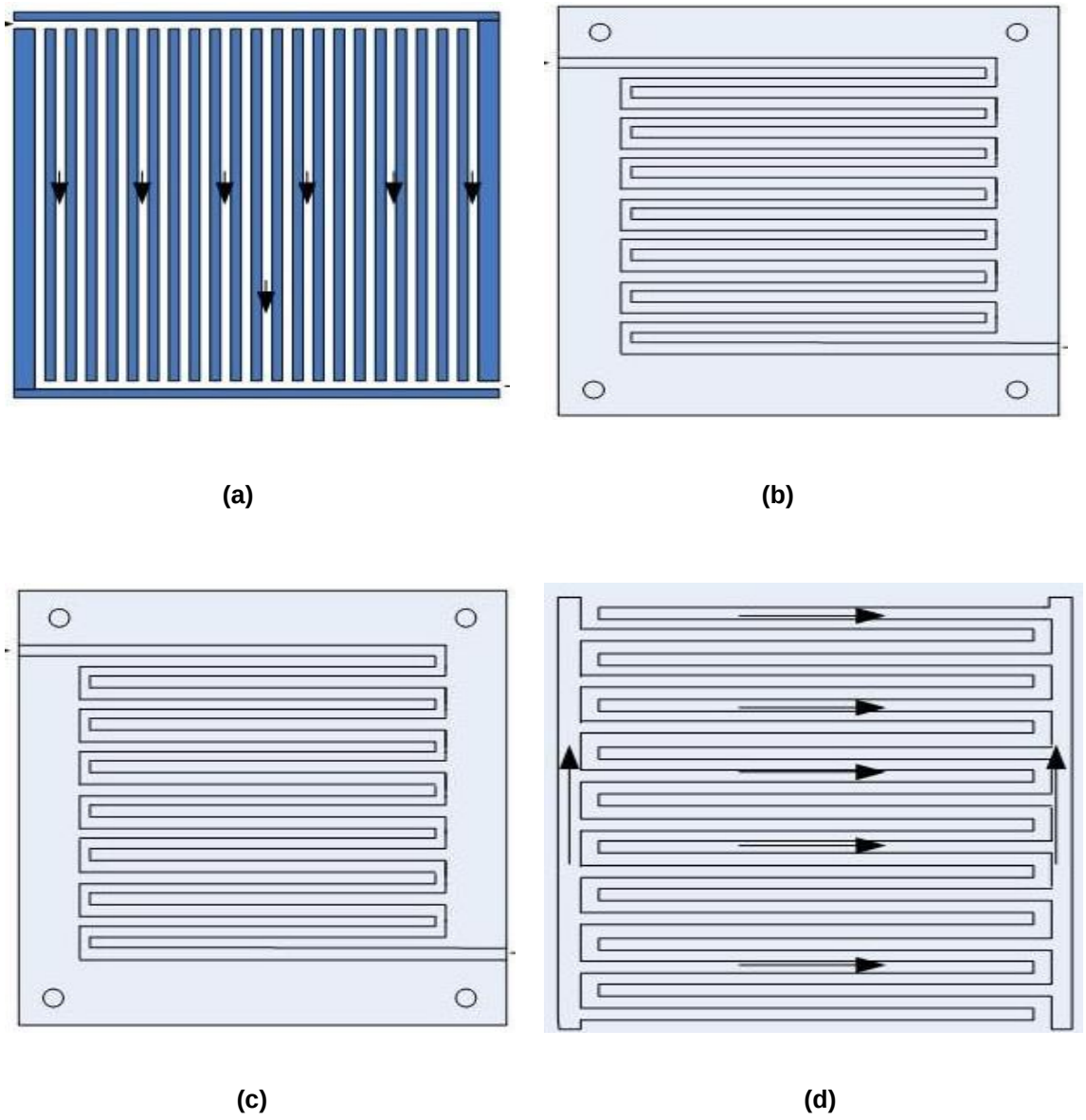

Figure 1.16 Schematics for (a) parallel, (b) single-pass serpentine, (c) multi-pass serpentine, and (d) interdigitated channel configurations [25].

1.6.5 Endplates and sealing gaskets.

- A complete PEM fuel cell stack is designed with bipolar plates and endplates (also known as clamp plates) which lie in parallel to each other. The

endplates are supplied in the fuel cell stack to apply the needed contact pressure on the PEM fuel cell components – the MEA and the bipolar plates to prevent the gas reactants from escaping and to minimise the contact resistance between the PEM fuel cell components [23]. They are also designed with holes, as shown in Figure 1.6, to fasten the tie-rods and bolts as well as for the inlet and outlet manifolds. Endplates must have high mechanical strength and stability to support the fuel cell stack and distribute the compression pressure uniformly to all the major surfaces of each PEM fuel cell in the fuel cell stack [23]. Hence the endplates must have the following characteristic properties:

- High compressive and mechanical strength
- Sufficient stability
- High tolerance and thermal stability as well as
- Shock and vibration resistance

The gas sealing gaskets provide the compressive pressure necessary to prevent potential reactant gases from leaking. The thickness of the sealing gaskets is of major importance as it determines how much the flow fields are allowed to pinch into the electrodes. This helps minimise the contact resistance between the gas diffusion layer and the bipolar plate. The gaskets used in PEM fuel cells must have the following properties:

- Long term chemical stability
- Sufficient strength to prevent reactant gases from mixing with one another and prevent the gases from leaking out.

- Ability to withstand shock and vibrations
- Electrically insulating
- Thermal stability and
- Excellent sealing capabilities

1.6.6 Gas diffusion media

The gas diffusion media (GDM) consists of the macroporous carbon substrate, which is generally made of carbon fibre paper, and a carbon particle-based teflonated microporous layer (MPL) [26]. The GDM is responsible for the transport of gas reactants to the active sites of the catalyst layers. It provides the electrical contact between the catalyst layer and the flow field plates for transport of electrons as well as mechanical support to the catalyst layer. It is also responsible for heat and liquid water removal from the MEA. They are distinct from the gas diffusion electrodes (GDEs) of which the catalyst is coated on the gas diffusion media and then bonded with the membrane to form the MEA [26].

The main functions are as follows:

- To provide the pathway for the reactants gases to flow from the gas channels to the catalyst layers.
- To remove the liquid water produced for the reactions in the catalyst layer to the flow field channels. To prevent flooding in the cell and allow reactant to get to reactive sites for the smooth operation of the cell.

- To keep water (in vapour) in the surface of the membrane for effective ionic conductivity.
- To electrically connect the catalyst layer to the bipolar plates so that the electrons can flow effectively.
- To conduct the heat produced from the reactions in the catalyst layer to the bipolar plates.
- To provide the mechanical strength to hold the MEA and prevent it from sagging due to water absorbance.

Therefore, they must have the following properties:

- Have enough porosity to allow for reactant transport to the reactive sites and liquid water removal from the catalyst layers.
- Have good thermal and electrical conductivity.
- Have good mechanical strength together with some flexibility to allow for good electrical contacts.

Since the topic of the thesis is about the GDLs, Section 2.1 has been entirely allocated to describing in detail the gas diffusion media and its roles in the transport of quantities within the PEM fuel cell.

1.7 Motivation and research objectives

Numerical modelling is considered an effective and reliable alternative to expensive and time-consuming experiments [27]. Unlike the case of experiments, a wide range of real-life cases, innovative designs, and novel materials could be investigated using numerical models [28]. However, it is observed in the literature that majority

of the numerical models of PEM fuel cells do not fully capture the anisotropic nature of the gas diffusion layers, neglecting the multidimensional effects of the anisotropy of the GDL on the transport of mass, heat, and charge through the MEA of the PEM fuel cell; these multi-dimensional effects are caused by the fact that the carbon fibres are preferentially oriented in the in-plane direction. Though the literature also shows that there have been some attempts to investigate the impact of the anisotropic GDL on the performance of the numerically modelled PEMFCs, as seen done by [27-33] to mention but a few, there have been no three-dimensional numerical PEMFC models that incorporates experimentally measured multidimensional values of each of the gas diffusivity, the gas permeability, the thermal conductivity, and the electrical conductivity of the GDLs.

In regard to the above, the first objective of this thesis is to numerically investigate the effect of not capturing the GDL anisotropy for each of the above-mentioned transport properties on the performance of the modelled PEMFC and how this impacts on the distribution of the key variables of current density and oxygen concentration within the GDL, providing useful insights on how to improve the efficiency of the PEMFC To meet this objective, realistic experimentally characterised transport properties of the GDL (the gas permeability, gas diffusivity, thermal conductivity, and electrical conductivity) are employed in the three-dimensional CFD modelling of the PEM fuel cell using the commercial ANSYS Fluent software.

Conventional GDLs used in PEM fuel cells are generally treated with PTFE and coated with a thin microporous layer (MPL) at the interface between the GDL and the catalyst layer. While the PTFE treatment increases the hydrophobicity of the GDL, the MPL helps remove excess liquid water from the MEA and reduce the

contact resistance between the GDL and the catalyst layer in the PEM fuel cell structure. The MPL is discussed in further details in **Chapter 2** of the thesis. Virtually, no extensive investigations have been reported in the literature on the effects of double side MPL-coated GDLs on the performance of the PEM fuel cell, where the conventionally applied MPL is facing the catalyst layer and the other proposed MPL is facing the bipolar plate. This could be of great importance as much of the contact resistance lies in the GDL and bipolar plate interface (especially where the catalyst layer is deposited on the gas diffusion media instead of the electrolyte membrane). Also, there is not much literature on the investigation of novel designs of the GDL/MPL structure with graded porosity. Therefore, the other objective of this thesis is to numerically investigate such effects of double side MPL-coated GDLs and graded porosity distributions in the cathode GDL and cathode MPL on the overall performance of the PEM fuel cell. A summary of the objectives of the thesis are presented as follows:

- To numerically investigate the effect of the GDL anisotropy on the overall fuel cell performance as well as the local distribution of oxygen and current density in the cathode gas diffusion layer of the PEM fuel cell.
- To numerically investigate the effect of the contact resistance between the PEM fuel cell components on the overall fuel cell performance and the distribution of the key variables within the cathode GDL.
- To numerically investigate the effect of the double side MPL-coated GDLs on the overall performance of the fuel cell and the distribution of the key variables within the GDL.

- To numerically investigate the effect of graded porosity of the cathode GDL and cathode MPL on the overall performance of the fuel cell and the distribution of the key variables within the GDL.

1.8 Structure of the thesis

The thesis is divided into 7 chapters. **Chapter 1** describes the transition from fossil fuels combustion technologies to renewables and hydrogen technology as a clean and sustainable alternative for energy generation. Section 1.3 describes the basic principles of fuel cells as well as the fuel cell systems. The advantages, limitations, types, and applications of the fuel cells are discussed in Sections 1.4 and 1.5. The polymer electrolyte membrane (PEM) fuel cell, its major components, and the gas diffusion media is presented in Section 1.6. This chapter is concluded by describing the motivation, the objectives, and the structure of the thesis.

In **Chapter 2** of the thesis, a theoretical background of the gas diffusion media used in PEM fuel cells is given in Section 2.1. The section details the roles, the treatments, properties, and manufacturing processes of the gas diffusion layers and the MPLs. In Section 2.2 of the chapter, the role of the gas diffusion media in the transport of mass, heat, and charge within the PEM fuel cells is presented. Section 2.5 describes the anisotropic transport properties of the gas diffusion layer and the characterisation (numerical and experimental) of the gas diffusion layer transport properties.

For the ‘technical’ chapters, **Chapters 3-6**, each chapter starts with an introduction which also states the motivation for the study, a literature review, the gaps in

knowledge, and the objectives of the investigation for each of the chapters. This is then followed by Section 3.2 which describes the model development and the transport equations for the model as well as the assumption for the model formulation. The third section presents and discusses the results, and the final section summarises the main findings of the study. This process has been implemented to maintain the fluency of the thesis and avoid the distraction that may result from referring to separate 'literature review' and 'methodology' chapters. The below is a summary of the content of each of the above chapters.

Chapter 3 discusses the transport of multicomponent gas species in the gas diffusion electrodes. Section 3.3.1 examines the effect of the anisotropic gas permeability of gas diffusion layers on the transport of reactant gases in the cathode gas diffusion electrode using ANSYS Fluent®. Section 3.3.2 discusses the sensitivity of the multicomponent gas reactant transport, in the cathode electrode, to the gas diffusivity and diffusivity ratio.

In **Chapter 4**, Section 4.3.1 shows the result of the comparison, of the performance of the PEM fuel cell model with the anisotropic GDL transport properties with those of the PEM fuel cell model having isotropic GDL transport properties. Sections 4.3.2 to 4.3.5 discuss the sensitivity of the PEFC performance to the anisotropic key transport properties of the GDL (the gas permeability, mass diffusivity, thermal conductivity, and electrical conductivity). Section 4.4 discusses the conclusions of the findings of the study.

The impact of double side coating of the gas diffusion layer as well as the effect of the interfacial contact resistance at the GDL-BPP and MPL-CL interfaces is numerically investigated in **Chapter 5**. In this chapter, the impacts of the interfacial

contact resistances between the GDLs and the bipolar plates as well as that between the MPLs and the catalyst layers are assessed in Sections 5.3.1 to 5.3.3. Section 5.3.4 compares the effects of a microporous layer (MPL), with property values for the carbon substrate (GDL), with that having distinct MPL properties. The sensitivity of the PEM fuel cell model to double side MPL-coated gas diffusion layers is evaluated and discussed in Section 5.4.

In **Chapter 6**, the sensitivity of the overall performance of the fuel cell and the local distribution of the key variables within the gas diffusion layer to the graded properties of the microporous layer (MPL) is numerically investigated and discussed.

Chapter 7 concludes of all the major results of the technical chapters of the thesis and discusses the recommendations for possible future work.

2 THEORETICAL BACKGROUND

This chapter details the theoretical background on the characteristics of the materials being investigated, namely the gas diffusion layers and the microporous layer, and the equations governing the transport of mass, heat, and electric charge, in PEM fuel cells. In addition, the platform used to discretise these governing equations, i.e., CFD, are reported.

2.1 Gas Diffusion Media

The gas diffusion media (GDM) are one of the most important components of the polymer electrolyte fuel cell. The GDM comprises of the carbon-based gas diffusion layer, which is conventionally made of carbon fibre paper or woven carbon cloth and is generally referred to as the microporous substrate (MPS) or simply carbon substrate, and a thin layer of carbon (Teflon-based carbon nanoparticles), which is coated on the side of the macroporous substrate that faces or is in contact with the catalyst layer (CL) [26]. The GDM provides mechanical strength and integrity to the membrane electrode assembly (MEA) as well as being responsible for the transfer of mass (reactant gases), heat and charge within the MEA (and between MEA and the gas flow field) during operation of the PEM fuel cell. A good understanding of the role the gas diffusion media plays in the operation of the PEM fuel cell, as well as its optimum design for better/ higher efficiency in the transport of gas reactants and the liquid water (and heat) removal/management is imperative for improved PEM fuel cell performance. The role of the GDM is for the effective transport of gas reactants to the reactive sites in the catalyst, electronic and thermal conductivity, and water management in the PEM fuel cell. This depends on several properties, such as the pore size distribution, thickness of the MPS and the microporous layer,

the PTFE treatment of both the MPS and the microporous layer, and the carbonisation and graphitisation of the gas diffusion media [24,34]. Therefore, the gas diffusion media must have high porosity and adequate pore volume to allow for the effective transfer of reactant gases to the active sites of the electro catalysts, as well as the proper management of the water within the MEA. At the same time, it provides sufficient conductivity for the transport of heat and electrons. Figure 2.1 shows the schematic of the PEM fuel cell showing the gas diffusion media.

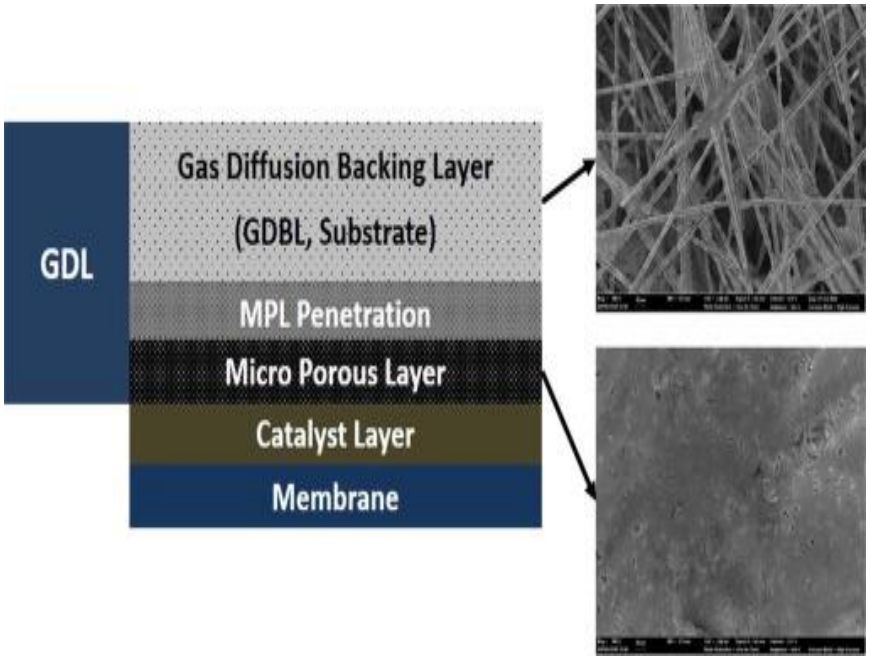

Figure 2.1 Schematic diagram of the PEM fuel cell showing the gas diffusion media [37].

2.1.1 Gas diffusion layers

The GDL is an important component of the MEA of the PEM fuel cell. It is a thin, porous material, which is situated between the bipolar plates and the catalyst layer of the PEM fuel cell. The GDL, together with the MPL, provides mechanical/ physical support to the catalyst layer and the membrane electrode assembly [36]. The GDL or the macroporous (carbon) substrates is impregnated with PTFE to increase its

contact angle to the water and increase the hydrophobicity of the GDL and have a thickness in the range of 100 to 300 mm [37]. The gas diffusion layer is generally made of a void phase as well as a solid phase. The void regions/pore spaces of the GDL allow for the free diffusion and effective transfer of the gas reactants from the gas channels to the reactive sites of the electro catalyst, and for the effective removal of dissolved and liquid water from the membrane electrode assembly to the gas channels. Its porous structure and void regions provide the pathway for the diffusion of gas reactant species from the gas channels to the catalyst active sites for the electrochemical reactions and for the removal of liquid water by-product (resulting from the ORR in the cathode catalyst layer) from the MEA to the gas channels in the flow field plates. The solid phase of the GDL serves as a thermal conductor that conducts the waste heat from the reactions in the electrodes, from the MEA to the bipolar plate. It also provides the pathway for the electrons to flow from the anode catalyst layer to the anode bipolar plate and from the cathode bipolar plate to the cathode catalyst layer for the Oxygen reduction reaction (ORR) to occur [26]. In addition to these functionalities, the GDL provides mechanical support to the MEA structure [1]. Conventional GDLs are made from carbon fibre materials (which could be woven carbon cloth, carbon fibre paper, carbon felt or carbon foam), because of the stability of the carbon allotropes in acidic environments – they are tolerant to the acid electrolytes. In addition, the carbon material has high gas permeability, thermal conductivity and electrical conductivity and high pore volume to allow for effective gas reactant transport and removal of liquid water. These conventional carbon-fibre based GDLs are treated with PTFE to increase their hydrophobicity. The PTFE affects the structure of the GDL (this effect is explained in detail in Section 2.5). The importance of the role of the gas diffusion layers in the

operations of PEM fuel cells requires numerous GDL parameters to be understood and their functioning effectively controlled. According to [37], the gas diffusion layers facilitates the management of heat and water in the membrane electrode assembly (MEA) by allowing the diffusion of water vapour/vapour phase water into the triple phase boundary consisting of the platinum catalyst agglomerate and the and the electrolyte membrane (for transport of the hydrogen proton and effective membrane ionic conductivity) & humidification. It also facilitates the removal of liquid/ dissolved by-product water from the oxygen reduction reaction in the cathode catalyst layer, preventing the flooding of the membrane electrode assembly. Therefore, as an ideal gas diffusion layer then it must offer the following properties: a superior gas and water vapour diffusion with optimum bending stiffness, sufficient porosity, surface contact angle, sufficient hydrophobicity and hydrophilicity, gas and hydraulic permeability, corrosion resistance, sufficient rigidity to mechanically support the MEA as well as some flexibility for good electrical contact with the catalyst layers and bipolar plates. Any weak spot in the design and architecture would adversely impact its functionality as well as the overall performance of the fuel cell [36]. Therefore, there are various ongoing research and investigations aimed at improving the design of PEMFC gas diffusion layers and control its properties for improved PEM fuel cell performance.

2.1.2 Materials and Types of gas diffusion layers

An ideal gas diffusion layer is required to fulfil the following requirements: effective transport of mass (gas reactants) within the PEM fuel cell, effective management of heat and water transport, and the transport of electrons from the anode side of the PEM fuel cell to the cathode reactive sites. In addition, the GDL is required to provide mechanical support to the MEA, provide high thermal and chemical resistance as

well as excellent stability and durability. Scientists have in the last two decades, experimented using carbon-based materials (carbon paper, woven carbon cloth, carbon foam & carbon felt) and metal-based materials (such as metal mesh, metal foam and micro-machined metals) as gas diffusion layers. Metal-based materials such as stainless-steel fibre felts, titanium, metal foams and micromachined metal substrates have been experimented as gas diffusion materials, due to the excellent electrical and thermal conductivity, mechanical strength, plasticity, durability, low cost and engineered uniform pore structure (by perforation, micro machining, or the use of metal forms) [38]. For example, [39] performed series of experimental tests in the cold start operation of PEM fuel cell with nickel metal foam used as the cathode gas diffusion layer. They reported higher maximum net power density and limiting current density compared to that of conventional gas flow fields. This was attributed to the highly porous structure of the nickel metal foam together with the uniform directional mass and heat transport within their GDL. Moradizadeh et al. [40] fabricated and characterised the transport properties of a nickel mesh- based double-layer gas diffusion material containing graphene oxide (rGO). The various steps taken for the fabricated nickel meshed GDL with rGO and the SEM images after various coatings are shown in Figure 2.2.

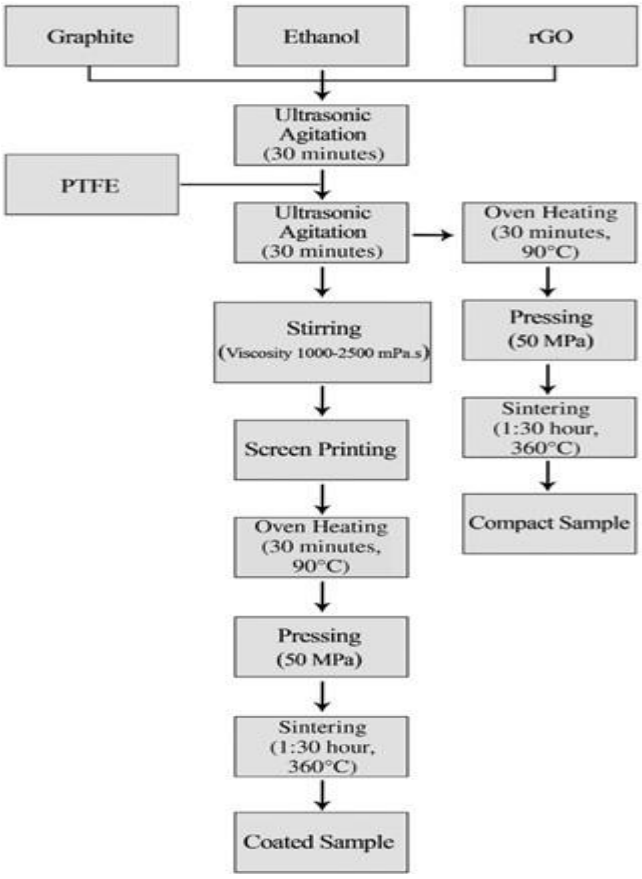

(a)

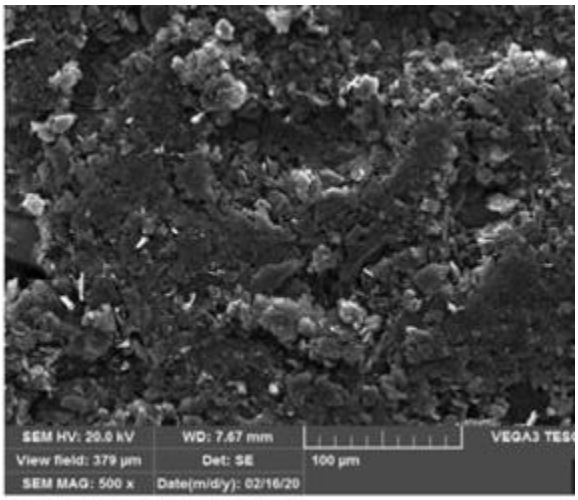

(b)

Figure 2.2 showing (a) step taken in the preparation of coated and compact samples (b) Surface SEM images of the coated sample with nickel mesh after four rounds of coating by [40].

They combined the graphene oxide with graphite to form the gas diffusion media. Then this fabricated material was treated with a PTFE, and this was made into a slurry with a suitable viscosity. They reported that the graphene oxide improved the permeability, diffusivity, and thermal conductivity of the nickel- based mesh GDL but resulted in a reduced electrical conductivity. While the PTFE only improved the contact angle and the GDL roughness. According to their report, the novel fabricated nickel mesh GDL performed better than the conventional Toray carbon paper GDL. Tanaka et al. [41] numerically and experimentally investigated the performance of a PEM fuel cell with a perforated metal sheet gas diffusion layer, which incorporated a conventional carbon-based microporous layer. They claimed an improvement in the performance of the PEM fuel cell model (with the perforated metal sheet GDL) when compared with that of the conventional carbon-based gas diffusion materials. Yi et al. [39] fabricated and characterised a gas diffusion layer made of sintered stainless-steel fibre felt (SSSFF), coated with amorphous carbon(a-C) film to enhance the corrosion resistance of the stainless steel GDL material as well as reduce the contact resistance when it was used with stainless steel bipolar plates in the PEM fuel cell. They compared the results of the PEM fuel cell performance using the sintered stainless-steel fibre felt to that of Toray TGP-H-060 carbon paper and reported their fabricated gas diffusion material to have similar morphological features, porosity, pore volume, and fibre diameter as that of the Toray paper but with higher compressive modulus, tensile strength, and ductility under compression. Zhang et al. [42] developed a micro-machined metal based GDL using thick copper foil with improved thermal and electrical conductivities, as well as controlled porosity. The GDL was micro- machined with straight pores allowing for proper water management at low flow rates, though the material had to be enhanced using

a carbon-based microporous layer with enhanced in-plane transport properties. Choi et al. [43] fabricated and compared the performance of Titanium foam (Ti) as the gas diffusion material with that of the Toray TGP-H-060 gas diffusion layer. They reported an improvement in performance of about 166% for the average output current density. In addition, they reported a superior performance of their fabricated GDL when compared to the SGL 35BC gas diffusion material. Several other investigations with different metal-based GDL materials such as titanium, copper, and aluminium [44-48] have reported an increase in the output power density of the PEM fuel cell by 40% and 32% for copper-based and aluminium, respectively, due to the decrease in electrical resistance with increased thermal conductivity. The model also reported an increase in the liquid water saturation due to uniform temperature distribution. Despite these reported breakthroughs with metal-based gas diffusion layer materials, there still exists some drawbacks, such as corrosion of the metals, which results in the degradation of the GDL and the PEM fuel cell. Hence, making carbon-based materials the most in demand for the use as the gas diffusion layers in PEM fuel cells. These carbon-based GDLs are still widely employed in the operation of PEM fuel cells due to their high gas permeability, high chemical stability, high electrical and thermal conductivities, and controllable pore structure. They are efficient and provide excellent characteristics in gas and heat (and water) transport during the PEM fuel cell operation. Several carbon- based gas diffusion materials exist in use and their distinction depends on their microstructural characteristic. These carbon- based gas diffusion layers vary in their manufacturing processes as well as the material used in their fabrication, their densities and thickness as well the output power density [36]. Based on these microstructural characteristics of the carbon-based gas diffusion layer, they are generally classified

into four groups, namely: carbon felts, carbon woven cloths, carbon fibre paper and carbon foams. The carbon felt gas diffusion layer material provides high surface area and high porosity as well as mechanical stability at low cost. They have randomly curved carbon fibres [37] The carbon fibre cloth GDL is made of woven carbon cloth fibres, with uniform microstructure [36,37]. Figure 2.3 shows the micrographs of carbon paper (Figure 2.3a) and carbon cloth GDLs where Figure 2.3b represents the SEM image and the woven structure of the typical carbon fibre cloth GDL used in PEM fuel cells. These GDLs provide excellent water removal properties at high relative humidity, as compared to the carbon fibre paper GDLs, due to their smaller tortuous path and rougher back surfaces with allows the water droplets to detach from the surfaces. However, they are more expensive to manufacture because of the high amounts of precious carbon fibre required [26]. In addition, the carbon cloth gas diffusion layers are less resistant to corrosion [36,37] due to their relatively low temperature heat treatment. The carbon fibre paper gas diffusion layers are typically a composite of carbon fibres, which are held together by a carbon binder [37]. They exhibit more or higher tortuosity and smoother surfaces which is a drawback as it allows for the retention and stagnation of water in the cathode side of the membrane electrode assembly. A micrograph of the carbon paper GDL is shown on Figure 2.3a. They are widely used as gas diffusion layer materials, and this is because they are less expensive to manufacture. Their higher tortuosity makes them most suitable for partially humidified PEM fuel cells at intermediate current densities. They are the most and conventionally used type of GDLs for PEM fuel cell operations especially at low relative humidity. In addition, carbon foams have also been reported to show some good performance when used as GDLs [37]. High electron conductivity in the PEM fuel with carbon foam GDL has

been reported [37], but the overall cell performance has been low generally. Carbon cloth (woven carbon fibre fabric) and in general, carbon fibre paper is used as GDL materials due to their high electrical conductivity, high porosity of 70-80%. In addition, they are non-corrosive with high hydrophobicity. The different types of conventional gas diffusion layers used in PEM fuel cells, together with their manufacturers are shown in Table 2.1.

(a)

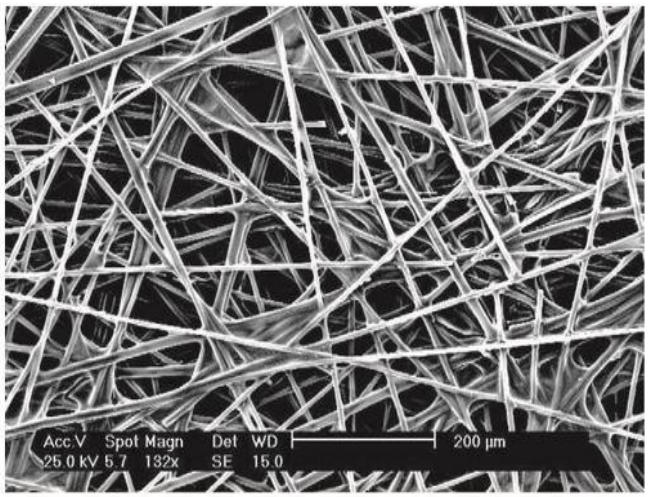

(b)

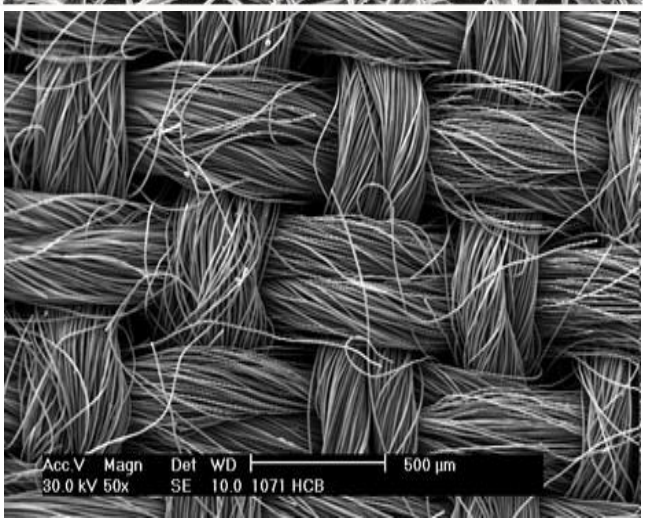

Figure 2.3 Micrographs for (a) carbon fibre paper, and (b) woven carbon cloth GDLs.

Table 2.1 Carbon based GDLs and their manufacturers [26].

Manufacturer	Type	Description
Ballard	1071HCB	Carbon cloth
	P50	Untreated carbon paper
	P50T	Teflonated carbon paper
	GDS1120	Teflonated carbon paper with coated MPL
	GDS2120	
	P75	Teflonated carbon paper with coated MPL
	P75T	
		Untreated carbon paper
		Teflonated carbon paper
Toray	TGP-H-030	Teflonated carbon papers with different thicknesses.
	TGP-H-060	
	TGP-H-090	
	TGP-H-120	
Freudenberg	C2	Felt fibres carbon paper based on H2315
	C4	
	I2 C6	Felt fibres carbon paper with coated MPL
	I2 C8	
		Felt fibres carbon papers based on H2315 with coated MPL

E-TEK	LT12001200WN LT	Non-woven carbon web GDL with coated MPL Woven carbon web GDL with coated MPL
Sigracet	SGL 10BA SGL 10BC SGL 24BA SGL 24BC SGL 25BA SGL 25BC SGL 34BA SGL 34BC SGL 34DC SGL 35BA SGL 35BC	3-D uncoated carbon fibre paper GDL 3-D MPL coated carbon fibre paper GDL Teflonated carbon fibre paper with/without MPL as follows: BA – 5% PTFE loading with no MPL BC – 5% PTFE loading with MPL DC- 20% PTFE loading with MPL
Tenax	TCC2660 TCC3250	Untreated woven carbon cloths
Cetech	N0S1005 N1S1007	Uncoated carbon paper

	GDS210	Carbon paper GDL with MPL coating
	GDS240	Uncoated carbon paper GDL
	GDS340	MPL coated carbon paper
	GDS370	Uncoated carbon paper substrate
	W0S1002	MPL coated carbon paper
	W0S1005	Carbon cloth
		Carbon cloth with MPL loading

2.1.3 Carbon fibre GDLs: Manufacture and treatment

The conventional GDLs used in PEM fuel cell designs comprise of carbon fibre materials also known as a carbon-carbon matrix. This is because of the excellent electrical conductivity of the carbon precursor material, their high stiffness, high strength, their light weight, the relative stability of the carbon element, high gas and hydraulic permeabilities as well as the elastic property of carbon when subjected to compression [36]. The two major types of carbon fibre GDLs widely used are the woven (carbon cloth) and non-woven (carbon fibre paper) GDLs. Woven carbon cloth GDLs exhibit higher power densities than the carbon papers [1]. Investigations by [39] found that the woven (carbon cloth) GDL exhibits better performance at high relative humidity, due to its lower tortuosity and rougher back surface, than carbon paper. However, the carbon papers are most preferred and commonly used owing to their low production cost and its low intrusion into the gas flow channels when assembled under load in the fuel cell stack, ease of MPL coating, ease of applying

of catalyst particles, their high gas permeability and electrical conductivity. Carbon fibre gas diffusion media are either fabricated from heavy fractions of petroleum or coal – the product fibres from this fabrication process are referred to as pitch precured -carbon fibres or from the copolymer of 90% or more of polyacrylonitrile (PAN). The woven carbon cloth or carbon fibre paper GDLs are produced from polyacrylonitrile (PAN) co-polymers due to its low cost (PAN) and the high carbon field of the precursor fibre (PAN) [36]. The manufacturing process of the carbon-paper GDL starts with the carbon fibre production, which involves the polymerization of acrylonitrile into co-polymers known as polyacrylonitrile (PAN) and then the spinning of the PAN co-polymers. The fibre from this manufacturing method are referred to as “PAN – percussed – carbon fibre. The PAN percussed -carbon fibre is used commonly as gas diffusion precursor materials because of their low-cost high carbon yield (50%-carbon) and excellent carbon-fibre properties. The various processing routes for the PAN -based carbon fibre GDL materials is shown in Figure 2.3. The PAN carbon fibre precursors are initially produced or formed from the PAN polymer using a solvent spinning process. The spinning process produces a continuous fibre comprising about 320000 filaments with an individual filament diameter of 12-14μm. Then the continuous carbon fibre material is stabilized in air at 230℃, transforming the fibres from a thermoplastic material into a thermoset one. Then the stabilised carbon thermoset material/ fibres is heat treated to a temperature 1200 - 1500℃ (high temperature). This heat treatment process, known as “carbonisation”, results in the elimination of nitrogen, oxygen and hydrogen elements contained in the thermoset resins, and this results in a 50% loss in weight of the fibre material. The process yields a carbon fibre with > 95% carbon, densities of 1.75-1.90 g/cm² and a fibre diameter of 7μm. Then the carbonised carbon fibre

paper is impregnated in phenolic resins, which allows the fibre to be moulded into the required and useful thickness and density. The material then undergoes a process called B-staging, which involves heating at 150℃ in air and results in the solvent evaporation and resin oligomerization. The carbon fibre paper is then graphitised at a temperature 2000℃, which changes its fibre structure from amorphous carbon into crystalline graphite with higher tensile modulus, increased thermal and electrical conductivity, higher density, and high oxidative resistance. The product of the graphitisation is a carbon fibre with > 99% carbon content, > 1400 MPa tensile strength, > 310000 MPa tensile modulus, densities ranging from 1.9 – 2.0 $\mathrm{g/cm^3}$ and fibre diameter between 6.5 – 7μm. This carbonisation and graphitisation processes serves to enhance the mechanical stability, thermal and electrical conductivities as well as adjust to the desired level of porosity.

For the carbon cloth gas diffusion material, the carbon material is woven from spun PAN yarns, carbonised and graphitised. This woven structure of the carbon cloth GDL accounts for the high mechanical integrity of the material as a GDL.

The finishing process of the manufacturing of carbon fibre GDLs involves the hydrophobic treatment of the carbon substrates with PTFE, commonly known as Teflon [1,26,36,37] where the manufactured carbon material is treated with 5 wt.% - 20wt.% PTFE to make it hydrophobic. The wetting of the carbon substrates also assists to make the surface of the substrate smoother for catalyst application, in the case of catalyst coated substrates (CCS), which helps reduce the contact resistance within the electrode. In addition, it prevents pore blockage by saturated liquid water from the ORR in the catalyst layer, which could obstruct the diffusion of reactants during operation [37]. This is done by dipping the GDL material into an aqueous

solution of PTFE, drying and heating at a temperature above 350℃ to sinter the PTFE particles on the surface of the GDL. Figure 2.4 show the manufacturing routes manufacturing routes for producing PEM fuel cell gas diffusion media materials using PAN-based carbon fibres.

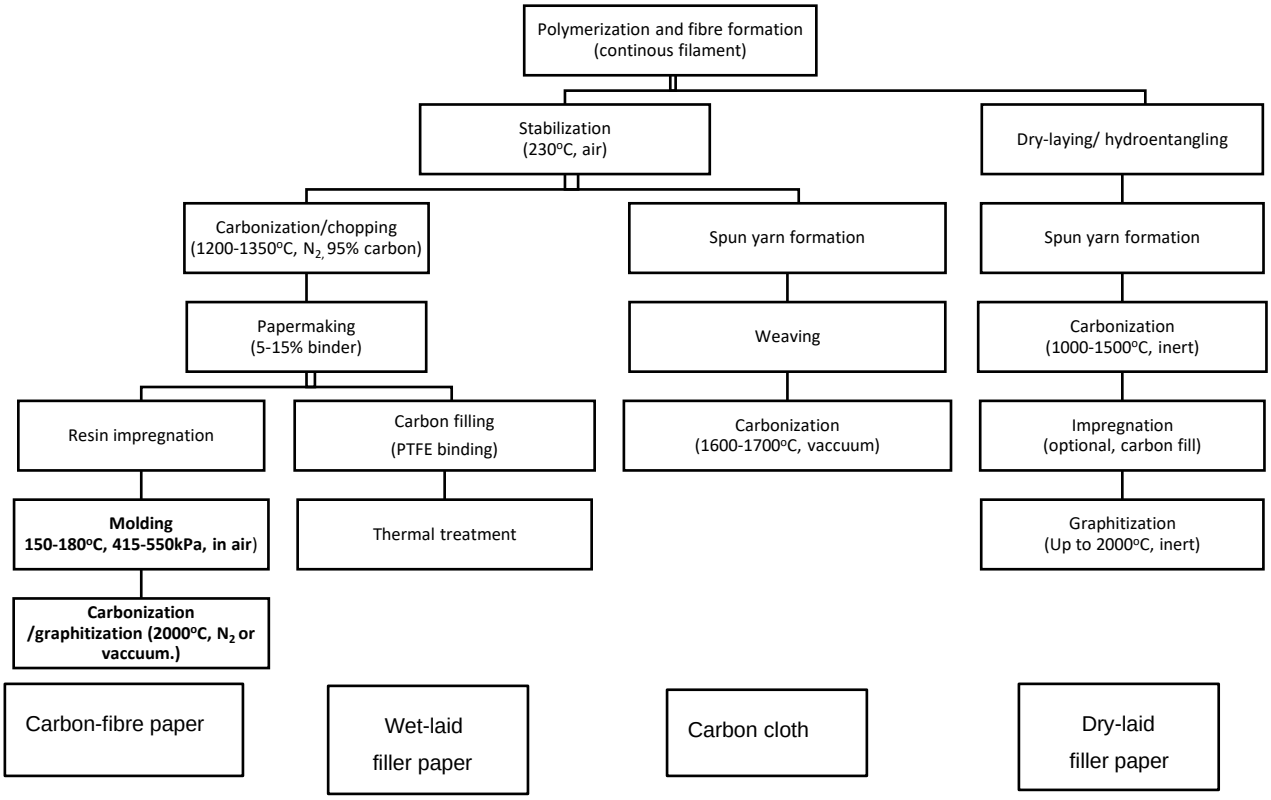

Figure 2.4. The various manufacturing routes for producing PEM fuel cell gas diffusion media materials using PAN-based carbon fibres. [36, 37].

2.1.4 Microporous layer (MPL)

Conventional gas diffusion layers are either designed as a single layer of the macroporous carbon substrate, made of either woven carbon cloth or carbon fibre paper, called gas diffusion layer (GDL). This is made hydrophobic using PTFE, or a dual layer gas diffusion media consisting of a macroporous carbon backing material (the MPS) and another layer which is a carbon-based microporous layer (the MPL). Usually, the MPL is applied on the interface between the gas diffusion layer and the catalyst layer. It is composed of agglomerates of carbon or graphite particles mixed with PTFE. The MPL is not a stand-alone layer (with distinct interface from the MPS) attached to the carbon substrate but a fluorinated polymer-based ink, which is deposited directly on the face of the macroporous substrate that interfaces the catalyst layer. The MPL have pore sizes within the range of 100 nm to 500 nm. They are made from a powdery mixture of carbon black (or other types of carbon particles) and the polymeric binder, PTFE, which is deposited on the carbon substrate and then sintered to allow the PTFE binder to bind the carbon particles and powder together. The pores of the MPL are several orders of magnitude smaller than those of the carbon substrate and the catalyst layer. This allows for the effective removal or wicking of liquid/dissolved water from the catalyst layer into the gas diffusion layer. In addition, the MPL is effective in reducing the ohmic losses within the PEM fuel cell during operation because of the effective humidification of the polymer electrolyte membrane, which results in increased ionic conductivity. Its impregnation and penetration into the macropores of the carbon substrate reduces the impact of the interfacial content resistance between the GDL and the catalyst coated membrane/ catalyst layer. Its effective liquid water removal enhances the transport of reactant gases to the reactive catalyst sites therefore minimize mass transfer

limitations, especially at higher current densities. It prevents the GDL from penetrating into the catalyst layer (which can result to reduced surface areas for the electrochemical reactions) when under assembly /compression pressure. In addition, the MPL prevents reactant crossover from the GDL into the membrane, when under assembly force by preventing the GDL from penetrating into the membrane. In addition, it could be used as substrate to deposit expensive and rare platinum catalyst particles.

The fabrication of a typical microporous layer involves the following three steps [36]:

- The carbon powder slurry/MPL slurry preparation.
- The deposition and
- Sintering

The carbon or graphite particles are mixed with the polymeric binder/hydrophobic agent (PTFE) to form an agglomerate. Then the mixture is dispersed in water or in organic additives to form a slurry. Thereafter, the MPL slurry is deposited on the surface of the carbon substrate. This is done by either brushing the slurry in the substrate, or by blading, spraying, or dipping of the substrate into the slurry. The MPL-deposited gas diffusion layer is then heat treated to a temperature of about 240℃ for a period of 30-40 minutes to dry (i.e., the drying process) [36]. Then the gas diffusion media is sintered at a temperature of 350℃ for about 30-60 minutes. This results in a uniform distribution of the hydrophobic agents within the gas diffusion media (GDM), producing a homogeneous surface morphology of the MPL and the gas diffusion layer. Table 2.2 shows the common types of carbon powder MPLs used in PEM fuel cells design together with their hydrophobic treatments and carbon loading.

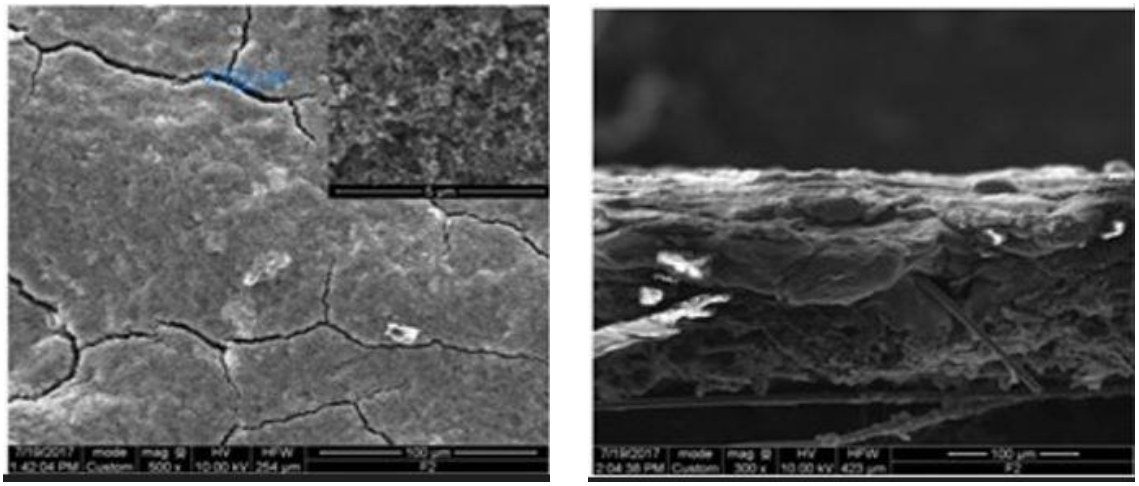

(a) **(b)**

Figure 2.5 SEM images of the MPL- deposited GDL; (a) face view of the untreated GDM comprising Avcarb EP40 carbon paper MPS and Vulcan XC-72R-based MPL, and (b) cross-sectional view of the GDM comprising Avcarb EP40, carbon paper and Vulcan XC-72R-based MPL, the image showing the uniform penetration profile of the MPL into the carbon gas backing layer [37].

Table 2.2 MPL Composition and carbon loadings [36].

Carbon powder	Hydrophobic agent	Optimum performance
Acetylene Black, Black Pearls 2000, Composite Carbon and Acetylene Black with 10% Black Pearls 2000	30 wt.% PTFE	Composite Carbon with 30 wt.% PTFE. $0.5\mathrm{mg/cm^2}$ Carbon loading

Vulcan XC-72	10-40 wt.% PTFE	Vulcan XC-72 with 20-30 wt.% PTFE. $3.5\mathrm{mg/cm^2}$Carbon loading
Carbon Black	24, 35, 45 wt.% PTFE	Carbon Black with 35 wt.% PTFE. $2.0\mathrm{mg/cm^2}$Carbon loading

2.2 Mass transport

A higher mass transfer rate always results in increased current densities in the PEM fuel cell, and high availability of reactant gases in the catalyst reaction sites thereby reducing the amount of platinum catalyst required for the electrochemical reactions in the cell [50]. To achieve this, GDL transport properties (such as permeability and diffusivity) required for the effective mass transport in the cell needs to be effectively controlled. A good number of PEM fuel cells are designed with serpentine flow fields. For this flow field, the diffusion of gases is the dominant mode of through-plane transport of reactants from the gas flow channels to the catalyst sites [51] with convection contributing an insignificant effect to the through-plane transport. Convective transport, however, contributes to the transport of reactants in the in-plane direction -parallel to the gas flow channels. This is due to the pressure difference, in the in-plane direction, between the inlets and outlets of the channels as well as the pressure drop across adjacent gas channels in the flow field [50, 52]. The gas convection in the GDL is proportional to the gas permeability of the GDL and is a function of its porous structure. At very low flow velocities, the gas

permeability is expressed, as a function of the pressure drop in the channel, using Darcy's law as follows [50]:

$$-\nabla P = \frac{\mu}{K}\vec{v} \quad \textbf{(2.1)}$$

Where K is the absolute gas permeability in m^2, μ is the viscosity of the gas mixtures, $\vec{v}$ is the fluid velocity and P is the fluid pressure.

At higher flow velocities, Darcy's law is combined with the Forchheimer equation which accounts for the inertial pressure loss resulting from the acceleration or deceleration of the fluid through the tortuous paths of the GDL [50]. The combined equation is expressed as follows:

$$-\nabla P = \frac{\mu}{K}\vec{v} + \beta\rho|\vec{v}|\vec{v} \quad \textbf{(2.2)}$$

where β is the inertial coefficient.

In the PEMFC, the liquid water content is always higher in the cathode catalyst layer (because of the ORR reaction in the cathode catalyst layer and the flow of water molecules, coupled to the protons transport through the membrane) than in the cathode GDL and the gas channels. As a result, a pressure gradient is developed but the higher region of saturated water (in the catalyst layer) and the lower saturation region thereby forcing the liquid water out of the cathode catalyst layer. The liquid water is the transported out of the GDE by capillary action in the GDL. At low permeability values, gas diffusion is the dominant mode of through-plane transport of gases from the channel to the catalyst layers [53-55]. Also, due to the presence of the MPL in the dual layer gas diffusion media (GDM), the pore sizes of the entire GDL ranges from tens of nanometre (in the MPL) to tens of micrometre

(in the MPS). Therefore, both ordinary and Knudsen diffusion usually occurs in the transport of reactant gases in the GDM.

2.3 Thermal transport

A major limitation to the optimal performance of PEMFCs is the two-phase water transport in the cell as the liquid water presence results in the blockage of the pores in the GDL and obstructs the flow of gases to the cathode catalyst layer [56]. The complex two-phase water transport in the PEMFC is strongly affect by the thermal management and temperature gradient in the cell [57]. The condensation of water vapour in the membrane releases large amounts of heat, which often results in undesirable hotspots that dehydrates the membrane and impedes effective transport of protons through it, thereby reducing the cell performance and membrane degradation if not effectively controlled [56]. Also, local variations of temperature (which can be attributed to the waste heat generated from the electrochemical reactions in the catalyst layers, losses from electrode overpotential and Joule heating) in the PEMFC can result to drying or flooding of the membrane or the catalyst layer, respectively. Either of these conditions can affect the cell performance [58]. Effective thermal management is crucial in PEMFCs as the cells are only able to withstand small deviations in temperature from their design point [55,59]. Therefore, the coupling of thermal transport and water transport in the PEMFC is necessary for improved performance of the PEMFC and its durability. Hence, the GDL must be carefully designed to be thermally conductive for removal of the excess heat in the MEA of the PEMFC for optimum performance [58].

2.4 Charge transport

The performance of the PEMFC depends largely on the electrical conductivity of the GDL (as it is responsible for the flow of electrons between the catalyst layers and the bipolar plates) as the ohmic losses are reduced with higher GDL electrical conductivity [60]. The measure of the ability of the GDL (or any material) to conduct electron is known as the electrical conductivity, σ, and it is a reciprocal of the electrical resistivity, ρ (which is a measure of the ability of the GDL to resist the flow of electrons through it). The SI unit for the electrical conductivity is S/m and that of the resistivity is $\Omega \cdot m$ [61]. Studies show that the transport of electrons through the GDL as well as the PEMFC performance is affected by the thickness of the GDL, the width of the ribs of the bipolar plates, the electrical conductivity and the contact resistance between the GDL-catalyst and GDL-bipolar plates [60]. Nitta et al. [62], in their study of the contact resistance between GDL and the catalyst layer reported the contact resistance between the GDL and catalyst layer to be an order of magnitude higher than that between the GDL and the bipolar plates and that a non-uniform compression of the GDL results in an uneven distribution of current in the MEA. They also investigated the effects of the contact resistance on different GDL types – woven and non-woven. They concluded that the contact resistance in carbon paper is higher than that of the woven carbon cloth. Studies by Higier and Liu [63] reported that the GDL contact resistance is affected by the width of the channel and that reducing the rib of the bipolar plate contributes to high increase of the contact resistance.

2.5 GDL structure and anisotropy

The gas diffusion layer microstructure and its design play an important role in the diffusion of gas reactants to the electrocatalyst reactive sites as well as the removal of liquid water from the MEA to the gas flow channels. Therefore, the fibre structure of the carbon fibre GDLs (whether woven or non-woven) has a strong effect in the pore size distribution (PSD) of the GDL, its electrical resistance as well as the overall performance of the PEM fuel cell. Non-woven (paper) carbon fibre GDLs are made of two groups, according to their fibre structure configuration, namely:

- The straight fibres
- The felt or spaghetti fibres.

Figure 2.6 shows SEM images of the fibre structural configurations of TORAY-060 and Freudenberg C2 carbon paper GDLs, respectively.

SEM images of the GDL cross-sectional and face views shown in Figures 2.5b and 2.6a show that the GDL is comprised of open pores of tens of micrometre (fibre diameter) which are formed by interconnection of individual carbon & fibres which are preferentially oriented in the in-plane or lateral direction. The manufacturing process of carbon paper GDL makes the carbon paper GDL to be highly anisotropic in nature – exhibiting different measured values of transport properties in different directions (through-plane and in-plane). These preferentially oriented fibres are randomly stacked according to their manufacturing process. The carbonisation and graphitisation (heat treatment) process of these randomly stacked carbon fibres results in a highly anisotropic microstructural configuration of the GDL. Also, the wetting or hydrophobic treatment of the carbon substrates results in a decrease in the pore size distribution, porosity, and tortuosity of the GDL. As reported by

[26,36,37], the deposition of the MPL on the MPS results in a reduction of the pore size of the GDM and less volume intrusion. This further reduces the bulk or overall porosity of the GDM.

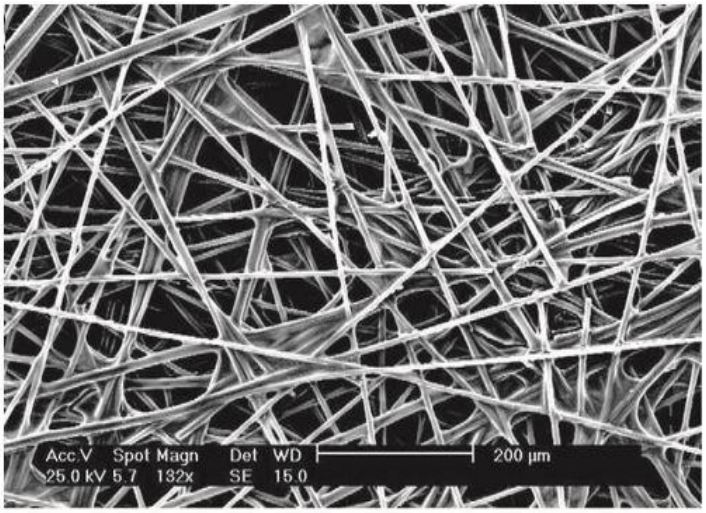

(a)

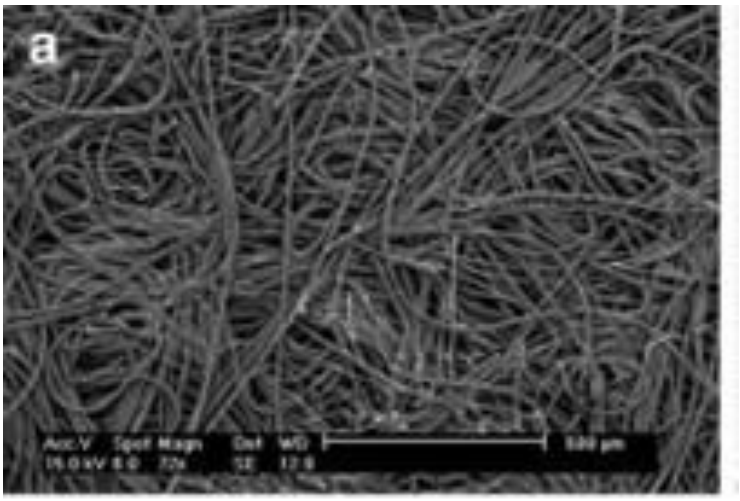

(b)

Figure 2.6 SEM images of (a) straight Toray H-060 fibre carbon paper, and (b) felt or spaghetti Freudenberg C2 fibre carbon paper [36,37].

Several reported studies in the literature show, both numerically and experimentally, that the transport properties of the gas diffusion layer differ in the different planes of orientation of the carbon fibre.

2.5.1 GDL Anisotropic transport properties

A good number of numerical investigations of GDL anisotropy existing in the literature have been based on numerical estimations and correlations of GDL anisotropy transport properties. Until lately, only a few models and investigations of GDL anisotropic transport properties have been based on experimentally characterized and realistic measurements of transport properties in the in-plane and through-plane directions of the GDL.

Most PEM fuel cell models available in the literature are based on the assumptions of the GDL to be spherical porous medium whereas they are fibrous porous medium. Hence, several correlations for the effective transport properties, based on the effective medium theory, such as that of [64-67] have been based on this assumption and therefore have failed to accurately predict the local and global performance of the PEM fuel cell. However, lately several experimental characterizations of the GDL transport properties have been conducted and are reported as below.

2.5.2 Gas permeability

The permeability of the GDL is a measure of the contribution of convection to the overall mass transport of the gases. [1]. The permeability of carbon fibre GDLs are reported to be with the range of 10^{-10} and $10^{-13}\mathrm{m}^2$. Tomadakis and Robertson [68] numerically correlated the anisotropic permeability for porous fibre materials as follows:

$$\mathrm{K} = \mathrm{r}^2 \frac{\varepsilon(\varepsilon-\varepsilon_\mathrm{p})^{\alpha+2}}{8(\mathrm{In}\varepsilon)^2(1-\varepsilon)^{\alpha}[(\propto+1)\varepsilon-\varepsilon_\mathrm{p}]^2} \quad \textbf{(2.3)}$$

Where r is the fibre radius, ε_p is the percolation threshold and $\propto$ is an empirical constant. The value of the percolation threshold was reported to be 0.11 and independent of the direction of flow while the empirical constant, $\propto$, was reported to be 0.785 and 0.521 for the through-plane and in-plane directions, respectively.

2.5.3 Effective diffusivity

There exists, in the open literature, many investigations (mainly numerical models and a few experimental observations) that aim to investigate the diffusion resistance of GDLs and its effect on fuel cell performance by estimating the effective diffusivity of the GDL. The effective diffusivity, D_{eff}, of the porous GDL is expressed as follows:

$$D_{eff} = f(\varepsilon)g(s)D_{bulk} \quad \textbf{(2.4)}$$

Where D_{bulk} is the bulk diffusivity, ε is the porosity, s is the water saturation, $g(s)$ is a function of the water saturation and $f(\varepsilon)$ is the diffusibility of the GDL -a function of its porosity.

The effective medium approximation which assumes that the GDL is made up of uniformly distributed spherical particles whereas the GDL is made up of randomly distributed cylindrical (non-spherical) fibres oriented in different directions (but preferentially in the in-plane direction) [1]. The Bruggeman diffusivity model is the most widely used approximation in PEMFC modelling and it is expressed as follows [69, 70,71]:

$$D_{eff} = D_{bulk}(\varepsilon)^{1.5}(1-s)^{1.5} \quad \textbf{(2.5)}$$

In addition, the effective medium approximation has been used by Neale and Nader [71] to estimate the effective diffusivity and their model is expressed as follows:

$$D_{eff} = D_{bulk}\left(\frac{2\varepsilon}{3-\varepsilon}\right) \quad \textbf{(2.6)}$$

Where the diffusibility, $f(\varepsilon)=\frac{2\varepsilon}{3-\varepsilon}$ **(2.7)**

Das et al. [72] extended the model of [73] to account for the presence of liquid water in the GDE and they expressed their model as follows:

$$D^{eff}_{flooded-GDL} = D_{bulk} + \frac{3(1-f_g)D_{bulk}}{f_g - \frac{3D_{bulk}}{D_{bulk}-D_l-\frac{3(1-f_l)D_l}{f_l-3(1-f_l)}}} \quad \textbf{(2.8)}$$

Where f_g and f_l are the volume fractions of gas and liquid phases, respectively. D_l is the diffusion coefficient of the vapor in the liquid.

Percolation theory has also been employed by Tomadakis and Sotirchos [74], considering the anisotropy of the GDL, to determine the effective diffusivity for the porous GDL. Their model is expressed as follows:

$$D_{eff} = D_{bulk}\left(\frac{\varepsilon-\varepsilon_p}{1-\varepsilon_p}\right)^{\propto} \quad \textbf{(2.9)}$$

Typical values for ε_p and $\propto$ are shown in Table 2.3.

Table 2.3 Parameters for percolation threshold and empirical constant in equation (2.9) [77].

	Direction of diffusional flow	ε_p	$\propto$
1-D	In-plane	0	0
	Through-plane	0.33	0.707

2-D	In-plane Through-plane	0.11 0.11	0.521 0.785
3-D	All directions	0.037	0.661

The model by [74] was extended by Nam and Kaviany [73] to account for the presence of saturated water in the GDL of a two-dimensional PEMFC model. Their model may be expressed as follows:

$$D_{eff} = D_{bulk}\left(\frac{\varepsilon-0.11}{1-0.11}\right)^{0.785}(1-s)^2 \quad \textbf{(2.10)}$$

Other numerical models for effective diffusivity of the GDL includes the pore network model by Wu et al. [75,76] in which they used a porosity value of 0.46 to calculate the through-plane diffusibility for Toray carbon paper. [77-79] correlated the effective diffusivity using 3-D reconstruction of the GDL pore network. In addition, X-ray computed tomography (X-CT) has been used by [80-81].

Experimental characterization of the GDL effective diffusivity has been carried out by [82] using limiting current technique. Loschimdt cell method has been used by as well as electrochemical diffusimetry method by Kramer et al. [83] and Fluckiger et al. [84].

2.5.4 Effective thermal conductivity

Thermal management in the PEM fuel cell (especially in the MEA) is very important as the PEM fuel cells produce almost the same amount of heat as they produce electricity and can only withstand a minimal temperature variation [58]. Thermal management in the PEM fuel cell is complicated further by the heat coupling with water transport in terms of the release of heat from the condensation of water

vapour, during cell operation [58]. Hence, many numerical studies and investigations exist in the literature on how to control the temperature distribution and thermal transport in the fuel cell.

The effective thermal conductivity is a property of porous materials, which measures the contribution of the solid and void (fluid) phases to the thermal conductivity of the material. It is widely used in modelling of heat transport and temperature distribution in PEM fuel cells. The effective thermal conductivity of the GDL is function of the porosity and the thermal conductivities of the solid carbon, gas species and liquid water in the GDL as well as the saturation. It is expressed as follows [58]:

$$\mathrm{K}_{\mathrm{eff}} = \mathrm{f}(\mathrm{K}_{\mathrm{sol}}, \mathrm{K}_{\mathrm{g}}, \mathrm{K}_{\mathrm{l}}, \varepsilon, \mathrm{s}) \quad \textbf{(2.11)}$$

Where $\mathrm{K}_{\mathrm{eff}}$ is the effective thermal conductivity of the GDL, ε is its porosity, K is the thermal conductivity, $\mathrm{sol}, \mathrm{g}\ \mathrm{and}\ \mathrm{l}$ denote solid phase, gases, and water, respectively. s is the water saturation.

Estimating effective thermal conductivity in the fibrous GDL has been the focus of several theoretical/analytical, numerical, and experimental studies [1, 58]. Unlike for the effective diffusivity, there is no specific correlation for the effective thermal conductivity for the GDLs [58]. Theoretical estimation of the carbon paper GDL effective thermal conductivity has been developed using arithmetic and geometric mean correlations by [85-87]. Other theoretical estimations such as those by [88-91] found the effective thermal conductivity of carbon paper GDL to be within the range of 0.15 W/m·K to 65 W/m·K [1, 58].

In addition, numerical models of the effective thermal conductivity have been developed by Veyret et al. [92] and Zamel et al. [58] by using a three-dimensional

(3-D) reconstruction of the GDL pore morphology. The fractal approach was used by Nikoee et al. [93] to estimate the through-plane effective thermal conductivity. Veyret et al. [92] reported that an increase in PTFE loading in the GDL increases the thermal resistance created in the GDL thereby leading to decrease in its thermal conductivity. Zamel et al. [58] found the effective thermal conductivity to be highly sensitive to the carbon fibre orientation in the GDL. They [58] concluded that the effective thermal conductivity is higher in the in-plane direction than that of the through-plane. They [58] also developed their own numerical correlation for both in-plane and through-plane effective thermal conductivities.

Ramousse et al. [94], experimentally, measured and investigated the effects of the carbonization and graphitization of the carbon paper as well as the PTFE treatment on the effective thermal conductivity of Quintech carbon paper. They reported the minimum and maximum ranges to be 0.3-1.36 W/m·K and 0.20-1.36 W/m·K, respectively. Khandelwal and Mench [57], experimentally, investigated the through-plane effective thermal conductivity for Toray TGP-H-060 and SIGRACET carbon papers, under different PTFE loadings. They reported a decrease from 1.8 ± 0.27 W/m·K to 1.24 ± 0.19 W/m·K at increased temperature, of 26 ℃- 73 ℃, as well as a drastic reduction when treated with PTFE for Toray TGP-H-060. For the Sigracet carbon paper, at a temperature of 58 ℃ and with different amounts of PTFE treatment of 0, 5 and 20% wt. the measured effective thermal conductivity was found to be 0.48 ± 0.09 W/m·K, 0.31 ± 0.06 W/m·K and 0.22 ± 0.04 W/m·K, respectively. Other experimental measurements and investigations of effective thermal conductivity exist in the literature.

2.5.5 Effective electrical conductivity

According to Mathias et al. [38], the performance of the PEMFC directly relates to the electrical conductivity of the GDLs. Usually, the electrical conductivity of the porous carbon paper GDL is described by the effective electrical conductivity, which is a function of the electrical conductivities of the solid carbon and the void fraction of the porous GDL [95]. This may be expressed as follows:

$$\sigma_{\mathrm{eff}} = \sigma_{\mathrm{s}} \mathrm{f}(\varepsilon) \quad \textbf{(2.12)}$$

Where σ_{eff} is the effective electrical conductivity, σ_{s} is the bulk electrical conductivity of the solid carbon material and $\mathrm{f}(\varepsilon)$ is a function of the porosity of the GDL. Usually, the effective electrical conductivity of the carbon paper (as well as other porous materials) is described based on the effective medium theory (EMT) [1]. The Bruggeman approximation for the effective electrical conductivity is the most widely used in PEMFC models, and it is expressed as follows:

$$\sigma_{\mathrm{eff}} = \sigma_{\mathrm{s}} (1 - \varepsilon)^{1.5} \quad \textbf{(2.13)}$$

Where $(1 - \varepsilon)$ is the fraction of the solid particles [69].

Looyenga [96], also using the EMT estimated the effective electrical conductivity for the carbon GDL as follows:

$$\sigma_{\mathrm{eff}} = \sigma_{\mathrm{s}} (1 - \varepsilon)^{3} \quad \textbf{(2.14)}$$

Das et al. [76] also developed their own model based on the Maxwell equation (another form of the effective medium theory) for the effective electrical conductivity. They proposed the following correlation:

$$\sigma_{\mathrm{eff}} = \sigma_{\mathrm{s}} \left(\frac{2 - 2\varepsilon}{2 + \varepsilon} \right) \quad \textbf{(2.15)}$$

There are, however, some limitations to the effective medium theory used in estimating the effective electrical conductivity for the GDL as using the theory assumes the GDL to be homogeneous in all directions, hence ignoring the dependence of the electrical conductivity on the anisotropy of the GDL [1, 98].

Several numerical models to characterize the effective electrical conductivity of the GDL have been developed. Becker et al. [80] investigated the effective electrical conductivity of Toray TPGH-90 carbon paper using 3-D reconstruction of the pore morphology. Zamel et al. [95] estimated the in-plane and through-plane electrical conductivities using 3-D reconstruction of the GDL. Their results, however, showed much variation when compared with experimental data due to the failure of their numerical model to capture certain properties of realistic GDLs such as the cracks upon compression, binder effects, etc. [1]. However, they [95] showed the effect of the GDL anisotropy and porosity on the effective electrical conductivity. They also reported the through-plane effective electrical conductivity to be lower than that of the in-plane due to the high electrical resistance between the carbon fibres in the through-plane direction. They [95] developed their own correlation for the effective electrical conductivity of the GDL.

Experimental measurements and investigations of the effective electrical conductivity of GDLs have been carried out, and this has been reported in the literature such as [97-99]. Williams et al. [97] measured the in-plane electrical conductivity for SGL and Toray carbon papers using the “Standard Test Method for Electrical Resistivity of Manufactured Carbon and Graphite Articles at Room Temperature” (ASTM C611-98), employing four-point method. They reported the electrical conductivity to be dependent on the MPL coating and PTFE treatment of the GDL. Nitta et al. [98] also measured the in-plane and through-plane electrical

conductivity of SGL Sigracet 10-BA carbon paper at different compressive loads. They reported that the electrical conductivity increases linearly with increased compression. Ismail et al. [99] measured the in-plane electrical conductivities for SGL 10BC (25% treated) and SGL 10BE (50% treated) as well as their through-plane contact resistances using the four-probe technique. They reported no effect of the PTFE loading on the in-plane electrical conductivity because the electrons travel through the solid carbon fibres instead of the void regions. They also found that the through-plane electrical resistance increases with increased PTFE treatment. Reports in the literature have established the fact that the conventional carbon fibre GDLs used in PEMFCs are oriented in both the through-plane and the in-plane directions of the fuel cell. Hence, there is the need for the anisotropy of the GDL to be fully captured in the modelling of PEMFCs. This allows for more accurate predictions of the performance of the modelled fuel cells. Also, it is important that realistic experimentally characterised GDL transport properties are implemented in CFD models of the PEMFC so as to fully understand the effects of these transport properties on the PEMFC performance. To emphasize this, the study in Chapter 4 of the thesis incorporates experimentally characterised GDL transport properties along the through-plane and the in-plane directions, such as the experimentally measured diffusivity by Kramer et al. [83] and the electrical conductivity measured by Ismail et al. [99]. The three-dimensional PEMFC model investigates the impact of these anisotropic GDL transport properties on the PEMFC performance.

2.6 Numerical and experimental characterisation of the GDL transport properties

Ismail et al. [99] experimentally measured /characterised the in-plane electrical conductivity of PTFE treated and MPL coated SGL carbon paper GDLs. They investigated the anisotropic electrical conductivity of the GDL samples, using Smit method, and their sensitivity to the hydrophobic agent (PTFE) and MPL coating, as well as the effect of cell clamping or assembly pressure on the interfacial contact resistance of GDLs. They reported an almost constant in-plane conductivity for the PTFE treated GDL samples while the in-plane electrical conductivity was higher for the SGL 10BC with 50wt.% PTFE loading as compared to that of SGL 10BC with 25wt.% PTFE loading. They also reported that there is a significant anisotropy of the electrical conductivity in the in-plane direction. Aldakheel et al. [100] experimentally measured the through-plane gas permeability, hydrophobicity (contact angle), thickness and the surface morphology for Toray (TGP-H-090) and SGL (24-BA,10-BA,34-BA, and 35-BC) carbon paper GDLs, with and without PTFE loading, before and after compression test. They reported that the Toray paper GDL had the least thickness and gas permeability reduction after being compressed due to its relative high density and low porosity. In addition, they found that the MPL penetrated the SGL35BC carbon GDL more than the SGL34BC and for all tested GDLs, the contact angles decreased after compression. Mukherjee et al. [101] experimentally measured the in-plane and through-plane permeability of GDL samples using an in-house dedicated PEM fuel cell, for both MPL coated and uncoated carbon paper GDLs. They showed that the gas permeability of the GDL in the in-house built PEM fuel cell can be estimated using Darcy's law for both the

through- plane and the in-plane directions. Ismail et al. [102] experimentally measured the through -plane gas permeability of MPL-coated SGL carbon paper GDLs - 10BC (treated) and 10BE (50% PTFE treated), as well as for an MPL-coated GDS 3215(Ballard) untreated paper. They used an in-house set up of the fuel cell rig. They reported an increase in the through-plane gas permeability of the tested GDL samples with increased hydrophobicity (PTFE loading) of the MPL. They also found the permeability of the MPLs to be 2-3 orders of magnitude lower than that of their corresponding carbon substrates. Orogbemi et al. [103] experimentally estimated the through-plane gas permeability of SGL 10 BA carbon substrate coated with Ketjenblack EC-300J (in one case) and Vulcan XC-72R, with 60wt.% PTFE treatment for various carbon loadings. They reported a decrease, by at least an order of magnitude, of the GDL sample gas permeability for both cases of MPL coating with the MPL permeability being 2-3 orders of magnitude lower than that of the uncoated carbon substrate. They also reported that the MPL sintering slightly decreased the GDL gas permeability. Chan et al. [104] experimentally estimated the following:

- the effective diffusivity of Toray-TGP-H-60 and TGP-H-120 GDL samples with 0wt.%, 30wt.%, and 60wt.% PTFE loading,
- the Solvicore Type A,
- the SGL series GDL (uncoated) with 0wt.% and 5wt.% PTFE loading, and
- the SGL 10 series without MPL coating but with PTFE loadings of 0wt.% and 5wt.% and the SGL 25 series with MPL coating and PTFE loading of 20wt.%.

They used a Loschimdt cell with an oxygen- nitrogen mixture at room temperature conditions. Their results showed that the effective diffusivity of the MPL contributes

only about 21% of that the carbon substrate while the Knudsen diffusion accounts for 80% of the diffusivity of coated GDLs. Zenyuk et al. [105] investigated the porosity, tortuosity, and pore-size distribution of the GDL under varying assembly forces using X-ray completed tomography (X-CT). They reported that MRC and Freudenberg GDLs exhibited the lowest tortuosity while the Toray paper GDLs showed the highest and the SGL values of tortuosity was in-between the two. Hwang & Weber [106] experimentally characterised the effective diffusivity of PTFE treated, and untreated GDLs using ex-situ electrochemical limiting current method for uncompressed GDLs with different percentages of PTFE loadings. They investigated Toray TGP-H-120, SGL10 series, and Freudenberg H2315 to measure the effective through-plane diffusivity. They observed that the porosity is the major factor that controls the diffusion of gases in the gas diffusion layer of the PEM fuel cell. Garcia- Salaberri et al. [107] characterised the effective diffusivity of dry and partially saturated Toray TGP-H-120 carbon fibre paper using Lattice Boltzmann (LB) Simulation method in X-ray tomographic reconstructed GDLs. They found that the effective diffusivity of the GDL sample reduced when treated with PTFE which reduced the pore volume and resulted in higher tortuosity. They reported a strong sensitivity of the finite-size porous media GDL to local conditions. Rashapov and Gostick [108] experimentally measured the porosity, thickness, skeletal and bulk density different Toray (060, 090,120) and SGL (24,25,34, and 35) series, and Freudenberg (H2315 series). All samples were uncoated. They employed the buoyancy method for these measurements. Their results showed that the porosity decreased with increased PTFE treatment. Xiao et al. [109] employed fractal theory to analytically characterise the gas permeability of the carbon fibre GDL in terms of porosity, tortuosity fractal dimension, pore area fractal dimension, water, and gas

phase fractal dimensions. Tayarani- Yoosefabadi et al. [110] developed a stochastic microstructural model of the Toray GDL to characterise the GDL transport properties under various amounts of PTFE loadings and liquid water saturation levels. They proposed a novel stochastic microstructural model of the GDL with which the investigated the anisotropic transport properties of the GDL. They reported a decrease in the GDL porosity, diffusivity and gas permeability with increased PTFE loading and liquid water saturation. Moosavi et al. [111] developed an in-situ X-ray computed tomography model to characterise the GDL. They employed pore-level simulations to characterise the transport properties of partially saturated GDLs with and without PTFE loadings (using Toray TGP-H-120). They developed mathematical correlations to determine the pore size distribution of liquid water and gaseous phases at different saturation levels. They also reported that the relative permeability and the effective relative diffusivity of air is not affected by the PTFE treatment of the GDL. However, the water permeability or hydraulic permeability is significantly improved by the treatment with PTFE. Zamel et al. [73] developed a numerical correlation to estimate the through-plane and the in-plane diffusibility of a TORAY carbon paper GDL based on a 3-D simulation of the GDL. They proposed different correlations for two different ranges of the GDL porosity ($\varepsilon_p \leq \varepsilon$<0.9) and (0.33$\leq \varepsilon <$1). Mangal et al. [112] experimentally estimated the through-plane viscous permeability and effective molecular diffusivity of carbon fibre GDLs. They found that the permeability varies, with PTFE loading, between 1.13×10^{-11} - 0.35×10^{-11} m² while the diffusibility varies in the range of 0.209-0.071. Rashapov and Gostick [108] measured the in-plane effective diffusivity of GDL as a function of compression and PTFE loading. They reported a decrease in the effective diffusivity

when compression and PTFE loadings were increased. Sadeghifar et al. [113] measured the through-plane thermal conductivity of SGL 24,25,34,35 series gas diffusion layers with coated MPL under different cell assembly ranging 2-14 bar at 60℃ temperature. Also, they developed a novel numerical model to predict the through-plane thermal conductivity of the PTFE treated GDL samples. They reported an increase in the thermal contact resistance for the treated and coated GDL samples as well as a reduction in the thermal conductivity. Molaeimanesh and Akbari [114] developed a 3-D Lattice- Boltzmann model of the cathode electrode in which they characterised the anisotropic transport properties of the GDL and investigated the effects of the GDL microstructure on reactant and current density distributions. Chevalier et al. [115] deployed in-operando synchrotron X-ray radiography to measure the through-plane liquid water saturation profiles of the GDL and X-ray computed tomography to determine the GDL porosity distributions. They also investigated the GDL effective diffusivity using electrochemical impedance spectroscopy (EIS). Bosomoiu et al. [116] numerically characterised the thermal and electrical conductivity of fresh and aged Sigracet 34BC GDLs samples using X-ray computed tomography. They also investigated the capillary pressure and the GDL samples. Zamel et al. [58] experimentally measured the in-plane thermal conductivity of Toray TGP-H-120 carbon with 0,5,20 and 50 wt.% PTFE loadings using thermal diffusivity measurements method for a temperature range of -20 to +120℃.They observed that the thermal conductivity decreased as the temperatures of the tested samples were increased. Loading for the treated samples, they found that thermal conductivity lies in the range of 10.1-14.7 W/m·K and also deduced empirical correlations to measure the thermal diffusivity and thermal conductivity. Zamel et al. [58] employed a thermal capacitance (slug) method to experimentally

characterise the through-plane thermal conductivity of TORAY carbon paper for a temperature range -50 to +120℃ as well as the effect of cell compression and PTFE loading in the thermal conductivity. They found that the thermal resistance decreased with increased assembly force and the thermal resistance is highly dependent in temperature and PTFE loading. Zamel et al. [95] numerically estimated the effective electrical conductivity of the carbon fibre paper GDL by developing a three-dimensional reconstruction of the GDL. They reported a higher electrical resistivity in the through-plane direction. They also proposed empirical relations to estimate the effective electrical conductivity of the carbon paper GDL and found the tortuosity of GDL to be 1.7 and 3.4 in the in-plane and through-plane directions respectively. Alhazmi et al. [117] employed parallel thermal conductance (PTC) method to experimentally measure the in-plane thermal conductivity and thermal contact resistance of SGL 10 Series Sigracet GDLs. They found the in-plane thermal conductivity to decrease with increased loading of PTFE and MPL. Alhazmi et al. [117] experimentally characterised the through-plane thermal conductivity and thermal contact resistance for Sigracet SGL 10 Series GDL samples. They found that the through-plane thermal conductivity of the samples is lower than those of the in-plane. However, most of the experimental and numerical approaches of characterisation of the GDL has been mostly ex-situ without the GDL being physically incorporated in the full fuel cell and measured. Hence, the need for these characterised value of the GDL to be used in CFD models of the PEMFC. Hence, in the Chapters of the thesis, experimentally measured values of the GDL transport properties in the through-plane and in-plane directions have been incorporated so have to effectively predict the impact of the transport properties on the PEMFC.

2.7 CFD Modelling

Computational Fluid Dynamics (CFD) is a branch of fluid mechanics that employs numerical methods and algorithms to study the transport processes and phenomena in the fluid flow. It combines the physics, numerical mathematics, and computer numerical codes to analyse complex fluid flow problems involving fluid-fluid structural interaction, fluid-solid or fluid-gas interaction, etc. It is a potential tool used in simulating the transport phenomena that occurs in the fuel cell (as well as in other engineering designs), and compute flows in multi-phases, multi-dimensions, and for multi-component species. It has been widely recognised as a competent alternative to experiments due to its flexibility as different approaches, assumptions, and parameter values can be formulated to obtain accurate/desired results. CFD has been widely employed in fuel cell technology [118] to develop novel designs and architecture of the fuel cells and its components. Using CFD, the PEM fuel cell can be divided into finite elements or control volumes, which are called ‘grids or mesh’ where the transport equations are solved for individual grids. This process of dividing the computational domain or geometry into grids is known as grid/mesh generation. The grids can be classified into structured- quadrilateral for two-dimension and hexahedral for three-dimensional geometries, and unstructured (triangles and tetrahedral shapes for two and three-dimensional geometries of complex shapes, respectively). Analysis in CFD comprises the following processes:

- The pre-processing process which involves model formulation and transformation into idealised and discretised numerical models, model assumptions, mesh generation, and the setting of boundary conditions.

- The solving of these formulated and discretised numerical models, together with the boundary conditions. This involves the use of several commercial solvers developed based on different numerical discretisation methods.
- The post-processing process, which involves the analysis and visualisation of the obtained results. This can be graphics, tables, charts, images, and animations.

2.7.1 Numerical Discretisation Methods

Numerical methods used in solving transport equations in CFD include the finite difference method (FDM), finite volume method (FVM), and finite element method (FEM). The finite element method (FEM) uses structured and unstructured grids and, hence it is widely employed for fluid flow in complex geometries, and in non-Newtonian fluids. To obtain high accuracy, more grids are used at boundaries and for regions where problem is to be solved. The method employs degree of freedom-total number of points multiplied by number of unknowns, the shape function-variation of solution in a mesh, and the weak formulation. The finite difference method (FDM) is a simple discretisation method that uses the Taylor's expansion series to solve the different equations for fluid flow. The finite difference method gives high-order accuracy for spatial discretisation but can only be used on structured grids. Finite volume method is also known as the control volume method. This method is employed in commercial solvers such as ANSYS Fluent, ANSYS CFX, and STAR-CD for transport computations. Here the fluxes are discretised at the boundaries of each finite volume/control volumes, which are small volumes of fluid that surround each nodal point on the grid. The fluxes of the finite volume

method are generally conservative so that the flux entering a given finite volume from a neighbouring finite volume is equal and opposite to that existing the control volume into the neighbouring control volume.

Fuel cell modelling, in the literature, fall into two main categories, namely empirical and numerical models. Empirical models combine theoretically derived equations with empirically (or experimentally) determined relationships. However, most of these empirical fuel cell models are concerned about the global performance of the fuel cell, which is graphically represented by the polarisation curve, without much investigation of the distribution of key variables within the GDL and other components of the PEM fuel cell model. They predict the current density based on a given cell voltage (and/or vice versa) [120] and are only useful for making quick predictions of the PEM fuel cell global performance. However, they cannot accurately predict the fuel cell performance outside the range of operating conditions under which they have been developed. Furthermore, empirical fuel cell models cannot be used to in the development of novel designs of the fuel cell or its components, or to investigate and optimise the local distribution of key parameters of temperature, pressure, current density, species concentrations, etc. in the fuel cell [124]. Experimental characterisation and investigations on the other hand have been time and cost consuming. They do not allow for changes in design and are limited in the ability to examine or investigate different materials, architecture under various operating conditions of the fuel cell.

Whereas CFD fuel cell models allow for the experimenting with novel designs, architecture, and materials, and the optimisation the influential parameters and operating conditions of the fuel cell and have received a good deal of attention over the last three decades. They are based on a number of conservation or transport

equations that can be applied to all the components of the fuel cell to investigate global performance as well as the distribution of key variables in the fuel cell. These equations describe the transport phenomena that take place in the fuel cell components and the differences between these fuel cell components can be accounted for by the use of source terms in the numerical computation. [120]. The set of conservation equations are solved in the commercial ANSYS Fluent software using the finite volume discretisation numerical techniques. This method and commercial code has been adopted in this thesis to model and investigate the PEM fuel cell.

3 TWO-DIMENSIONAL MODELLING OF THE MULTICOMPONENT SPECIES TRANSPORT IN THE CATHODE GDL OF THE PEMFC

3.1 Introduction

In the PEMFC operation, reactant gas species are consumed in the electro catalyst reaction sites which results in the depletion of the gas reactants and the production of liquid water. The depletion of the reactant gases creates a concentration gradient of the reactant gas species in the catalyst reaction sites. The porous carbon fibre GDL helps transport the gas species from the gas flow channels to maintain a constant supply at the catalyst reaction sites by convection and the multicomponent diffusion of the gases. According to [121], a constant concentration gradient, decreasing background concentrations, results in a moderate increase of the diffusion coefficients. Generally, PEMFC models in the literature have the mass, heat and charge transport coupled and solved together. For example, [122] investigated the multicomponent transport of gases in the porous GDL using volume averaging method. [123] investigated the mass and charge transport for a three-dimensional single phase PEMFC model with straight and interdigitated flow field configurations. They showed that the oxygen concentration decreased from the gas flow channels to the catalyst layers due to its consumption in the electrochemical reaction occurring in the PEMFC. [124] developed a 3-D model of the PEMFC to investigate the transient convective and diffusive transport of the gas reactants in the PEMFC. They reported that the oxygen concentration in the region of the GDL lying below the current collector rib is smaller than that of the region of GDL lying below the gas flow channels due to the diffusion and consumption of the reactant

gases. However, these studies have assumed the GDL to be isotropic and having its transport properties in one direction. On the other hand, Hossain et al. developed a two-phase model of the PEMFC to investigate the anisotropic GDL gas permeability effects on the PEMFC performance. They reported that a high isotropic gas permeability or a combination of a high in-plane and low through-plane gas permeability of the GDL results in an improved PEMFC performance while the performance decreased with a combination of low in-plane gas permeability and high through-plane permeability. Yang et al. developed a two-phase mass transport anisotropic model of the GDL to study the effects of the GDL anisotropic mass transport property. They reported that the anisotropy of the GDL significantly impacts the local distribution of current density within the cathode GDL. Stockie et al. [125] also developed a mathematical model of the fuel cathode electrode to investigate the multicomponent gas transport for an anisotropic GDL. They studied the impact of the GDL anisotropic gas permeability and gas diffusivity on the transport of reactant species within the cathode GDL. In this study, the sensitivity of the transport of reactant gas species, within the porous carbon fibre GDL, to the GDL anisotropic gas permeability and gas diffusivity is investigated. The study builds on the initial work of [125]. The model considers only the mass transfer of gases from the gas flow channel of the cathode to the catalyst layer of the cathode.

3.2 Model formulation

This section details the conservation equations that govern the transport of the gas species through the cathode gas diffusion layer of the PEMFC, their source terms in the ORR occurring at the catalyst layer, and the coupled boundary conditions.

However, the convective transport of the gas reactants within the gas flow channels of the cell is not considered in the model. Also, to simplify the model and restrict it to the transport of gas species in the cathode GDL of the PEMFC, the ionic transport in the membrane, liquid water transport within the MEA, heat, and charge transport are ignored.

3.2.1 Model assumptions

The following assumptions were made to simplify the model:

I. Steady state flow of species.

II. Flow is laminar, incompressible, and isothermal.

III. Water exists in vapour form only; therefore, the flow is single phase.

IV. Gas mixtures are ideal and uniform throughout the depth of the channel - concentration in channel is same as that immediately inside the GDL.

V. Catalytic reaction in the catalyst layer is immediate and irreversible so that the concentration inside the catalyst layer is negligible.

VI. The force of gravity is neglected, and pressure drop between the two channels is zero.

3.2.2 Model geometry

The computational domain for the model is shown in Figure 3.1. It represents a two-dimensional cross section through the cathode GDL of the PEMFC which is labelled as Ω. Where **H** represents the thickness of the GDL, $\mathbf{L_c}$ is the width of the gas flow channel, $\mathbf{L_s}$ is the width of the current collector rib between the channels on the flow field plate, **L** is the total width of model computational domain. The lower boundary of Ω at $y = 0$, represents the interface between the GDL and either the current

collector at segment **I** or the gas flow channels at segment **II**. Segment **III** represents the permeable boundary between GDL and the catalyst layer where the immediate and irreversible ORR occurs, while segment **IV** on both sides of Ω represent the periodic boundaries at $\mathbf{x = 0}$ and $\mathbf{x = L}$.

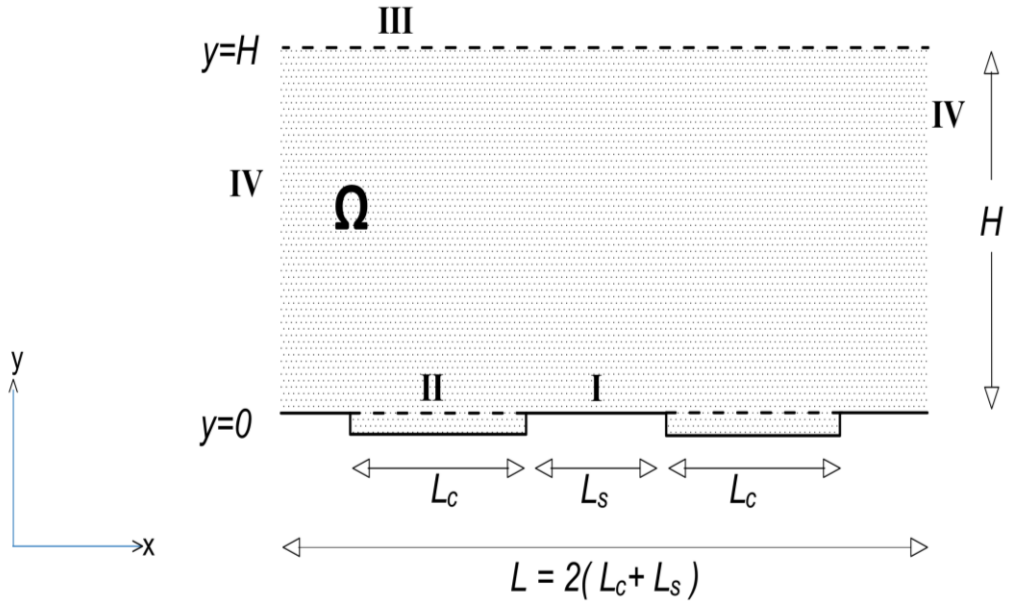

Figure 3.1 Dimensions of the computational domain.

3.2.3 Transport equations

The 2-D model developed in this investigation accounts for reactant species transport, only, within the cathode GDL. After consideration of the assumptions mentioned above and the substitution of the source terms, the convection-diffusion equation which governs the flow is presented as follows [123, 125]:

$$\nabla \cdot (\rho \vec{v} Y_i) = -\nabla \cdot \vec{J}_i + R_i + S_i \qquad \textbf{(3.1)}$$

where R_i is the net rate of production of species i by the electrochemical reaction taking place in the cathode catalyst layer, $\vec{v}$ is the molar-averaged velocity, Y_i is the mass fraction of each species i, and ρ is the gas density which is given as follows:

$$\rho = \sum_i M_i C_i \quad \textbf{(3.2)}$$

where M_i is the molar mass of each species i and C_i is the concentration of species i. The species diffusive flux vector, $\vec{J}_i$, is given as follows:

$$\vec{J}_i = -\sum_{j=1}^{n-1} \rho D_{ij} \nabla Y_j \quad \textbf{(3.2)}$$

where Y_j is the mass fraction of each species j, D_{ij} is the multicomponent diffusivity.

The corresponding source terms, S_i, for the ORR reaction in the cathode catalyst layer is given as [54]:

$$S_{O_2} = -\frac{i_c a_c}{4F} M_{O_2} \quad \textbf{(3.4)}$$

$$S_{H_2O} = \frac{i_c a_c}{2F} M_{H_2O} \quad \textbf{(3.5)}$$

i_c is the cathode current density and a_c is the cathode catalyst specific surface area and F is the Faraday constant.

3.2.4 Boundary conditions and numerical procedure

The following boundary conditions were specified and implemented for each of the four segments of the model domain:

- At segment **I**, a no slip boundary condition is specified at the wall boundary between the GDL and the current collector rib so that there is no flow across this boundary.
- For segment **III**, where y = H, it is assumed that the electrochemical reaction in this layer is spontaneous and irreversible therefore a pressure outlet boundary condition is specified here.

- At x = 0 and x = L in segment **IV**, the solution is assumed to be periodic along the x- direction and hence a symmetry boundary condition is specified in this region.
- Mole fractions for oxygen and water vapour shown in Table 3.1 are also specified at the inlet for segment **II**.

The cathode channel inlet velocity was calculated as shown in Equation 4.24 based on a typical operating current density (i_o) of 1.0 A/cm², the active area of the fuel cell (A_{act}), the channel cross-sectional area (A_{ch}). The stoichiometric ratio (ξ) of the reactant gas which was set as 2 for both hydrogen and oxygen gases.

$$u_c = \xi_c \frac{i_o}{4F} A_{act} \frac{1}{X_{O_2}} \frac{RT}{P_c} \frac{1}{A_{ch}} \quad \textbf{(4.24)}$$

The model geometrical, physical, and operational parameters are as shown in Table 3.1.

Table 3.1. Parameter values used for the two-dimensional GDE model [125].

Property	Value
GDL thickness, H	5×10^{-4} m
Model domain width, L	1.0×10^{-2} m
Channel width, L_c	2.5×10^{-3} m
Land area width, L_s	2.5×10^{-3} m
GDL permeability	1.0×10^{-12} m²
GDL porosity	0.74

Operating temperature	346.15 K
Relative humidity of inlet gases	100%
Oxygen/nitrogen molar ratio in air	0.21/0.79
Catalyst layer porosity	0.4
Viscosity, μ	2.24×10^{-5}
$D_{O_2-H_2O}$	$1.24 \times 10^{-5}\ m^2/s$
$D_{O_2-N_2}$	$1.04 \times 10^{-5}\ m^2/s$
$D_{H_2O-N_2}$	$1.23 \times 10^{-5}\ m^2/s$
Oxygen molar mass	0.032 kg/mol
Water molar mass	0.018 kg/mol
Nitrogen molar mass	0.028 kg/mol
Oxygen mole fraction	0.21
Water mole fraction	0.10
Nitrogen mole fraction	0.69
Cathode reference exchange current density, $i_{0,c}^{ref}$	$1.0 \times 10^4\ A/m^2$
Cathode specific surface area, a_c	$1.0 \times 10^7\ m^{-1}$
Faraday's constant	96485 C/mol

Universal gas constant	8.314 J/(mol-K)
inlet velocity	0.075m/s

3.2.5 Mesh independence test

To check that the solution of the gas species conservation equation does not change significantly with the mesh size, and to ensure accuracy in the model prediction, four different mesh systems were built with different mesh dimensions of X×Y= 16×12, 32×24, 64×48, and 128×96 and a mesh independence test was performed for the model with the various mesh sizes. The result of the test is shown in Figure 3.2. A mesh size of 32×24 was used for accuracy and to save computational time.

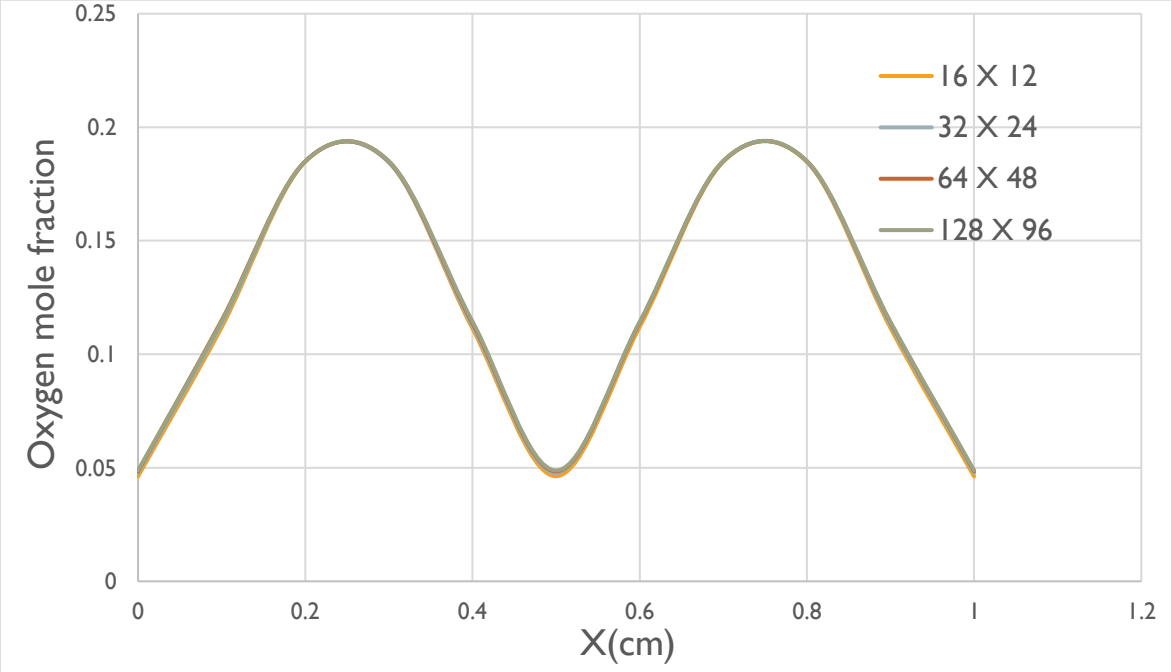

Figure 3.2 Mesh independence test.

3.3 RESULTS AND DISCUSSIONS

3.3.1 Base Case model

The result of the simulated base case model of the species transport through the GDL, based on the gas mixtures and transport properties shown in Table 3.1, are discussed in this section of the thesis. Figure 3.3 shows the contour plot of the distribution of the oxygen mole fraction within the cathode GDL for the base case model, where it is assumed that the through-plane and the in-plane components of the gas permeability and gas diffusivity are equal. Hence, the anisotropic gas permeability and anisotropic gas diffusivity ratios are equal to 1. Therefore, the GDL species transport coefficient are assumed and modelled as being isotropic. The result in Figure 3.3 shows that where there is no pressure gradient, the distribution of the oxygen mole fraction in the cathode GDL is symmetrical about the centreline x=**L**/2. The contour plot shows the decrease in the mole fraction distribution, along the through-plane direction, from the gas channel towards the GDL-catalyst layer interface. This depletion in the concentration of the of oxygen gas is as a result of the utilization of the oxygen in the ORR occurring within the catalyst layer of the fuel cell. Also, the distribution of the oxygen mole fraction narrows as we approach the GDL-catalyst layer interface. This shows that around the midpoint of the region of the GDL lying below the gas flow channels, the electrochemical reaction is enhanced and therefore more of the oxygen reactant is consumed in the catalyst layer above this region. Again, there is noticeable variation in the mole fraction distribution of the oxygen reactant along the in-plane direction, that is from x=0 to x = **L**. As can be seen, the oxygen distribution is low (along the through plane direction) for the region of the GDL lying below the current collector rib as compared to the region of the GDL below the gas flow channel. This shows that the oxygen

reactant is more consumed in electrochemical reaction in the catalyst layer around this region and therefore the oxygen is more utilised in the catalyst around this region. This observation can be explained by the fact that the compression from the current collector ribs increases the porosity of the region of the GDL under compression and hence the effective diffusion of the gas reactant from the gas channel to the catalyst layer is enhanced around this region.

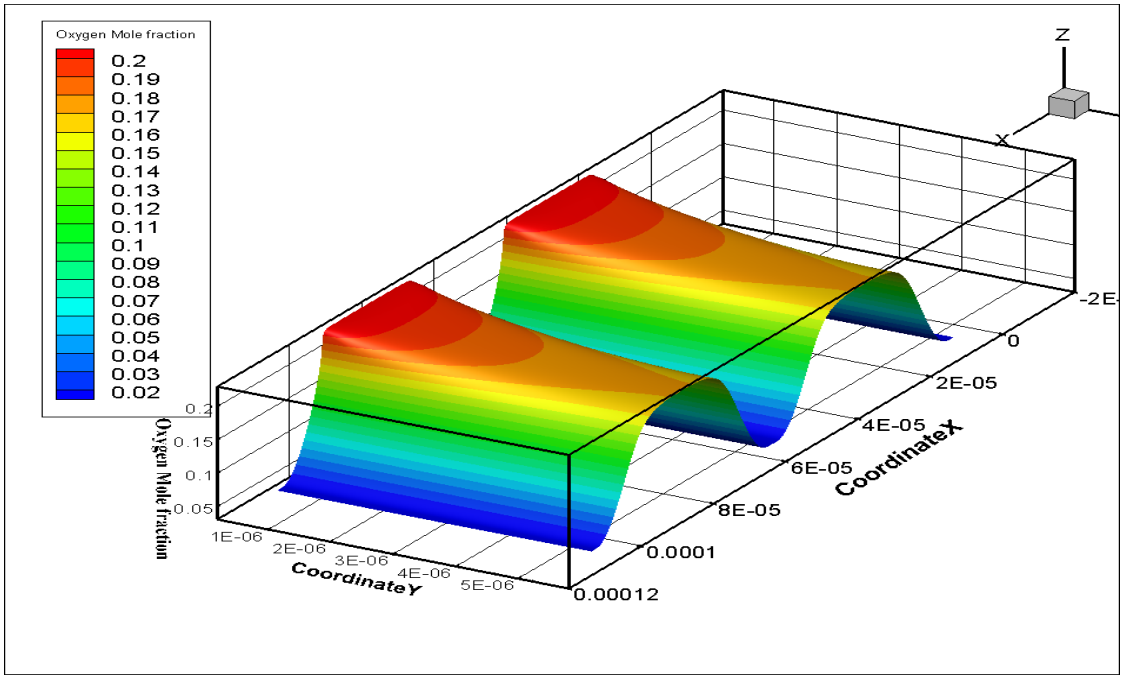

Figure 3.3 Contour plot of the oxygen mole fraction in the cathode GDL for base case.

3.3.2 Sensitivity to gas permeability

Two different cases were investigated for the effects of the anisotropy of the GDL on the GDL gas permeability. The computed cases are shown in Table 3.2. Case 1 represents the base Case where the in-plane gas permeability ($K_{=}$) and the through-plane gas permeability ($K_{\perp}$) are assumed to be equal so that the ratio of the in-plane gas permeability ($K_{=}$) to that of the through-plane gas permeability ($K_{\perp}$) is equal to 1. This represents the case where the GDL is assumed to be isotropic. For Case 2,

the in-plane gas permeability is taken to be 10 orders of magnitude higher than that of the through-plane gas permeability so that the anisotropic gas permeability ratio is equal to 10.

Table 3.2 List of computational cases investigated.

Case No.	Anisotropic Permeability ratio ($K_{=}$: $K_{\perp}$)
1.(base Case)	1
2.	10

The results of the sensitivity of the model to the GDL anisotropic gas permeability are shown in Figures 3.4 – 3.6. Figure 3.4 shows the reactant distribution at the GDL-catalyst interface for the Cases 1 (which is isotropic) and 2 (which has an anisotropic ratio equal to 10). The distribution is however symmetric. Although there is a minimal variation in the flux profiles between the isotropic and anisotropic case, the sensitivity of the model to the anisotropic permeability is less pronounced. As can be seen in Figure 3.4, the distribution of the oxygen gas reactant at the GDL-catalyst layer interface is almost insensitive to the gas permeability of the GDL. This is understandable and expected as there is no cross flow between channels and the pressure difference between the gas channels is not considered in the model. Also, the model is in single phase and the gas permeability is low, hence there is minimal or almost zero convective effect especially where the flow velocity is low. Again, the mole fraction distribution at the GDL-catalyst in Figure 3.4 shows that the gas reactant supply increases from the middle of the region of the GDL lying below the current collector rib till it reaches the peak at the middle of the region below the gas

flow channels. Again, this is due to the increased porosity due to GDL compression by the current collector. Figures 3.5 and 3.6 show the contour plots of the oxygen mole fraction for cases 1 and 2, respectively. The plots of both figures show the oxygen mole fraction to be uniform and with low concentration at all the regions of the GDL lying below the current collector rib. At the region of the GDL lying below the gas flow channels, the mole fraction decreases and narrows from the channels towards the GDL-catalyst layer interface. However, the contour plots in both Figures 3.5 and 3.6 do not show any significant variation of the mole fraction distribution for both cases (1 and 2). These plots of Figures 3.5 and 3.6 agree with the gas reactant flux of the GDL-catalyst interface shown in Figure 3.4. These results clearly show that, at low flow velocities and low permeability, the convective transport of the gas reactant species within the PEMFC is less dominant and has no significance in a steady state, single phase, and straight channel model of the transport of gas reactant species through the porous GDL of the PEMFC.

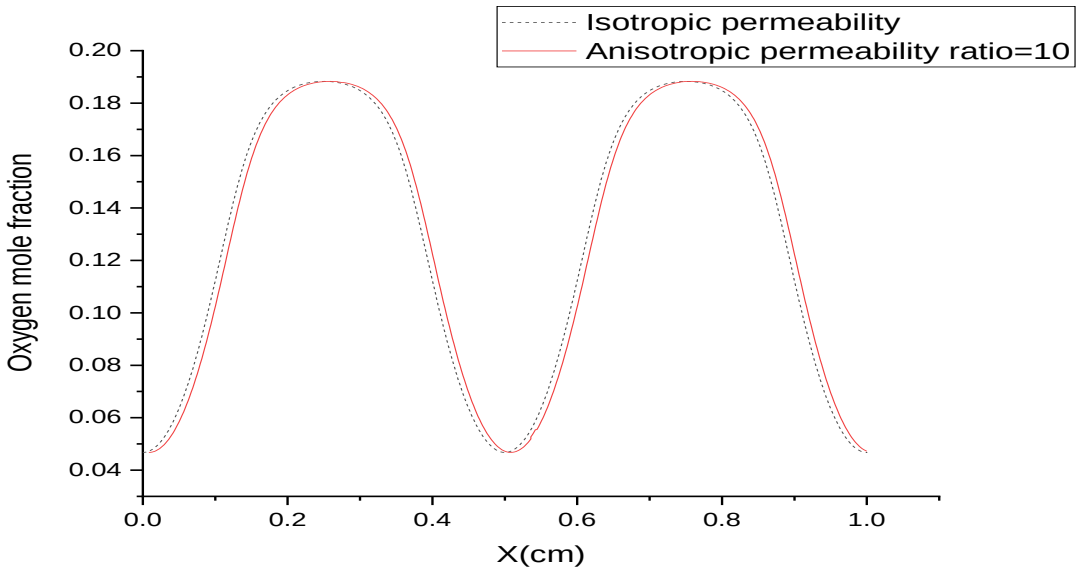

Figure 3.4 Oxygen mole fraction distribution at the GDL- catalyst layer interface for cases shown in Table 3.2, investigated for GDL gas permeability.

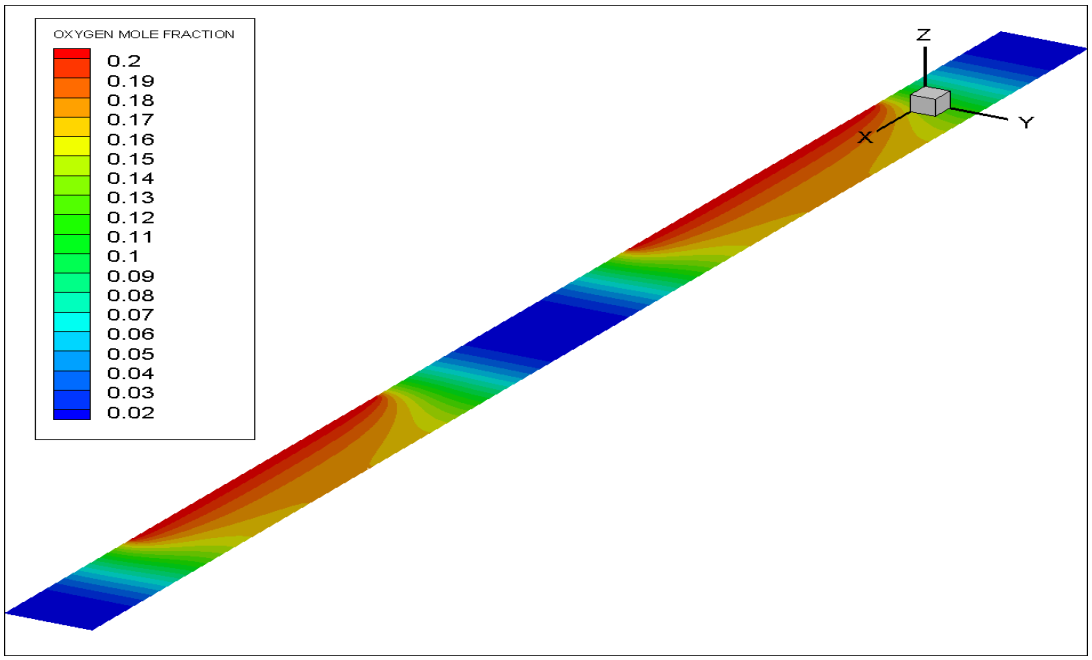

Figure 3.5 Contour plot of oxygen mole fraction in the cathode GDL for Case 2 of Table 3.2.

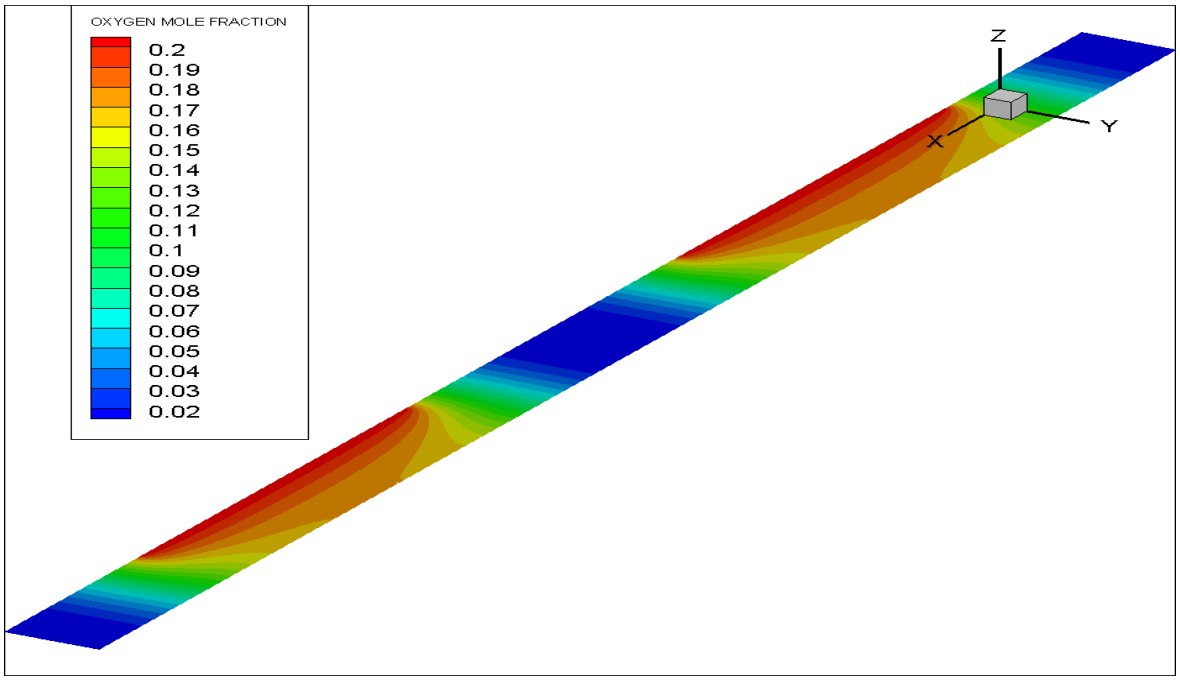

Figure 3.6 Contour plot of oxygen mole fraction in the cathode GDL for Case 3 of Table 3.2.

3.3.3 Sensitivity to gas diffusivity

Three different cases of anisotropic gas diffusivity ratios, shown in Table 3.3, were investigated for the effect of the GDL anisotropy on the diffusive transport of the gas reactant species from the gas channel to the GDL and then to the catalyst layer.

Table 3.3 List of computation cases investigated.

Case No.	Anisotropic Diffusivity ratio ($D_{=}$: $D_{\perp}$)
1(base Case)	1
2	2
3	4

$D_{=}$ and $D_{\perp}$ are the in-plane and the through-plane gas diffusivities, respectively. Case 1 represents the isotropic case where the in-plane and the through-plane diffusivities are equal. For Case 2, the in-plane diffusivity is two times that of the through-plane component, while for Case 3 the in-plane diffusivity is four times that of the through-plane. The oxygen reactant flux distribution at the GDL-catalyst layer interface is shown in Figure 3.7 for all three cases. The plot of the oxygen flux in Figure 3.7 shows that the transport of the oxygen gas reactant within the cathode GDL is sensitive to the GDL anisotropic gas diffusivity. Also, Figure 3.7 shows clearly that diffusion is the dominant mode of transport of the gas reactant species, from the gas channels to the catalyst reaction sites of the PEMFC. Considering the oxygen reactant mole fraction distribution at the GDL-catalyst layer interface shown in Figure 3.7, it is observed that at the region of the GDL lying below the gas flow channel the mole fraction distribution is overestimated for Case 1 – which is the isotropic gas diffusivity case. This is due to the Bruggemann's correlation [69,] used

in the ANSYS Fluent module. Also, the in-plane gas diffusivity is not incorporated, therefore allowing the through-plane component of the gas diffusivity to have an overall effect on the transport of the oxygen species. Thus, this shows that the Bruggemann's correlation for the gas diffusivity which is commonly used in PEMFC modeling overestimates the diffusion transport of the gas species within the PEMFC and hence does not give a realistic prediction of the mass transport in the PEMFC and its global performance. Again, considering Cases 2 and 3 in Figure 3.7, we can observe that at the region of the GDL lying below the gas flow channels, Case 2 is overestimated compared to Case 3. This can be attributed to the influence of the through-plane gas diffusivity. In this region of the GDL, the compression pressure has an insignificant effect and therefore the in-plane gas diffusivity is low so that the through-plane component of the gas diffusivity dominates the diffusive transport of the oxygen gas reactant within this region of the GDL. The region of the GDL below the current collector rib shows that Case 1 has a better oxygen consumption compared to Case 2 and Case 3. This is as a result of the influence of the Bruggemann's correlation of the diffusivity used for the isotropic diffusivity case (Case 1) of Table 3.3 which is higher and not unrealistic and also the low value of the in-plane diffusivity in Case 2 as compared to that of Case 3. The in-plane gas diffusivity helps improve the consumption of the oxygen gas reactant in the region of the GDL lying below the gas channel. Figures 3.8 to 3.10 further emphasizes the effect of the in-plane GDL gas diffusivity on the transport of the oxygen gas reactant within the GDL. It can be seen from the contour plots, of Figures 3.8-3.10, that the oxygen gas is more utilised when the gas diffusivity ratio of the GDL is increased (as shown in the cases of Table 3.3). Figure 3.10 shows an improved distribution of the oxygen mole fraction within the GDL for the region of the current collector rib as

compared to those of Case 1 and Case 2 in Figures 3.8 and 3.9, respectively. This further shows the influence of the in-plane gas diffusivity in the transport of the gas reactants withing the GDL of the PEMFC. Also, in Figure 3.10 we see that in the region of the GDL lying below the current collector ribs, the oxygen gas is well utilised. This means that the in-plane diffusivity as well as the through-plane gas diffusivity play very important roles in the local distribution of the gas reactants within the GDL of the PEMFC and helps improve its local performance within the GDL.

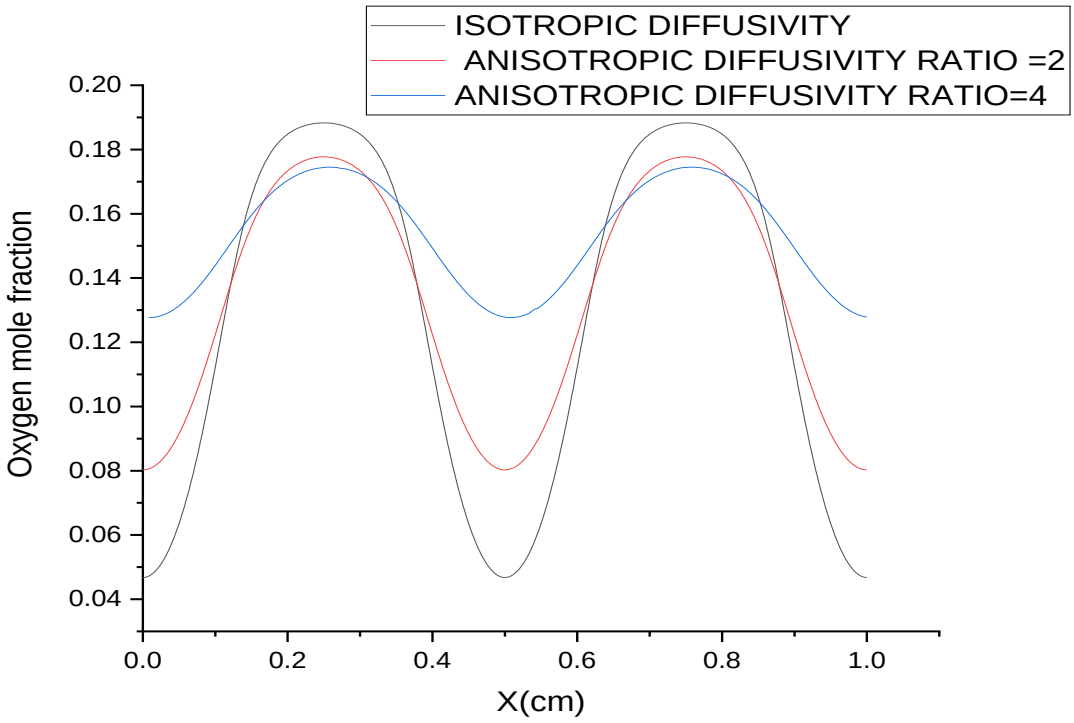

Figure 3.7 Oxygen mole fraction distribution at the GDL- catalyst layer interface for the cases investigated in Table 3.3.

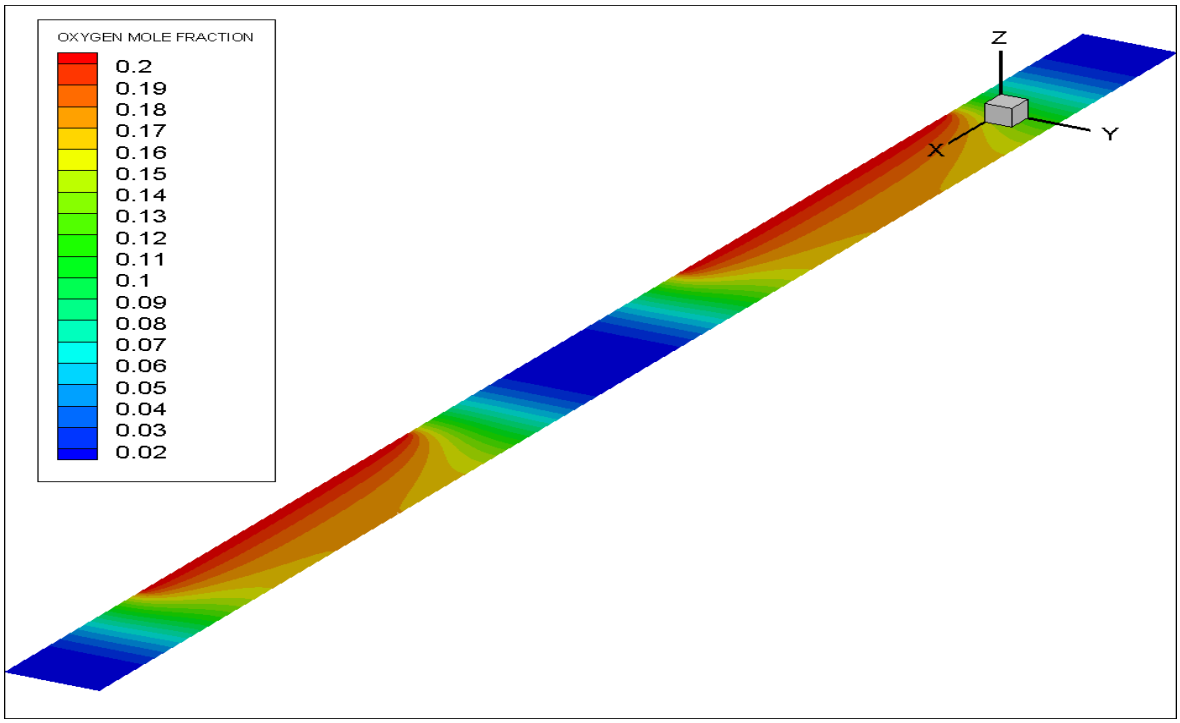

Figure 3.8 Contour plot of oxygen mole fraction in the cathode GDL for Case 1 of Table 3.3.

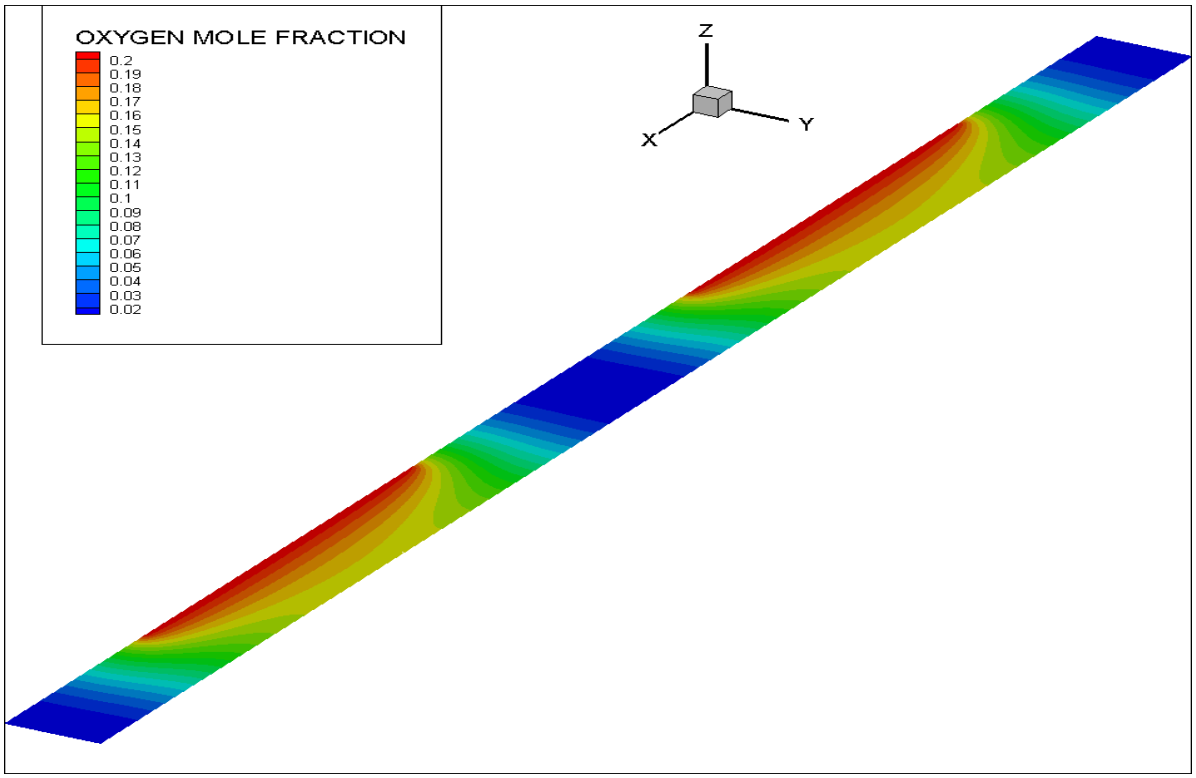

Figure 3.9 Contour plot of oxygen mole fraction in the cathode GDL for Case 2 of Table 3.3.

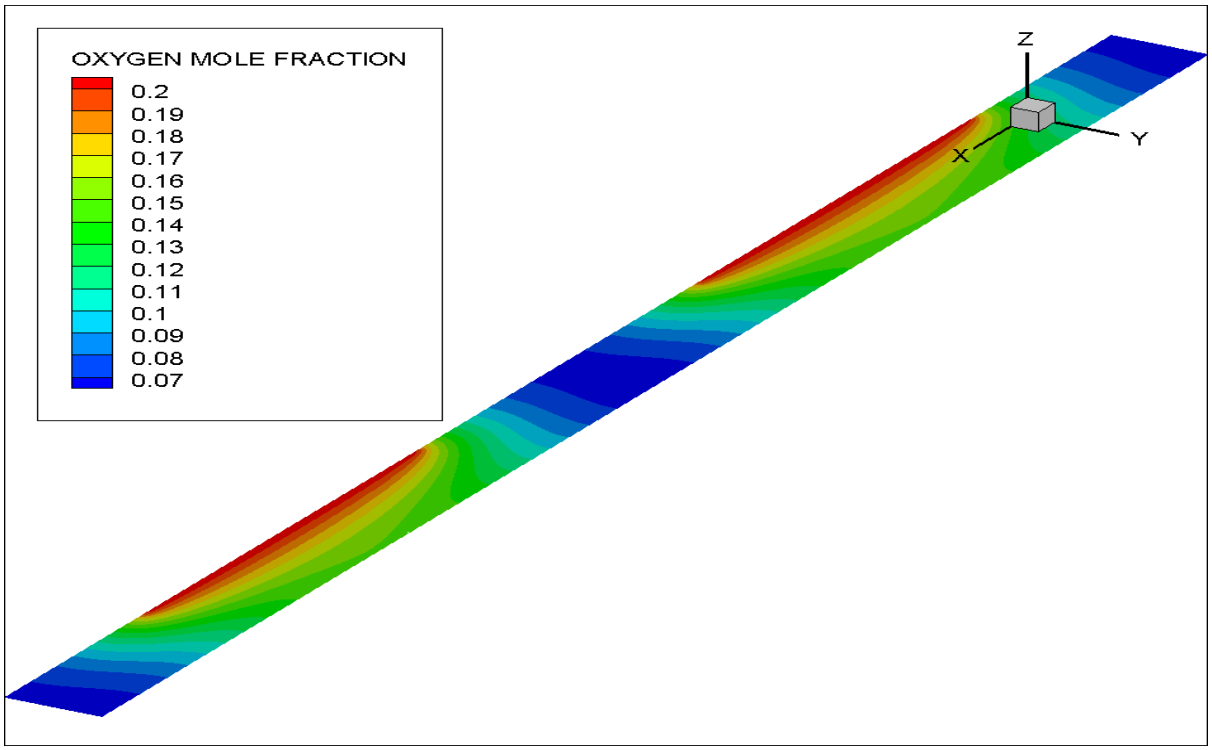

Figure 3.10 Contour plot of oxygen mole fraction in the cathode GDL for Case 3 of Table 3.3.

3.4 Conclusions

A 2-D model of the multicomponent transport of gas species within the cathode GDL was developed in **Chapter 3** of the thesis, using ANSYS Fluent software, to investigate the sensitivity of the transport of reactant gas species to the GDL anisotropic gas permeability and the gas diffusivity. A parametric study using the anisotropic ratios (in-plane vs through-plane) of the gas permeability and gas diffusivity were used to test the sensitivity of the species transport to the anisotropy of the GDL. the key findings and observations of both investigations are as follows:

- At low flow velocities and gas permeability, the convective transport of the gas reactant species from the channel to the catalyst reaction sites is less

dominant and has no significance in a steady state, single phase model of the GDE. While the transport of species is dominated and controlled by the diffusion mechanism in the GDL.

- the distribution of the oxygen gas reactant at the GDL-catalyst layer interface is almost insensitive to the gas permeability of the GDL. This is understandable and expected as there is no cross flow between channels and the pressure difference between the gas channels is not considered in the model.
- The compression of the GDL by the current collector ribs increases the porosity of the GDL in the region lying under the current collector rib so that the diffusion of the gas reactant from the gas channel to the catalyst layer is increased around this region. As a result, the oxygen is more utilized in the catalyst layer.

4 EFFECTS OF GAS DIFFUSION LAYER ANISOTROPIC TRANSPORT PROPERTIES ON THE PEM FUEL CELL PERFORMANCE

4.1 Introduction

The gas diffusion layer of the polymer electrolyte membrane fuel cell is made up of solid (carbon, binder, and PTFE) and void phases. It is a crucially important component for the PEMFC as it is responsible for the transport of gas reactants, heat and electrons between the flow-field plates and the catalyst layers, and the provision of mechanical support to the delicate catalyst layers [26,82]. It is evident that limited transfer rate of gas reactants to the catalyst layers results in a decreased overall PEMFC performance. On the other hand, high availability of reactant gases in the catalyst reaction sites does not only improve the fuel cell performance but also reduces the amount of precious platinum catalyst required for the electrochemical reactions in the cell, thus making the PEMFC more efficient and cost-effective [82]. To this end, the GDL should possess high mass transport properties (i.e., gas diffusivity and permeability) to quickly supply enough reactant gases to the catalyst layers and at the same time effectively remove excess water generated at the cathode catalyst layer. Equally, the GDL should demonstrate high electrical conductivity to minimise ohmic losses and high thermal conductivity to dissipate heat generated within the membrane electrode assembly (MEA) and subsequently prevent the dry-out of the membrane electrolyte.

The conventional GDLs are made from carbon fibres, which are preferentially oriented in the in-plane directions, thus resulting in anisotropic transport properties

[129]. To this end, there have been a good number of experimental and numerical studies on investigating the anisotropic nature of the GDL and estimating its transport properties in different principal directions. Zamel et al. [95] developed a 3-D reconstruction model of a carbon paper GDL to numerically estimate the effective electrical conductivity, at different values of porosity, for both through -plane and in-plane directions. They found the in-plane electrical conductivity to be higher than that in the through-plane direction by about 25% for high GDL porosity values between 0.7 to 0.9, and at low porosity values of 0.4 to 0.6, about 43.7%. Also, they proposed mathematical correlations to determine the effective electrical conductivity for the carbon fibre paper GDL and found the tortuosity factor to be 3.4 in the through-plane direction while that of the in-plane was reported to be 1.7. Zamel et al. [58] numerically estimated the effective thermal conductivity of untreated carbon fibre paper GDL, using GeoDict code to reconstruct a realistic 3-D morphology of the carbon paper GDL. They found the thermal conductivity to be higher in the in-plane as compared to that of the through-plane by a factor of 2. Also, they found that the effective thermal conductivity increased with a decrease in the porosity of the GDL. Wu et al. [75,76] developed a 3-D pore network model of a TGP-H-60 Toray carbon paper with spherical pores and cylindrical throats. They proposed two correlations for the gas diffusibility and water saturation function. Veyret and Tsotridis [92] developed a 3-D numerical model to estimate the effective thermal conductivity of the GDL. They reported that the anisotropic ratio for the GDL thermal conductivity (i.e., the ratio between the in-plane and the through- plane thermal conductivity) increases with increasing GDL porosity. Nikooee et al. [93], using pore fraction approach, numerically estimated the effective thermal conductivity of untreated carbon paper GDL. They proposed a fractal equation to determine the

through-plane thermal conductivity of the GDL. Zamel et al. [79] experimentally measured the effective diffusivity of carbon paper GDL using Loschimdt cell. They reported that the diffusibility of the GDL is not affected by temperature but reduces when GDL is treated with PTFE. Kramer et al. [83] applied electrochemical impedance spectroscopy (EIS) to measure the effective diffusivity in the in-plane and through -plane directions as a function of the compression of the GDL paper. Fluckiger et al. [84], using the electrochemical diffusimetry method initially developed by [83], measured the in-plane and through-plane diffusivities for three different carbon fibre paper materials, namely TGP-H-060, GDL24 and GDL25. They investigated the effect of the binder structure and the Teflon treatment on the anisotropy and the effective diffusivity of the different GDL samples. They showed that an improved through-plane diffusivity is essential for high limiting current densities. Also, they reported that the ratio of the in-plane diffusivity to the through-plane diffusivity depends on the orientation of the carbon fibres, the properties of the binders, the PTFE treatment as well as the GDL compression. Khandelwal and Mench [55] experimentally measured the through-plane thermal conductivity and the thermal contact resistance of several GDLs from various manufacturers (SIGRACET and TORAY), at different temperatures, for treated and untreated GDLs. They employed the steady state measurement method. They found the thermal conductivity for the Toray carbon paper to be around 1.80 W/m·K at 26℃, and it decreases when the temperature is increased. For the SIGRACET manufactured carbon paper GDLs, the thermal conductivity for 0 (i.e., untreated GDL), 5 and 20 wt.% PTFE treated GDLs were found to be around 0.48, 0.31 and 0.22 W/m·K respectively. In addition, they reported a decrease in GDL thermal conductivity with an increase in PTFE content. Building upon the work of Khandelwal

and Mench [57], Ramousse et al. [94] theoretically and experimentally estimated the thermal conductivity of Quintech and SGL GDLs. They showed that the thermal conductivity of the different GDLs is highly orthotropic. Ismail et al. [129] experimentally measured the in-plane gas permeability for five different SGL carbon substrates varying in PTFE content. They reported a decrease in the in-plane gas permeability of the carbon substrate with an increase in the PTFE content. They also reported that the in-plane gas permeability of the carbon substrate decreases by an order of magnitude when coated with the microporous layer (MPL). Gostick et al. [49] measured the gas permeability in three perpendicular directions for several carbon fibre GDL substrates including SGL and Toray GDLs. They also measured the in-plane permeability of the GDL samples as a function of compression. They reported that the GDL samples with the most highly aligned fibres displayed the highest anisotropy, and their permeability could differ by a factor of 2. They also showed that the compression of any one sample to half its thickness decreases the in-plane gas permeability of the substrates by an order of magnitude. Becker et al. [80] combined both experimental and numerical approaches to characterise the anisotropic transport properties of a Toray TGP-H-060 carbon paper, considering the effects of GDL compression on these transport properties. They reported the in-plane diffusivity to be twice that of the through-plane and that GDL compression ratio of about 23% reduces the diffusivity of the GDL in both directions by 30%. They also found the in-plane permeability to be four times higher than the through-plane permeability. Likewise, the in-plane electrical conductivity was found to be an order of magnitude higher than that in the through-plane direction. Using periodic surface modelling, Didari et al. [77] numerically characterised the gas permeability and relative diffusivity for a Toray TGP-H-060

carbon GDL. They reported a larger binder volume fraction effect on the permeability, diffusibility and tortuosity factor of the GDL as compared to the actual tortuosity of the GDL. They also reported that these GDL morphological characteristics and transport properties have larger changes along the through-plane direction as compared to the in-plane. Chan et al. [104] used a Loschimdt cell with oxygen-nitrogen mixture to measure the effective through-plane diffusibility of coated and uncoated GDL samples. They found that the Bruggeman correlation [69] over-predicts the effective diffusivity of the GDL material by at least 60%. Tomadakis & Sotirchos [74] numerically characterised the effective diffusivity in both the through-plane and the in-plane directions of the GDL, using a Monte Carlo simulation scheme. They reported the effective diffusivity to be strongly dependent on the orientation of the fibres, the porosity of the GDL and the Knudsen number. Gostick [130] developed a 3D pore network model of the GDL to numerically characterize the gas diffusivity of the GDL. The author numerically estimated the relative effective diffusivity in partially saturated GDL pore networks and reported a decay of approximately 1-S_w for both through-plane and in-plane directions which is lower than the exponent of 5 used in existing literature. James et al. [80] used X-ray computed tomography of the GDL to numerically estimate transport properties of an SGL carbon substrate: 30BA. They reported that the computationally obtained effective gas diffusivity is at least 15% lower than approximated using Bruggeman correlation [69]. They also showed that the effective electrical conductivity and diffusivity in the in-plane directions are four times larger than in the through-plane direction. Nam and Kaviany [78] developed a numerical model to estimate the effective diffusivity of carbon fibre GDL as a function of the porosity of the GDL and water saturation. They showed that the fibre alignment in the lateral direction, where

there is no pore blockage, results in a higher in-plane effective diffusivity. Also, at low porosities (less than 0.45), the through-plane diffusivity was found to be larger than that in the in-plane direction.

Clearly not capturing the anisotropic nature of the GDL in the PEFC models would negatively impact the accuracy of the predictions of these models. The literature shows that there have been some attempts to investigate the impact of the anisotropic GDL on the performance of the modelled PEFCs. Pharaoh et al. [33] investigated the effect of the anisotropic diffusivity and electrical conductivity on the performance of the modelled PEFC cathode. They showed that treating the electrodes as isotropic porous media yields significantly different current density predictions than anisotropic treatments. Using a 2-D single phase numerical PEFC, Bapat and Thynell [31] investigated the effects of the anisotropic thermal conductivity and the thermal contact conductance on temperature distribution in the PEFC. They reported that though an increase in the in-plane thermal conductivity of the GDL resulted in smaller temperature gradients, and the improvement in the heat transport is limited by the thermal contact resistance between the GDL and the bipolar plates. Pasaogullari et al. [55] developed a 2-D, non-isothermal, two-phase cathode side PEFC model to investigate the effect of the GDL anisotropy on the coupled heat and mass transfer within the cathode of the PEFC. They showed that the maximum temperature difference in the GDL is a strong function of the of the GDL anisotropy. Also, they reported that relatively high in-plane thermal conductivity values result in significantly different liquid water saturation distributions. Ju [56] developed a 3-D, two -phase PEFC model to study the effects of GDL anisotropic transport properties on PEFC performance as well as on heat and water transport in the cell. The author reported a significant variation of the PEFC temperature along

the through-plane direction when the in-plane thermal conductivity is an order of magnitude higher than the through-plane thermal conductivity. Alhazmi et al. [131] numerically investigated the effect of the GDL anisotropic thermal conductivity at three different PEFC operating temperatures, using a 3-D multiphase model of the PEFC. They reported a greater sensitivity of the temperature gradients within the PEFC to the in-plane thermal conductivity of the GDL as opposed to that of the through -plane direction. They also reported an increase in the power density of the PEFC when the in-plane and through-plane thermal conductivities are increased. Xing et al. [132] studied the effect of GDL anisotropy on transport of species, electric charge, heat, and liquid water in PEFCs operated at various loads, using a non-isothermal multi-phase flow numerical model of the PEFC. They reported that the anisotropic gas diffusivity does not influence PEFC cell performance at low current densities but at higher current densities. Their results showed negligible influence of the anisotropic gas permeability and thermal conductivity on the PEFC performance. Yoshimune et al. [133] experimentally measured the through-plane diffusivity for Toray carbon paper GDL, TGP-H-060 using infrared absorption carbon dioxide sensor. They found the through-plane diffusivity of the GDL sample to be 0.36 ± 0.02 at a temperature $25℃$. Taş and Elden [134] experimentally measured the through-plane and in-plane electrical conductivities of SGL34BA and SGL34BC (a bilayer gas diffusion layer with a microporous layer) Sigracet gas diffusion layers. They investigated the effects of the PEFC operating temperature, the relative humidity, and the clamping pressure on the anisotropic electrical conductivities of the tested gas diffusion materials. They reported no significant change in the in-plane electrical conductivity, of both the SGL34BA and SGL34BC GDL samples, with increasing PEFC operating temperature and clamping pressure. However,

there was significant change in the in-plane electrical conductivity for the measured GDL samples under different relative humidity. For a RH range of 70-100%, temperature range of 50-80℃, and clamping pressure of 2-8bars. They also reported an increase in the through-plane electrical conductivity, of both GDL samples, with increased cell operating temperature and clamping pressure. However, there was no remarkable change in the through-plane electrical conductivity when the cell was operated at different relative humidity values. Taş and Elden [135] numerically developed a three-dimensional PEFC model in which they integrated their previously experimentally measured values of anisotropic electrical conductivities for SGL34BA and SGL34BC carbon gas diffusion layers. In their model, they investigated the effects of the PEFC operating temperature and the relative humidity on the anisotropic electrical conductivities of the GDL samples. They reported an increase in the output current densities in the in-plane direction with an increase in temperature. For the through-plane directional component, they reported a maximum value of current density in the region of the GDL lying underneath the ribs of the bipolar plates. They also reported that the anode electrical potential increases gradually with increased relative humidity for both the in-plane and through-plane directions. In addition, they observed and reported an increase in the current density with increasing relative humidity for both the in-plane and the through-plane electrical conductivity. Zhang et al. [136] developed a three-dimensional multiphase PEFC model to investigate channel and gas diffusion layer flows in the PEM fuel cell. They investigated the effect of the GDL anisotropic effective electrical conductivity, the anisotropic gas diffusivity, and the anisotropic intrinsic permeability on the performance of the PEFC model. However, the effect of anisotropic thermal conductivity was not investigated in their developed model.

They used the Bruggeman correlation to model the effective electrical conductivity and the effective gas diffusivity. Therefore, their model showed a higher cell overpotential for the case with anisotropic GDL transport properties when compared to that with isotropic GDL transport properties. They reported the oxygen mass fraction distribution to be under predicted for the anisotropic GDL model while it is over predicted for the case with isotropic GDL transport properties. In addition, they reported that there is no significant change or difference for the intrinsic permeability of the isotropic and anisotropic GDL. They reported a lower liquid water saturation in the GDL region lying under the rib for the case with anisotropic transport properties while that of the isotropic GDL was over predicted. This, they claim was due to the higher intrinsic in-plane permeability of the anisotropic GDL. Wang et al. [137] proposed and developed a three-dimensional multiphase PEFC model with through-plane and in-plane synergetic gradient porosity distribution in the cathode gas diffusion layer. They investigated the effects of the through-plane graded porosity distribution, the in-plane graded porosity distribution, and the uniform porosity distribution on the overall performance of the PEFC model as well as on the distribution of current density and oxygen mass fraction within the cathode GDL. They reported that a higher porosity within the region of the GDL lying close to the flow channel (for the through-plane gradient porosity distribution), while there is a higher or lower porosity at the section of the cathode outlet for the in-plane gradient porosity distribution. This improves the transport of the gas reactants and the liquid water removal from the PEFC. This results in a uniform distribution of oxygen and current density within the cathode GDL. Yu et al. [138] also developed a three-dimensional, non-isothermal, two-phase agglomerate PEFC model incorporating the difference in porosities of the region of the GDL under the rib and that under the

gas flow channel. They investigated the effects of the GDL anisotropic transport properties - electrical conductivity, thermal conductivity, gas permeability, and the gas diffusivity on the current density distribution within the PEFC, temperature distribution, liquid water, and gas reactant concentrations. They reported that the in-plane values of these GDL transport properties are several orders of magnitude higher than those in the through-plane direction. In addition, they reported lower current density distribution at the region of the GDL lying under the gas channel when the cell is operated at lower cell voltages. They also reported that the effects of the GDL gas permeability is insignificant. They showed that the integral values of the GDL anisotropic transport properties are lower than that of the isotropic GDL model. Ismail et al. [127] developed a 3-D PEFC model of an in-house built PEFC to study the effects of GDL anisotropic gas permeability and electrical conductivity on the performance of the PEFC. They found the PEFC performance to be almost insensitive to the GDL anisotropic permeability and highly sensitive to the GDL anisotropic electrical conductivity. Li et al. [28] developed a 3-D, two-phase, non-isothermal model of the PEMFC in which they investigated the effects of GDL anisotropic gas permeability, gas diffusivity thermal conductivity and electrical conductivity on PEMFC performance. They demonstrated that the temperature of the anisotropic case is more uniform and lower than that of the isotropic case owing to the relatively high in-plane thermal conductivity at high current densities. They also reported severe liquid water saturation in the isotropic GDL case model as compared to that of the anisotropic case.

It should be noted that in all the above studies, there have been no three-dimensional numerical PEMFC models that have incorporated the experimentally measured multidimensional values of each of the gas diffusivity, the gas

permeability, the thermal conductivity, and the electrical conductivity of the GDLs. Therefore, to improve the predictions, a three-dimensional PEMFC model was built, which accounts for the anisotropic nature of the GDLs though employing experimentally measured values of the above key transport properties. After validating the model, we have performed a parametric study by realistically increasing/decreasing the base experimentally estimated value of each of the above-mentioned transport properties. This is performed to investigate the impact of not capturing the anisotropy for each of the above-mentioned transport properties on the performance of the modelled PEM fuel cell and the distribution of the key variables of current density and oxygen concentration, and subsequently obtain insights on how to improve the fuel cell efficiency.

4.2 Model description and transport equations

This section details the conservation equations that govern the transport of the physical quantities and their source terms as well as the electrochemical reactions, which occur within the PEM fuel cell. The PEMFC model developed in this study is based on the PEMFC model of Berning et al. [62].

4.2.1 Model assumptions

The following assumptions are made to simplify the PEMFC model:

- Steady-state operation.
- Laminar and incompressible flow.
- Membrane is impermeable to the reactant gases.
- Uniform compression on all components of the fuel cell.

- Water exists in vapour phase only to isolate the impact of water saturation and solely focus on the impact of the GDL anisotropy.

4.2.2 Model geometry

The computational domain of the PEMFC model consists of cathode and anode bipolar plates (or current collectors), cathode and anode flow channels, cathode and anode catalyst layers and the membrane electrolyte. The computational domain is, to save computational time, limited to a portion incorporating cathode and anode straight gas flow channels. Further, due to symmetry, only half channel width is considered; see Figure 4.1. The geometrical, operational, and physical parameters are presented in Table 4.1.

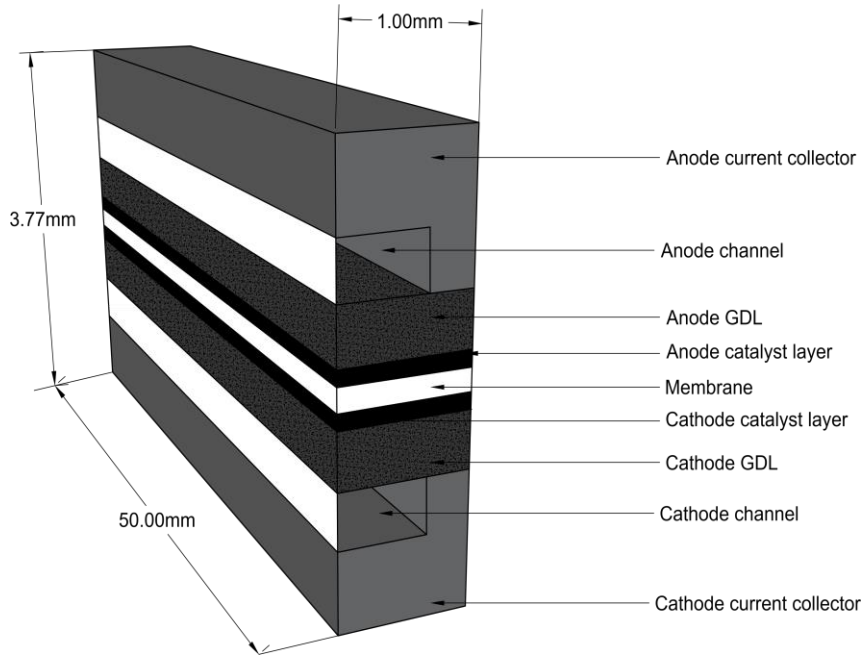

Figure 4.1 Schematic geometry of the computational domain.

4.2.3 Transport equations

The following equations govern the transport of the physical quantities in all components of the modelled PEMFC [28, 31, 67, 127,130, 131, 139]:

Mass transport equation

$$\nabla \cdot (\varepsilon \rho \vec{u}) = 0 \quad \textbf{(4.1)}$$

where ρ is the gas mixture fluid density, ε is the porosity and $\vec{u}$ is the fluid velocity vector.

Momentum transport equation

$$\nabla \cdot (\varepsilon \rho \vec{u}\vec{u}) = -\varepsilon \nabla P + \nabla \cdot (\mu \nabla \varepsilon \vec{u}) + \frac{\varepsilon^2 \mu \vec{u}}{K} \quad \textbf{(4.2)}$$

where P is the pressure of gas mixtures, μ is the dynamic viscosity of the fluid and K is the permeability of the porous medium.

Species transport equation

$$\nabla \cdot (\varepsilon \rho \vec{u} Y_i) = \nabla \cdot (\rho D_{ij}^{eff} \nabla Y_i) + S_i \quad \textbf{(4.3)}$$

where Y_i is the mass fraction of species i and D_{ij}^{eff} is the effective binary diffusivity of species j into i. D_{ij}^{eff} is calculated using the Bruggeman's correlation as follows [67]:

$$D_{ij}^{eff} = \varepsilon^{\tau} D_{ij} \quad \textbf{(4.4)}$$

where τ is the tortuosity of the porous medium and D_{ij} is bulk binary diffusivity of species i into j. S_i is the source term that represents either consumption/production of species k (H_2, O_2 or H_2O) and is given as follows [127]:

$$S_{H_2} = -\frac{i_a a_a}{2F} M_{H_2} \quad \textbf{(4.5)}$$

$$S_{O_2} = -\frac{i_c a_c}{4F} M_{O_2} \quad \textbf{(4.6)}$$

$$S_{H_2O} = \frac{i_c a_c}{2F} M_{H_2O} \quad \textbf{(4.7)}$$

where i_a and i_c are the anodic and cathodic local current density respectively, a_a and a_c are the anodic and cathodic specific surface areas respectively, F is Faraday constant (96485 C/mol) and M_{H_2}, M_{O_2} and M_{H_2O} are the molecular weights for hydrogen, oxygen, and water, respectively.

Energy transport equation

$$\nabla \cdot \left(\rho c_p \vec{u} T\right) = \nabla \cdot (K_{eff} \nabla T) + S_e \quad \textbf{(4.8)}$$

where T is the temperature, c_p is the specific heat capacity of the gas mixtures, K_{eff} is the effective thermal conductivity. S_e is the heat source term and takes one of the following forms in each fuel cell component [28]:

$$S_e = \begin{cases} i_s^2/\sigma_s \text{ for anode and cathode GDLs} \\ i_{0,a}\left[\eta_a - \frac{T\Delta S_a}{2F}\right] + \frac{i_s^2}{\sigma_s} + \frac{i_m^2}{\sigma_m} \text{ for anode catalyst layer} \\ i_{0,c}\left[-\eta_c - \frac{T\Delta S_c}{2F}\right] + \frac{i_s^2}{\sigma_s} + \frac{i_m^2}{\sigma_m} \text{ for cathode catalyst layer} \end{cases} \quad \textbf{(4.9)}$$

where $i_{0.a}$ and $i_{0,c}$ are the anode and cathode exchange current densities, i_s and i_m are the solid phase and membrane phase current densities, σ_s and σ_m are the electrical and ionic conductivities of the solid and membrane phases respectively, and η_a and η_c are the anodic and cathodic overpotential, ΔS_a and ΔS_c are the reaction entropies at anode and cathode catalyst layers respectively.

Charge transport equations

Two potential equations for the electronic and ionic conduction are solved. The equations are expressed as follows:

$$\nabla \cdot (\sigma_s \nabla \phi_s) = S_{\phi,s} \quad \textbf{(4.10)}$$

$$\nabla \cdot (\sigma_m \nabla \phi_m) = S_{\phi,m} \quad \textbf{(4.11)}$$

where ϕ_s and ϕ_m are the electrical (solid phase) and ionic (membrane phase) potentials respectively. $S_{\phi,s}$ and $S_{\phi,m}$ are the solid-phase potential and membrane-phase potential, respectively and are given as follows [131]:

$$S_{\phi,s} = \begin{cases} j_a \text{ at the anode CL} \\ -j_c \text{ at the cathode CL} \end{cases} \quad \textbf{(4.12)}$$

$$S_{\phi,m} = \begin{cases} -j_a \text{ at the anode CL} \\ j_c \text{ at the cathode CL} \end{cases} \quad \textbf{(4.13)}$$

where j_a and j_c are the volumetric exchange current density (A/m³) at the anode and cathode catalyst layers, respectively, and are obtained using Butler-Volmer equations [139]:

$$j_a = i_a^{ref} a_a \left(\frac{c_{H_2}}{c_{H_2}^{ref}}\right)^{0.5} \left[\exp\left(\frac{\alpha_{a,a} F}{RT}\eta_{act,a}\right) - \exp\left(\frac{\alpha_{a,c} F}{RT}\eta_{act,a}\right)\right] \quad \textbf{(4.14)}$$

$$j_c = i_c^{ref} a_c \left(\frac{c_{O_2}}{c_{O_2}^{ref}}\right) \left[\exp\left(\frac{\alpha_{c,a} F}{RT}\eta_{act,c}\right) - \exp\left(\frac{\alpha_{c,c} F}{RT}\eta_{act,c}\right)\right] \quad \textbf{(4.15)}$$

where $i_a^{ref}$and i_c^{ref} are the reference anodic and cathodic exchange current density respectively, $\alpha_{a,a}$ and $\alpha_{a,c}$ are respectively the anode and cathode transfer coefficients for the electrochemical reactions in the anode catalyst layer, $\alpha_{c,a}$ and $\alpha_{c,c}$ are, respectively, the anode and cathode transfer coefficients in the cathode catalyst layer, $c_{H_2}^{ref}$ and $c_{O_2}^{ref}$are the reference hydrogen and oxygen concentration, respectively, F is the Faraday's constant and R is the universal gas constant. $\eta_{act,a}$ and $\eta_{act,c}$ are the anodic and cathodic overpotential and are given as follows:

$$\eta_{act,a} = \phi_s - \phi_m \quad \textbf{(4.16)}$$

$$\eta_{act,c} = \phi_s - \phi_m - E_0 \quad \textbf{(4.17)}$$

where E_0 is the reference potential of the electrodes and is equal to zero for the anode, while for the cathode it is equal to the equilibrium cell potential (E_r) [31, 130]:

$$E_r = 1.482 - 0.000845T + 0.0000431T\ln\left(P_{H_2} P_{O_2}^{0.5}\right) \quad \textbf{(4.18)}$$

The membrane ionic conductivity, σ_m, is estimated using an empirical correlation developed by [140]:

$$\phi_m = (0.005139\lambda - 0.00326)\exp\left[1268\left(\frac{1}{303} - \frac{1}{T}\right)\right] \quad \textbf{(4.19)}$$

where λ is the membrane water content which is empirically correlated by [139]:

$$\boldsymbol{\lambda} = \begin{cases} 1.409 + 11.26ac - 18.77ac^2 + 16.21ac^3, 0 < ac \leq 1 \\ 10.11 + 2.944(ac - 1), 1 < ac \leq 3 \\ 16.8, \ ac > 3 \end{cases} \quad \textbf{(4.20)}$$

where ac is the water activity and is given as [127]:

$$ac = \frac{P_v}{P_s} \quad \textbf{(4.21)}$$

where P_v is the partial pressure of water vapour and P_s is the pressure of saturated water vapor which is given by [127]:

$$\log(P_s) = -2.1794 + 0.02953(T - 273.15) - 9.1837 \times 10^{-5}(T - 273.15)^2 + 1.4454 \times 10^{-7}(T - 273.15)^3 \quad \textbf{(4.22)}$$

4.2.4 Boundary conditions and numerical procedure

Velocity inlet boundary conditions are specified for the anode and cathode gas flow channels. The operating temperature (353K) and the species mass fractions are specified at the flow channel inlets. The fluid inlet velocity is defined as a function of a typical operating current density (i_{op}) which is in this case 500 mA/cm², the active

area of the fuel cell (A_{act}), the channel cross-sectional area (A_{ch}), and the stoichiometric ratio (ξ) of the reactant gas which was set as 2 for both hydrogen and oxygen gases. Therefore, the anodic and the cathodic inlet velocities are given as follows [62]:

$$u_a = \xi_a \frac{i_{op}}{2F} A_{act} \frac{1}{X_{H_2}} \frac{RT}{P_a} \frac{1}{A_{ch}} \quad \textbf{(4.23)}$$

$$u_c = \xi_c \frac{i_{op}}{4F} A_{act} \frac{1}{X_{O_2}} \frac{RT}{P_c} \frac{1}{A_{ch}} \quad \textbf{(4.24)}$$

Zero-flux boundary conditions are specified for all wall boundaries, except for the anode and cathode terminals (i.e., the top surfaces of the current collectors). The pressure outlet boundary conditions are specified at the outlet of the gas flow channels. Potentiostatic boundary conditions are specified for the anode and cathode current collector terminals of the cell, respectively, with the electrical potential for the anode set to zero (ground voltage) and that of the cathode set to the cell operating voltage (V_{cell}). A constant operating temperature of 353K is set for both the anode and cathode terminals. The equations governing the transport of mass, heat, and charge in the PEMFC model and the coupled boundary conditions were solved iteratively, using the commercial software ANSYS FLUENT. The Semi-implicit Method for Pressure Linked Equations (SIMPLE) algorithm is employed for the pressure–velocity coupling with the second-order upwind discretization scheme for the conservation of momentum, species, energy, and charge equations. The model was found to give mesh-independent solution with a mesh of about 1.4 million cells; doubling this number result in a variation of less than 0.3% in the key performance indicator which is, in this case, the average current density at 0.55 V. The distribution of the mesh is shown in Figure 4.2.

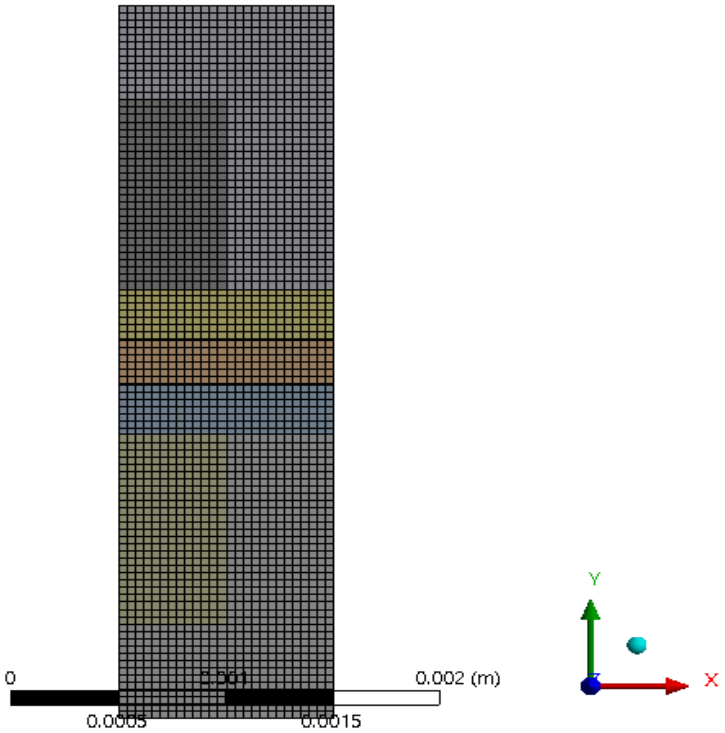

Figure 4.2 The mesh profile of the front view of the geometry. Note that the number of elements in the z-direction is 350.

Table 4.1 Geometrical and physical properties for the base case of the PEMFC model. [64,128,139]

Property	**Value**
Channel length	5×10^{-2} m
Channel height	1.0×10^{-3} m
Channel width	1.0×10^{-3} m
Land area width	1.0×10^{-3} m
GDL thickness	0.26×10^{-3} m

Catalyst layer thickness	1.0×10^{-5} m
Membrane thickness	0.23×10^{-3} m
Operating temperature	353 K
Gauge pressure at anode	5 atm
Gauge pressure at cathode	3 atm
Relative humidity of inlet gases	100%
Oxygen/nitrogen molar ratio in air	0.21/0.79
Catalyst layer porosity	0.4
GDL porosity	0.7
GDL permeability	4.97×10^{-13} m^2
Reference hydrogen concentration, $c_{H_2}^{ref}$	40 mol/m^3
Reference oxygen concentration, $c_{O_2}^{ref}$	40 mol/ m^3
Electrical conductivity of solid phase	6000 S/m
Ionic conductivity of the membrane	0.6 S/m
Catalyst layer permeability	1×10^{-13} m^2
Membrane permeability	1.8×10^{-18} m^2
Thermal conductivity of GDLs	75 W/(m-K)
Thermal conductivity of catalyst layers	75 W/(m-K)
Thermal conductivity of Bipolar plates	75 W/(m-K)

Thermal conductivity of the membrane	0.67 W/(m-K)
Faraday's constant	96485 C/mol
Universal gas constant	8.314 J/(mol-K)
Active area	11.56×10^{-4} m^2
Anode inlet mass fraction of hydrogen	0.37
Anode inlet mass fraction of water	0.63
Cathode inlet mass fraction of oxygen	0.21
Cathode inlet mass fraction of water	0.103
Cathode inlet mass fraction of nitrogen	0.69
Anode concentration exponents	0.5
Cathode concentration exponents	1
Anode reference exchange current density, $i_{0,a}^{ref}$	6000 A/m²
Cathode reference exchange current density, $i_{0,c}^{ref}$	0.0044 A/m²
Transfer coefficients for anode reaction	0.5
Transfer coefficients for cathode reaction	1
Anode specific surface area, a_a	1.0×10^7 m^{-1}
Cathode specific surface area, a_c	1.0×10^7 m^{-1}

4.3 RESULTS AND DISCUSSIONS

The modelled PEMFC was simulated for different cell voltages and the polarisation curve was then generated. Figure 4.3 shows that the modelling data results are in good agreement with the experimental data extracted from [141]. However, the model slightly under-predicts the performance of the fuel cell at lower cell voltages, and this is most likely since the physics of liquid water (which at higher current densities increases the water content of the membrane electrolyte phase to be of the order of 20s rather than 10s. This subsequently improves the ionic conductivity [152] has not been captured in this model which is single-phase and not multi-phase.

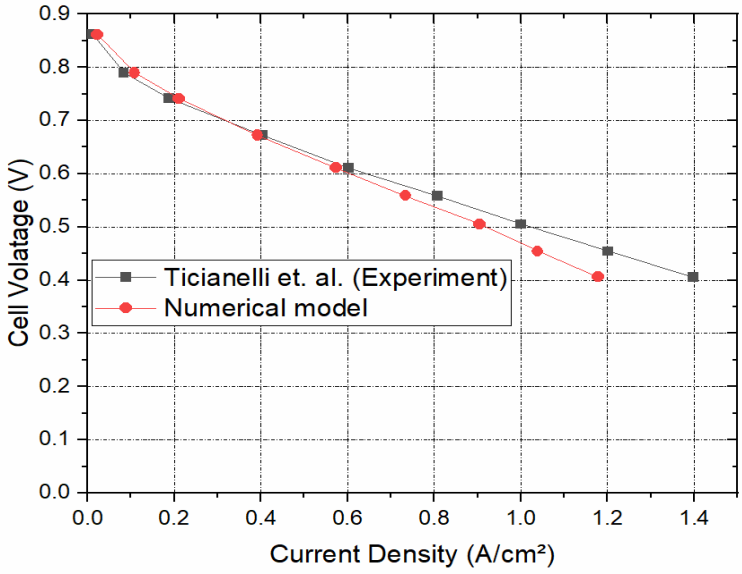

Figure 4.3 The polarization curve generated from the numerical model as compared to the experimental polarization curve taken from [141].

4.3.1 Anisotropic GDL versus isotropic GDLs

Experimentally measured and realistic GDL anisotropic transport properties (gas permeability, gas diffusivity, thermal conductivity, and electrical conductivity) of the PEMFC obtained from literature, as shown in Table 4.2, are fed into the PEMFC

model. We strived for all the experimentally estimated transport properties to be of the same GDL material (i.e., SGL 10BA) [3,139] However, for the gas diffusibility values, we used those of [87] and this was due to the unavailability of the corresponding values for SGL 10BA; nonetheless, this should not affect the general trends and the overall conclusions drawn. The polarisation curve of the modelled PEFC with the anisotropic GDL transport properties as well as the local distribution of key variables (the current density and oxygen mass fraction) within its cathode GDL are compared with those for the modelled PEFC model having isotropic GDL transport properties; see Figure 4.4. The isotropic transport properties are assumed to be the same as those of the through-plane direction for Case 2 and the same as those for the in-plane direction for Case 3; see Table 4.2.

Table 4.2 Key GDL transport properties in through-plane and in-plane directions.

	Case 1		Case 2	Case 3
Transport properties	**Through-plane**	**In-plane**	**Isotropic (Through-plane)**	**Isotropic (In-plane)**
Permeability (m^2) [128]	4.97×10^{-13}	1.87×10^{-12}	4.97×10^{-13}	1.87×10^{-12}
Diffusibility (m^2/s). [83]	0.3	0.5	0.3	0.5
Thermal Conductivity (W/m-K) [30]	1.7	21	1.7	21
Electrical Conductivity (S/m) [128]	48	4000	48	4000

Figure 4.4a shows that the model over-predicts the fuel cell performance if the GDL transport properties are assumed to be isotropic and having the same values as those of the in-plane direction; for example, at 0.4 V, the current density is over-predicted by about 38%. On the other hand, the model under-predicts the fuel cell performance if the GDL transport properties are assumed to be isotropic and having the same values as those of the through-plane direction. However, the model is less sensitive the “isotropic through-plane” assumption (Case 2) compared to the “isotropic in-plane” assumption (Case 3). Namely, at 0.4 V, the current density is under-predicted by about 25% when switching from Case 1 to Case 2. Figure 4.4b compares the current density distribution at 0.55 V within the cathode GDL, halfway along the length of the channel of the PEMFC, for both isotropic (through-plane and in-plane) and anisotropic cases. The local current density distribution in all cases have similar trends. For all three cases, the local current density is minimum at the section of the GDL which lies under the midpoint of the channel. It then increases

steadily towards the interface between the collector rib and the gas channel where it peaks and then drops at the region beneath the current collector rib (this is more evident for Cases 1 and 3). This is attributed to the fact that the interface between the flow channel and the current collector is where the supply of oxygen and the transport of electrons are both optimised. It should be noted that the transport of oxygen to the catalyst layer is a minimum beneath the mid-point of the rib and the transport of electrons is a minimum beneath the mid-point of the flow channel. The local current density is significantly higher in Case 3 compared to Cases 1 and 2 and this evidently is due to the significantly higher in plane electrical conductivity which is assumed to be having the same value as the experimentally estimated in-plane conductivity shown in Table 4.2 (i.e., 4000 S/m). Case 2 shows that the current density saturates beneath the rib of the current collector, and this is due to lack of high in-plane conduction; this should be compared with Case 1 where the high in-plane conduction (4000 S/m) is responsible for “spreading” the current density more uniformly within the GDL. As expected, Figure 4.4c shows that, for all cases, the concentration of oxygen (in the form of oxygen mass fraction) is maximum under the midpoint of the flow channel and minimum under the mid-point of the rib of the current collector. Note that Case 3 demonstrates lower oxygen concentration within the GDL, and this is due to the consumption of higher amount of oxygen at the cathode catalysts layer compared to Cases 1 and 2; this is induced by the higher overall electrical conduction of Case 3.

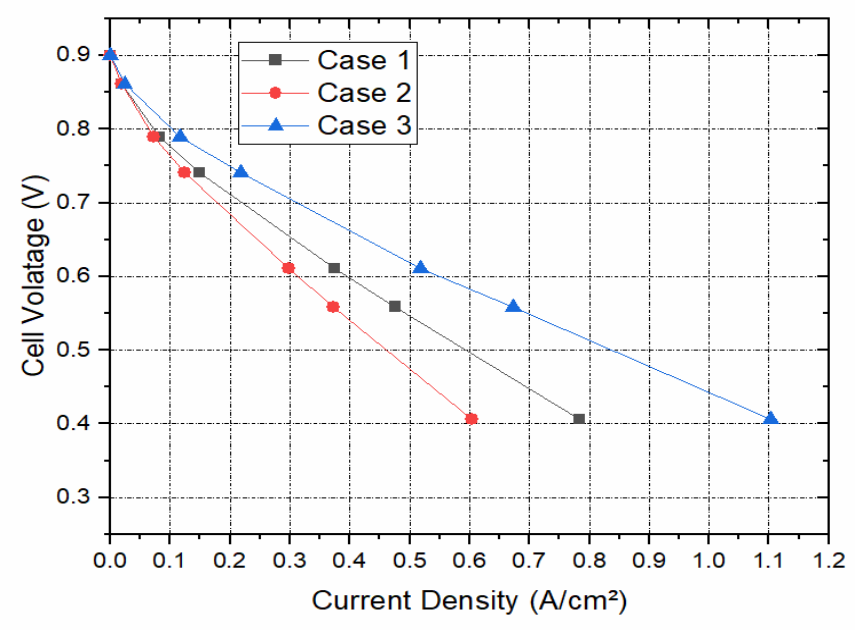

(a)

Figure 4.4 (a) The polarisation curves. Case 1 (where the GDL transport properties are anisotropic), Case 2 (where the GDL transport properties are isotropic and having the same values as those of the through-plane direction) and Case 3 (where the GDL transport properties are isotropic and having the same values as those of the in-plane direction).

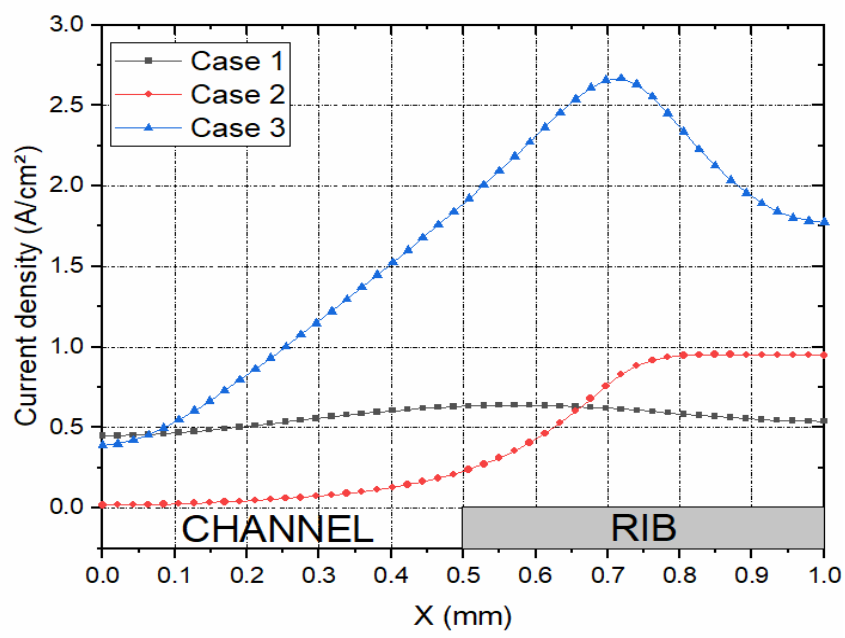

(b)

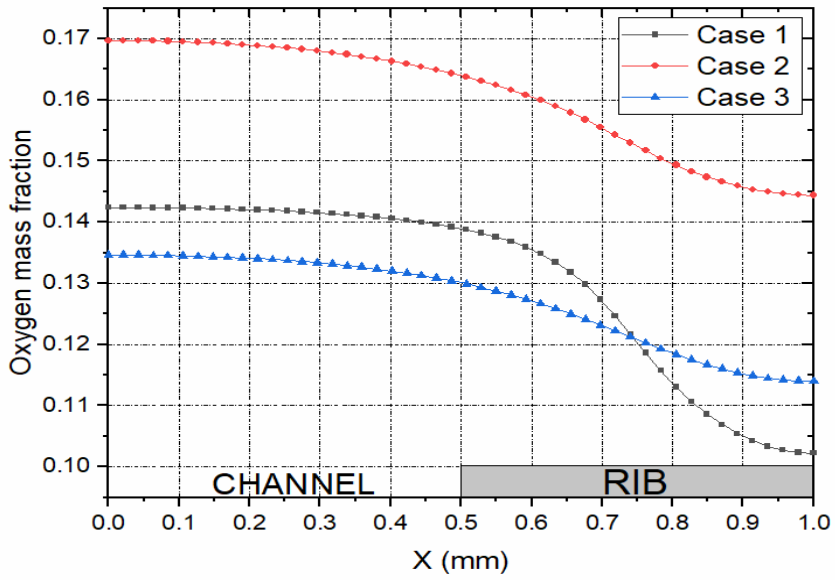

(c)

Figure 4.4 (b) the distribution of current density within the cathode GDL at 0.55 V and (c) the distribution of oxygen mass fraction within the cathode GDL at 0.55 V for the investigated cases. Case 1 (where the GDL transport properties are anisotropic), Case 2 (where the GDL transport properties are isotropic and having the same values as those of the through-plane direction) and Case 3 (where the GDL transport properties are isotropic and having the same values as those of the in-plane direction).

4.3.2 Parametric study

As this study is aimed at investigating the sensitivity of the PEMFC performance to the anisotropic key transport properties of the GDL (the gas permeability, mass diffusivity, thermal conductivity, and electrical conductivity), a parametric study of the individual transport properties of the GDL was examined.

4.3.3 Anisotropic gas permeability

Table 4.3 shows the 5 computational cases considered to investigate the impact of the gas permeability. Case 1 is the case in which the experimentally estimated gas permeability in through-plane and in-plane directions were fed into the model. In Cases 2 and 3, the experimentally measured through-plane gas permeability is kept constant and the experimentally measured in-plane gas permeability is decreased and increased by an order of magnitude respectively. Likewise, in Cases 4 and 5, the experimentally measured in-plane gas permeability is kept constant and the experimentally measured through-plane gas permeability is decreased and increased by an order of magnitude. The results of the simulated cases are represented in Figure 4.5. Figure 4.5a shows the result of the sensitivity of the PEM fuel cell polarization curves of the five cases investigated to the anisotropic gas permeability. The polarization curves of all five cases overlap each other. The plot of the polarisation curves for the five cases shows that for a given realistic range of gas permeability values, the performance of the PEM fuel cell model does not change with the gas permeability of the GDL. This indicates an insignificant impact of the gas permeability on the overall PEM fuel cell performance in the range of the realistic gas permeability values. This shows that the anisotropic gas permeability has a limited impact on the cell performance for the single-phase PEM fuel cell

model with straight channel configuration. There is an absence of the in-plane pressure gradient effect, and this could result in the crossover flow under the lands and resulting in a substantial decrease in the pressure drop required to drive the flow. This finding agrees with prior investigations of Ismail et al.[128] and Gostick et al [130]. Figure 4.5b shows that the linear profiles of the current density within the cathode GDL almost overlap with each other; the same can be observed, in Figure 4.5c, about the profiles of the oxygen concentration within the cathode GDL at 0.55 V. Further, the average current density at 0.55 V for all the cases shows a very minimal variation between the cases (the variation lies in the fourth decimal place). This signifies the very minimal impact of the GDL gas permeability on the performance of the fuel cell. As mentioned in prior works of Ismail et al. [128] and Zamel et al. [70] observed that the main mode of transport within the GDL is diffusion, not convection.

Table 4.3 Computation cases for the GDL gas permeability investigation [128].

Case Number	**Permeability (m²)**		**Average Current density (A/cm²) at 0.55 V**
	Through-plane, $K_{\perp}$	**In-plane,** $K_{=}$	
1	4.97×10^{-13}	1.87×10^{-12}	0.5016
2	4.97×10^{-13}	1.87×10^{-13}	0.5015
3	4.97×10^{-13}	1.87×10^{-11}	0.5017
4	4.97×10^{-14}	1.87×10^{-12}	0.5016
5	4.97×10^{-12}	1.87×10^{-12}	0.5017

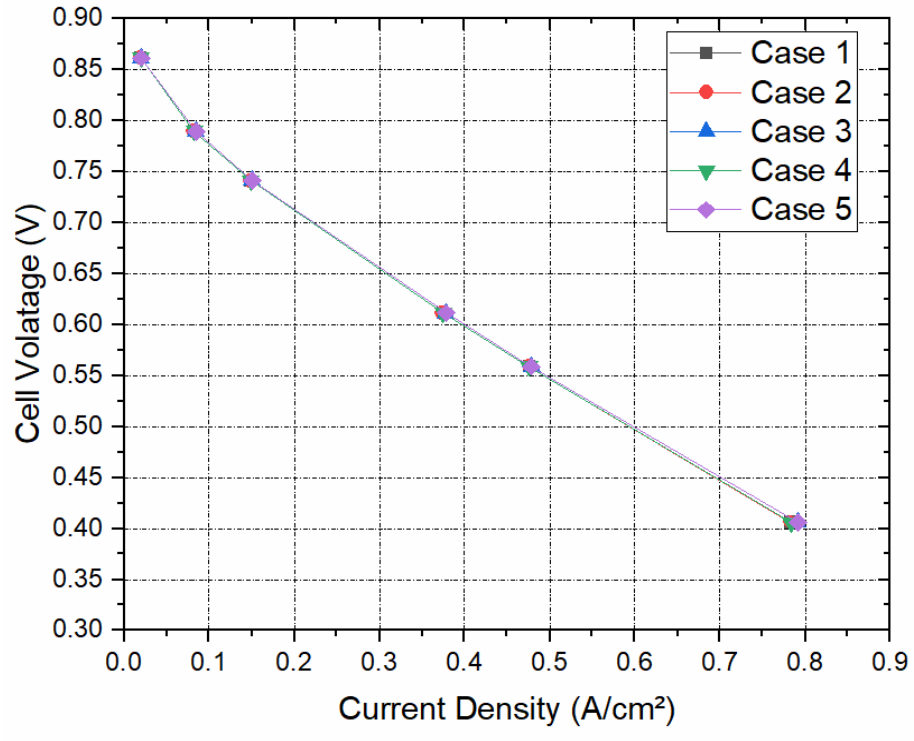
Case 1
Case 2
Case 3
Case 4
Case 5
Cell Volatage (V)
Current Density (A/cm²)
0.90
0.85
0.80
0.75
0.70
0.65
0.60
0.55
0.50
0.45
0.40
0.35
0.30
0.0
0.1
0.2
0.3
0.4
0.5
0.6
0.7
0.8
0.9

(a)

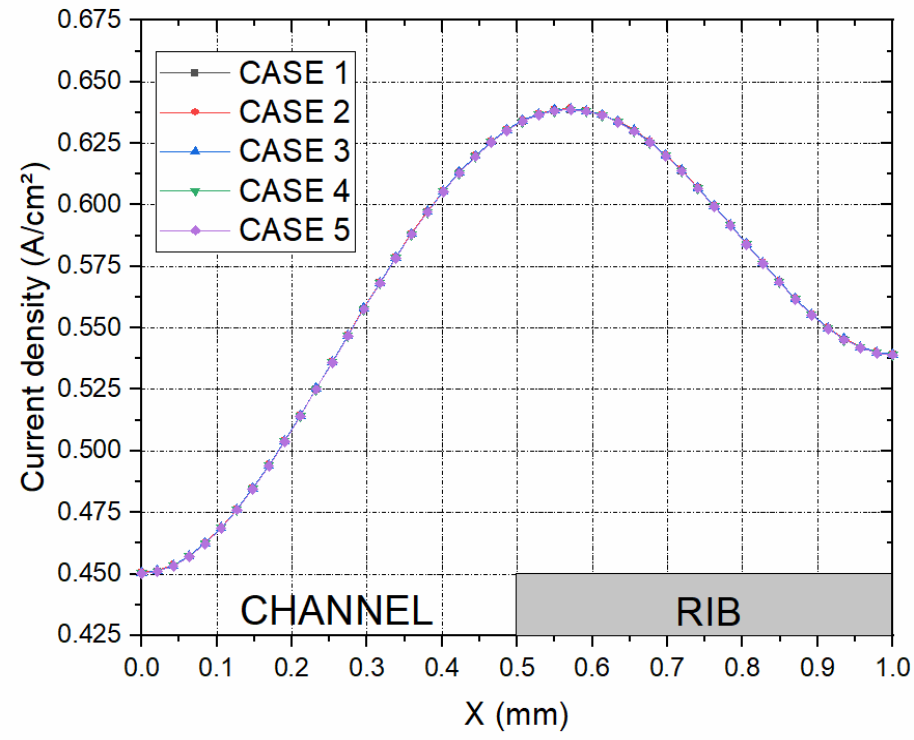
CASE 1
CASE 2
CASE 3
CASE 4
CASE 5
Current density (A/cm²)
X (mm)
CHANNEL
RIB
0.675
0.650
0.625
0.600
0.575
0.550
0.525
0.500
0.475
0.450
0.425
0.0
0.1
0.2
0.3
0.4
0.5
0.6
0.7
0.8
0.9
1.0

(b)

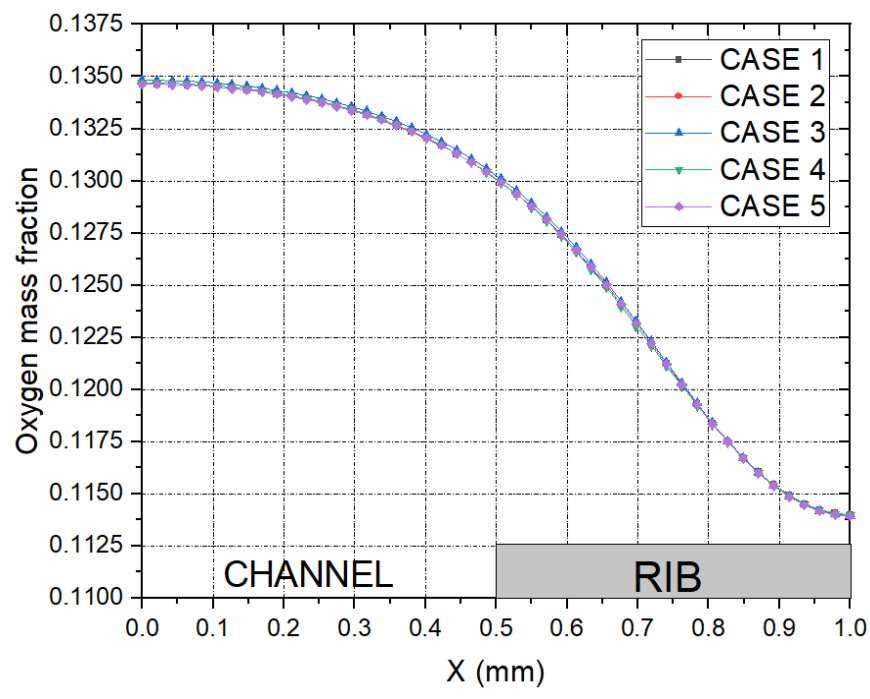

(c)

Figure 4.5 (a) Polarisation curves and, the distribution of (b) current density, and (c) oxygen mass fraction within the cathode GDL gas permeability computation cases shown in Table 4.3.

4.3.4 Anisotropic effective diffusivity

The effective diffusivity within the GDL is often estimated using Bruggeman's correlation which is ε^{τ} in Equation (4.4). The ratio between the effective diffusivity and the bulk diffusivity (which is Bruggeman's correlation in our case) is called the diffusibility. As with gas permeability, the experimentally estimated diffusibility in Case 1 has been realistically decreased and increased in the through-plane and in-plane directions; see Table 4.4. This table shows that the average current density at 0.55 V changes very slightly with the changes in the in-plane diffusibility (compare Cases 1, 2 and 3). However, the average current density becomes more sensitive to changes in the through-plane diffusibility (compare Cases 1, 4 and 5); for example, the current density, for a given in-plane diffusibility of 0.5, increases by around 5% when the through-plane diffusibility increases from 0.1 to 0.5. Figure 4.6 shows the current density, and the oxygen concentration profiles within the cathode GDL. Figure 4.6a shows the cell polarisation curves for all five cases investigated for the anisotropic gas diffusivity. The polarisation curves show that Case 5, which has the highest value of through-plane diffusibility (0.5) and the second highest value of the in-plane diffusibility (0.5) exhibits the best performance. At lower cell voltages, the cell polarisation curve for Case 5 is about 11% overestimated when compared to Cases 1, 2 and 3 while it is overestimated when compared with that of Case 4, which has the lowest value of through-plane diffusibility, by a factor of 4. Despite having an in-plane diffusibility value of 0.5, Case 4 shows the lowest cell performance compared to the other cases investigated. This is because Case 4 having the lowest through-plane diffusibility value of 0.1. This shows that through-plane diffusion is the most dominant mode

of gas reactant transport from the gas flow channels to the electrocatalyst reaction sites. Therefore, increasing the through-plane diffusivity of the gas diffusion layer improves the overall PEM fuel cell performance in terms of the cell polarisation. As with the average current density, Figure 4.6b shows that, compared to the base case (Case 1), the local current density is more sensitive to the through-plane diffusibility (Cases 4 and 5) than the in-plane diffusibility (Cases 2 and 3). This is since the through-plane direction is the direction through which the reactant gas (oxygen in this case) is transported from the flow channel to the catalyst layer where it is consumed, thus completing the reaction, and generating the electrical current. For example, the mean local current density (averaged over the distance considered within the cathode GDL) increases by around 11% when the GDL diffusibility increases from 0.1 to 0.5. Figure 4.6c shows that the oxygen mass fraction within the region of the cathode GDL under the flow channel is the lowest for Case 5 where the through-plane diffusibility is the largest. Thus, signifying that a higher amount of oxygen is consumed compared to other cases; this in line with the cell polarisation curves and the current density profiles shown in Figures 4.6a and 4.6b which demonstrates that the overall PEM fuel cell performance (the cell polarisation) and the current density is in general the highest for Case 5. On the other hand, the oxygen concentration under the rib is the lowest for Case 2. This is because the in-plane diffusibility is the lowest for this case and as such the transport of oxygen from the regions below the flow channel to the regions below the rib is most hindered compared to other cases. On a related note, Cases 1, 2 and 3 do not show any remarkable difference in the distribution of oxygen in the region of the GDL below the channel. This shows that the in-plane diffusibility has

no major impact on the oxygen distribution within this region. The in-plane diffusibility begins to dominate the distribution of oxygen as we approach the interface between the channel and the collector rib.

Table 4.4 Computation cases for the GDL gas diffusivity investigation [83].

Case Number	Diffusibility		Average Current density (A/cm²) at 0.55 V
	Through-plane, $f(\varepsilon)_{\perp}$	In-plane, $f(\varepsilon)_{=}$	
1	0.3	0.5	0.5115
2	0.3	0.3	0.5109
3	0.3	0.7	0.5119
4	0.1	0.5	0.4932
5	0.5	0.5	0.5155

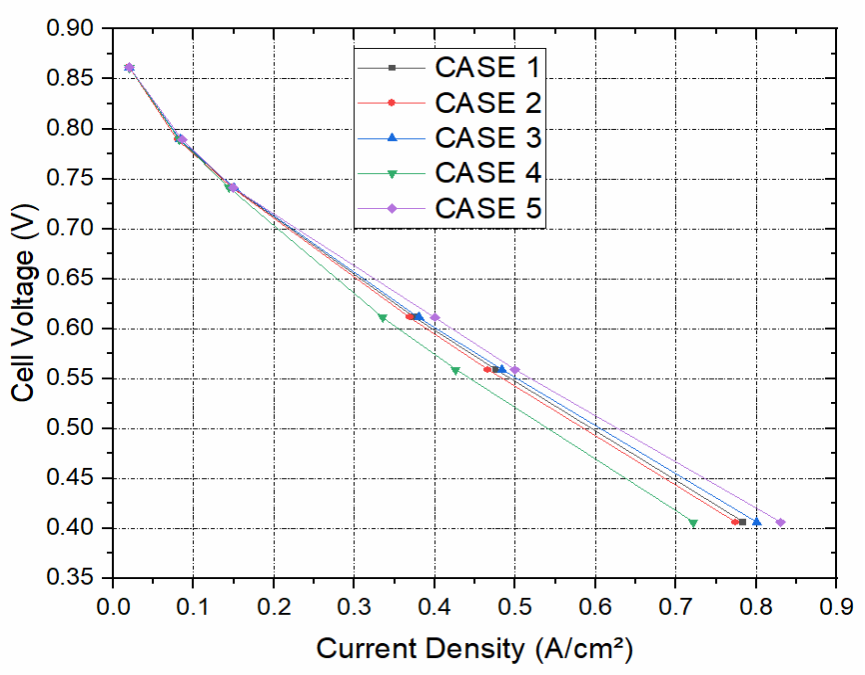
CASE 1
CASE 2
CASE 3
CASE 4
CASE 5
Cell Voltage (V)
Current Density (A/cm²)
0.90
0.85
0.80
0.75
0.70
0.65
0.60
0.55
0.50
0.45
0.40
0.35
0.0
0.1
0.2
0.3
0.4
0.5
0.6
0.7
0.8
0.9

(a)

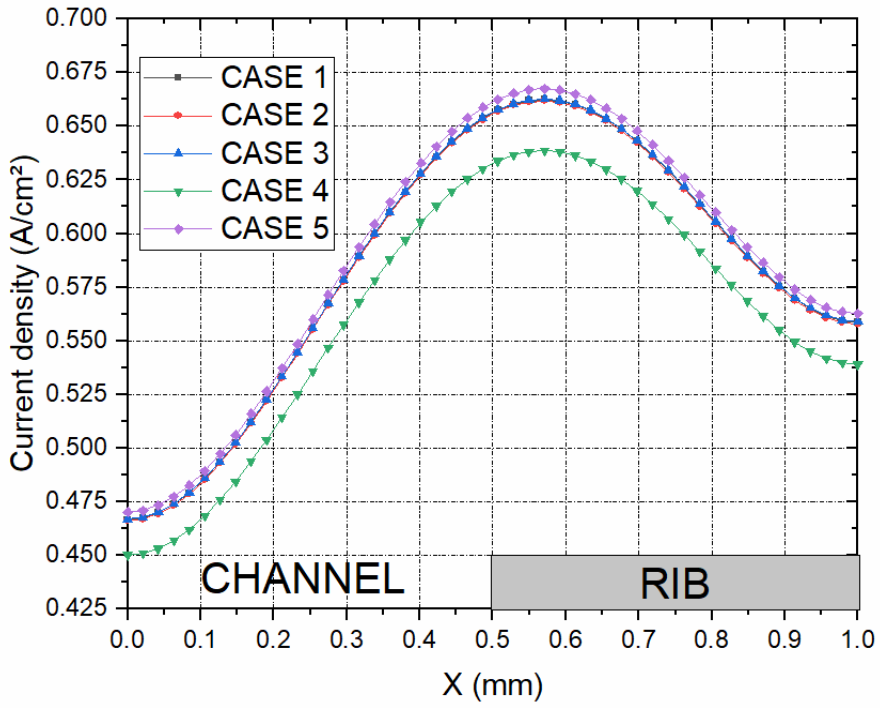
CASE 1
CASE 2
CASE 3
CASE 4
CASE 5
Current density (A/cm²)
X (mm)
CHANNEL
RIB
0.700
0.675
0.650
0.625
0.600
0.575
0.550
0.525
0.500
0.475
0.450
0.425
0.0
0.1
0.2
0.3
0.4
0.5
0.6
0.7
0.8
0.9
1.0

(b)

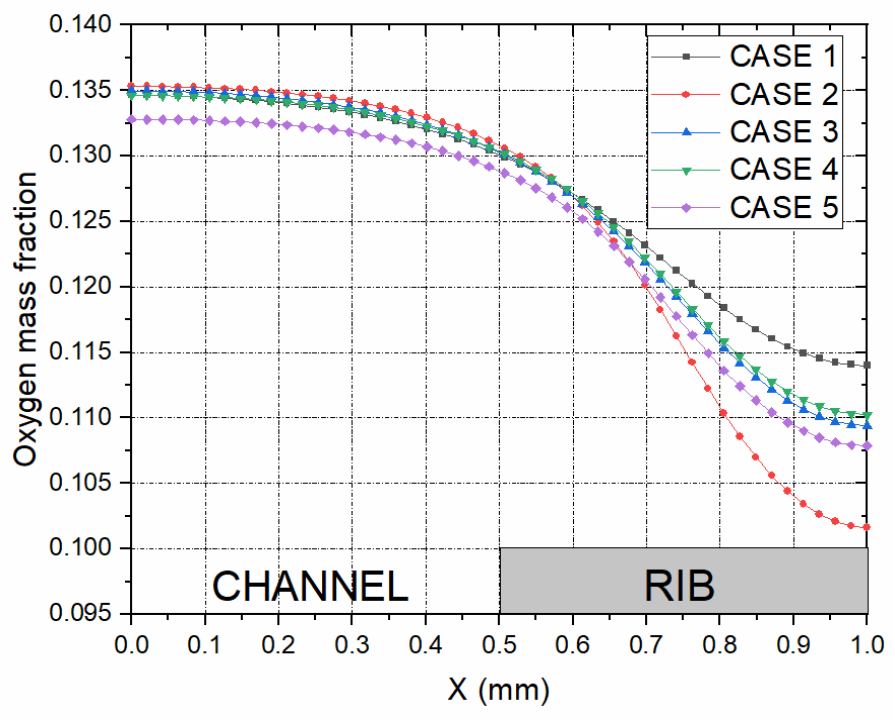

(c)

Figure 4.6 (a) Polarisation curves and, the distribution of (b) current density, and (c) oxygen mass fraction within the cathode GDL at 0.55 V for the GDL gas diffusivity computation cases shown in Table 4.4.

4.3.5 Anisotropic thermal conductivity

As with the GDL gas permeability and diffusibility, Table 4.5 shows five cases. Case 1 is the case with the experimentally estimated values for the through- and in-plane thermal conductivity. The other 4 cases are the cases where the through-plane and the in-plane thermal conductivity values are realistically changed to investigate the sensitivity the fuel cell performance to the anisotropic GDL thermal conductivity. Overall, the impact of the GDL thermal conductivity on the fuel cell

performance is, compared to electrical conductivity or even gas diffusivity, rather small; the difference in the average current density at 0.55 V between the best case (Case 4) and the worst case (Case 5) is just about 13.4 mA/cm^2. The reason that Case 4 shows the best performance is that the significantly reduced through-plane thermal conductivity (i.e., 0.01 W/m·K) decreases the heat dissipation rate and increases the cell temperature. This subsequently increases the rate of reaction (as evidenced from the Butler-Volmer equation shown in Equations (4.14) and (4.15)) and the membrane conductivity (as evidenced from the Springer's model shown in Equation (4.19). In general, any decrease in either the in-plane thermal conductivity (compare Cases 1, 2 and 3) or the through-plane conductivity (compare Cases 1, 4 and 5) results in a slight improvement to the fuel performance. The cell polarisation curves for the five cases investigated and the distribution of current density within the cathode GDL (Figures 4.7a-b) are in line with the average current density results shown in Table 4.6; marginal gain are obtained with decreasing either the in-plane or the through-plane GDL thermal conductivities. Evidently, better fuel cell performance means higher oxygen consumption rate and subsequently less oxygen concentration within the gas diffusion layer and that is why Case 4 demonstrates the least oxygen mass fraction within the cathode GDL (Figure 4.7c).

Table 4.5 Computation cases for the GDL thermal conductivity investigation [131].

Case Number	Thermal Conductivity (W/m·K)		Average Current density (A/cm²) at 0.55 V
	Through-plane	In-plane	
1	0.1	10	0.5029
2	0.1	1	0.5054
3	0.1	100	0.5017
4	0.01	10	0.5089
5	1	10	0.4955

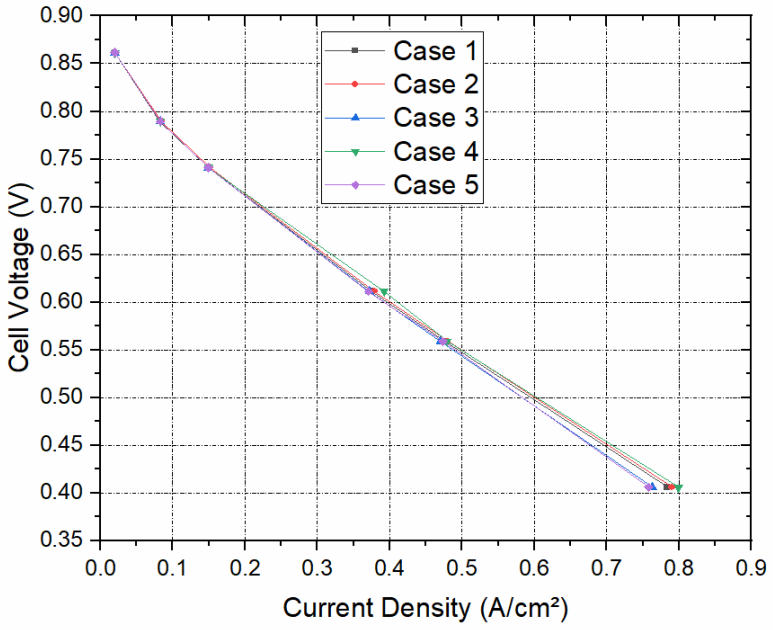

(a)

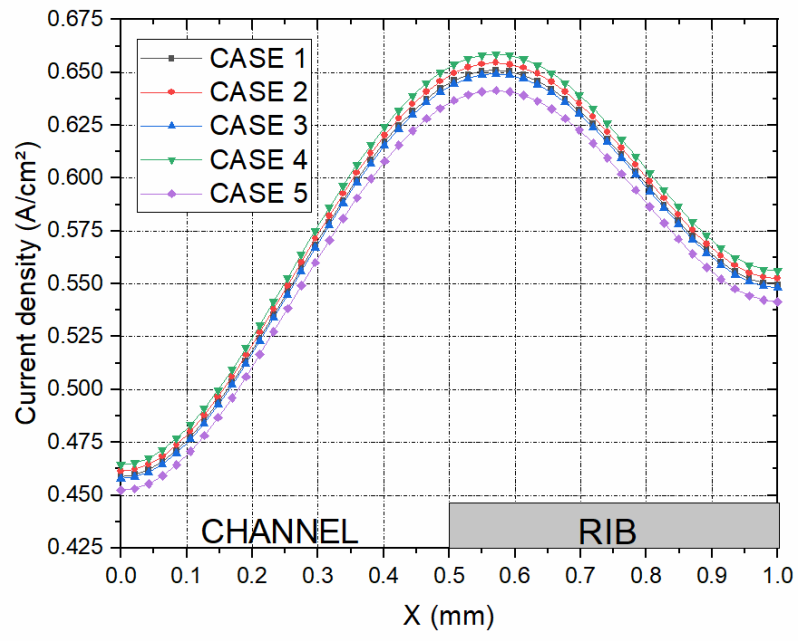

(b)

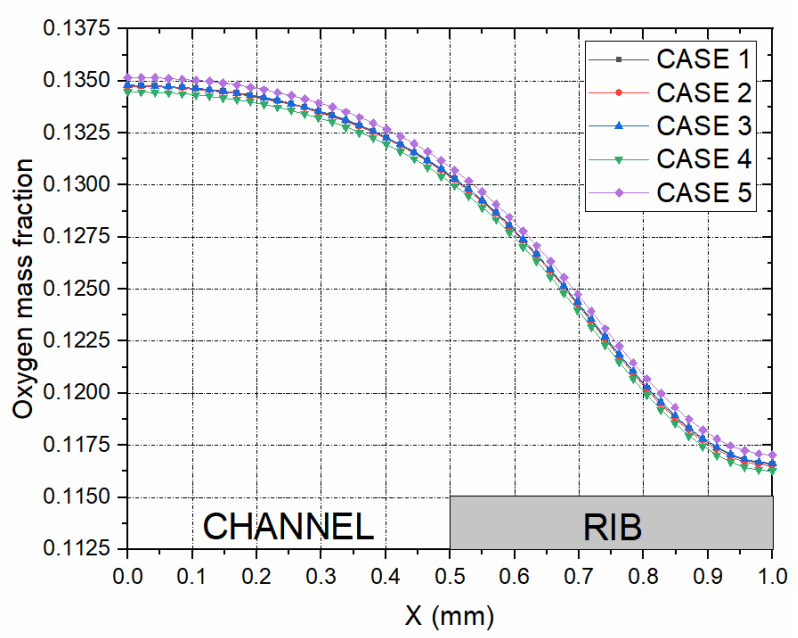

(c)

Figure 4.7 (a) Polarisation curves and, the distribution of (b) current density, and (c) oxygen mass fraction within the cathode GDL at 0.55 V for the GDL thermal conductivity computation cases shown in Table 4.5.

4.3.6 Anisotropic electrical conductivity

Table 4.6 shows 5 computation cases. The first case (Case 1) is the case with the experimentally estimated values for the through- and in-plane electrical conductivity and the other 4 cases are the cases where the through-plane and the in-plane electrical conductivity values are realistically changed to investigate the sensitivity the fuel cell performance to the anisotropic GDL electrical conductivity. Further, Figure 4.8 displays cell polarisation curves, the distribution of current density, and oxygen concentration within the cathode GDL at 0.55 V. The first observation that may be extracted from Table 4.6 and Figure 4.8 is that the overall fuel cell performance and the distributions of current density and oxygen concentration are much more sensitive to the GDL electrical conductivity than the other transport properties. The reason behind this is that the electrical conductivity is associated with the ohmic losses which are the main potential losses for typically operating cell voltages (0.5 - 0.6 V). The second observation is that the fuel cell performance is significantly more sensitive to the through-plane electrical conductivity (compare Cases 1, 4 and 5) than to the in-plane electrical conductivity (compare Cases 1, 2 and 3). To illustrate, the average current density at 0.55 V increases by more than 50% when increasing the through-plane GDL conductivity from 24 S/m (Case 4) to 96 S/m (Case 5). On the other hand, the average current density increases by less than 5% when increasing the in-plane GDL electrical conductivity from 2000 S/m (Case 2) to 8000 S/m (Case 3). This is mainly since the shortest (and the least resistive) pathway for the electrons to reach the catalyst layers (where they combine with oxygen and protons to produce water) is across the thickness of the GDL, not along the plane of the GDL.

Figure 4.8b shows that, for a given through-plane electrical conductivity, as the in-plane electrical conductivity increases (Cases 1, 2 and 3), the linear distribution of current density within the GDL expectedly becomes more uniform due to decreased in-plane electrical resistance. Further, in accordance with the average current density results at 0.5 V, it is evident that local current density is much more sensitive to the through-plane electrical conductivity (compare Cases 1, 4 and 5) than to the in-plane electrical conductivity (compare Cases 1, 2 and 3). This observation is also applicable to the distribution of oxygen distribution; the largest gap is between Case 4 and Case 5 where the through-plane electrical conductivity are 24 and 48 S/m respectively. As expected, the lowest oxygen concentration within the GDL is demonstrated by Case 5 where the oxygen consumption rate is the maximum for this case.

Table 4.6 Computation cases for the GDL electrical conductivity investigation [128].

Case Number	Electrical Conductivity (S/m)		Average Current density (A/cm²) at 0.55 V
	Through-plane	In-plane	
1	48	4000	0.493
2	48	2000	0.480
3	48	8000	0.503
4	24	4000	0.386
5	96	4000	0.580

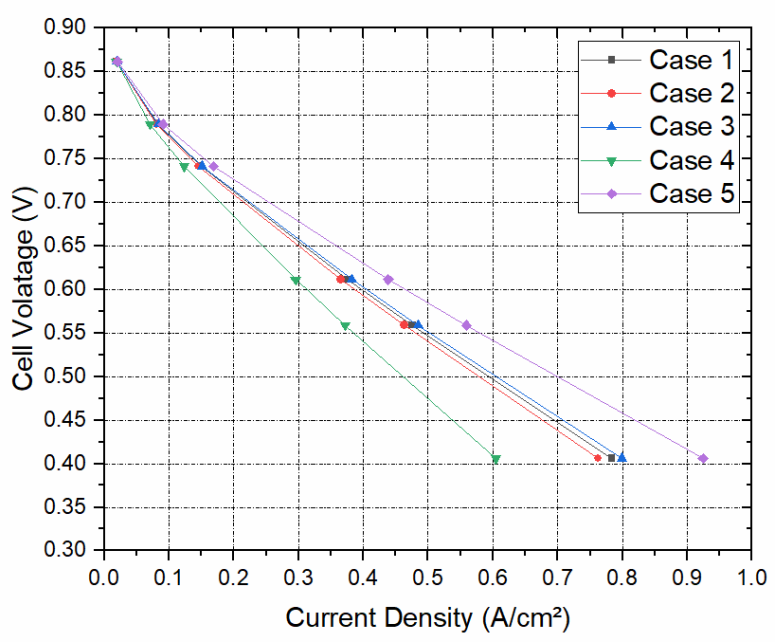
Case 1
Case 2
Case 3
Case 4
Case 5
Cell Volatage (V)
Current Density (A/cm²)
0.90
0.85
0.80
0.75
0.70
0.65
0.60
0.55
0.50
0.45
0.40
0.35
0.30
0.0
0.1
0.2
0.3
0.4
0.5
0.6
0.7
0.8
0.9
1.0

(a)

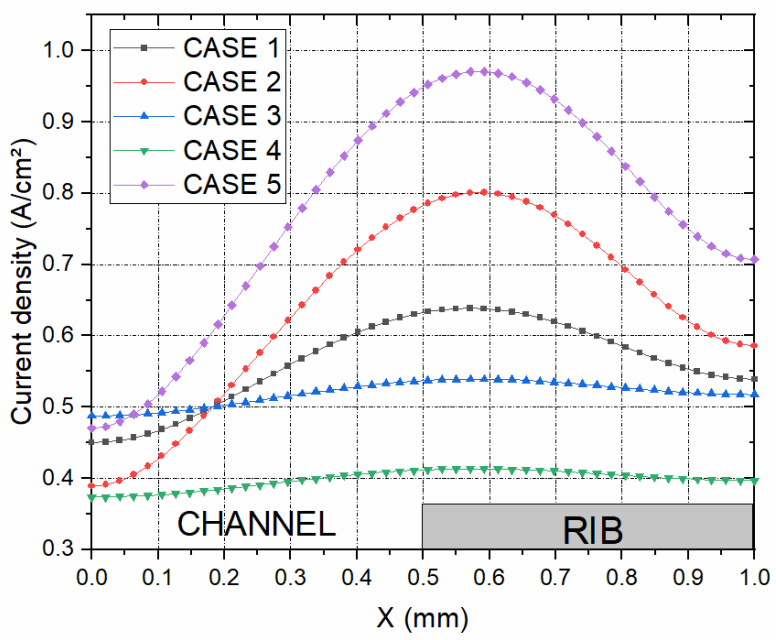
CASE 1
CASE 2
CASE 3
CASE 4
CASE 5
Current density (A/cm²)
X (mm)
CHANNEL
RIB
1.0
0.9
0.8
0.7
0.6
0.5
0.4
0.3
0.0
0.1
0.2
0.3
0.4
0.5
0.6
0.7
0.8
0.9
1.0

(b)

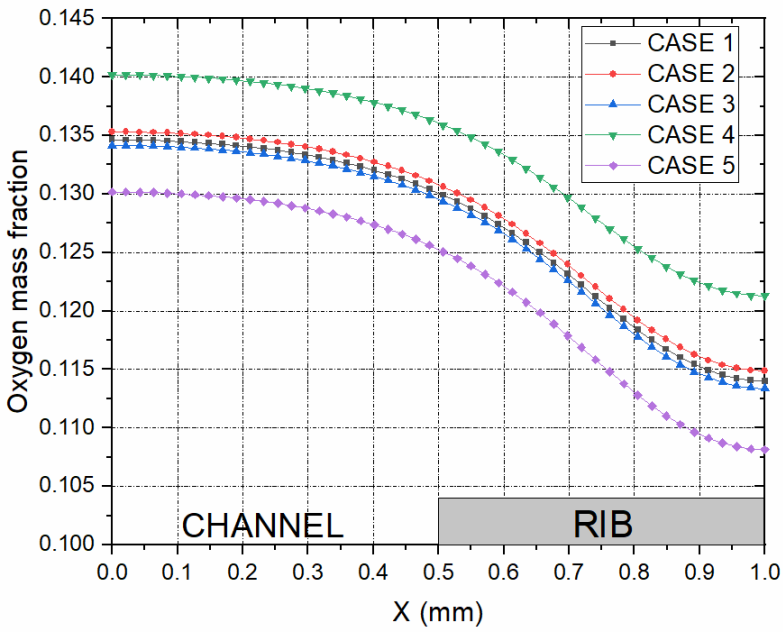

(c)

Figure 4.8 (a) Polarisation curves and, the distribution of (b) current density, and (b) oxygen mass fraction within the cathode GDL at 0.55 V for the GDL electrical conductivity computation cases shown in Table 4.6.

4.4 Conclusions

A three-dimensional straight channel PEFC model has been developed. The main purpose of this study is to investigate the sensitivity of the fuel cell performance and the distributions of the key variables within the GDL (current density and oxygen concentration) to the anisotropy in the key transport properties of the GDL: gas permeability, gas diffusivity, thermal conductivity, and electrical conductivity. The key findings and observations are as follows:

- The anisotropic nature of the conventionally used GDLs need to be captured in the PEMFC models. Overlooking this GDL's attribute leads to either significant overestimation (if the in-plane values of the transport properties

are considered) or underestimation (if the through-plane values of the transport properties are considered) of the modelled fuel cell current density by up to 50% at typical cell voltages.

- The fuel cell performance and the distribution of current density and oxygen concentration within the GDL are, compared to other transport properties, highly sensitive to the electrical conductivity of the GDL, particularly in the through-plane direction. Quadrupling the through-plane GDL electrical conductivity increases the average current density of the fuel cell at 0.55 V by more than 50%.
- On the other hand, the fuel cell performance, and the distributions of the above key variables within the GDL are almost insensitive to the through-plane or in-plane gas permeability of the GDL as the main mode of transport within the GDL is diffusion.
- The fuel cell performance is moderately sensitive to both the gas diffusivity (represented by the diffusibility in this study) and, to a lesser extent, the thermal conductivity of the GDL. This observation is more evident with the through-plane diffusibility and the thermal conductivity than with in-plane diffusibility or the thermal conductivity of the GDL. This is mainly since the mass and heat transport to/from the catalyst layer from/to the flow channel/rib is in the through-plane direction. Notably, the fuel cell performance improves with decreasing the GDL through-plane thermal conductivity as it lowers heats dissipation and increases the reaction rate at the cathode catalyst layer.

- It is recommended that in the design and manufacture of the carbon fibre paper GDLs, the carbon fibre needs to be more oriented in the through-plane direction as against the conventional in-plane direction as the GDL transport properties in that direction will improve the performance of the PEMFC.

Based on the findings of the study, it is recommended to design GDLs with superior through-plane electrical conductivity and, to a lesser extent, through-plane diffusibility and thermal conductivity. This could be achieved by having more carbon fibres oriented in the through-plane direction.

5 SINGLE AND DOUBLE SIDED MPL COATED GDLs: A NUMERICAL STUDY

5.1 Introduction

The ohmic and concentration losses that occur in the PEM fuel cell operation has a major effect on the efficiency and performance of the cell, namely by lowering its efficiency. A way to mitigate these losses is to minimise the electrical resistance of the fuel cell and increase the pore volume available for the gas transport to the reactive sites. This can be achieved by minimising the contact resistances between the solid components of the fuel cell and designing the gas diffusion media for effective water management and gas reactant transport. Most PEMFC models tend to assume a high electrical conductivity for the GDL and the current collector (bipolar plates) and hence downplay the importance of the interfacial contact resistance between the GDL and the bipolar plates. However, experimental, and numerical studies in the literature have been done to characterise the GDL interfacial contact resistance and have reported its influence on the performance of the PEM fuel cell. For example, Zhou et al. [143,144] developed a micro-scale numerical model to estimate the contact resistance between the BPP and GDLs in PEM fuel cells by using FU436a graphite plates and Toray TGP-H-030 carbon paper. They reported that the contact resistance decreased with increasing the bipolar plate asperity peak density, by about 14%. Qiu et al. [145] showed that the interfacial contact resistance between the GDL and bipolar plates has significant influence on the PEM fuel cell performance by experimentally measuring the bulk resistance and investigating the microstructure for Toray carbon papers (TGP-H-060 and TGP-H-090), Tenax

carbon cloths (TCC2660 and TCC3250), and Freudenberg carbon felts (H2315 and H14) under cyclic and steady loads. Lai et al. [146] developed both mechanical - electrical FEM and experimental techniques to estimate the contact resistance between the bipolar plate and the GDL of PEM fuel cells and reported that the contact resistance decreases rapidly as the clamping pressure was increased. Zhang et al. [147] experimentally estimated the contact resistance between the GDL and bipolar plates using experimental and numerical approaches. They reported that the contact resistance between GDLs and the bipolar plates is influenced by the clamping pressure in the PEM fuel cell stack. Sow et al. [148] developed a novel technique to, numerically and experimentally, characterise the through-plane interfacial contact resistance and the through- plane bulk resistance for various SGL carbon paper GDL series, namely 25BA, 25BC, 25DC and 35DC. They reported that both the bulk and interfacial contact resistances of the GDL increased with PTFE treatment (for all samples), and that the bulk resistance of the GDL contributes only 10% of the total ohmic losses in the PEM fuel cell, while the interfacial contact resistance contributed significantly to the ohmic losses in the cell. Ismail et al. [149] experimentally measured the interfacial contact resistance between the graphite bipolar plates and uncoated (carbon substrates) and MPL coated SGL carbon paper GDLs using a 4-probe BS401 ohmmeter. They reported that the contact resistance was significantly reduced with increasing the MPL loadings. Ye et al. [150] developed a multi-electrode probe technique to measure the contact resistance, distinctly, from that of the bulk resistivity for Toray TGP-H-120 carbon paper and carbon cloth (CCWP) GDLs. In addition, they reported that the addition of MPL coating had no effect on the bulk resistivity of either material but that the interfacial

contact resistance of both GDL materials reduced with the MPL coating but increased with hydrophobic treatment.

It has been reported in the literature [1,26,37,151] that the MPL deposition improves the water management in the cathode side of the PEMFC, and this is due to its relatively small pore size and increased hydrophobicity. Also, it provides mechanical strength, against clamping force, to the catalyst layer by increasing the surface contact between the catalyst layer and the GDL [149]. In addition, it improves the electrical conductivity of the GDL by reducing the interfacial contact resistance between the GDL and the catalyst layer as well as that between the GDL and bipolar plate by its penetration into the GDL. Ismail et al. [99] having experimentally characterised the anisotropic electric conductivity of uncoated, PTFE treated and coated SGL10AA,10BA,10CA,10DA,10EA,10BC and 10BE (with the last two being MPL coated) reported that the MPL coating reduced the interfacial contact resistance between the GDL and the bipolar plate. They attributed this to the compressibility of the MPL which allows it to penetrate the pores in the bipolar plate/ GDL surface and thereby establishing a good contact at the GDL-bipolar plate interface. There has been various studies in open literature on novel designs of the GDL-MPL structure to improve its pore structure. For example, Kitahara et al. [152] developed a water vapor exchange system of the PEM fuel cell comprising two distinct GDL architectures, one coated with hydrophobic MPL at the active reactive area and the other coated with hydrophilic MPL loaded with polyvinyl alcohol (PVA) and carbon black at the cathode water vapor exchange area for a self-humidifying PEM fuel cell. They reported that a 20 % mass coating of the MPL with hydrophilic PVA and carbon black material, improved the water transport and enhanced the overall PEMFC performance. Also, Kitahara et al. [153] developed a GDL with

double (hydrophobic and hydrophilic) MPL coating at the GDL-catalyst interface. The hydrophilic carbon black MPL was deposited on the carbon substrate while the hydrophilic MPL with carbon black and PVA was deposited on the hydrophobic MPL (and facing the catalyst layer). However, Chun et al. [154] developed a double MPL-coated GDL with a hydrophilic MPL deposited in between the carbon substrate and the hydrophobic MPL that is in contact with the catalyst layer. They reported better performance than a single type hydrophobic MPL coated GDL under low humidification condition. Wang et al. [155] fabricated a bi-functional pore structure MPL using carbon black composite of Acetylene Black and Black pearls 2000 carbon and reported improved power density of 0.91 W/cm for the MPL with 10wt.% Black Pearls 2000 in the composite carbon black. Wang et al. [156] also developed a composite carbon MPL consisting of Acetylene Carbon Black and Black Pearls 2000 carbon, having a bi-functional pore structure, for effective mass transport management in the fuel cell. They proposed a novel GDL with different MPLs deposited on each side of the of the GDL to provide improved pore structure and high electrical conductivity by reducing the interfacial contact resistance between the GDL and its adjoining components. An important finding in their study is that the absence of an MPL at the GDL-bipolar plate interface increased the electrical contact resistance between the GDL and the bipolar plate. They suggested a design of the GDL structure to incorporate an MPL on double sides of the carbon substrate for enhanced electrical conductivity/charge transport as well as gas/water transport. The outcome of their study, as well as that of [149], forms the motivation of the investigation performed in this chapter of the thesis. In this study, a three-dimensional multiphase model of the PEM fuel cell was developed to study the significance of the interfacial contact resistances of the PEMFC components and

also that of a double side MPL-coated GDL. After validating the model, parametric studies were performed on the PEMFC model with single side MPL-coated and double-sided MPL-coated GDLs, by realistically increasing or decreasing the base experimentally estimated value of each of the interfacial contact resistances between the GDM and its adjoining components. The result of this study gives many insights on the significance of the interfacial contact resistance and the MPL coatings on the performance of the PEM fuel cell.

5.2 Model description

The multiphase, isothermal PEM fuel model includes the transport of gas species, energy, charge, liquid, and dissolved water. This section details the conservation equations that govern the transport of these physical quantities as well as their source terms. The PEMFC model developed in this study is based on the model of [30,157]. Detailed descriptions of the conservation equations are given in the following subsections.

5.2.1 Model assumptions

To simplify the PEFC model and make it tractable, the following assumptions have been made:

- The fuel cell operates in steady state.
- Laminar and incompressible flow.
- The membrane is impermeable to the reactant gases.
- Uniform compression on all components of the fuel cell.

- The catalyst layer is coated on the gas diffusion media instead of the membrane.

5.2.2 Model geometry

The three-dimensional, straight gas flow channels computational domain of the PEMFC model is shown in Figure 5.1 and consists of cathode and anode bipolar plates (or current collectors), cathode and anode flow channels, cathode and anode catalyst layers, cathode and anode GDLs, cathode and anode MPLs, and the membrane electrolyte. Only half of the channel width is considered in the PEM fuel cell model due to symmetry and to reduce computational time.

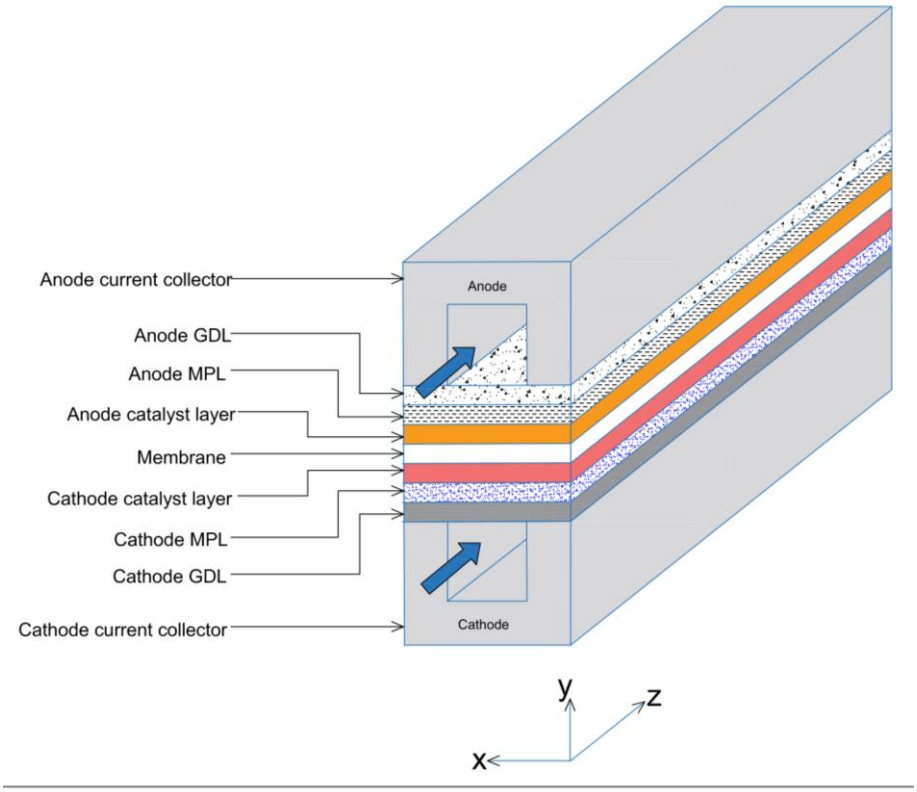

Figure 5.1 Schematic geometry of the computational domain for the base case PEM fuel cell model.

5.2.3 Governing equations

The equations which govern the transport of physical quantities are detailed in this section. However, equations (5.1) to (5.6) have already been defined in Section 4.2.3 of Chapter 4, of the thesis but are briefly stated here for easy reference. The details of these transport equations are as follows [157]:

Mass transport equation

$$\nabla \cdot (\varepsilon \rho \vec{u}) = 0 \quad \textbf{(5.1)}$$

Momentum transport equation

$$\nabla \cdot (\varepsilon \rho \vec{u}\vec{u}) = -\varepsilon \nabla P + \nabla \cdot (\mu \nabla \varepsilon \vec{u}) + \frac{\varepsilon^2 \mu \vec{u}}{K} \quad \textbf{(5.2)}$$

Species transport equation

$$\nabla \cdot (\varepsilon \rho \vec{u} Y_i) = \nabla \cdot (\rho D_{ij}^{eff} \nabla Y_i) + S_i \quad \textbf{(5.3)}$$

*****The diffusivity in Equation 5.3 is calculated using the correlation by [158].

Energy transport equation

$$\nabla \cdot \left(\rho c_p \vec{u} T\right) = \nabla \cdot (k_{eff} \nabla T) + S_e \quad \textbf{(5.4)}$$

Charge transport equations

$$\nabla \cdot (\sigma_s \nabla \phi_s) = S_{\phi,s} \quad \textbf{(5.5)}$$

$$\nabla \cdot (\sigma_m \nabla \phi_m) = S_{\phi,m} \quad \textbf{(5.6)}$$

Liquid water transport equations

$$\nabla \cdot \left(\rho_l \frac{K_{rl} \mu_g}{K_{rg} \mu_l} \vec{u}\right) = \nabla \cdot (\rho_l D_s \nabla s) + S_l \quad \textbf{(5.6)}$$

where K_{rl} and K_{rg} are the relative permeability of liquid water and the water in gaseous phase, respectively, and are given as follows [28]:

$$K_{rl} = s^3 \quad \textbf{(5.7)}$$

$$K_{rg} = (1 - s)^3 \quad \textbf{(5.8)}$$

The capillary diffusion coefficient, D_s, in Equation (5.6) is given as follows [28]:

$$D_s = \frac{Ks^3 dP_c}{\mu_l ds} \quad \textbf{(5.9)}$$

where P_c is the capillary pressure derived from the Leverett J function and is given as follows [28]:

$$P_c = \sigma \cos(\theta_c) \left(\frac{\varepsilon}{K}\right)^{0.5} (1.417s - 2.12s^2 + 1.263s^3) \quad \textbf{(5.10)}$$

where σ is the surface tension, θ_c is the contact angle, and K is the absolute permeability.

5.2.4 Boundary conditions and numerical procedure

Mass flow rate boundary conditions were specified for inlets of the anode and cathode gas flow channels. An operating temperature of 353K and the species mass fractions were also specified at the inlets of the gas flow channels with inlet liquid water saturation set to zero. The fluid mass flow rate is defined as a function of a typical operating current density (i_{op}) which is in this case is 1.0 A/cm², the active area of the fuel cell (A_{act}), and the stoichiometric ratio (ξ) of the reactant gas which was set as 1.5 and 2 for the hydrogen and oxygen gases, respectively. Therefore, the anodic and the cathodic mass flow rates are given as follows [28]:

$$Q_a = \frac{\xi_a M_{H_2}}{2FY_{H_2}} i_{op} A_{act} \quad \textbf{(5.28)}$$

$$Q_c = \frac{\xi_c M_{O_2}}{4FY_{O_2}} i_{op} A_{act} \quad \textbf{(5.29)}$$

The boundary conditions for the anode and cathode outlets and wall terminals are the same as those specified in Section 4.2.4 of Chapter 4 of the thesis.

The equations governing the transport of mass, heat, and charge, and liquid water in the PEFC model and the coupled boundary conditions were solved iteratively, using the commercial software ANSYS FLUENT with Semi-implicit Method for Pressure Linked Equations (SIMPLE) algorithm employed for the pressure–velocity coupling with the second-order upwind discretization scheme for the conservation of momentum, species, energy, charge, and liquid water equations. The model was found to give mesh-independent solution with a mesh of about 1.6 million elements. The deviations in the average current densities at 0.55V, when this number was doubled and when halved was 0.6 and 1.3%, respectively.

The model was found to give mesh-independent solution with a mesh of about 1.4 million cells; doubling this number result in a variation of less than 0.3% in the key performance indicator which is, in this case, the average current density at 0.55 V.

The mesh geometry is shown in Figure 5.2, while the geometrical, operational, and physical parameters of this model are presented in Table 5.1.

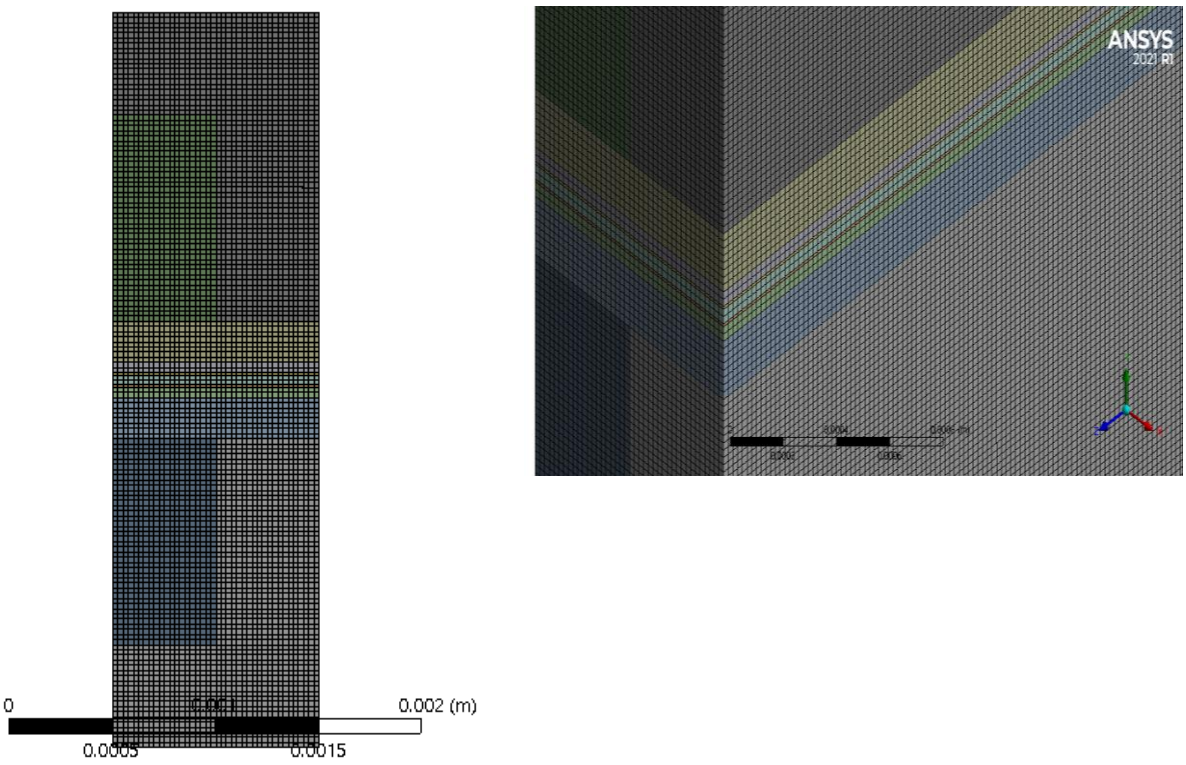

Figure 5.2 The mesh profile of the PEM fuel cell model geometry.

Table 5.1 Geometrical and physical properties for the base case of the PEFC model [30].

Property	**Value**
Channel length	5×10^{-2} m
Channel height	1.0×10^{-3} m
Channel width	1.0×10^{-3} m
Current collector rib width	1.0×10^{-3} m
Current collector height	1.5×10^{-3} m
GDL thickness	2.0×10^{-4} m

MPL thickness	5.0×10^{-5} m
Catalyst layer thickness	1.0×10^{-5} m
Membrane thickness	5.0×10^{-5} m
Operating temperature	353 K
Gauge pressure at anode	1 atm
Gauge pressure at cathode	1 atm
Relative humidity of inlet gases	100%
Stoichiometric ratio, anode	1.5
Stoichiometric ratio, cathode	2
Oxygen/nitrogen molar ratio in air	0.21/0.79
Catalyst layer porosity	0.2
GDL porosity	0.7
MPL porosity	0.6
Reference hydrogen concentration, $c_{H_2}^{ref}$	56.4 mol/m^3
Reference oxygen concentration, $c_{O_2}^{ref}$	3.39 mol/ m^3
Electrical conductivity of current collector	20000 S/m
Electrical conductivity of GDL	5000 S/m
Electrical conductivity of catalyst layer	2000 S/m
Electrical conductivity of MPL	5000 S/m

GDL permeability	3.0×10^{-12} m^2
MPL permeability	1.0×10^{-1} m^2
Catalyst layer permeability	2×10^{-13} m^2
Membrane permeability	1.8×10^{-18} m^2
Thermal conductivity of GDLs	1.7/21 W/(m-K)
Thermal conductivity of MPL	10 W/(m-K)
Thermal conductivity of catalyst layers	0.3 W/(m-K)
Thermal conductivity of current collector	100 W/(m-K)
Thermal conductivity of the membrane	0.25 W/(m-K)
GDL/MPL/CL contact angle	110/130/95
Faraday’s constant	96485 C/mol
Universal gas constant	8.314 J/(mol-K)
Anode inlet mass fraction of hydrogen	0.1105
Anode inlet mass fraction of water	0.8895
Cathode inlet mass fraction of oxygen	0.1503
Cathode inlet mass fraction of water	0.3541
Anode flow rate	1.3518e-07 kg/s
Cathode flow rate	1.10331e-06 kg/s
Anode concentration exponents	0.5

Cathode concentration exponents	1
Anode reference exchange current density, $i_{0,a}^{ref}$	100 A/m²
Cathode reference exchange current density, $i_{0,c}^{ref}$	0.0001760881 A/m²
Transfer coefficients for anode reaction	0.5
Transfer coefficients for cathode reaction	1
Anode specific surface area, a_a	1.0×10^7 m^{-1}
Cathode specific surface area, a_c	1.0×10^7 m^{-1}

5.3 RESULTS AND DISCUSSIONS

To further validate the accuracy of the computed multiphase PEM fuel cell model, the model was simulated for different cell voltages and the polarisation curve was generated. Figure 5.3 shows the polarization curve for the simulated PEM fuel cell model to be in good agreement with the experimental data of Wang et al. [34].

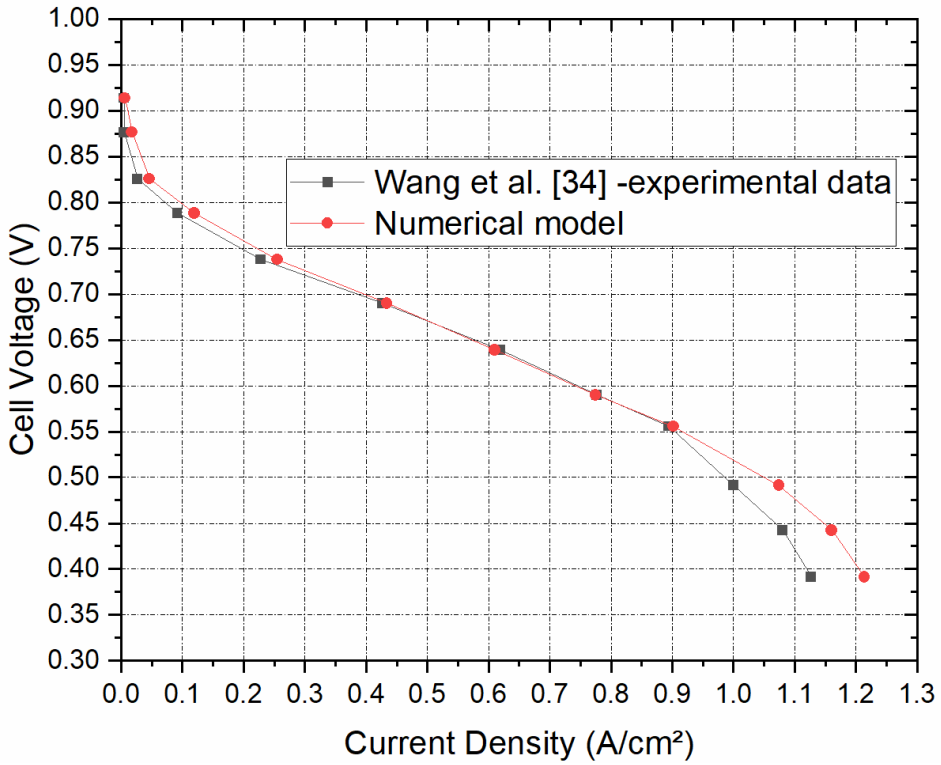

Figure 5.3 Comparison of the polarization curve generated from the numerical model to the experimental polarization curve taken from Wang et al. [170].

5.3.1 Parametric study on single-side MPL coated GDLs.

The first part of this investigation is aimed at studying the sensitivity of the PEM fuel cell model (with single side MPL-coated GDL) performance to the interfacial contact resistance between the fuel cell components. To achieve this aim, the experimentally estimated interfacial contact resistance values, measured by Ismail et al., 2015, for Sigracet SGL 10BC coated carbon paper at an assembly clamping pressure of 1.5 bar, are incorporated into the model and the effects are investigated. The outcomes of the study are discussed in Sections 5.3.2 to 5.3.4.

5.3.2 Contact resistance values of 12.5mΩ.cm², 15mΩ.cm², and 17.5mΩ.cm² at GDL-BPP

Three cases incorporating different values of 12.5mΩ.cm², 15.0mΩ.cm² and 17.5mΩ.cm², respectively, interfacial contact resistance between the GDL and the bipolar plates were simulated, and the results shown in Figure 5.4. Figure 5.4a shows the fuel cell polarisation curves for these three cases. As can be observed in Figure 5.4a, the global performance of the PEMFC model improves from Case 3 with 17.5mΩ.cm² contact to that of Case 2 with 15.0mΩ.cm² contact resistance at a percentage of 2.4%, and there is a 3.2% increase in the model performance when we compare Case 2 with Case 1. As can be observed, the polarization curves show that Case1 is over-estimated by 4.8% when compared to Case 3 for the current density values of 0.3 to 1.25A/cm². Again, Figure 5.4b shows the distribution of the current density taken at the midpoint of the cathode GDL, half the length of the fuel cell channel, at an average cell potential of 0.55V. It can be observed that the current density distribution, for all three Cases, increases from the region of the GDL lying below the Centre of the gas flow channel to the region below the interface of the gas flow channel and the current collector rib, where it reaches its peak value. Then it decreases from its peak value at the gas channel / collector rib interface towards the region of the GDL below the mid-point of the current collector rib. Also, Figure 5.4b shows that the distribution of current density for Case 1 is over-estimated by 11.8% as compared to the current density distribution of Case 3, while it is 5.5% over-estimated when compared to that for the Case 2. Also, Case 2 is 5.9% over-estimated when compared to that with the interfacial contact resistance of Case 3. Considering Figure 5.4c, which shows the distribution of the oxygen mass from fraction for the three cases, it can be observed that the Cases 1 and 2 show more

utilization of the oxygen gas reactants within the cathode GDL as compared to Case 3. The distribution of oxygen mass fraction for Cases 1 and 2 overlap each other but as we approach the region of the GDL lying directly below the middle of the current collector rib, we observe that Case 1 shows more utilization of oxygen in comparison to Case 2. Cases 2 and 3 show about 3.2% more consumption of oxygen when compared to Case 3. However, all three cases show that there is more consumption of the oxygen in the region beneath the collector rib compared to the region below the gas channel.

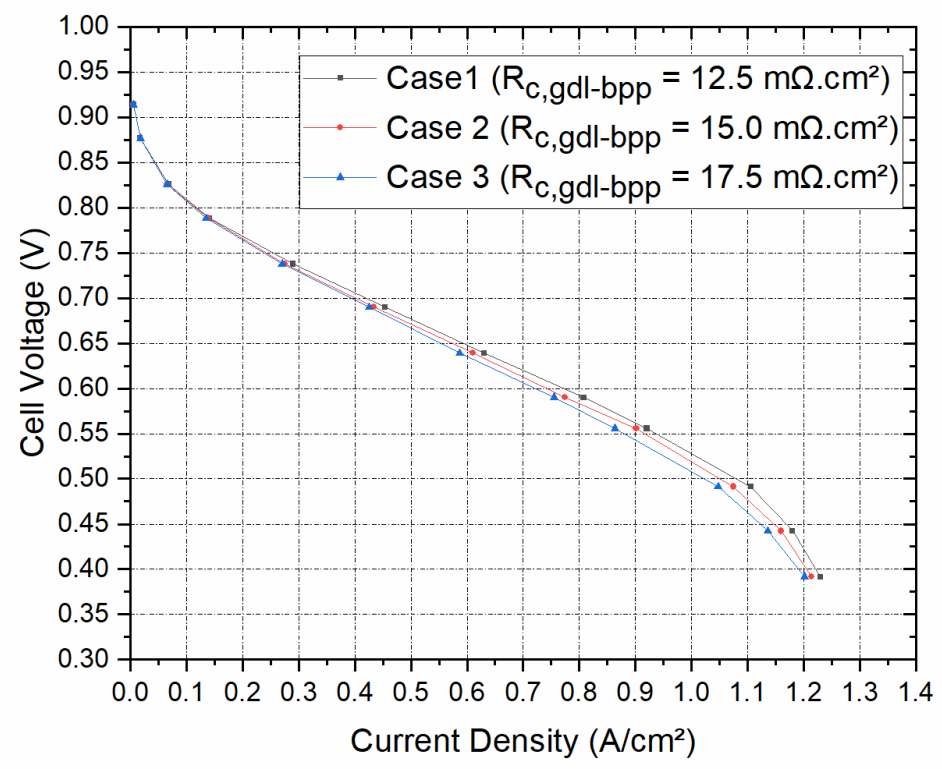

(a)

Figure 5.4 (a) Polarisation curves for the contact resistances.

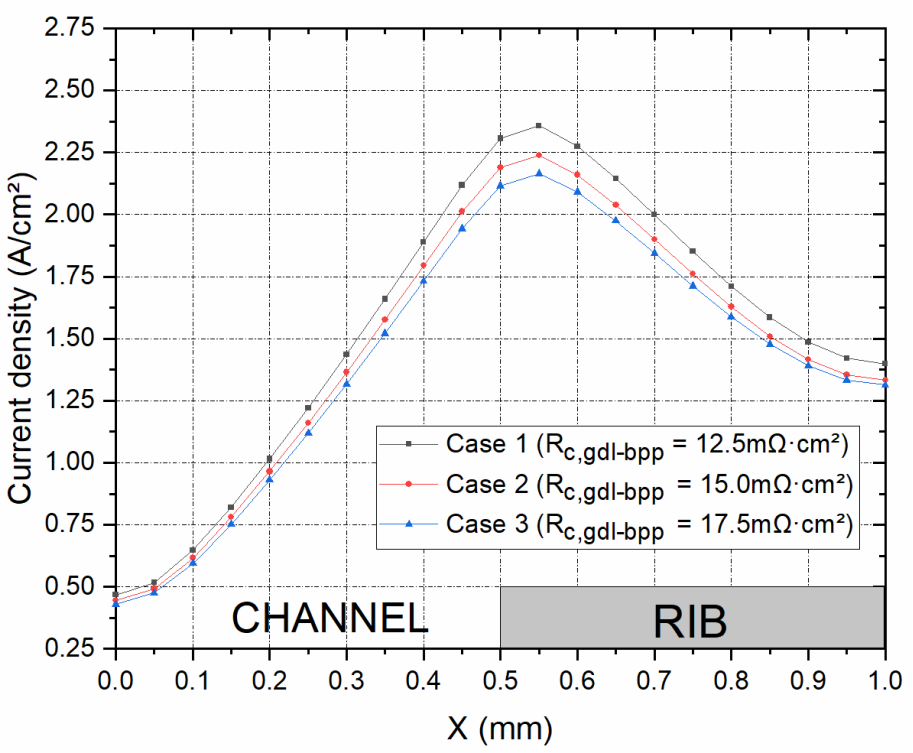

(b)

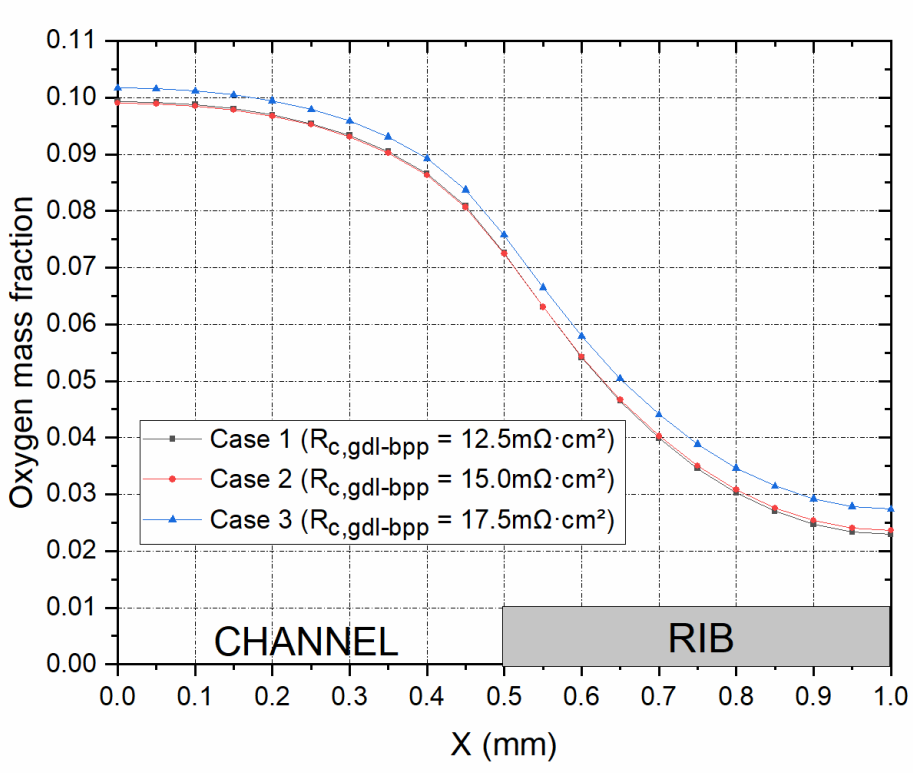

(c)

Figure 5.4 (b) the distribution of current density and (c) oxygen mass fraction within the cathode GDL at 0.55 V for the contact resistances.

5.3.3 Contact resistance values of 2.5mΩ.cm², 5mΩ.cm², and 7.5mΩ.cm² at the GDL-BPP interface

The PEM fuel model has been simulated for Cases 1, 2, and 3 where the interfacial contact resistance between the gas diffusion layer and the bipolar plates has been realistically reduced from the values used in Section 5.3.2 to those shown in Table 5.2 of this section. This has been done to highlight the impact of the interfacial contact resistance, between the GDL and the bipolar plate, on the global performance of the PEM fuel cell model and the local distribution of key variables (current density and oxygen) within the cathode GDL. It can be seen that the cases presented in Figure 5.5a show an improvement compared to the polarisation curves shown in Figure 5.4a in Section 5.3.2. This can be explained by the fact that the lower interfacial contact resistances allow for an improved transport of electrons from the bipolar plates to the GDL, also the bulk electrical resistance of the gas diffusion electrode is reduced as a result of the reduction in the interfacial contact resistance which contributes to the electrical resistance of the GDL. Therefore, more electrons are effectively transported to the electro catalyst for the reactions to occur. The influence of the improved electronic conductivity can also be seen in the mass transfer losses region as the polarisation curve improves at higher current density for Figure 5.5a as compared to Figure 5.4a. To emphasize this further, we consider the current density distribution plots of Figures 5.4b and 5.5b. Comparing Case 1 of Section 5.3.3 (with a contact resistance of 2.5mΩ.cm²) with Case 1 of Section 5.3.3 (with contact resistance of 12.5mΩ.cm²), shows that the current density distribution increases. Also, for Cases 2 and 3 of Figure 5.5a, it can be seen that the distribution improves the average when compared with the same Cases in Figure 5.4a. This is as a result of the reduced electrical resistance which arises due to the reduced

interfacial contact resistance. Also, the above observation is applicable to the distribution of the oxygen mass fraction within the cathode GDL. The case for the Section 5.3.3 shows that the oxygen is utilized more for the case with lower interfacial contact resistance. This shows that more oxygen is consumed with the lower resistance to the electronic transport in the cathode gas electrode.

Table 5.2 Interfacial contact resistance between the GDL and the bipolar plates.

	Case 1	**Case 2**	**Case 2**
Contact resistance	2.5mΩ.cm²	5mΩ.cm²	7.5mΩ.cm²

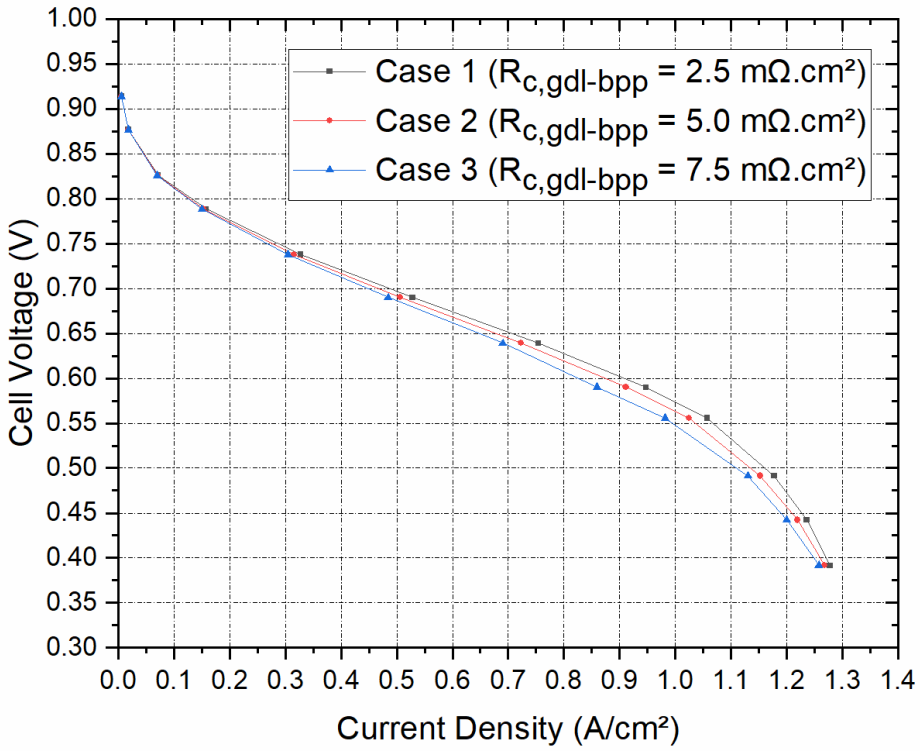

(a)

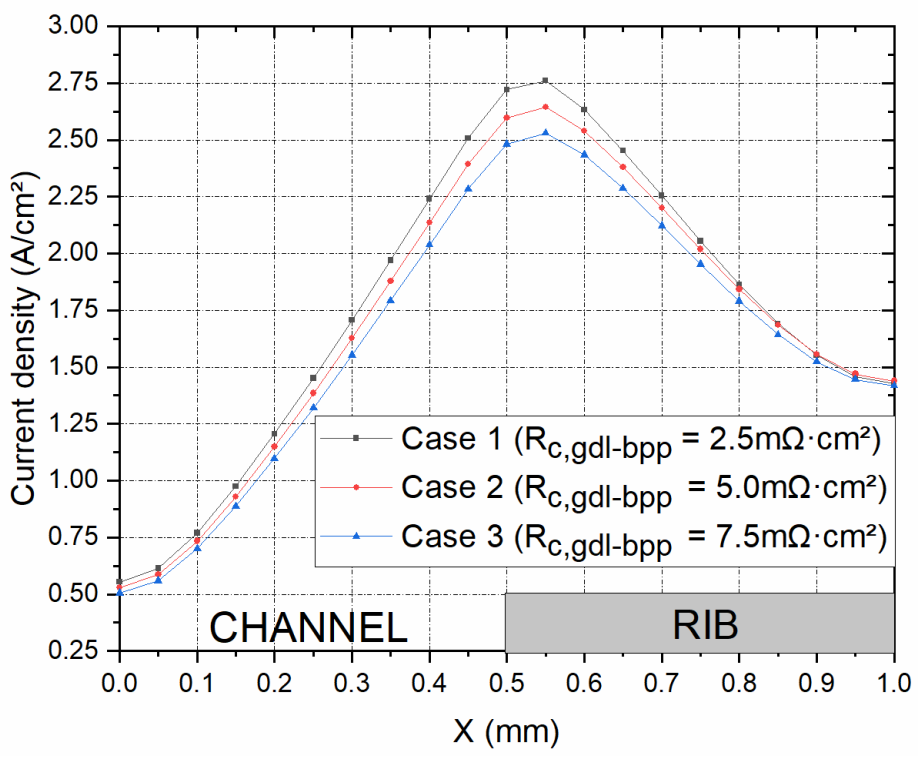

(b)

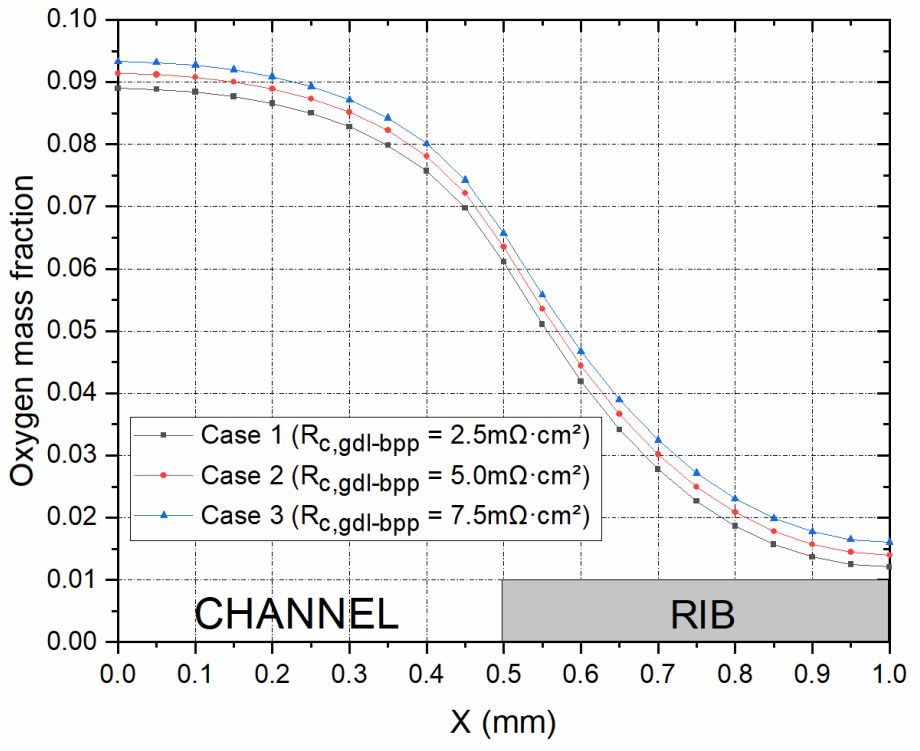

(c)

Figure 5.5 (a) Polarisation curves, and the distribution of (b) current density, and (c) oxygen mass fraction within the cathode GDL at 0.55 V for the contact resistances.

5.3.4 Effect of the contact resistance at the GDL-catalyst layer interface

One of the assumptions for this PEM fuel cell model was that the catalyst layer is deposited directly on the gas diffusion media instead of the membrane. Therefore, the interfacial contact resistance between the GDL and the catalyst layer was assumed to be negligible, and the gas diffusion electrode is assumed to be homogenous. The assumption has been made at the initial stage so as to simplify the model and also because there is no existing experimentally characterised values of the interfacial resistance between the MPL and the catalyst layer in the open literature. However, to investigate the sensitivity of the global PEM fuel cell performance, as well as the local distribution of the current density and oxygen mass fraction, within the cathode GDL, the interfacial contact resistance between the MPL and the catalyst layer has been assumed to be 2.5mΩ.cm² for the two scenarios of Section 5.3.2 and Section 5.3.3. Figure 5.6 shows the cell polarisation curves. as well as the local distribution of the current density and oxygen mass fraction within the cathode GDL for the different scenarios investigated. Figure 5.6a-b with shows that there is not much change in the PEM fuel cell polarisation curves for the scenario simulated. Therefore, we can state that for a catalyst coated GDM, the impact of the contact resistance between the MPL and the catalyst layer on the global performance of the PEM fuel cell is moderate or almost insignificant. Figure 5.6c shows the distribution of the current density within the cathode GDL at a cell potential of 0.55V for the scenarios investigated. As can be observed, the current density distribution is overestimated for the cases without the interfacial contact resistance at the MPL and catalyst layer interface. For example, considering Case 1 and Case 4 (of each scenario), we see that the current density is overestimated for Case 1 by an average of 5.4%. Also, Case 2 is overestimated by about 4.4%

when compared to Case 5. Likewise, Case 3 is overestimated by about 3.7% when compared to Case 6. Also, Figure 5.6d shows the same trend as that of Figure 5.6c. Case 1 is overestimated by about 5.5% when compared to case 4. Case 2 shows 5.1% over estimation compared to that of Case 5 and likewise, Case 3 is about 4% overestimated when compared to Case 6. The distribution of the oxygen mass fraction in Figure 5.6 e-f shows that the cases overlap each other for both scenarios so that the distribution of oxygen within the cathode GDL is not sensitive to the interfacial contact resistance between the MPL and the catalyst layer. The results of this section in the studying of the highlights of the impact of the contact resistance at GDL -bipolar plate interface (and to a minimal extent, that of the MPL and catalyst layer) on the global performance of the PEM fuel cell as well as in the local distribution of key variables within the cathode GDL. Hence, there is the need to investigate further the effect of the MPL coating of the GDL at the GDL-bipolar plate interface.

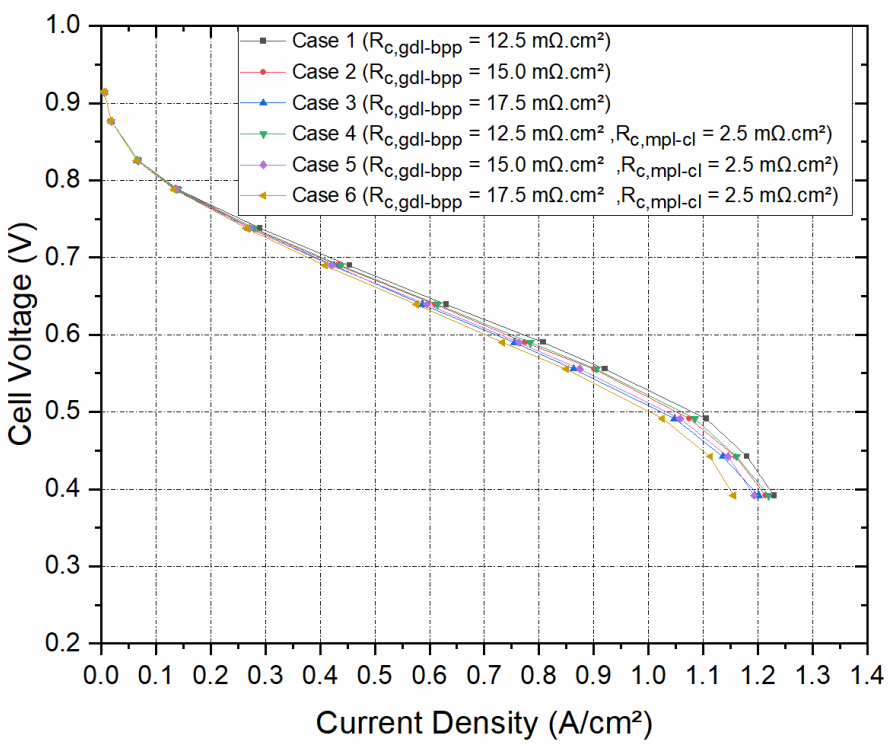

(a)

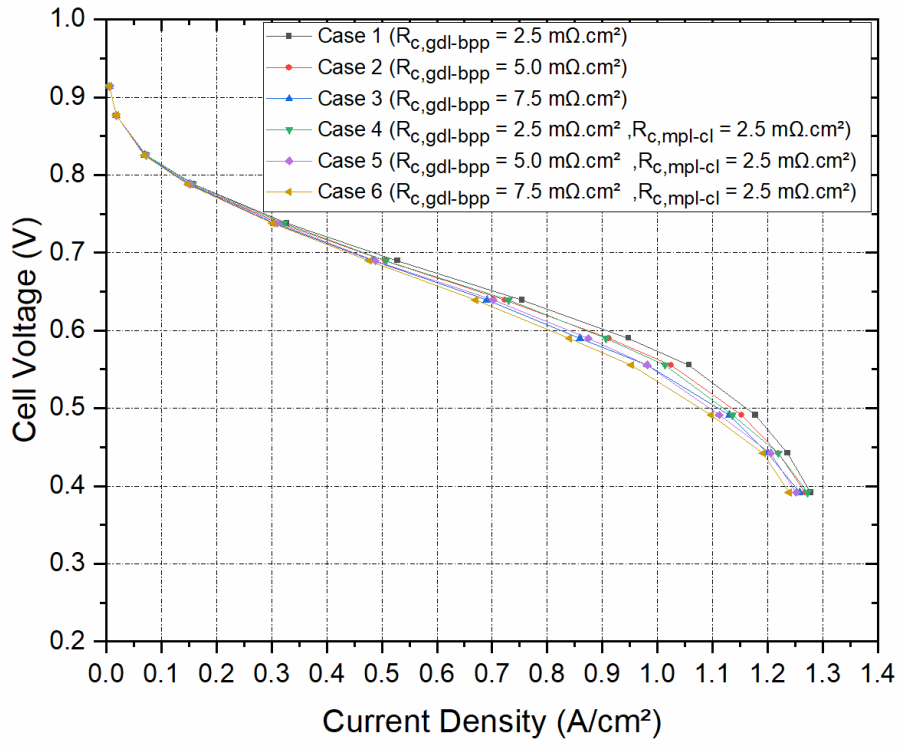
Case 1 ($R_{c,gdl-bpp}$ = 2.5 mΩ.cm²)
Case 2 ($R_{c,gdl-bpp}$ = 5.0 mΩ.cm²)
Case 3 ($R_{c,gdl-bpp}$ = 7.5 mΩ.cm²)
Case 4 ($R_{c,gdl-bpp}$ = 2.5 mΩ.cm² ,$R_{c,mpl-cl}$ = 2.5 mΩ.cm²)
Case 5 ($R_{c,gdl-bpp}$ = 5.0 mΩ.cm² ,$R_{c,mpl-cl}$ = 2.5 mΩ.cm²)
Case 6 ($R_{c,gdl-bpp}$ = 7.5 mΩ.cm² ,$R_{c,mpl-cl}$ = 2.5 mΩ.cm²)
Cell Voltage (V)
Current Density (A/cm²)

(b)

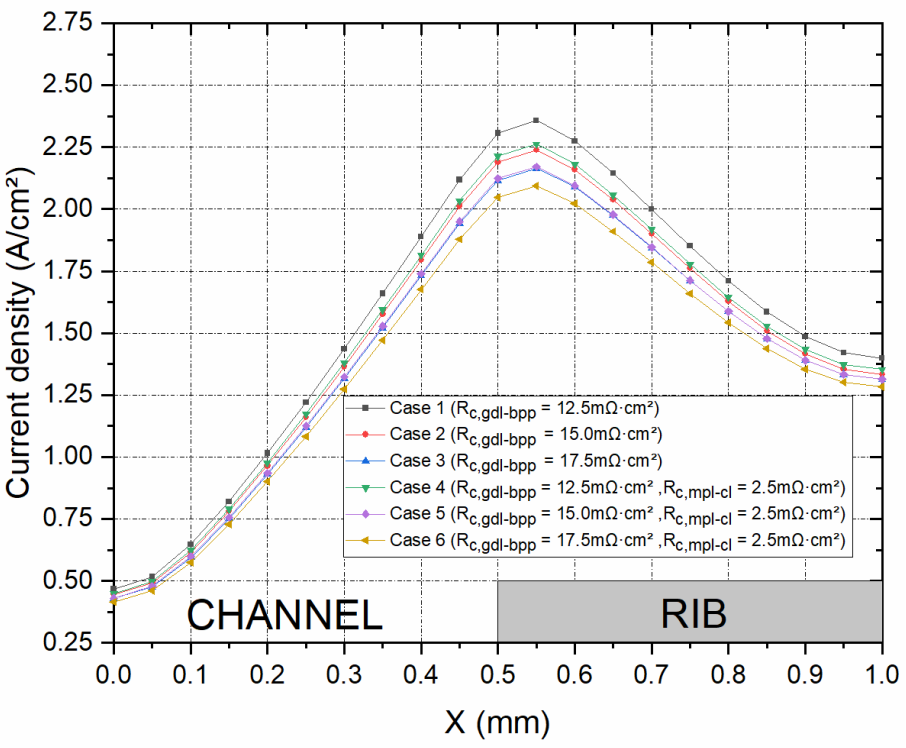
Case 1 ($R_{c,gdl-bpp}$ = 12.5mΩ·cm²)
Case 2 ($R_{c,gdl-bpp}$ = 15.0mΩ·cm²)
Case 3 ($R_{c,gdl-bpp}$ = 17.5mΩ·cm²)
Case 4 ($R_{c,gdl-bpp}$ = 12.5mΩ·cm² ,$R_{c,mpl-cl}$ = 2.5mΩ·cm²)
Case 5 ($R_{c,gdl-bpp}$ = 15.0mΩ·cm² ,$R_{c,mpl-cl}$ = 2.5mΩ·cm²)
Case 6 ($R_{c,gdl-bpp}$ = 17.5mΩ·cm² ,$R_{c,mpl-cl}$ = 2.5mΩ·cm²)
CHANNEL
RIB
Current density (A/cm²)
X (mm)

(c)

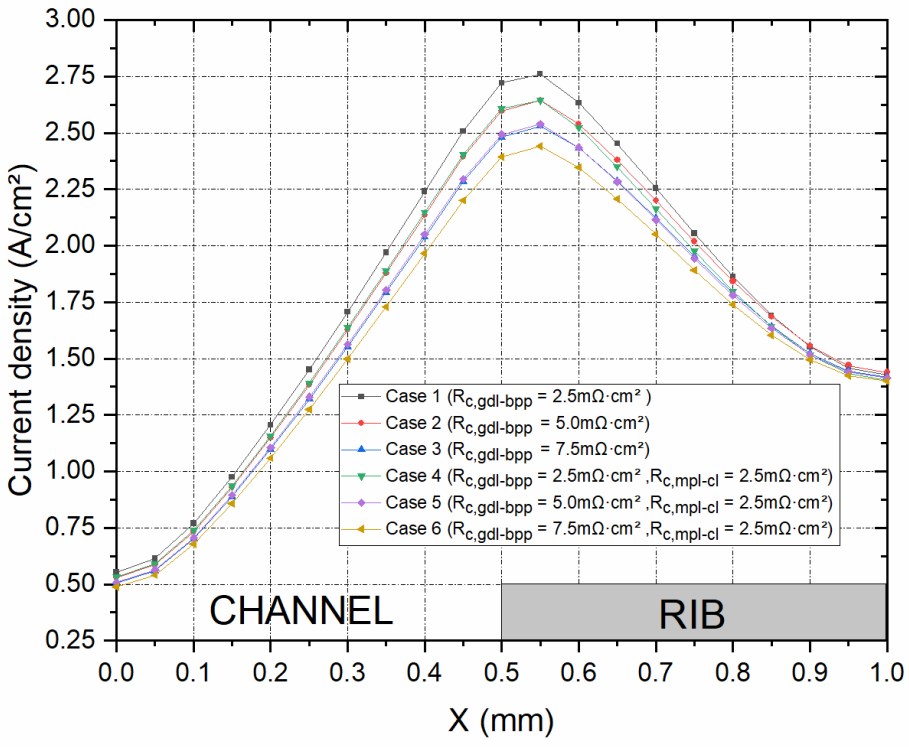
Current density (A/cm²)
X (mm)
CHANNEL
RIB
Case 1 (Rc,gdl-bpp = 2.5mΩ·cm²)
Case 2 (Rc,gdl-bpp = 5.0mΩ·cm²)
Case 3 (Rc,gdl-bpp = 7.5mΩ·cm²)
Case 4 (Rc,gdl-bpp = 2.5mΩ·cm² ,Rc,mpl-cl = 2.5mΩ·cm²)
Case 5 (Rc,gdl-bpp = 5.0mΩ·cm² ,Rc,mpl-cl = 2.5mΩ·cm²)
Case 6 (Rc,gdl-bpp = 7.5mΩ·cm² ,Rc,mpl-cl = 2.5mΩ·cm²)

(d)

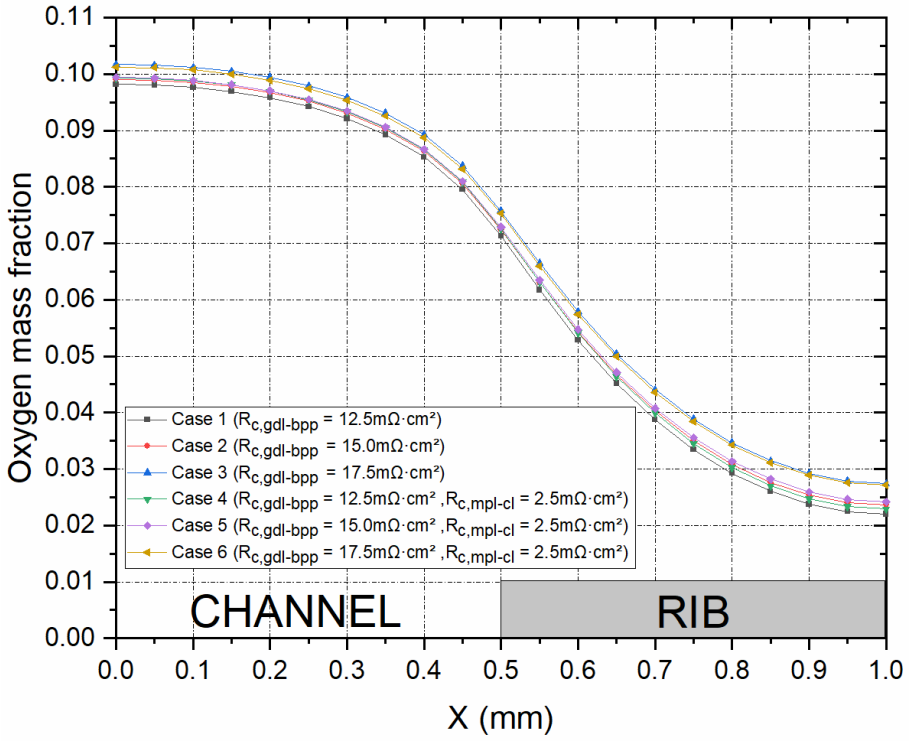
Oxygen mass fraction
X (mm)
CHANNEL
RIB
Case 1 (Rc,gdl-bpp = 12.5mΩ·cm²)
Case 2 (Rc,gdl-bpp = 15.0mΩ·cm²)
Case 3 (Rc,gdl-bpp = 17.5mΩ·cm²)
Case 4 (Rc,gdl-bpp = 12.5mΩ·cm² ,Rc,mpl-cl = 2.5mΩ·cm²)
Case 5 (Rc,gdl-bpp = 15.0mΩ·cm² ,Rc,mpl-cl = 2.5mΩ·cm²)
Case 6 (Rc,gdl-bpp = 17.5mΩ·cm² ,Rc,mpl-cl = 2.5mΩ·cm²)

(e)

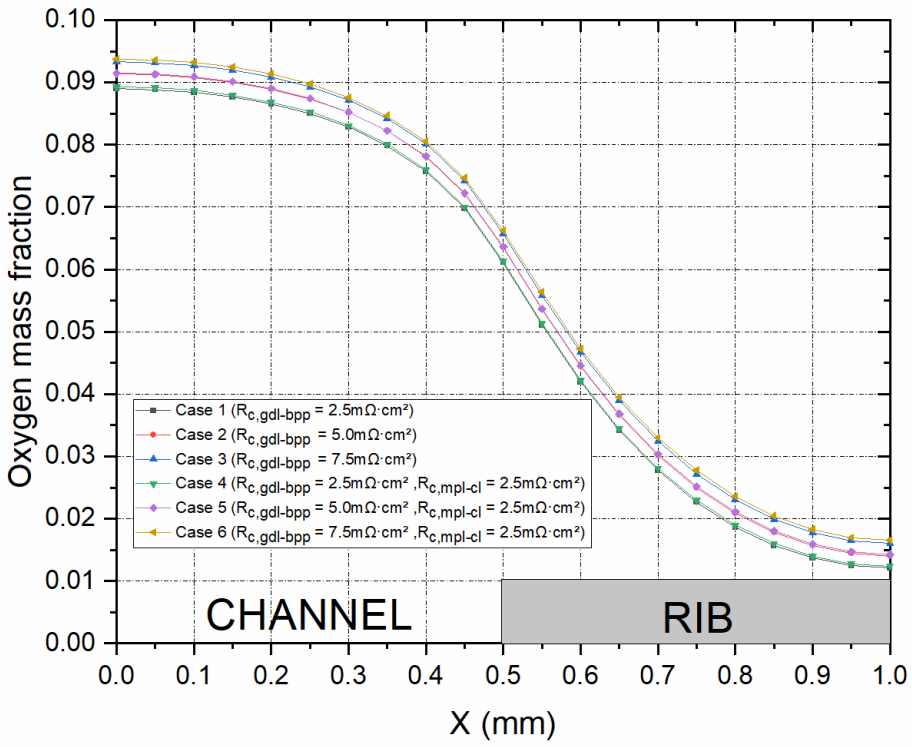

(f)

Figure 5.6 Polarisation curves of (a) the contact resistance values of 12.5mΩ.cm², 15.0mΩ.cm², and 17.5mΩ.cm² at GDL-BPP interface, (b) the contact resistance values of 2.5mΩ.cm², 5.0mΩ.cm², and 7.5mΩ.cm² at GDL-BPP interface; the distribution of the current density, (c) the contact resistance values of 12.5mΩ.cm², 15.0mΩ.cm², and 17.5mΩ.cm² at GDL-BPP interface, (d) the contact resistance values of 2.5mΩ.cm², 5mΩ.cm², and 7.5mΩ.cm² at GDL-BPP interface; and oxygen mass fraction distribution, (e) the contact resistance values of 12.5mΩ.cm², 15.0mΩ.cm², and 17.5mΩ.cm² at GDL-BPP interface, (f) the contact resistance values of 2.5mΩ.cm², 5mΩ.cm², and 7.5mΩ.cm² at GDL-BPP interface, within the cathode GDL at 0.55 V.

5.3.5 Double side MPL coated GDL

To investigate the effect of the double coating of the GDL carbon substrate, the PEM fuel cell model geometry has been modified to incorporate the MPL at the GDL-bipolar plate interface, for both the anode and cathode sides of the PEM fuel cell, as shown in Figure 5.7.

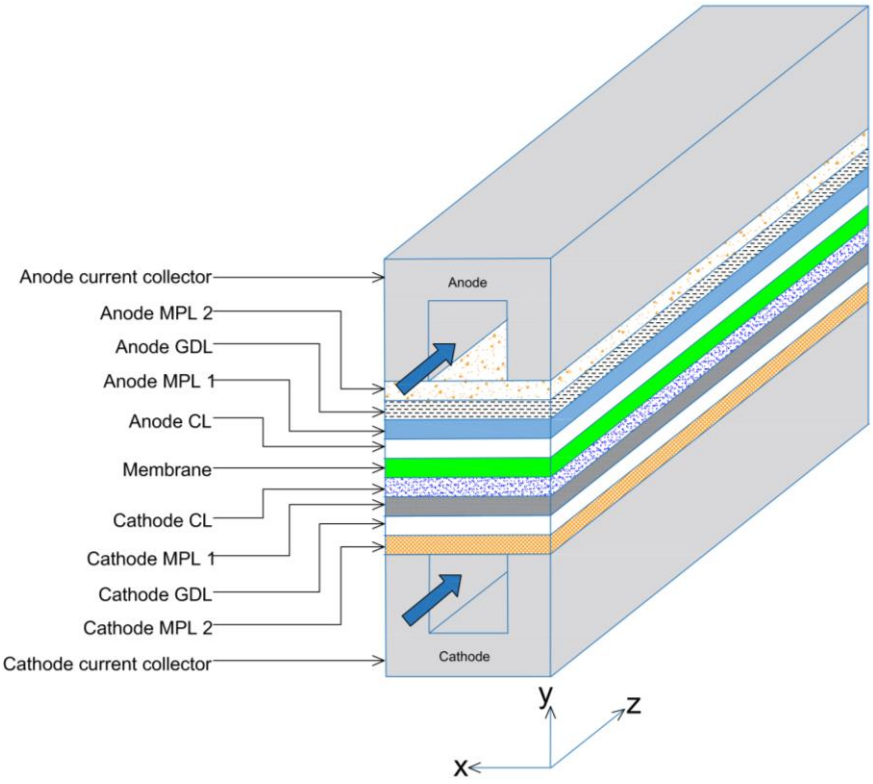

Figure 5.7 Schematic geometry of the computational domain incorporating the MPL at the GDL-bipolar plate interface.

5.3.6 Parametric study on the interfacial contact resistances

Four different Cases (1-4) shown in Table 5.3 were simulated to investigate the significance of the MPL coating at the GDL-bipolar plate interface on the global performance of the PEM fuel cell model. It is important to note that Case 1 is the base case of the PEM fuel cell model with a single side MPL coating at the GDL-catalyst layer while Cases 2, 3, and 4 represent the modified PEM fuel cell model which incorporates and extra MPL coating at the GDL-bipolar plate interface. The cell polarisation curves of the four Cases simulated are shown in Figure 5.8. The results show that for the range of cell voltage of 0.375-0.725V, Case 2 is overestimated by approximately 6% when compared to Case 1. Also, Cases 3 and

4 show approximately 3.8% and 1.5% overestimation, respectively, compared to Case 1 for the same range of cell voltage. Interestingly, Case 3 and Case 1 have the same values of interfacial contact resistances but Case 3 has an MPL coated between the GDL and the bipolar plate. This shows that the influence of the interfacial contact resistance is reduced with an MPL coating at the GDL-bipolar plate interface. Also, a parametric study was performed on the interfacial contact resistance between the MPL and the bipolar plate. The results show that a decrease in the contact resistance resulted in improved performance of the PEM fuel cell model as can be seen when we compare Cases 2, 3, and 4.

Table 5.3 Interfacial contact resistances for the cases investigated.

Contact resistance	Case 1 (Single-side MPL)	Case 2 (Double-side MPL)	Case 3 (Double-side MPL)	Case 4 (Double-side MPL)
$R_{c,gdl-bpp}$	5.0mΩ·cm²	-	-	-
$R_{c,mpl-cl}$	2.5mΩ·cm²	2.5mΩ·cm²	2.5mΩ·cm²	2.5mΩ·cm²
$R_{c,mpl-bpp}$	-	2.5mΩ·cm²	5.0mΩ·cm²	7.5mΩ·cm²

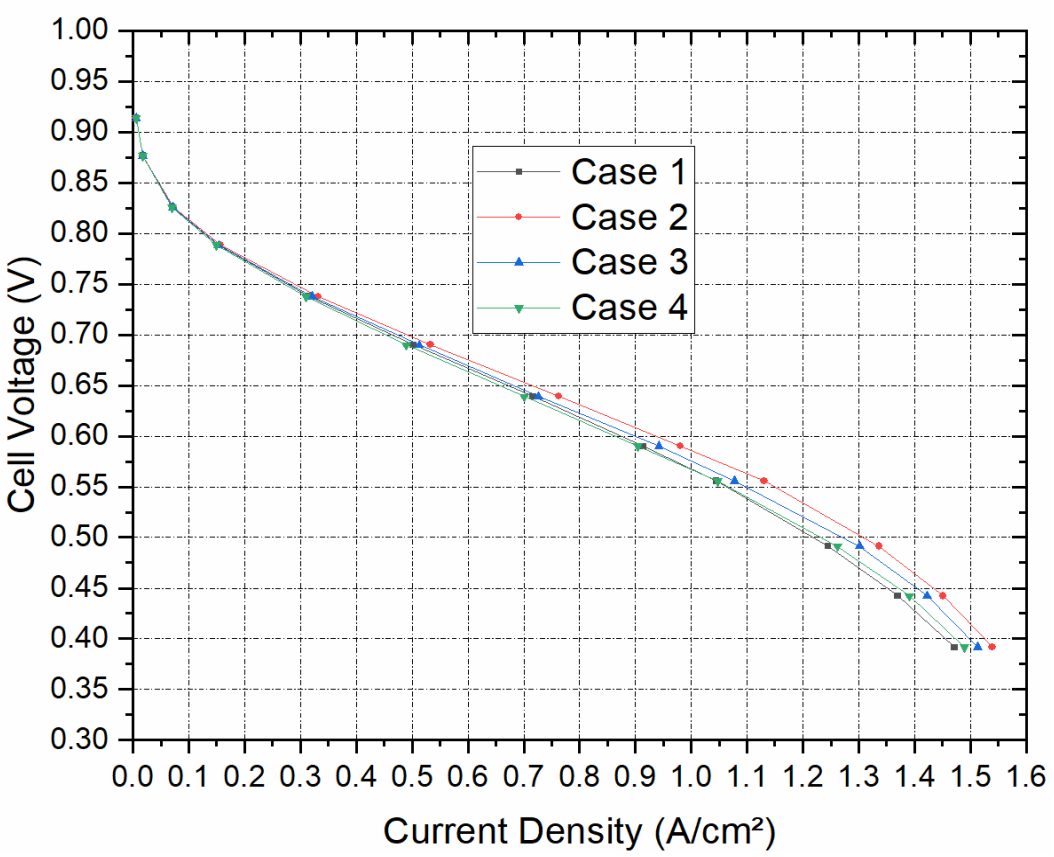

Figure 5.8 Polarisation curves for the contact resistances of single side and double side MPL-coated GDL computation cases shown in Table 5.3.

5.3.7 Parametric study on the porosity of double side MPL coated GDLs

A parametric study is carried out in this Section to investigate the effect of the porosities of the MPLs on both sides of the GDL substrate and the model simulated with various MPL porosities as shown in Table 5.4. Where $\varepsilon_{\mathrm{MPL1}}$ is the porosity of the MPL between the GDL and the catalyst layer and $\varepsilon_{\mathrm{MPL2}}$ is the porosity of the MPL coating between the GDL and the bipolar plate for both anode and cathode sides of the PEM fuel cell. The results of the study are shown in Figure 5.9. As can be seen, in Figure 5.9a, the model begins to show sensitivity to the porosities at the ohmic and concentration losses region of the cell polarisation curve. The PEM fuel cell polarisation curve is overestimated for Case 9 where $\varepsilon_{\mathrm{MPL1}}$ and $\varepsilon_{\mathrm{MPL2}}$ are

equal to 0.8. Also, considering Cases 1,2,3 and 4, where Case 1 is the base case (with single side MPL coating between the GDL and the catalyst layer), it is observed that at this region of concentration losses, Case 2 with $\varepsilon_{\mathrm{MPL1}}$ and $\varepsilon_{\mathrm{MPL2}}$ equal to 0.6 is underestimated compared to Case 1 with the single side MPL coating and having a porosity value of 0.6. This is understandable as the addition of the MPL makes the gas diffusion media thicker, hence increasing the tortuous path for gas reactants to travel from the gas channel to the catalyst reaction sites. Case 3 is underestimated by 20% when compared to Case 1. Also, it is underestimated by 14.7% when compared with Case 2 and underestimated by 25% compared to Case 4. Also, Case 4 is overestimated by 3.6% compared to Case 1 (the base case with single side MPL coating). This emphasizes the fact that the global performance of the PEM fuel cell model is sensitive to the MPL loading at the GDL-bipolar plate interface. It can be stated from this observation that the double side MPL-coated GDL with improved porosity significantly improves the global performance of the PEM fuel cell. Also, the results emphasize the importance of the porosity of the MPL coating between the GDL and the bipolar plates. It shows that a reduction in the porosity of this MPL limits the diffusive transport of gas reactants from the gas flow channel to the gas diffusion layer and the catalyst reaction sites. Also, for Cases 5, 6 and 7, where the porosity of the MPL between the GDL and the catalyst layer is kept constant at 0.4, it is observed that an increase in the porosity of the MPL which lies between the GDL and the bipolar plates significantly improves the performance concentration polarisation regions. A Case-by-Case comparison shows that the cell polarisation curve of Case 6 is overestimated by 14.7% compared to that of Case 5, while Case 7 is overestimated by about 22.9% compared to Case 5. Also, when Case 7 is compared with Case 6, we observe that the cell polarisation curve

increases by a factor of 2. Again, for Cases 8, 9 and 10, the cell polarisation curve of Case 10 is about 23.5% overestimated when compared to Case 8. Also, Case 9 is about 15.1% overestimated compared to Case 8. To further emphasize the significance of the porosity of the MPL coating between the GDL and the bipolar plate and its importance in improving the global performance of the PEM fuel cell model, we can compare to Case 3, Case 6, Case 4 to Case 9 and Case 7 with Case 8. It can be observed, in all these cases, that where $\varepsilon_{\mathrm{MPL2}}$ is decreased the cell polarisation curve is underestimated. Whereas, increasing $\varepsilon_{\mathrm{MPL2}}$ increases the cell performance. The same trend observed can be seen in Figure 5.9b which shows the distribution of current density within the mid-point of the gas diffusion layer, at a cell potential of 0.55V. Figure 5.9b shows that the MPL coating between the GDL and the bipolar plate significantly impacts the local distribution of the current density in the cathode GDL. This is more pronounced in the region of the GDL which lies below the current collector rib. This is more pronounced at the region of the GDL that lies below the current collector rib. The plots show that the local distribution of the current density is improved where $\varepsilon_{\mathrm{MPL2}}$ is greater than $\varepsilon_{\mathrm{MPL1}}$. For example, the distribution for Case 10 is overestimated when compared to Cases 8 and 9, while Case 9 is better compared to Case 8. Case 4 is overestimated compared to Cases 2 and 3 while Case 2 shows better distribution when compared to Case 3. The trend is the same for Cases 5, 6, and 7. Also, Case 4 shows better distribution compared to Case 9. Likewise, Case 7 is better than Case 8 and Case 6 is better than Case 3. This emphasizes the fact that the MPL coating between the GDL and the bipolar plate improves the electronic transport by reducing the contact resistance in that interface. However, for the distribution of oxygen mass fraction in the cathode

GDL shown in Figure 5.9c, it is observed that the oxygen is more consumed where $\varepsilon_{\mathrm{MPL1}}$ is greater than $\varepsilon_{\mathrm{MPL2}}$. This can be attributed to the fact that a decrease in porosity, along the through plane direction, will allow for more reactants to be supplied to the catalyst layer.

Table 5.4 Cases investigated for the MPL porosities.

Case No.	$\varepsilon_{\mathrm{MPL1}}$	$\varepsilon_{\mathrm{MPL2}}$
1 (Single MPL)	0.6	NA
2	0.6	0.6
3	0.6	0.4
4	0.6	0.8
5	0.4	0.4
6	0.4	0.6
7	0.4	0.8
8	0.8	0.4
9	0.8	0.6
10	0.8	0.8

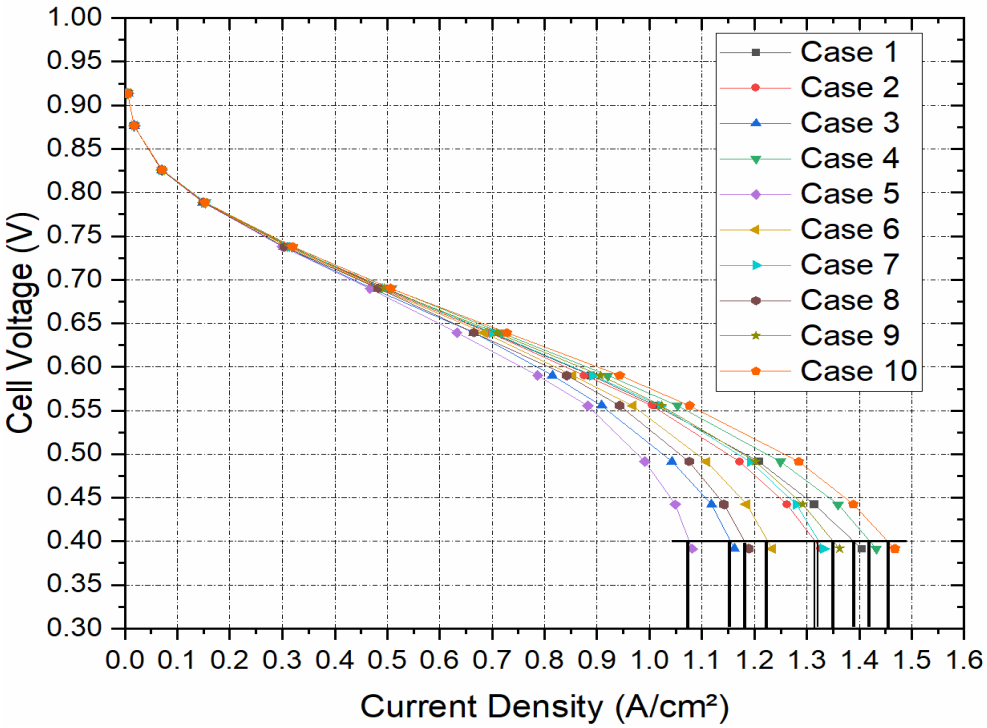
Cell Voltage (V)
Current Density (A/cm²)
Case 1
Case 2
Case 3
Case 4
Case 5
Case 6
Case 7
Case 8
Case 9
Case 10

(a)

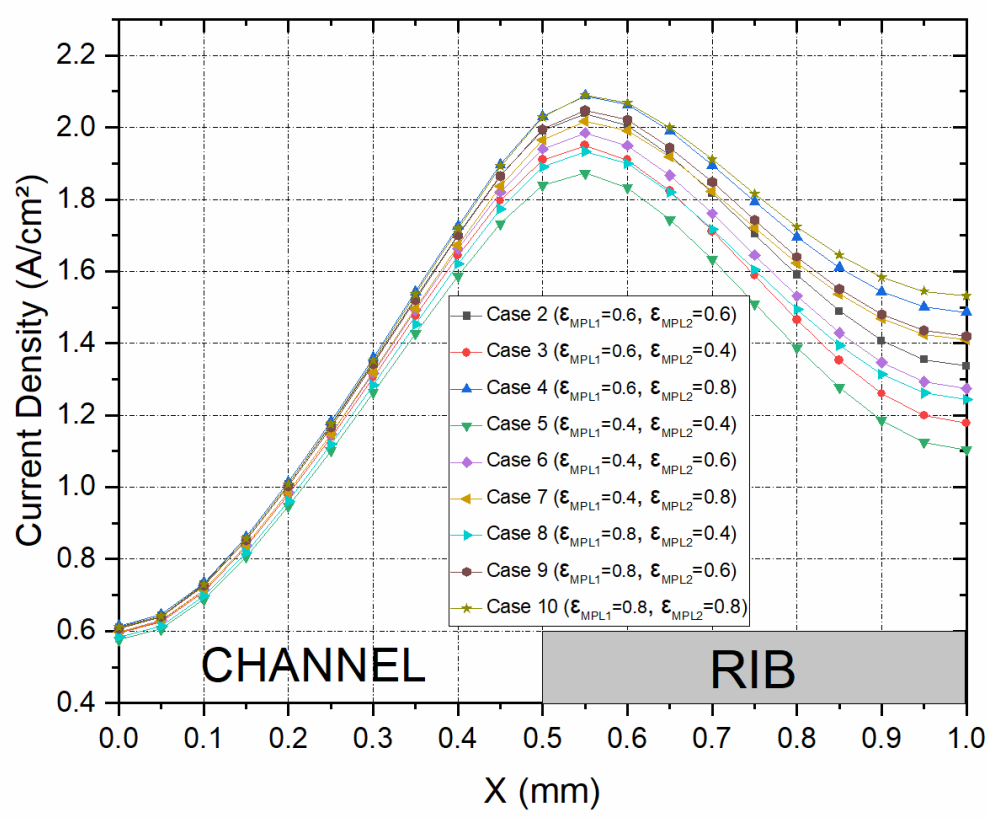
Current Density (A/cm²)
X (mm)
Case 2 (ε_MPL1=0.6, ε_MPL2=0.6)
Case 3 (ε_MPL1=0.6, ε_MPL2=0.4)
Case 4 (ε_MPL1=0.6, ε_MPL2=0.8)
Case 5 (ε_MPL1=0.4, ε_MPL2=0.4)
Case 6 (ε_MPL1=0.4, ε_MPL2=0.6)
Case 7 (ε_MPL1=0.4, ε_MPL2=0.8)
Case 8 (ε_MPL1=0.8, ε_MPL2=0.4)
Case 9 (ε_MPL1=0.8, ε_MPL2=0.6)
Case 10 (ε_MPL1=0.8, ε_MPL2=0.8)
CHANNEL
RIB

(b)

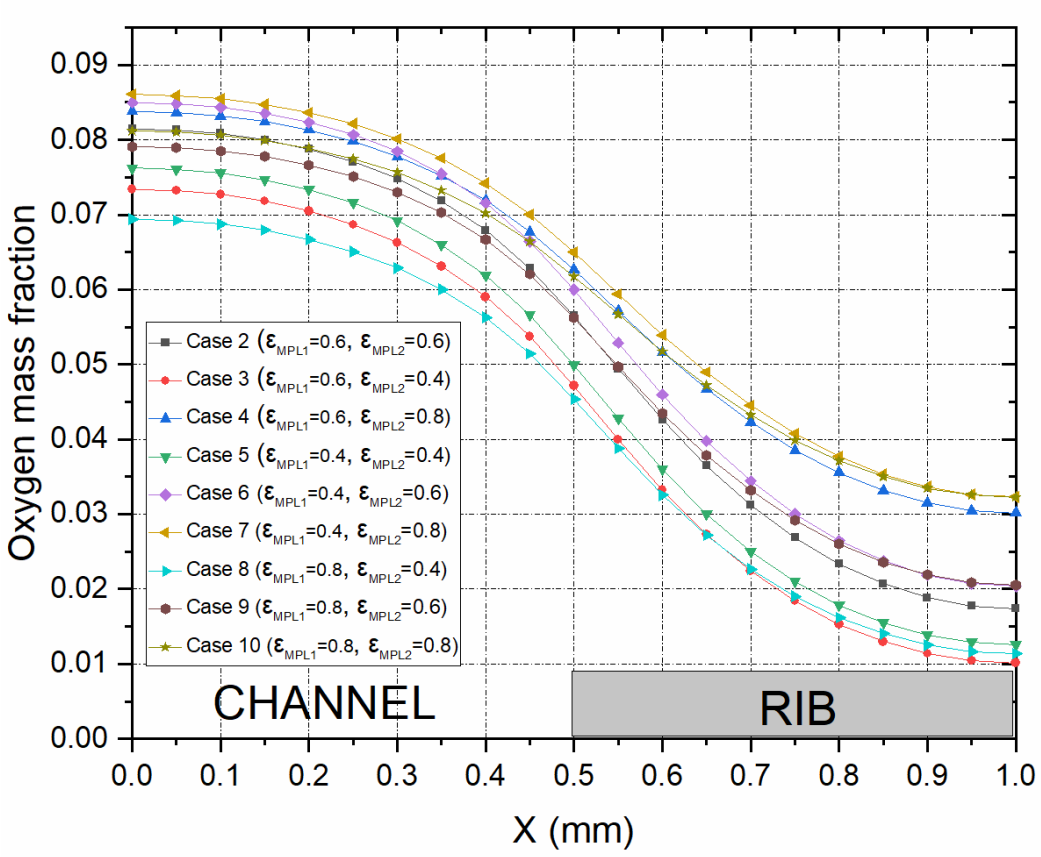

(c)

Figure 5.9 (a) Polarisation curves and, the distribution of (b) current density, and (c) oxygen mass fraction within the cathode GDL at 0.55 V for the porosities of single side and double side MPL-coated GDL computation cases shown in Table 5.4.

Table 5.5 shows the current density, at a cell voltage of 0.4V, for each of the cases plotted in Figure 5.9a.

Table 5.5 Current Density values for the cases shown in Fig. 5.9a, at 0.4 V.

Case No.	Current Density (A/cm²)
1 (Single MPL)	1.39
2	1.36
3	1.16
4	1.42
5	1.07
6	1.23
7	1.37
8	1.18
9	1.35
10	1.47

5.4 Conclusions

A three-dimensional, multiphase PEM fuel cell model with a straight channel has been developed. Parametric studies on the interfacial contact resistance of the PEMFC components, and effects of single side and double side MPL-coated GDLs were performed. The key findings and observations of the study are as follows:

- The interfacial contact resistance between the GDLs and the bipolar plates of the PEM fuel cell showed significant influence on the performance of the fuel cell, as well as the distribution of the current density and oxygen within the cathode GDL. Therefore, there is the need for experimentally measured

values of the contact resistance to be captured in the PEMFC models to give an accurate and realistic prediction of the performance of the PEM fuel cell.

- The fuel cell performance shows moderate sensitive to the interfacial contact resistance between the MPL and the catalyst layer. This can be attributed to the fact that the catalyst layer is directly deposited on the gas diffusion media and the presence of the MPL allows for improved contact at this surface, hence reducing the electron transport resistance.
- Incorporating an extra MPL at the interface between the GDL and the bipolar plate significantly improves the fuel cell performance as well as the local distribution of the current density and oxygen within the cathode GDL by reducing the contact resistance at that interface.
- Also, double side MPL-coating of the GDL improves the electrical contact between the GDL and each of the bipolar plate and the catalyst layer and subsequently improves the fuel cell performance significantly.
- It is recommended that in the design and manufacture of the PEM fuel cell GDLs, the MPL can be deposited on both sides of the carbon substrate as this improves the performance of the PEMFC.

In conclusion, based on the findings of this study, it is strongly recommended to design GDLs with double side MPL coatings.

6 GRADED GDL AND MPL POROSITIES: A NUMERICAL STUDY

6.1 Introduction

One of the challenges in the PEMFC operation is the effective liquid water management and the efficient transport of the gas reactants from the inlets of the gas channels to the catalyst layer where the electrochemical reactions take place. The gas diffusion layer which is responsible for the proper management of water and gas transport in the PEMFC has been widely investigated with modifications aimed at improving its architecture to meet this requirement. To this end, several studies exist in the literature on ways to increase the pore size and improve the porosity distribution of the cathode gas diffusion layer. For example, Zhang et al. [159]. developed a two-dimensional model of a PEMFC, which they validated with their experimental data, to study the effect of a functionally graded cathode GDL porosity of the PEMFC. They investigated the optimum porosity distribution along the PEMFC length that could yield maximum power density and limit the variation in the current density along the channel length. They reported that the current density variation at an operating cell voltage of 0.35 V reduced from 102 % to 10 % while at a cell voltage of 0.5 V, the current density variation reduced from 12 % to 5%. They concluded that an optimally graded porosity distribution of the cathode GDL significantly improves the uniformity in the local current density distribution along the PEMFC channel length by a factor of 10 and also produces maximum power. Carcadea et al. [160] developed a three-dimensional numerical multiphase model of the PEMFC in which they investigated the effect of the graded porosity of the

cathode GDL on the global performance of the PEMFC. They reported an improved performance with more effective liquid water rejection compared to the conventional cathode GDL design with uniform porosity. Also, Liu et al. [161] developed a three-dimensional model to study the effects of grading the cathode GDL into 5 layers with different porosities along the through-plane direction on the mass transport process and on the PEM fuel cell performance. They reported that larger gradients in the cathode GDL porosity results in poor uniformity of the gas diffusion coefficient distribution and reduces the mass transport of gas reactants within the fuel cell. However, a smaller porosity gradient results in a more uniform gas diffusion, higher electrochemical reaction rate, and improved PEMFC performance. Chen et al. [162] also investigated the effect of the graded porosity of the cathode GDL and reported improvements in performance. Kanchan et al. [1634] studied the effects of the non-uniform porosity distribution of the cathode GDL, along the PEMFC length, on the performance of the fuel cell. They reported an optimal performance when the GDL porosity is logarithmically graded along the PEMFC length. However, the PEMFC performed poorly with a sinusoidal decrease in the GDL porosity along the PEMFC length. In general, they reported superior PEMFC performance for all cases with non-uniform cathode GDL porosity compared to that of uniform porosity. However, most of these investigations have focused only on the GDL neglecting the MPL. Also, these studies have assumed low porosities for the GDL therefore failing to accurately predict the optimal linear porosity gradient required for improved fuel cell performance.

In this study, the three-dimensional multiphase model of the PEM fuel cell, developed in Chapter 5 of the thesis, has been used to study the effects of a linear gradient of the porosities of the cathode GDL and the cathode MPL. Parametric

studies were performed to show the optimal design arrangements for improved global performance of the PEMFC as well as the local distribution of the current density and oxygen concentration in the cathode side of the MEA.

6.2 RESULTS AND DISCUSSIONS

The PEM fuel cell model developed and validated in **Chapter 5** of the thesis has been used in this Chapter to investigate the effects of gradient porosity distributions of the cathode GDL and MPL of the PEMFC on the global performance of the fuel cell as well as on the local distribution of current density and oxygen concentration at the MPL-catalyst layer interface in the cathode of the PEM fuel cell. However, the conventional Brueggemann correlation [69] for the gas diffusivity of the GDL has been employed for this investigation instead of that proposed by [158] (used in Chapter 5 of the thesis). This is because the ANSYS Fluent PEMFC module is limited in terms of UDFs and expression for a graded diffusibility. Table 6.1 shows the cases investigated in this Chapter of the thesis for through-plane and in-plane graded GDL and MPL porosities. For Case 1, which is the base case, the porosity of either the cathode GDL or the cathode MPL is uniform and with a constant value of 0.6. The results of the study are discussed in detail in the following sections of this chapter.

Table 6.1 Cases investigated for the graded GDL and MPL porosities.

Case No.	ε_1	ε_2
1. (Uniform GDL porosity)	**0.6**	**0.6**
2.	0.6	0.2
3.	0.6	0.4
4.	0.6	0.8
5.	0.2	0.6

where ε_1 represents the half of the cathode GDL in contact with the bipolar plates (and for the graded MPL, it represents the half of the cathode MPL directly interfacing the cathode GDL). ε_2 represents the other half of the cathode GDL in contact with the cathode MPL (and for the graded MPL, it represents the half of the cathode MPL directly interfacing the cathode catalyst layer).

6.2.1 Graded GDL Porosity

The five cases of the cathode GDL porosity distribution, along the through-plane direction, shown in Table 6.1 were simulated and the overall PEMFC performance in terms of the cell polarisation curves as well as the current density and oxygen mass fraction distribution at the cathode side MPL-catalyst layer interface are shown in Figure 6.1. Considering Figure 6.1a, the cell polarisation shows moderate change with the different cases investigated. However, the cell polarisation curves for these cases show that the PEMFC model overestimated when the GDL graded porosity is linearly increased instead of decreasing. For example, Case 2 with decreasing GDL porosity gradient in the through-plane direction of the GDL is underestimated

when compared with Case 1 (the base case) with a uniform porosity value of 0.6. Cases 1 and 5 overlap each other. The polarisation curves also show that the grading of the porosity needs to be from a lower to a higher value for there to be improvements in the global fuel cell performance. Also, in Figure 6.1a, Case 2 is underestimated by about 16% compared to Cases 1 and 5, while it is about 11% underestimated when compared with Case3. Case 4 is about 5% overestimated when compared with the base case model (Case 1). The local distribution of the current density and oxygen concentration at the interface of the MPL and the catalyst layer, however, shows significant sensitivity to the gradient in the porosity of the cathode GDL, as can be seen in Figures 6.1a and b. In Figure 6.1b, it can be seen that Cases 2 and 3 with decreasing gradient porosity distributions are about 15% and 7%, respectively, underestimated compared to Case 1. While Case 5 is overestimated by about 5% when compared with Case 1, though the cell polarisation curves of these two cases (1 and 5) overlap each other. Case 4 is overestimated by about 18% when compared with Case 1. The same trend can be seen in Figure 6.1c which represents the plot of the oxygen mass fraction distribution at the MPL- catalyst layer interface of the cathode side of the PEMFC. The oxygen is more consumed at the catalyst layer for Case 4, with increasing gradient porosity compared to all other cases. Also, Case 5 that the oxygen is more consumed when compared to the base case. However, Case with decreasing porosity gradient (from 0.6 to 0.2) shows the least consumption of the oxygen gas reactant in the catalyst layer.

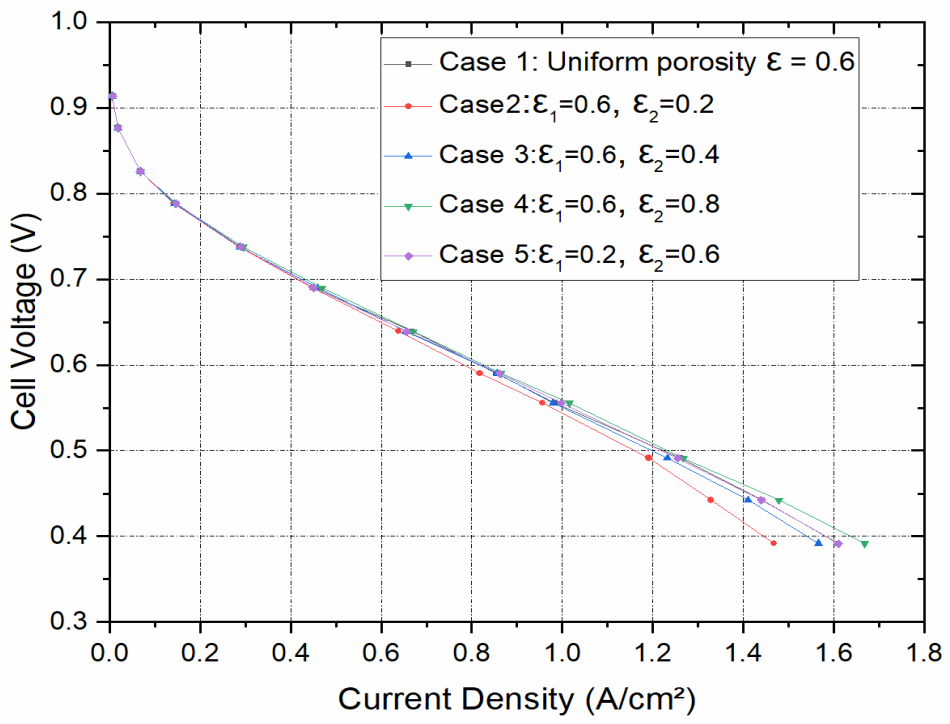
Case 1: Uniform porosity ε = 0.6
Case2:ε1=0.6, ε2=0.2
Case 3:ε1=0.6, ε2=0.4
Case 4:ε1=0.6, ε2=0.8
Case 5:ε1=0.2, ε2=0.6
Cell Voltage (V)
Current Density (A/cm²)
1.0
0.9
0.8
0.7
0.6
0.5
0.4
0.3
0.0
0.2
0.4
0.6
0.8
1.0
1.2
1.4
1.6
1.8

(a)

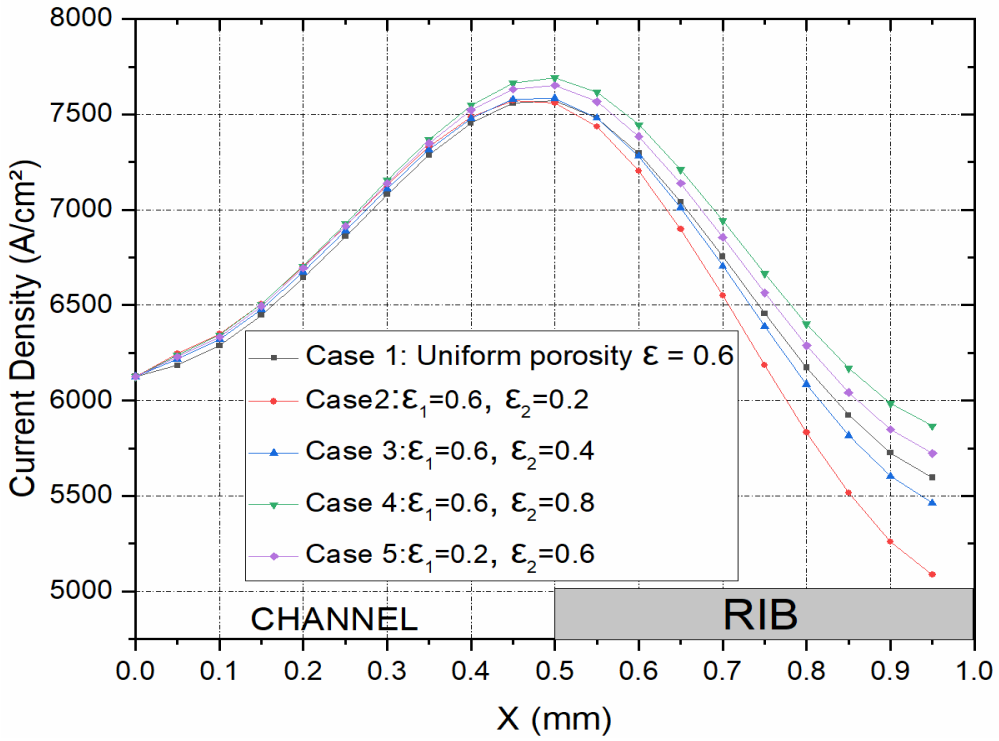
Case 1: Uniform porosity ε = 0.6
Case2:ε1=0.6, ε2=0.2
Case 3:ε1=0.6, ε2=0.4
Case 4:ε1=0.6, ε2=0.8
Case 5:ε1=0.2, ε2=0.6
CHANNEL
RIB
Current Density (A/cm²)
X (mm)
8000
7500
7000
6500
6000
5500
5000
0.0
0.1
0.2
0.3
0.4
0.5
0.6
0.7
0.8
0.9
1.0

(b)

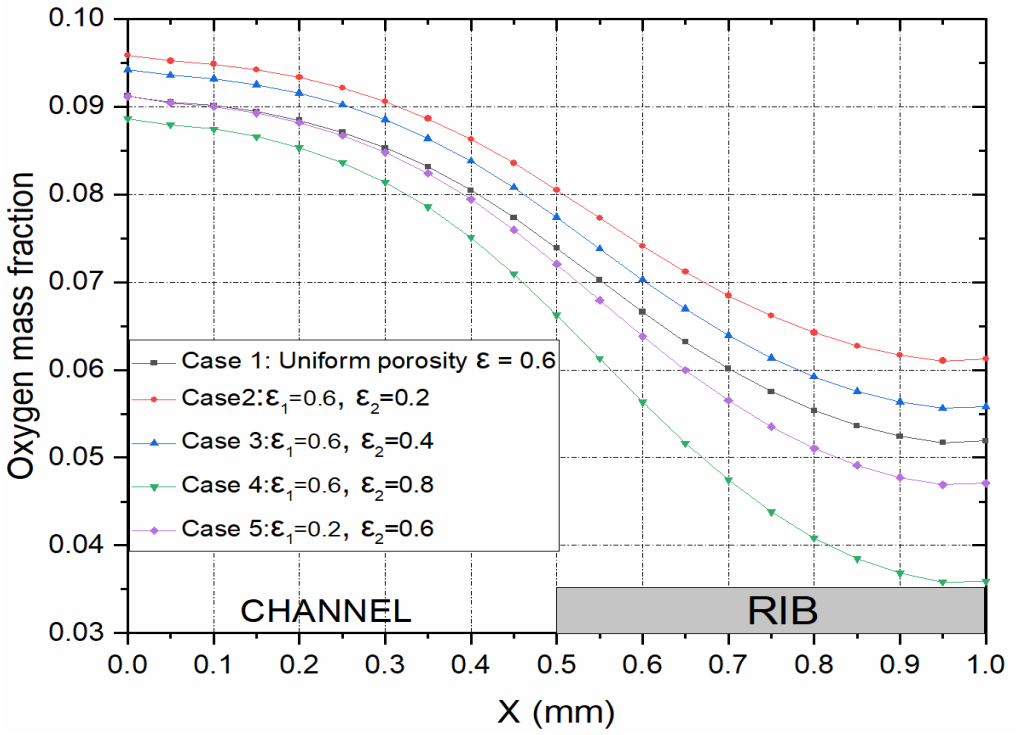

(c)

Figure 6.1 (a) Polarisation curves and, the distribution of (b) current density, and (c) oxygen mass fraction within the cathode GDL at 0.55 V for the cases shown in Table 6.1.

6.2.2 Graded MPL Porosity

The PEM fuel model was further investigated to see the effect of the linear gradient of the cathode MPL porosity on the PEMFC performance and the results are as shown in Figure 6.2. Though there are significant variations in the results for the local distribution of the key variables withing the cathode of the PEMFC, the results of the cell polarisation curves for the five cases of Table 6.1 implemented in the simulations show slight improvements for Case 2,3,4,5 of Figure 6.2 as compared to the same Cases in Figure 6.1 of Section 6.2.1. This can be attributed to the MPL being very thin (50 micron). Hence, the effect of the porosity gradient might be too

small to be seen in this study. However, it has been recommended in the Chapter 7 of this thesis for the graded MPL to be investigated further, using a thicker MPL. The distribution of the current density shown in Figure 6.2b shows that Case 4 overlaps Case 5. While Case 4 and 5 show about 40% improvement in the distribution when compared to Case 1. Both cases show about a 100% improvement in distribution when compared to Case 3 and more than 100% compared to Case 2, which has the least performance. For Figure 6.2c which shows the distribution of the oxygen mass fraction at the MPL-catalyst layer interface, Case 4 shows about 17% more consumed at the catalyst layer when compared with that of Case 5, especially in the area under the current collector rib. Again, Case 4 shows better consumption of the oxygen by over a 100% when compared with Case 6 while for Cases 2 and 3 the overestimation is about 140%. Though there is not much variation in the results with graded MPL porosity, it supports the fact that the grading of the porosity of the MPL and that GDL has to be in increasing order for there to be improvements in the performance of the PEM fuel cell model.

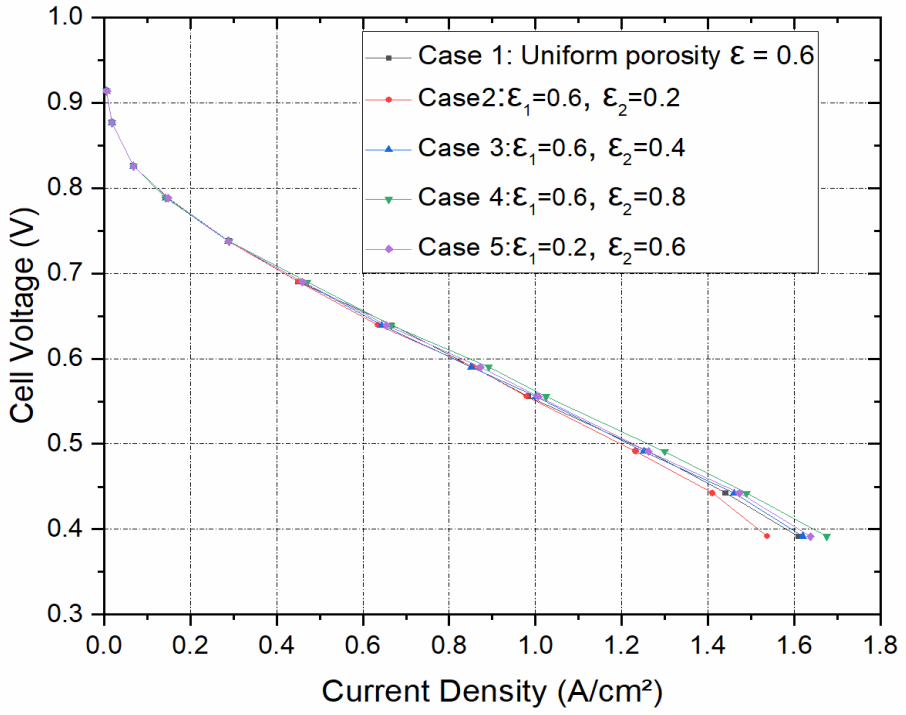
Case 1: Uniform porosity ε = 0.6
Case2:ε1=0.6, ε2=0.2
Case 3:ε1=0.6, ε2=0.4
Case 4:ε1=0.6, ε2=0.8
Case 5:ε1=0.2, ε2=0.6
Cell Voltage (V)
Current Density (A/cm²)
1.0
0.9
0.8
0.7
0.6
0.5
0.4
0.3
0.0
0.2
0.4
0.6
0.8
1.0
1.2
1.4
1.6
1.8

(a)

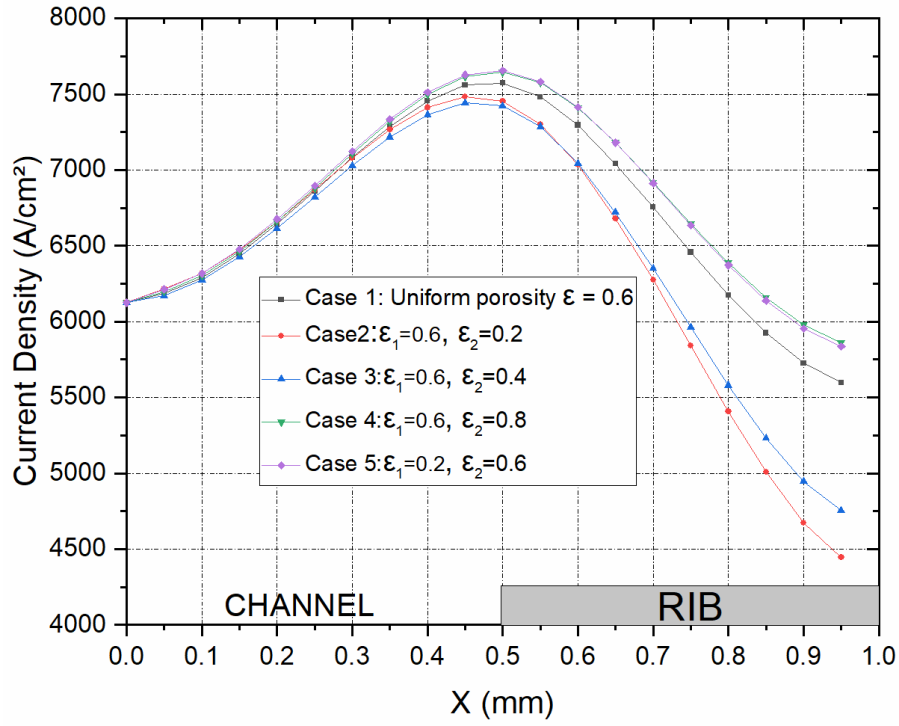
Case 1: Uniform porosity ε = 0.6
Case2:ε1=0.6, ε2=0.2
Case 3:ε1=0.6, ε2=0.4
Case 4:ε1=0.6, ε2=0.8
Case 5:ε1=0.2, ε2=0.6
CHANNEL
RIB
Current Density (A/cm²)
X (mm)
8000
7500
7000
6500
6000
5500
5000
4500
4000
0.0
0.1
0.2
0.3
0.4
0.5
0.6
0.7
0.8
0.9
1.0

(b)

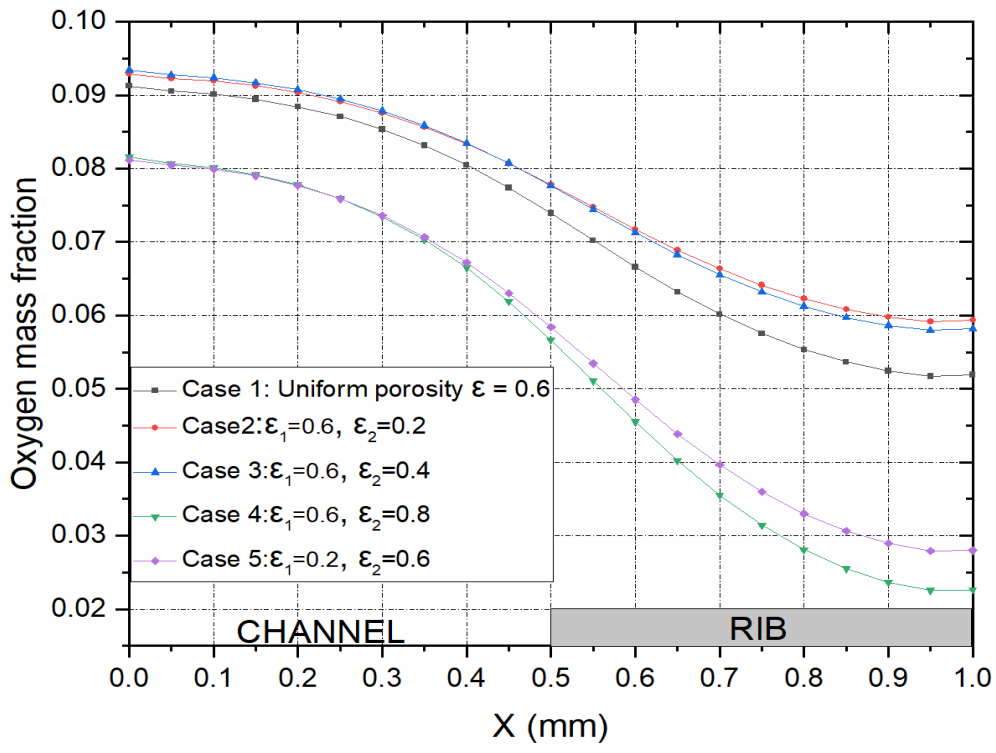

(c)

Figure 6.2 (a) Polarisation curves and, the distribution of (b) current density, and (c) oxygen mass fraction within the cathode GDL at 0.55 V for the cases in Table 6.1.

6.3 Conclusions

A sensitivity analysis was carried out on the effects of a linear gradient porosity distribution in the cathode GDL of the PEMFC on the PEM fuel cell performance, using the PEMFC cell model developed and validated in Chapter 5 of the thesis. However, the Brueggemann correlation for the GDL diffusivity was used in this investigation to account for the GDL diffusivity instead of that earlier used in Chapter 5 by Ismail et al. [169] which represents a more realistic formulation. The conclusions of the study are as follows:

- A gradient in the porosity of the cathode GDL has a moderate impact on the PEM fuel cell global performance. However, the local distribution of current density and oxygen mass fraction at the MPL-catalyst layer interface of the fuel cell is highly sensitive to the gradient porosity distribution of the cathode GDL.
- Also, a gradient in the porosity of the cathode MPL showed slight improvements compared to that of the cathode GDL for the global fuel cell performance, in terms of the cell polarisation curve. However, the distribution of the key parameters – current density and oxygen mass fraction at the interface of the MPL and the catalyst layer shows increased variations for each case compared to that of the graded GDL.
- Both investigations in Sections 6.2.1 and 6.2.2 show that all though the fuel cell performance is impacted by the gradient in the GDL and MPL porosities, a gradient in decreasing order, that is from high to low reduces the fuel cell performance. Whereas, increasing gradient, from low to higher porosity improves the performance of the PEMFC.

7 CONLUSIONS AND FUTURE WORK

7.1 Introduction

In this thesis, numerical models (2-D and 3-D) of the cathode gas diffusion electrode and the PEMFC were developed to study the sensitivity of the fuel cell performance and the local distributions of current density and oxygen concentration (within the cathode GDL of the PEMFC) to the anisotropy of the GDL. Realistic experimentally measured through-plane and in-plane gas permeability, gas diffusivity, thermal conductivity, and electrical conductivity of the GDL have been incorporated into the 3-D numerical model of the PEMFC to evaluate their impact on the global and local performance of the PEMFC. The modelled PEMFC was simulated using ANSYS Fluent software for all the cases investigated in this study, and the results obtained have been validated with experimental data obtained from existing literature. The outcome of this investigation shows that the GDL anisotropic transport properties needs to be fully captured in PEMFC models to avoid overestimating or underestimating the performance of the fuel cell.

In addition, the effects of the interfacial contact resistances that the GDL make with both the catalyst layer and the bipolar plate and the beneficial impact that double-sided MPL-coated GDL on the PEMFC performance have been investigated. Furthermore, the effect of a gradient porosity distribution in the cathode MPL, and the cathode GDL, on the PEMFC performance has been studied. The conclusions as well as recommended possible future works on these three major investigations in the thesis are discussed in detail in the following sections of this chapter, in line with the objectives stated in Chapter 1 of the thesis.

7.2 Effects of GDL anisotropic transport properties

A 2-D model of the multicomponent transport of gas species within the cathode GDL was developed in **Chapter 3** of the thesis, using ANSYS Fluent software, to investigate the sensitivity of the transport of reactant gas species to the GDL anisotropic gas permeability and the gas diffusivity. A parametric study using the anisotropic ratios (in-plane vs through-plane) of the gas permeability and gas diffusivity were used to test the sensitivity of the species transport to the anisotropy of the GDL.

In **Chapter 4**, a 3-D single phase model of the PEMFC was developed to investigate the effect of the GDL anisotropic transport properties – gas permeability, gas diffusivity, thermal conductivity, and electrical conductivity on the global performance of the PEMFC and the local distribution of current density and oxygen concentration within the cathode GDL. The developed 3-D PEMFC model was validated using experimental data from the literature and the key findings and observations of both investigations are as follows:

- At low flow velocities and gas permeability, the convective transport of the gas reactant species from the channel to the catalyst reaction sites is less dominant in terms of transporting the gases to the catalyst layer. The transport of species is dominated and controlled by the diffusion mechanism in the GDL.
- The distribution of the oxygen gas reactant at the GDL-catalyst layer interface is almost insensitive to the gas permeability of the GDL. This is understandable and expected as there is no cross flow between channels

and the pressure difference between the gas channels is not considered in the model.

- The compression of the GDL by the current collector ribs increases the porosity of the GDL in the region lying under the current collector rib so that the diffusion of the gas reactant from the gas channel to the catalyst layer is increased around this region. As a result, the oxygen is more utilized in the catalyst layer.
- The anisotropic transport properties of conventionally used carbon fibre GDLs need to be fully captured in the PEMFC models. Overlooking this GDL's attribute leads to either significant overestimation (if the in-plane values of the transport properties are only considered) or underestimation (if the through-plane values of the transport properties are only considered) of the modelled fuel cell current density by up to 50% at typical cell voltages (e.g., 0.5 V).
- Compared to the other GDL transport properties, the local distribution of current density and oxygen concentration within the GDL as well as the global PEMFC performance are highly sensitive to the electrical conductivity of the GDL, particularly in the through-plane direction. Quadrupling the through-plane GDL electrical conductivity increases the average current density of the fuel cell at 0.55 V by more than 50%.
- On the other hand, the through-plane or in-plane gas permeability of the GDL has an insignificant effect on the PEMFC performance, and the distributions of the above key variables within the GDL. This is because gas diffusion is

the dominant mode of transport of the gas species between the gas channel and the catalyst layer.

- The fuel cell performance is moderately sensitive to both the gas diffusivity (represented by the diffusibility in this study) and, to a lesser extent, the thermal conductivity of the GDL. This observation is more evident with the through-plane diffusibility and the thermal conductivity than with in-plane diffusibility or the thermal conductivity of the GDL. This is mainly attributed to the fact that the mass and heat transport between the catalyst layer and the flow channel/rib is in the through-plane direction. Notably, the fuel cell performance improves with decreasing the GDL through-plane thermal conductivity as it lowers heats dissipation and increases the reaction rate at the cathode catalyst layer.
- It is recommended that, when designing the carbon fibre paper GDLs, the carbon fibres are more oriented in the through-plane direction than in the through-plane direction to maximise traverse transport properties, in particular electrical conductivity, thermal conductivity, and gas diffusivity.

7.3 Effects of double sided MPL coated GDL and gradient porosities of the GDL and the MPL

In **Chapters 5 and 6**, a three-dimensional, multiphase PEM fuel cell model with a straight channel has been developed to investigate the effects (i) of the interfacial contact resistance between the PEM fuel cell components, (ii) double-side MPL-coated GDLs, and (iii) a graded porosity of the cathode GDL on the global performance of the PEMFC as well as the local distribution of key variables within the cathode GDL. Upon validation of the modelled PEMFC with experimental data

from the literature, parametric studies on the interfacial contact resistance of the PEMFC components, effects of single side and double side MPL-coated GDLs, and graded porosity of the cathode GDL and MPL have been performed. The key findings and observations of the study are as follows:

- The global performance of the PEM fuel cell model, as well as the local distribution of the current density and oxygen concentration within the cathode GDL, is significantly impacted by the interfacial contact resistance between the GDLs and the bipolar plates. For accurate predictions of PEM fuel cell performance, realistic experimentally measured values of the contact resistance need to be captured in the PEM fuel cell models.
- The fuel cell performance and the distributions of the above key variables within the cathode GDL are moderately sensitive to the interfacial contact resistance between the MPL (which is part of the GDL) and the catalyst layer. This can be attributed to the assumption that in the design of the MEA, the catalyst is mostly directly deposited on the gas diffusion media. Also, the presence of the MPL allows for improved contact at the GDM-catalyst layer interface, hence reducing the contact resistance.
- Incorporating double side MPL-coated GDLs significantly improves the fuel cell performance as well as the uniformity local distribution of the current density and oxygen within the cathode GDL by reducing the electrical resistance within the PEMFC and this leads to improved electrical conductance within the fuel cell.

- Also, double side MPL-coating of the GDL improves the electrical contact between the GDL and each of the bipolar plate and the catalyst layer and subsequently improves the fuel cell performance significantly.
- Increasing the porosity of the MPL at the GDL-BPP interface highly improves the performance of the fuel cell compared to that of single MPL coating at the GDL-catalyst interface.
- It is recommended that, when designing and manufacturing the PEM fuel cell GDLs, the MPL is deposited on both sides of the carbon substrate as this was shown to improve the performance of the PEMFC.
- Also, a cathode MPL with graded porosity showed a slight improvement in fuel cell performance compared to a cathode GDL with graded porosity. Also, the distribution of the key parameters (the current density and oxygen mass fraction at the interface of the MPL and the catalyst layer) shows increased variations with the graded-porosity MPL compared to the graded-porosity GDL.
- Both investigations in Sections 6.2.1 and 6.2.2 show that the fuel cell performance is sensitive to how the porosity of the GDL and the MPL is graded. Namely, increasing MPL or GDL porosity form the catalyst layer improves the fuel cell performance.

7.4 Overall Conclusion

In final conclusion, the results of the numerical investigation on the importance of the implementing the GDL anisotropy in PEMFC modelling provides the researcher with useful insights into the impact of the multi-directional components on the performance of the fuel cell. It allows for a full knowledge of the effect of the GDL

anisotropy on each of the transport properties. Also, the results show that the through-plane component of the GDL transport properties has more impact on the PEFC performance and therefore the carbon fibres need to be more oriented in the through-plane design during its design and manufacture.

Also, the numerical investigation into the effects of double side MPL-coated GDLs showed that the PEMFC performance was maximized and also the effect of the interfacial contact resistance is reduced (and also the total resistance). Therefore, the transport of electrons is improved in the PEMFC so that the current density distribution is maximised. Also, the grading of the cathode porous transport medium of the PEMFC shows that the at optimum design with increasing gradient, the PEMFC global performance as well as the local distribution of the key parameters is improved. This allows for an effective management of the liquid water transport and allows the gas reactant to be effectively transported to the catalyst layer. Therefore, improving the overall performance of the fuel cell.

7.5 Possible future work

This study highlights the effects of double sided MPL-coated GDLs and graded-porosity cathode GDL and MPL on the performance of the PEM fuel cell.

However, it would be of great interest to develop numerical PEMFC models to further investigate the effects of (i) the three-layered graded-porosity GDL and MPL in the through-plane direction and (ii) the in-plane graded-porosity GDL and MPL on the fuel cell performance. This could provide very useful insights in terms of designing GDLs for a more improved PEMFC performance.

One of the main limitations of this study is the fact that the PEM fuel cell module in ANSYS Fluent is limited in terms of modifications that one could do the code. To

this end, it is quite challenging to perform a wide range of novel designs to optimise the GDL and the PEMFC performance. Therefore, experimental designs and fabrications of GDL with double side MPL coatings would be very interesting and could result in improved results. Also, the GDL and the MPL can be fabricated with different porosity distributions as well as with different MPL materials to allow for improved pore distribution and also effective water manage within the MEA.

.

REFERENCES

[1] N. Zamel and L. Xianguo, “Effective transport properties for polymer electrolyte membrane fuel cell-With focus on the gas diffusion layer,” Progress in Energy and Combustion Science, vol.39, pp. 111-146, 2013.

[2] L. Xianguo, “Diversification and localization of energy systems for sustainable development and energy security,” Energy Policy, vol.33, pp. 2237-2243, 2005.

[3] IEA, Key World Energy Statistics from the IEA. www.iea.org/ statist/keyworld2002/keyworld2002.pdf, 2003.

[4] IEA, Global Energy Review: CO_2 Emissions in 2021. www.iea.org/reports/global-energy-review-co2-emissions-in-2021-2

[5] https://ourworldindata.org/energy

[6] Moomaw, W., F. Yamba, M. Kamimoto, L. Maurice, J. Nyboer, K. Urama, T. Weir, “Introduction. In IPCC Special Report on Renewable Energy Sources and Climate Change Mitigation” [O. Edenhofer, R. Pichs-Madruga, Y. Sokona, K. Seyboth, P. Matschoss, S. Kadner, T. Zwickel, P. Eickemeier, G. Hansen, S. Schlömer, C.von Stechow (eds)], Cambridge University Press, Cambridge, United Kingdom and New York, NY, USA, 2011.

[7] https://ec.europa.eu/transport/sites/transport/files/themes/strategies/doc/2001_white_paper/lb_texte_complet_en.pdf

[8] S. Ramesohl, and F. Merten, “Energy system aspects of hydrogen as an alternative fuel in transport,” Energy Policy, vol. 34, pp. 1251–1259, 2006.

[9] https://www.weforum.org/agenda/2021/06/4-technologies-accelerating-green-hydrogen-revolution/

[10] https://www.iea.org/reports/hydrogen-supply

[11] European Commission, “Green paper, Towards a European Strategy for Security of Supply. Directorate-General for Transport and Energy,” 2001c.

[12] https://www.csiro.au/en/work-with-us/services/consultancy-strategic-advice-services/CSIRO-futures/Energy-and-Resources/hydrogen-commercial-aviation

[13] F. Barbir, PEM Fuel Cells: Theory and Practice, Chapter 1. First ed. 2005, Oxford: ELSEVIER Academic Press.

[14] Fuel Cell Handbook, Chapter 1. Seventh ed. 2004, Morgantown, West Virginia: US Department of Energy.

[15] A. Lanz, Hydrogen Fuel Cell Engines and Related Technologies: Rev 0, module 4, 2001, USA: College of the Desert, Energy Technology Training Centre.

[16] Hoogers G., Fuel Cell Technology Handbook, Chapter 1. First ed. 2003, Boca Raton, Florida: CRC Press.

[17] T. Sutharssan, D. Montalvao, Y. K. Chen, W-C. Wang, C.Pisac, H. Elemara, “A review on prognostics and health monitoring of proton exchange membrane fuel cell,” Renewable and Sustainable Energy Reviews, Vol. 75, pp. 440-450, 2017.

[18] Larmine, J. and A. Dicks, Fuel Cell Systems Explained, Chapter 5. Second ed. 2003, Chichester (UK): John Wiley & Sons.

[19] https://www.fuelcellstore.com/blog-section/introduction-alkaline-fuel-cells

[20] https://www.energy.gov/eere/fuelcells/types-fuel-cells

[21] M. Kamran, Chapter 7 - Fuel cell, Renewable Energy Conversion Systems, Academic Press, 2021, pp. 221-242.

[22] Barbir, F., PEM Fuel Cells: Theory and Practice, Chapter 4. First ed. 2005, Oxford: ELSEVIER Academic Press.

[23] https://www.fuelcellstore.com/blog-section/direct-methanol-fuel-cell-improvements.

[24] https://www.fuelcellstore.com/fuel-cell-components/plates/end-plates.

[25] https://www.fuelcellstore.com/blog-section/fuel-cell-gaskets-spacers-and-end-plates.

[26] A. El-kharouf, B.G. Pollet, Chapter 4-Gas Diffusion Media and Their Degradation, in Polymer Electrolyte Fuel Cell Degradation, Academic Press, Boston, 2012, pp. 215-247.

[27] H.K. Versteeg and W. Malalasekera, An Introduction to Computational Fluid Dynamics: The Finite Volume Method, Chapter 1. Second ed. 2007, Harlow (UK): Pearson Education Limited.

[28] D. Kuzmin, “A Guide to Numerical Methods for Transport Equations,” First ed. 2010, Nurnberg: Friedrich Alexander University.

[29] X. Zhang, D. T. Song, Q. P. Wang, C. Huang, and Z. S. Liu, “Influence of anisotropic transport properties of the GDL on the performance of PEMFCs,” ECS Transactions, Vol. 16, no.2, pp. 913-923, 2008.

[30] S. Li, J. Yuan, M. Andersson, G. Xie, and B. Sunden, “Influence of anisotropic gas diffusion layers on transport phenomena in a proton exchange membrane fuel cell,” Int. J. Energy Res, vol. 41, pp. 2034-2050, 2017.

[31] C. Bapat and S.T. Thynell, “Effect of anisotropic electrical resistivity of gas diffusion layers (GDLs) on current density and temperature distribution in a Polymer Electrolyte Membrane (PEM) fuel cell,” Journal of Power Sources, vol.185, no.1, pp. 428-432, 2008.

[32] C. Bapat and S.T. Thynell, “Effect of anisotropic thermal conductivity of the GDL and current collector rib width on two-phase transport in a PEM fuel cell, “Journal of Power Sources, vol.179, no.1, pp. 240-251, 2008.

[33] J. G. Pharaoh, K. Karan, and W. Sun, “On effective transport coefficients in PEM fuel cell electrodes: Anisotropy of the porous transport layers,” Journal of Power Sources, vol.161, no.1, pp. 214-224, 2006.

[34] T. Zhou, and H. Liu, “Effects of the electrical resistances of the GDL in a PEM fuel cell,” Journal of Power Sources, vol.161, no.1, pp. 444-453, 2006.

[35] H. Meng and C. Y. Wang, “Electron Transport in PEFCs,” J. Electrochemical Society, vol. 151, no.3, pp. A358-A367, 2004.

[36] A. Kharouf, T. J. Mason, D. J. I. Brett, and B. G. Pollet, “Ex-situ characterization of gas diffusion layers for proton exchange membrane fuel cells,” J. Power Sources, vol. 218, pp. 393-404, 2012.

[37] A. Ozden, S. Shahgaldi, X. Li, and F. Hamdullahpur, “A review of gas diffusion layers for proton exchange membrane fuel cells—With a focus on characteristics, characterization techniques, materials and designs,” Progress in Energy and Combustion Science, vol. 74, pp. 50-102, 2019.

[38] M. Mathias, J. Roth, J. Fleming, and W. Lehnert, “Handbook of FUEL cells-fundamentals, technology and applications-chapter 46: diffusion media materials and characterization,” John Wiley &Sons, Ltd; 2003.

[39] P. Yi, L. Peng, X. Lai, M. Li, J. Ni,” Investigation of sintered stainless-steel fibre felt as gas diffusion layer in proton exchange membrane fuel cells,” International Journal of Hydrogen Energy, Vol 37, no. 15, pp.11334-1134, 2012.

[40] L. Moradizadeh, M. H. Paydar, P. Yazdanpanah, and G. Karimi, “Fabrication and characterization of metal-based gas diffusion layer containing rGO and graphite for proton exchange membrane fuel cells,” International Journal of Energy Research, pp. 1-14, 2022.

[41] S. Tanaka, W. W. Bradfield, C. Legrand, and A. G. Malan, “Numerical and experimental study of the effects of the electrical resistance and diffusivity under clamping pressure on the performance of a metallic gas-diffusion layer in polymer electrolyte fuel cells,” Journal of Power Sources, vol 330, pp. 273-284, 2016.

[42] F-Y. Zhang, S. G. Advani, and A. K. Prasad, “Performance of a metallic gas diffusion layer for PEM fuel cells,” Journal of Power Sources, vol 176, pp. 293-298, 2008.

[43] H. Choi, O-H. Kim, M. Kim, H. Choe, Y-H. Cho, and Y-E. Sung, “Performance of a metallic gas diffusion layer for PEM fuel cells,” Journal of Power Sources, vol 176, pp. 293-298, 2008.

[44] Y. Tang, W. Yuan, M. Pan, and Z. Wan, “Feasibility study of porous copper fibre sintered felt: a novel porous flow field in proton exchange membrane fuel cells,” Int J Hydrogen Energy, vol 35: pp. 9661- 9967.

[45] Y. Tang, W. Zhou, M. Q. Pan, H. Q. Chen, W. Y. Liu, and H. Yu,” Porous copper fibre sintered felts: an innovative catalyst support of methanol steam reformer for hydrogen production,” Int J Hydrogen Energy, vol 33, pp. 2950-2956, 2008.

[46] W. Zhou, Y. Tang, M. Q. Pan, X. L. Wei, H. Q. Chen, J. H. Xiang, “A performance study of methanol steam reforming microreactor with porous copper fibre sintered felt as catalyst support for fuel cells, “Int J Hydrogen Energy, vol34, pp. 9745-9753, 2009.

[47] F. Y. Zhang, S. G. Advani, and A. K. Prasad, “Performance of a metallic gas diffusion layer for PEM fuel cells,” Journal of Power Sources, vol 176, pp. 293-298, 2008.

[48] K. Fushinobu, D. Takahashi, and K. Okazaki, “Micromachined metallic thin films for the gas diffusion layer of PEFCs,” Journal of Power Sources, vol 158, pp. 1240-1245, 2006.

[49] J.T. Gostick, M. W. Fowler, M. D. Pritzker, M. A. Ioannidis, and L. M. Behra, “In-plane and through-plane gas permeability of carbon fibre electrode backing layers,” Journal of Power Sources, vol.162, no.1, pp. 228-238, 2006.

[50] M.V. Williams, H.R. Kunz, and J.M. Fenton, “Influence of convection through gas-diffusion layers on limiting current in PEMFCs using a serpentine flow field,” Journal of the Electrochemical Society, vol.151, no.10, pp. A1617-A1627, 2004.

[51] L. Carrette, K.A. Friedrich, and U. Stimming, “Fuel cells: Principles, types, fuels, and applications,” Chemphyschem, vol.1, no.4, pp. 162-193, 2000.

[52] R.L. Busby, Hydrogen and Fuel Cells: A Comprehensive Guide, Chapter 2. First ed., Oklahama: PennWell, 2005.

[53] S.M. Haile, “Fuel cell materials and components,” Acta Materialia, vol.51, no.19, pp. 5981-6000, 2003.

[54] K. Malek and M. O. Coppens, “Knudsen self-and Fickian diffusion in rough nanoporous media,” Journal of Non-Crystalline Solids, vol.225, no.1, pp. 293-297, 1998.

[55] U. Pasaogullari and P.P. Mukherjee, C. Y. Wang, and K. S. Chen, “Anisotropic Heat and Water Transport in a PEFC Cathode Gas Diffusion Layer,” Journal of the Electrochemical Society, vol.151, no.3, pp. A399-A406, 2004.

[56] H. Ju, “Investigation of the effects of the anisotropy of gas-diffusion layers on heat and water transport in polymer electrolyte fuel cells,” J. Power Sources, vol.191, pp. 259-268, 2009.

[57] M. Khandelwal and M.M. Mench, “Direct measurement of through-plane thermal conductivity and contact resistance in fuel cell materials” J. Power Sources, vol.161, no.2, pp. 1106-1115, 2006.

[58] N. Zamel, L. Xianguo, J. Shen, J. Becker, and A. Wiegmann, “Estimating effective thermal conductivity in carbon paper diffusion media,” Chemical Engineering Science, vol.65, no.13, pp. 3994-4006, 2010.

[59] E. Sadeghi, N. Djilali, and M. Bahrami, “Effective thermal conductivity and thermal contact resistance of gas diffusion layers in proton exchange membrane fuel cells. Part 1: Effect of compressive load,” J. Power Sources, vol,196, no.1, pp. 246-254, 2011.

[60] M. S. Ismail, “On the Transport Properties of Gas Diffusion Layers used in Proton Exchange Membrane Fuel Cells,” PhD Thesis, University of Leeds, 2011.

[61] V. Mishra, F. Yang, and R. Pitchumani, “Measurement and Prediction of Electrical Contact Resistance Between Gas Diffusion Layers and Bipolar Plate for Applications to PEM Fuel Cells,” Journal of Fuel Cell Science and Technology, vol.1, no.1, pp. 2-9, 2004.

[62] I. Nitta, O. Himanen, and M. Mikkola, “Contact resistance between gas diffusion layer and catalyst layer of PEM fuel cell,” Electrochemistry Communications, vol.10, no.1, pp. 47-51, 2008.

[63] A. Higier and H. Liu, “Effects of the difference in electrical resistance under the land and channel in a PEM fuel cell,” Int J Hydrogen Energy, vol..36, pp.1664–1670, 2011.

[64] T. Berning, D. M. Lu, and N. Djilali, “Three-dimensional computational analysis of transport phenomena in a PEM fuel cell,” Journal of Power Sources, vol 106, pp. 284–294, 2002.

[65] H. Wu, P. Berg, and X. G. Li, “Modeling of PEM fuel cell transients with finite rate phase transfer processes, “Journal of the Electrochemical Society, vol 157(1), pp. B1–12, 2010.

[66] C. Y. Jung, W. J. Kim, C. S. Yoon, D. H. Kim, and S. C. Yi, “Computational modeling of proton exchange membrane fuel cells including gas-crossover behaviour, “International Journal of Energy Research, vol 37, pp. 1981–1991, 2013.

[67] H. Meng, “Numerical studies of liquid water behaviours in PEM fuel cell cathode considering transport across different porous media,” International Journal of Hydrogen Energy, vol 35, pp. 5569–5579, 2010.

[68] M. M. Tomadakis and T. J. Robertson, “Viscous Permeability of Random Fibre Structures: Comparison of Electrical and Diffusional Estimates with Experimental and Analytical Results,” The Journal of Composite Materials, vol.39, No. 2, pp. 163-188, 2004.

[69] D.A.G. Bruggeman, “Calculation of various physics constants in heterogeneous substances I dielectricity constants and conductivity of mixed bodies from isotropic substances, “Annalen der Physik (Leipzig), vol. 24, pp. 636-664, 1935.

[70] N. Zamel and X. Li, “Non-isothermal multi-phase simulation of PEM fuel cell cathode,” Int. J. Energy Research, Vol.34: pp. 568 -584, 2010.

[71] G. H. Neale and W. K. Nader, “Prediction of transport processes within porous media: diffusive flow processes within a homogeneous swarm of spherical particles,” AIChE Journal, vol.19, pp. 112- 119, 1973.

[72] P. K. Das, X. Li, and Z. S. Liu, “Effective transport coefficients in PEM fuel cell catalyst and gas diffusion layers: beyond Bruggeman approximation,” Applied Energy, vol.87, pp. 2785-2796, 2010.

[73] J. H. Nam, and M. Kaviany, “Effective diffusivity and water-saturation distribution in single-and two-layer PEMFC diffusion medium,” Int. J. Heat Mass Trans, vol.46, pp. 4595-4611, 2003.

[74] M. M. Tomadakis and S. V. Sotirchos, “Ordinary and transition regime diffusion in random fiber structures,” AIChE Journal, vol.39, pp. 397-412, 1993.

[75] R. Wu, Q. Liao, X. Zhu, and H. Wang, “Liquid and oxygen transport through bilayer gas diffusion materials of proton exchange membrane fuel cells,” Int. J. Heat Mass Trans, vol.55, pp. 6363-6373, 2012.

[76] R. Wu, X. Zhu, Q. Liao, H. Wang, Y. D. Ding, J. Li, et al “Determination of oxygen effective diffusivity in porous gas diffusion layer using a three-dimensional pore network model,” Electrochim Acta, vol.55, pp. 7394-7403, 2010.

[77] S. Didari, A. Asadi, Y. Wang, and T.A.L. Harris, “Modeling of composite fibrous porous diffusion media, “Int. J. Hydrogen Energy, vol.39, pp. 9375-9386, 2014.

[78] T. Rosen, J. Eller, J. Kang, N. I. Prasianakis, J. Mantzaras, and F. N. Buchi, “Saturation dependent effective transport properties of PEFC gas diffusion layers,” J. Electrochem Soc, vol.159, pp. 536-544, 2012.

[79] N. Zamel, X. Li, and J. Shen, “Correlation for the effective gas diffusion coefficient in carbon paper diffusion media, “Energy Fuels, vol.23, pp. 6070-6078, 2009

[80] J. P. James, H.W. Choi, and J. G. Pharaoh, “X-ray computed tomography reconstruction and analysis of polymer electrolyte membrane fuel cell porous transport layers,” Int. J. Hydrogen Energy, vol.37, pp. 18216-18230, 2012.

[81] J. Becker, R. Fluckiger, M. Reum, F.N. Buchi, F. Marone, and M. Stampanoni, “Determination of Material Properties of Gas Diffusion Layers: Experiments and Simulations Using Phase Contrast Tomographic Microscopy,” J. Electrochem Soc, vol.156, no.10, pp. 1175- 1181, 2009.

[82] N. Zamel, N. G. C. Astrath, X. Li, and J. Shen, J. Zhou, F. B. G. Astrath, et al. “Experimental determination of effective diffusion coefficient of oxygen-nitrogen mixture in carbon paper, “Chemical Engineering Science, vol.65, pp. 931-937, 2010.

[83] D. Kramer, S. A. Freunberger, R. Flückiger, I. A. Schneider, A. Wokaun, F. N. Büchi, et al. “Electrochemical diffusimetry of fuel cell gas diffusion layers,” J. Electroanal Chem, vol.612, no. 1, pp. 63-77, 2008.

[84] R. Flückiger, S. A. Freunberger, D. Kramer, A. Wokaun, G. G. Scherer, and F. N., Büchi, “Anisotropic, effective diffusivity of porous gas diffusion layer materials for PEFC,” Electrochim Acta, vol.54, no.2, pp. 551-559, 2008.

[85] J. J. Baschuk and X. Li, “A general formulation for a mathematical PEM fuel cell model, “J. Power Sources, vol. 142, pp. 134 -153, 2005.

[86] H. T. Aichlmayr and F. A. Kulacki, “The effective thermal conductivity of saturated porous media, “In: G. Greene, (Ed.), Advances in Heat Transfer, Academic Press, New York, vol. 39, pp. 377 – 460, 2006.

[87] H. Wu, P. Berg, and X. Li, “Non-isothermal transient modeling of water transport in PEM fuel cells,” J. Power Sources, vol. 165, pp. 232-243, 2007.

[88] Y. Shan and S. Y. Choe, “A high dynamic PEM fuel cell model with temperature effects,” J. Power Sources, vol. 145, pp. 30-39, 2005.

[89] J. Hwang, “Thermal-electrochemical modeling of a proton exchange membrane fuel cell, “J. Electrochem Soc, vol. 153, pp. A216-224, 2006.

[90] E. Sadeghi, M. Bahrami, and N. Djilali, “Analytic determination of the effective thermal conductivity of PEM fuel cell gas diffusion layers,” J. Power Sources, vol. 179, pp. 200 -208, 2008.

[91] G. Maggio, V. Recupero, C. Mantegazza, “Modelling of temperature distribution in a solid polymer electrode cell stack,” J. Power Sources, vol. 62, pp. 167-174, 1996

[92] D. Veyret and G. Tsotridis, “Numerical determination of the effective thermal conductivity of fibrous materials: application to proton exchange

membrane fuel cell gas diffusion layers," J. Power Sources, vol. 195, pp. 1302-1307, 2010

[93] E. Nikooee, G. Karimi, and X. Li, "Determination of the effective thermal conductivity of gas diffusion layers in polymer electrolyte membrane fuel cells: a comprehensive fractal approach," International Journal of Energy Research, vol.35, 1351-1359, 2011.

[94] J. Ramousse, S. Didierjean, O. Lottin, and D. Maillet, "Estimation of the effective thermal conductivity of carbon felts used as PEMFC Gas Diffusion Layers," Int. J. Thermal Sciences, Vol. 47, no.1, pp. 1-6, 2008.

[95] N. Zamel, X. Li, and J. Shen, "Numerical estimation of the effective electrical conductivity in carbon paper diffusion media," Applied Energy, vol. 93, pp. 39-44, 2012.

[96] H. Looyenga, "Dielectric constants of heterogeneous mixture, "Physica, vol. 31, pp. 401-406, 1965.

[97] M. V. Williams, E. Begg, L. Bonville, R. Hunz, and J. M. Fentona, "Characterization of gas diffusion layers for PEMFC," J. Electrochem Soc, vol. 151, pp. A1173-1180, 2004.

[98] I. Nitta, T. Hottinen, O. Himanena, and M. Mikkola, "Inhomogeneous compression of PEMFC gas diffusion layer: Part I. Experimental," J. Power Sources, vol. 172, pp. 26-36, 2007.

[99] M. S. Ismail, T. Damjanovic, D. B. Ingham, M. Pourkashanian, and A. Westwood, "Effect of polytetrafluoroethylene-treatment and microporous layer-coating on the electrical conductivity of gas diffusion layers used in

proton exchange membrane fuel cells," J. Power Sources, vol. 195, no. 9, pp. 2700 –2708, 2010.

[100] F. Aldakheel, M.S. Ismail, K.J. Hughes, D.B. Ingham, L. Ma, M. Pourkashanian, D. Cumming, and R. Smith, "Gas permeability, wettability and morphology of gas diffusion layers before and after performing a realistic ex-situ compression test," Renewable Energy, vol 151, pp. 1082 – 1091, 2020.

[101] M. Mukherjee, C. Bonnet, and F. Lapicque, "Estimation of through-plane and in-plane gas permeability across gas diffusion layers (GDLs): Comparison with equivalent permeability in bipolar plates and relation to fuel cell performance," International journal of hydrogen energy, vol 45, pp. 13428 -13440, 2020.

[102] M. S. Ismail, T. Damjanovic, K. Hughes, D. B. Ingham, L. Ma, M. Pourkashanian, et al., "Through-plane permeability for untreated and PTFE-treated gas diffusion layers in proton exchange membrane fuel cells," J. Fuel Cell Sci Technol, vol. 7, pp. 051016–051017, 2010.

[103] O.M. Orogbemi, D.B. Ingham, M.S. Ismail, K.J. Hughes, L. Ma, and M. Pourkashanian," On the gas permeability of the microporous layer used in polymer electrolyte fuel cells," Journal of the Energy Institute, vol 91, pp. 894-901, 2018.

[104] C. Chan, N. Zamel, X. Li, and J. Shen, "Experimental measurement of effective diffusion coefficient of gas diffusion layer/microporous layer in PEM fuel cells," Electrochimica Acta, vol 65, pp. 13-21, 2012.

[105] I. V. Zenyuk, D.Y. Parkinson, L.G. Connolly, A.Z. Weber, “Gas-diffusion-layer structural properties under compression via X-ray tomography,” J. Power Sources, vol 328, pp. 364–376, 2016.

[106] G. S. Hwang and A. Z. Weber, “Effective Diffusivity Measurement of Partially-Saturated Fuel-Cell Gas – Diffusion Layers,” Journal of The Electrochemical Society, vol 159, no.11, pp. 683-692, 2012.

[107] P.A. García-Salaberri, I. V. Zenyuk, A. D. Shum, G. Hwang, M. Vera, A. Z. Weber, and J.T. Gostick, “Analysis of representative elementary volume and through-plane regional characteristics of carbon-fibre papers: diffusivity, permeability and electrical/thermal conductivity,” International Journal of Heat and Mass Transfer, vol 127, pp. 687–703, 2018.

[108] R. R. Rashapov, and J. T. Gostick, “In-Plane Effective Diffusivity in PEMFC Gas Diffusion Layers,” Transp Porous Med, vol115, pp. 411–433, 2016.

[109] B. Xiao, J. Fan, and F. Ding, “A fractal analytical model for the permeabilities of fibrous gas diffusion layer in proton exchange membrane fuel cells,” Electrochimica Acta, vol 134, pp. 222–231, 2014.

[110] Z. Tayarani-Yoosefabadi, D. Harvey b, J. Bellerive b, and E. Kjeang, “Stochastic microstructural modeling of fuel cell gas diffusion layers and numerical determination of transport properties in different liquid water saturation levels,” Journal of Power Sources, vol 303, pp. 208-221, 2016.

[111] S. Mohamad Moosavi, M. Niffeler, J. Gostick, and S. Haussener, “Transport characteristics of saturated gas diffusion layers treated with

hydrophobic coatings," Chemical Engineering Science, vol 176, pp. 503–514, 2018.

[112] P. Mangal, L. M. Pant, N. Carrigya, M. Dumontier, V. Zingan, S. Mitra, and M. Secanell, "Experimental study of mass transport in PEMFCs: Through plane permeability and molecular diffusivity in GDLs," Electrochimica Acta, vol 167, pp. 160–171, 2015.

[113] H. Sadeghifar, N. Djilali, and M. Bahrami, "Effect of Polytetrafluoroethylene (PTFE) and micro porous layer (MPL) on thermal conductivity of fuel cell gas diffusion layers: Modeling and experiments," Journal of Power Sources, vol 248, pp. 632-641, 2014.

[114] G.R. Molaeimanesh, and M.H. Akbari, "A three-dimensional pore-scale model of the cathode electrode in polymer-electrolyte membrane fuel cell by lattice Boltzmann method," Journal of Power Sources, vol 258, pp. 89-97, 2014.

[115] S. Chevalier, J. Lee, N. Gea, R. Yip, P. Antonacci, Y. Tabuchi, T. Kotakab, A. Bazylak, "In operando measurements of liquid water saturation distributions and effective diffusivities of polymer electrolyte membrane fuel cell gas diffusion layers," Electrochimica Acta, vol 210 pp. 792–803, 2016.

[116] M. Bosomoiu, G. Tsotridis, T. Bednarek, "Study of effective transport properties of fresh and aged gas diffusion layers," Journal of Power Sources, vol 285, pp. 568-579, 2015.

[117] N. Alhazmi, M.S. Ismail, D.B. Ingham, K.J. Hughes, L. Ma, and M. Pourkashanian, "The in-plane thermal conductivity and the contact resistance

of the components of the membrane electrode assembly in proton exchange membrane fuel cells," Journal of Power Sources, vol 241, pp. 136-145, 2013.

[118] N. Alhazmi, M.S. Ismail, D.B. Ingham, K.J. Hughes, L. Ma, and M. Pourkashanian," The through-plane thermal conductivity and the contact resistance of the components of the membrane electrode assembly and gas diffusion layer in proton exchange membrane fuel cells," Journal of Power Sources, vol 270, pp. 59-67, 2014.

[119] H.K. Versteeg and W. Malalasekera, An Introduction to Computational Fluid Dynamics: The Finite Volume Method, Chapter 1. Second ed. 2007, Harlow (UK): Pearson Education Limited.

[120] K. Z. Yao, K. Karan, K. B. McAuley, P. Oosthuizen,B. Peppley, and T. Xie,"A Review of Mathematical Models for Hydrogen and Direct Methanol Polymer Electrolyte Membrane Fuel Cells," Fuel Cells, vol 4(1-2), pp. 3-29, 2004.

[121] S. Scheiner, P. Pivonka, and D.W. Smith, "Electro-diffusive transport in macroscopic porous media: Estimation of effective transport properties using numerical upscaling," Computers and Geotechnics, vol 48, pp. 283–292, 2013.

[122] M. Quintard, L. Bletzacker, D. Chenu, and S. Whitaker, "Nonlinear, multicomponent, mass transport in porous media," Chemical Engineering Science, vol 61, pp. 2643 – 2669, 2006.

[123] E. Carcadea, H. Ene, D.B. Ingham, T, R. Lazar, L. Ma, M. Pourkashanian, and I. Stefanescu, "Numerical simulation of mass and charge

transfer for a PEM fuel cell," International Communications in Heat and Mass Transfer, vol 32, pp. 1273 – 1280, 2005.

[124] J. Peng, J.Y. Shin, T.W. Song, "Transient response of high temperature PEM fuel cell," Journal of Power Sources, vol 179, pp. 220–231, 2008.

[125] J. M. Stockie, K. Promislow, and B. R. Wetton, "A finite volume method for multicomponent gas transport in a porous fuel cell electrode," International Journal for Numerical Methods in Fluids, vol 41, pp. 577-599, 2003.

[126] ANSYS Fluent. Fuel cell module manual. Lebanon, New Hampshire (USA): Fluent Inc.; 2010.

[127] E. Carcadea, H. Ene, D. B. Ingham, R. Lazar, L. Ma, M. Pourkashanian, and I. Stefanescu, "A computational fluid dynamics analysis of a PEM fuel cell system for power generation", International Journal of Numerical Methods for Heat and Fluid Flow, Vol. 17, No. 3, pp. 302-312, 2007.

[128] M. S. Ismail, K. J. Hughes, D. B. Ingham, L. Ma, and M. Pourkashanian, "Effects of anisotropic permeability and electrical conductivity of gas diffusion layers on the performance of proton exchange membrane fuel cells,". Applied Energy, vol. 95, pp. 50 – 63, 2012.

[129] M. S. Ismail, T. Damjanovic, D. B. Ingham, L. Ma, and M. Pourkashanian, "Effect of polytetrafluoroethylene-treatment and microporous layer-coating on the in-plane permeability of gas diffusion layers used in proton exchange membrane fuel cells," J. Power Sources, vol. 195, pp. 6619 – 6628, 2010.

[130] J. T. Gostick, “Random pore network modeling of fibrous PEMFC gas diffusion media using Voronoi and Delaunay tessellations, “J. Electrochem Soc, vol.160, pp. 731- 743, 2013.

[131] N. Alhazmi, D. B. Ingham, M.S. Ismail, K. J. Hughes, L. Ma, and M. Pourkashanian, “Effect of the anisotropic thermal conductivity of GDL on the performance of PEM fuel cells,” Int. J. Hydrogen Energy, vol.38, pp. 603-611, 2013.

[132] L. Xing, P. K. Das, X.G. Song, M. Mamlouk, K. and Scott, “Numerical analysis of the optimum membrane/ionomer water content of PEMFCs: the interaction of Nafion ionomer content and cathode relative humidity”, Applied Energy, Vol 138, pp.242–257, 2015.

[133] W. Yoshimune, S. Kato, M. Inagaki, and S. Yamaguchi, S. “A simple method to measure through-plane effective gas diffusivity of a gas diffusion layer for polymer electrolyte fuel cells”, International Journal of Heat and Mass Transfer, Vol 191 No. 122887, pp.1-7, 2022.

[134] M. Taş, and G. Elden, “An Experimental Investigation of the Effects of Operating Conditions on Anisotropic Electrical Conductivity in a PEM Fuel Cell”, Fuel Cells, Vol. 20 No. 5, pp. 531-539, 2020.

[135] M. Taş, and G. Elden, “Three-dimensional and anisotropic numerical analysis of a PEM fuel cell”, International Journal of Hydrogen Energy, Vol. 47, pp. 19758-19771, 2022.

[136] G. Zhang, L. Fan, J. Sun, and K. Jiao, “A 3D model of PEMFC considering detailed multiphase flow and anisotropic transport properties”, International Journal of Heat and Mass Transfer, Vol 115, pp.714-724, 2017.

[137] Y. Wang, X. Wang, Y. Qin, L. Zhang, and Y. Wang, “Three-dimensional numerical study of a cathode gas diffusion layer with a through/in plane synergetic gradient porosity distribution for PEM fuel cells”, International Journal of Heat and Mass Transfer, Vol 188, No. 122661, pp.1-15, 2022.

[138] R. J. Yu, H. Guo, and F. Ye, “Study on transmission coefficients anisotropy of gas diffusion layer in a proton exchange membrane fuel cell”, Electrochimica Acta, Vol. 414, pp. 1-18, 2022.

[139] T. A. Zawodzinski, T. E. Springer, F. Uribe, and S. Gottesfeld, “Characterisation of polymer electrolytes for fuel cell applications”, Solid State Ionics, Vol 60, pp.199–211, 1993.

[140] T. E. Springer, T. A. Zawodzinski, and S. Gottesfeld, “Polymer electrolyte fuel-cell model”, Journal of the Electrochemical Society, Vol 138, pp.2334–42, 1991.

[141] E. A. Ticianelli, C. R. Derouin, A. Redondo, and S. Srinivasan, “Methods to Advance Technology of Proton Exchange Membrane Fuel Cells,” J. Electrochem. Soc., vol. 135, no. 9, pp. 2209–2214, 1988, doi: 10.1149/1.2096240.

[142] Q. Duan, H. Wang, and J. Benziger, “Transport of liquid water through Nafion membranes”, Journal of Membrane Science, Vol.392-393, pp. 88-94, 2012.

[143] P. Zhou, C.W. Wu, G.J. Ma, “Contact resistance prediction and structure optimization of bipolar plates,” Journal of Power Sources, vol159 pp. 1115–1122, 2006.

[144] Y. Zhou, G. Lin, A.J. Shih, S.J. Hu,” A micro-scale model for predicting contact resistance between bipolar plate and gas diffusion layer in PEM fuel cells,” Journal of Power Sources, vol 163, pp. 777–783, 2007.

[145] D. Qiu, H. Janßen, L. Peng, P. Irmscher, X. Lai, and W. Lehnert, “Electrical resistance and microstructure of typical gas diffusion layers for proton exchange membrane fuel cell under compression,” Applied Energy, vol 231, pp.127-137, 2018.

[146] X. Lai, D. Liu, L. Peng, J. Ni,” A mechanical–electrical finite element method model for predicting contact resistance between bipolar plate and gas diffusion layer in PEM fuel cell,” Journal of Power Sources, vol 182, pp. 153–159, 2008.

[147] L. Zhang, Y. Liu, H. Song, S. Wang, Y. Zhou, S. J. Hu, “Estimation of contact resistance in proton exchange membrane fuel cells,” Journal of Power Sources, vol 162, pp.1165–1171, 2006.

[148] P. K. Sow, S. Prass, P. Kalisvaart, W. Merida, “Deconvolution of electrical contact and bulk resistance of gas diffusion layers for fuel cell applications,” International Journal of Hydrogen Energy, vol 40, pp. 2850 – 2861, 2015.

[149] M.S. Ismail, D.B. Ingham, L. Ma, M. Pourkashanian, “The contact resistance between gas diffusion layers and bipolar plates as they are

assembled in proton exchange membrane fuel cells," Renewable Energy, vol 52, pp. 40-45, 2013.

[150] D. Ye, E. Gauthier, J. B. Benziger, and M. Pan, "Bulk and contact resistances of gas diffusion layers in proton exchange membrane fuel cells," Journal of Power Sources, vol 256, pp. 449-456, 2014.

[151] F.C. Lee, M.S. Ismail, D.B. Ingham, K.J. Hughes, L Ma, S.M. Lyth, M. Pourkashanian," Alternative architectures and materials for PEMFC gas diffusion layers: A review and outlook," Renewable and Sustainable Energy Reviews, Vol 166, pp.1-33, 2022.

[152] T. Kitahara, T. Konomi, and H. Nakajima," Microporous layer coated gas diffusion layers for enhanced performance of polymer electrolyte fuel cells," Journal of Power Sources, vol 195 pp. 2202–2211, 2010.

[153] T. Kitaharaa , H. Nakajimaa , K. Moria and M. Inamoto," Influence of Hydrophilic and Hydrophobic Double MPL Coated GDL on PEFC Performance," ECS Transactions, vol 50, no.2, pp. 437-444, 2012.

[154] J. H. Chun, K. T. Park, D. H. Jo, J.Y. Lee, S. G. Kim, S. H. Park, E. S. Lee, J-Y. Jyoung, S. H. Kim," Development of a novel hydrophobic/hydrophilic double micro porous layer for use in a cathode gas diffusion layer in PEMFC," International Journal of Hydrogen Energy, Vol 36, No. 14, pp.8422-8428, 2011.

[155] X. Wang, H. Zhang, J. Zhang, H. Xu, X. Zhu, J. Chen, B. Yi," A bi-functional micro-porous layer with composite carbon black for PEM fuel cells," Journal of Power Sources, vol162, pp.474–479, 2006.

[156] X.L. Wang, H.M. Zhang, J.L. Zhang, H.F. Xu, Z.Q. Tian, J. Chen, H.X. Zhong, Y.M. Liang, B.L. Yi, “Micro-porous layer with composite carbon black for PEM fuel cells,” Electrochimica Acta, vol 51 pp. 4909–4915, 2006.

[157] I.C. Okereke, M.S. Ismail, D.Ingham, K.J. Hughes, L. Ma, M.Pourkashanian,” The effects of GDL anisotropic transport properties on the PEFC performance,” International Journal of Numerical Methods for Heat & Fluid Flow, DOI: https://doi.org/10.1108/HFF-05-2022-0284.

[158] M.S. Ismail, D.B. Ingham, K.J. Hughes, L. Ma, M. Pourkashanian,” Effective diffusivity of polymer electrolyte fuel cell gas diffusion layers: An overview and numerical study,” International Journal of Hydrogen Energy, Vol 40, no. 34, pp. 10994-11010, 2015.

[159] L. Wang, A. Husar, T. Zhou, H. Liu,” A parametric study of PEM fuel cell performances,” International Journal of Hydrogen Energy, vol 28 pp. 1263 – 1272, 2003.

[160] E. Carcadea, M. Varlam, M. S. Ismail, D. B. Ingham, A. Marinoiu, M. Raceanu, C. Jianu, L. Patularu, D. Ion-Ebrasu,” PEM fuel cell performance improvement through numerical optimization of the parameters of the porous layers,” International Journal of Hydrogen Energy, Vol 45, no. 14, pp.7968-7980, 2020.

[161] Y. Liu, S. Wu, Y. Qin, M. Zhang, X. Liu, J. Zhang, and Y. Yin,” Mass transport and performance of proton exchange membrane fuel cell considering the influence of porosity distribution of gas diffusion layer”,

International Journal of Green Energy, doi.org/10.1080/15435075.2021.2007389.

[162] F. Chen, M-H. Chang, and P-T. Hsieh," Two-phase transport in the cathode gas diffusion layer of PEM fuel cell with a gradient in porosity," International Journal of Hydrogen Energy, vol 33 pp.2525– 2529, 2008.

[163] B. K. Kanchan, P. Randive, S. Pati, "Implications of non-uniform porosity distribution in gas diffusion layer on the performance of a high temperature PEM fuel cell," International Journal of Hydrogen Energy, vol 46 pp. 18571-18588, 2021.

APPENDIX A

A.1. User Defined Function for Graded Porosity of the GDL

```
#include "udf.h"

#define h      0.0016


DEFINE_PROFILE (porosity, t, i)

{

  cell_t c;

  real z;

  real x[3];

  real por;

  begin_c_loop (c, t)

    {

              C_CENTROID (x, c,t);

       z=x[2];

       if (0.0015<z<=h)

          {

          por=0.6;

           }

       else

         {

           por=0.2;

           }

       C_PROFILE(c,t,i)=por;

    }
```

```
    end_c_loop(c,t)
}
DEFINE_PROFILE (permeability, t, i)
{
  cell_t c;
  real y;
  real x [3];
  real permeab;
  begin_c_loop (c, t)
    {
            C_CENTROID (x, c,t);
       y=x[2];
       if (0.0015<y<=h)
         {
         permeab=3.96e-13;
          }
       else
        {
          permeab=3e-12;
          }
       C_PROFILE(c, t,i) =permeab;
    }
    end_c_loop(c,t)
}
```

A.2. User Defined Function for Graded Porosity of the MPL

```
#include "udf.h"

#define h      0.00175

DEFINE_PROFILE (porosity, t,i)

{

  cell_t c;

  real z;

  real x[3];

  real por;

  begin_c_loop(c,t)

    {

            C_CENTROID(x,c,t);

       z=x[2];

       if (0.0017<z<=h)

          {

          por=0.6;

           }
```

```
        else
          {
            por=0.2;
            }
        C_PROFILE(c,t,i)=por;
     }
     end_c_loop(c,t)
}
DEFINE_PROFILE (permeability, t, i)
{
  cell_t c;
  real y;
  real x[3];
  real permeab;
  begin_c_loop(c, t)
     {
               C_CENTROID(x,c,t);
```

```
        y=x [2];
        if (0.0017<y<=h)
          {
          permeab=3.96e-13;
           }
        else
         {
           permeab=3e-12;
           }
        C_PROFILE (c, t, i) =permeab;
    }
    end_c_loop (c, t)
}
```